UNIVERSITÉ DE GRENOBLE

浙江大學

THÈSE

Pour obtenir le grade de

DOCTEUR DE L'UNIVERSITÉ DE GRENOBLE

Spécialité : **2MGE : Matériaux, Mécanique, Génie civil, Electrochimie**

Arrêté ministériel : 7 août 2006

Et de

DOCTEUR DE L'UNIVERSITÉ DE ZHEJIANG

Spécialité : **MATERIAL SCIENCE**

Présentée par

Liyan SHEN

Thèse dirigée par **Catherine PICART** et codirigée par **Jian JI**

préparée au sein du **Laboratoire des Matériaux et du Génie Physique (LMGP UMR CNRS 5628)**
dans **l'École Doctorale IMEP2**
et du **Department of Polymer Science and Engineering**
à **ZHEJIANG UNIVERSITY (Hangzhou, Chine)**

Membranes auto-supportées et nanocomposites à base de films multicouches de polyélectrolytes

Thèse soutenue publiquement le **7 mars 2012**
devant le jury composé de :

M. Gero DECHER
Professeur, Université de Strasbourg, Rapporteur
M. Boris LAKARD
Professeur, Université de Franche Comté, Rapporteur
M. Didier DELABOUGLISE
Professeur, INP de Grenoble, Président
M. Jiacong SHEN
Professeur, Université de Zhejiang, Membre
M. Jian JI
Professeur, Université de Zhejiang, Membre, Co-directeur de thèse
Mme Catherine PICART
Professeur, INP de Grenoble, Directrice de thèse

Membranes auto-supportées et nanocomposites à base de films multicouches de polyélectrolytes

Résumé

La technique d'auto-assemblage couche par couche de polyélectrolytes, permettant de construire des films appelés « multicouches », s'est grandement développée au cours des deux dernières décennies. Cette technique permet non seulement de modifier des surfaces de matériaux mais également d'élaborer des membranes auto-supportées. Dans cette thèse, j'ai étudié la croissance de deux systèmes multicouches assemblés dans des conditions extrêmes de pH pour accélérer leur croissance. Les films à base de poly(ethylene imine) et d'acide poly(acrylique) ont été utilisés pour réaliser, d'une part, des membranes possédant une capacité à répondre à l'humidité, et d'autre part, des membranes asymétriques présentant des propriétés anti-bactériennes. Les films à base de poly(L-lysine) et de hyaluronane ont été réalisé par croissance amplifiée par le pH, et l'effet du poids moléculaire du HA sur la croissance et les propriétés interne des films a été étudié. Ces films ont servi de réservoir pour le piégeage de précurseurs métalliques, qui ont ensuite été réduit *in situ* par irradiation UV, afin de former des nanoparticules. Ainsi, des films nanocomposites contenant des particules d'argent et des particules d'or ont été synthétisés.

Mots Clefs: assemblage couche par couche, membrane, nanocomposite, pH, réduction *in situ*.

Free-standing films and nanocomposites based on pH-amplified polyelectrolyte multilayer films

Abstract

Layer-by-layer assembly has witnessed great development during the last two decades and has expanded its application from surface modification to membrane construction. In this thesis, I studied the buildup of layer-by-layer films assembled at extreme pH (i.e. pH-amplified). I first focused on the fabrication of free-standing film made of poly(ethylene imine) and poly(acrylic acid). An application was to use these films as humidity sensors and a second one was to load silver ions in the films to create anti-bacterial membranes. Then, I worked on poly(L-lysine)/hyaluronan films and I investigated the effect of HA molecular weight on film growth and internal properties. Finally, nanocomposites were made via *in situ* synthesis of metal NPs in (PLL/HA) films: silver NP loaded (PLL/HA) free-standing films were constructed and their mechanical properties were tested; well dispersed gold NPs with sizes ranging from ~2 nm to ~9 nm were synthesized in (PLL/HA) films.

Key words: layer-by-layer assembly, free-standing film, nanocomposite, pH, *in situ* reduction

Laboratoire:

Institut Polytechnique de Grenoble - Laboratoire des Matériaux et du Génie Physique - 3 parvis L.NEEL 38016 Grenoble, France

Zhejiang University - Department of Polymer Science and Engineering - 38 Zheda Road, 310027 Hangzhou, China

Acknowledgements

This manuscript reports most of my work over the past three years. The thesis was a first professional experience in scientific research for me, and it was generally an experience with numerous discoveries and encounters. In these few words, I would like to thank everyone who helps me in one way or another to make this experience possible and as enjoyable and rewarding.

First of all, I would like to extend my sincere gratitude to Prof. Gero Decher from Université de Strasbourg and Prof. Boris Lakard from Université de France Comté for giving me the honor of judging my thesis. Also, I would like to thank Prof. Didier Delabouglise from INP Grenoble to chaire the thesis committee.

High tribute shall be paid to my supervisors Prof. Catherine Picart and Prof. Jian Ji. Both of them are of great help during the thesis, not only in the research but also in daily life. They two perfectly fulfilled the role of guiding me to be a qualified researcher, and provided me sufficient freedom in my experiments and work organization. In particular, I would like to thank both of them for their confidence in me and for their strong and continuous support that I can clearly feel during the three years.

Half of my work was done in LMGP (Laboratoire des Matériaux et du Génie Physique) at MINATEC. I would like to thank all the members in the lab for their friendship, kindness and efforts that have helped make me feel comfortable at work. Special thanks should go to Prof. Michel Langlet, Prof. Didier Delabouglise and Prof. Roland Madar for their fruitful discussion and to Mr. Patrick Chaudouet and Ms. Laetitia Rapenne for their assistant in SEM and TEM characerizations. Many thanks also go to Mr. Simon LeDemnat in nanoplatform for AFM tests.

Another half of my work was carried out in the Lab of Biomimetic Self-assembly Interfaces and Nano-Biomedical Materials at Zhejiang University. I thank all the members in the lab for their cooperation and helpful discussion. I would particularly thank Prof. Jiacong Shen, who is also my advisor, for his profound knowledge, rigorous attitude for research and great care and concern for students. I also thank Prof. Kefeng Ren for his kind suggestions.

During the three years, I had the chance to develop real friendship in the lab. I owe my deepest gratitude to Uyen, Claire, Raphael, Fabien, Laure, Flora, Varvara, Ofelia, Thomas.

Thank you for all that you gave me. Thank you for your support in working for thesis, for the very crowded memories of life in the lab and for your friendship.

I would like to show my gratitude to the financial support from French government through an “Eiffel Doctorate” fellowship, the Rhône-Alpes region through a CMIRA fellowship, and the French Embassy in China through a “France-China co-trained doctorate” scholarship.

Finally, I am indebted to my parents and my husband for their continuous support and encouragement.

Table of content

List of abbreviations

Polymers

ALG: Alginate
CHI: Chitosan
DNA: Deoxyribonucleic acid
DXS: Dextran sulfate
HA: Hyaluronic acid (Hyaluronan)
HEP: Heparin
LPEI: Linear poly(ethylene imine)
PAA: Poly(acrylic acid)
PAH: Poly(allylamine hydrochloride)
PAMAM: Polyamidoamine dendrimer
PAMPS: Poly(acrylamidosulfonic acid)
PDAC: Poly(diallyldimethylammonium chloride)
PDDA: Poly(diallyldimethylammonium chloride)
PEI: Poly(ethylene imine)
PET: Poly(ethylene terephthalate)
PEG: Poly(ethylene glycol)
PGA: Poly(L-glutamic acid)
PLA: Poly(lactic acid)
PLL: Poly(L-lysine)
PSS: Poly(styrene sulfonate)
PVPON: Poly(vinylpyrrolidone)
PVTAC: Poly(4-vinylbenzyltrimethylammonium chloride)
PVA: Poly(vinyl acetate)
PXV: Polyhexylviologen
RNA: Ribonucleic Acid

Other chemicals

EDC: 1-Ethyl-3-(3-dimethylaminopropyl) carbodiimide
FITC: Fluoresceinisothiocyanate
S-NHS: N-hydroxysulfosuccinimide
SWNT: Single wall carbon nanotube
HEPES: 4-(2-Hydroxyethyl)-1-piperazineethanesulfonic acid
MTM: Montmorillonite platelets
MWNT: Multiwall carbon nanotube
PBS: Phosphate Buffered Saline
Rho/Rhod: Rhodamine
rhBMP-2: Human recombinant bone mophogenic protein 2
TAT: Trans-activating transcriptional factor peptide
TR: Texas red
VEGF: Vascular endothelial growth factor

Techniques

AFM: Atomic force microscopy
ATR: Attenuated total reflectance
CLSM: Confocal laser scanning microscopy
CVD: Chemical vapor deposition
FRAP: Fluorescence recovery after photobleaching
FRAPP: Fluorescence recovery after patterned photobleaching
FTIR: Fourier transform infrared spectroscopy
ICP-MS: Inductively coupled plasma mass spectrometry
OWLS: Optical waveguide lightmode spectroscopy
QCM-D: Quartz crystal microbalance with dissipation monitoring
SEM: Scanning electron microscopy
TEM: Transmission electron microscopy
XPS: X-ray photoelectron spectroscopy

Chapter 1 Introductions

1.1 Layer-by-layer self-assembly

Living bodies are the products of millions of years of evolution and their biological functions are realized through the weak interactions between a large number of macromolecules, such as proteins, nucleic acids, lipids…The realization of biological functions is largely dependent on the spontaneously formed complex and ordered structures (Zhang et al. 1999; Shen et al. 2000). Single molecules are not able to demonstrate such function and bioactivity. Supramolecular self-assembly has been developed based on the principles of nature, that employs advantageously molecular self-assembly and self-organization. It refers to the building blocks that spontaneously form ordered structures in the absence of human intervention. It is based on the large possibility of weak interactions between molecules, including electrostatic interactions, van der Waals forces, hydrogen bonds, hydrophobic interactions, coordination bonds… (Lehn et al. 1995)

Based on molecular self-assembly and self-organization, several techniques have been developed to design thin films at the molecular level, including Langmuir blodgett (LB) (Blodgett et al. 1937) and Self-assembled monolayers (SAM) (Bigelow et al. 1946). A LB film can be defined as one or more monolayers of molecules deposited from a liquid surface onto a solid substrate by dipping the substrate through a floating monolayer at a constant molecular density, and a SAM is an organized layer of amphiphilic molecules in which one end of the molecule, the “head group”, shows a specific, reversible affinity for a substrate. Both of the techniques showe great advantage in precisely controlling film structure and thickness, but their limitations are obvious. The most problematic are probably the poor stability and high cost of LB films, and the need for the presence of thiols on the molecules and only for noble metals and silane substrates in order to deposit SAMs. Therefore, much easier and more versatile deposit methods are needed.

Firstly discovered by Iler in 1966 (Iler 1966) and then further developed by Decher, Moehwald and Lvov in early 90s’ (Decher et al. 1991; Lvov et al. 1993; Decher 1997), the layer-by-layer (LbL) self-assembly technique aims to assemble multiple layers of polyelectrolytes at a solid/liquid interface in a very simple manner. The principle is mostly based on ionic interactions. As shown in **Figure 1.1**, the substrate with positive surface

charges was placed in a polyanion solution to deposit a layer of polyanion on the surface and render the surface negatively charged (1). Then, the substrate was rinsed in water to remove the loosely bond polyanion (2). After that, the substrate was immersed into a polycation solution to form a new layer of polycation (3) followed by a second rinse (4). Multilayered film was achieved by repeating the above four steps. Within the past two decades, the technique has expanded and there are now experimental proofs that the driving force for layer-by-layer self-assembly can be of various type, including electrostatic interaction (where the entropy gain due to the release of counterions was proved to be the main reason (Bucur et al. 2006; Klitzing 2006)), hydrogen bonding (Stockton et al. 1997; Sukhishvili et al. 2002), molecular recognitions (Muller et al. 1993), covalent bonding (Chen et al. 1999; Gill et al. 2010), coordinate bonding (Yang et al. 1993), and host-guest interactions (Crespo-Biel et al. 2005). The technique can be used to prepare thin coatings in the nanometer to hundreds of nanometer range and event extent to form micrometer (or even more) thick coatings. It presents very interesting advantages: (i) it is easy to perform and needs only mild conditions; (ii) films can be formed on any kind of substrates independent of their shape and size (Crisp et al. 2003); (iii) it can incorporate a large range of charged as well as uncharged polymers, or other small molecules as building blocks; and (iv) the physico-chemical properties of the formed film can be precisely controlled. All these advantages render this technique very interesting and popular in various fields of applications, including optics (Shimomura et al. 2010), energy (Lutkenhaus et al. 2007), biosensors (Tang et al. 2006; Iost et al. 2011; Lakard et al. 2011), surface modification of biomaterials (Leguen et al. 2007; Boudou et al. 2010), controlled drug release (Schneider et al. 2009; Sun et al. 2009; Delcea et al. 2011), separation (Bolto et al. 2011), tissue engineering (Mjahed et al. 2008; Grossin et al. 2009) and so on.

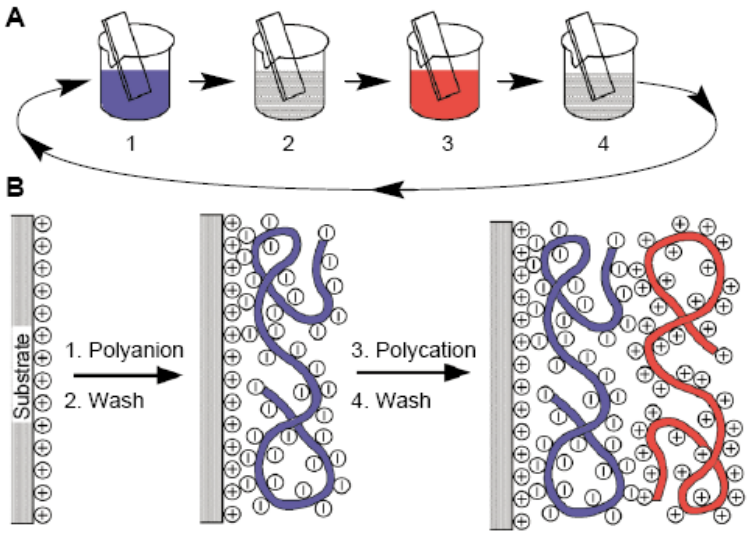

Figure 1.1 Scheme of the assembly of a layer-by-layer film onto a positively charged substrate. (Reproduced from (Decher 1997)).

1.1.1 Linear versus exponential growth mode

The entropy gain due to the release of the counterions was shown to play an important role in the film buildup for electrostatic layer-by-layer assemblies (Bucur et al. 2006; Klitzing 2006). It provides the driving force for the next layer deposition, and ensures the self-assembly can go on and on. Usually, charge overcompensation on the multilayer film surface occurred during polyelectrolyte deposit steps. Zeta potential measurements have shown that the charge is reversed after the deposition of each successive layer (Decher et al. 1994; Caruso et al. 1999).

For a large number of polyelectrolyte pairs, the amount of polyelectrolyte adsorbed onto the surface is the same for each step. That is to say, the mass or thickness of the film grows linearly as a function of the number of deposited layers (**Figure 1.2**). This is the so-called "linear growth mode" of the films. Many polyelectrolyte systems based on the strong polyelectrolytes and most of the weak polyelectrolytes follow the linear growth mode. The most common examples are (Poly(styrene sulfonate)/Poly(allylamine hydrochloride), PSS/PAH) (Decher et al. 1991; Caruso et al. 1997) and (Poly(acrylic acid)/PAH, PAA/PAH) (Yoo et al. 1998) systems (**Figure 1.2)**. The thickness of a single layer pair can range from several angstrom to several nanometers (Decher et al. 2003). Although linearly growing films with thickness increments of 50-200 nm per layer have also been observed due to brush-like polymer conformations(Zhang et al. 2003), this kind of phenomenon is quite rare.

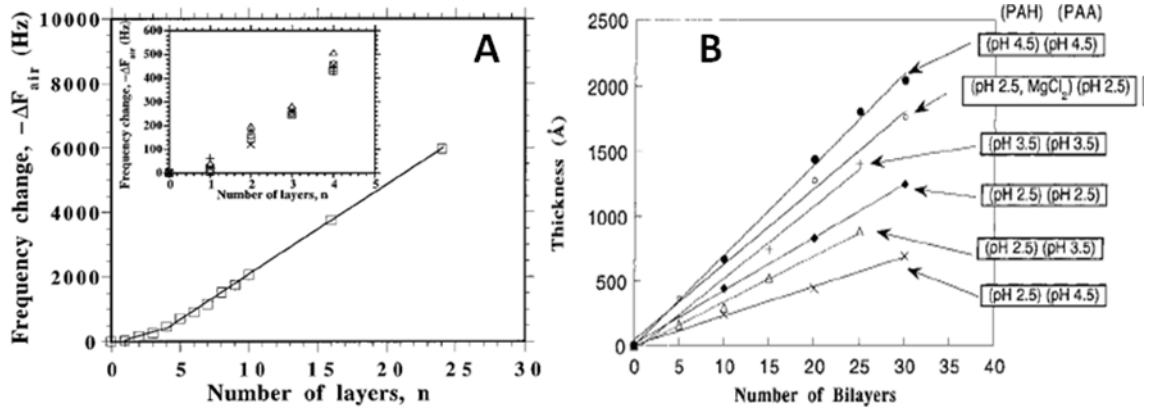

Figure 1.2 (A) Quartz crystal microbalance (QCM) data for $(PSS/PAH)_i$ film growth (Reproduced from (Caruso et al. 1997)) (*i* being the number of layer pairs) and (B) thickness of $(PAH/PAA)_i$ film measured by ellipsometry for films built at different pH (Reproduced from (Yoo et al. 1998)). These films follow a linear growth mode.

Few years later, another kind of layer-by-layer growth mode was evidenced, where the film mass and thickness grow exponentially with the number of deposited layers. This growth mode was first evidenced for films made of polysaccharides and polypeptides by Hubbell and co-workers, who studies (Poly(L-lysine)/Alginate, PLL/ALG) films (Elbert et al. 1999). Voegel and co-workers observed a similar behavior for (PLL/Hyaluronan, PLL/HA) films (Picart et al. 2001). **Figure 1.3** shows the growth of these two polyelectrolyte multilayer films followed either by ellipsometry or by quartz crystal microbalance with dissipation monitoring (QCM-D).

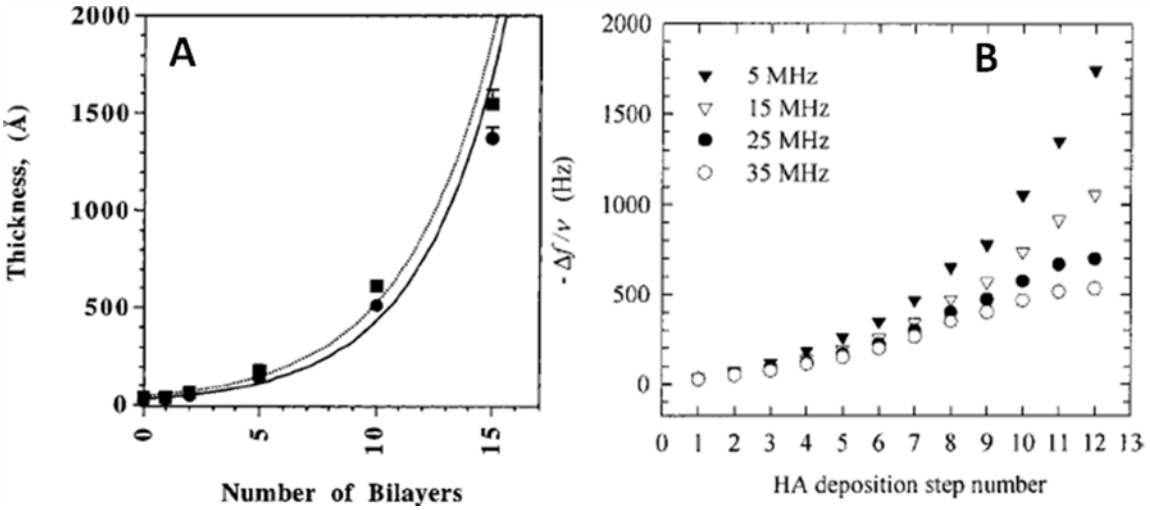

Figure 1.3 (A) Dry thickness of (PLL/ALG) films measured by ellipsometry as a function of the number of layer pairs (Reproduced from (Elbert et al. 1999)); (B) QCM data for (PLL/HA) film growth (Reproduced from (Picart et al. 2001)). These films follow an exponential growth mode.

Two main mechanisms have been proposed to explain this unusual exponential growth, which had indeed been also observed for (PSS/PAH) films (Ruths et al. 2000) and for (PSS/PDDA) films (McAloney et al. 2001) when the salt concentration in the deposit solutions was increased. The first mechanism of exponential growth is related to the roughness of the film, which increased when the number of deposited layers increased. With this increased roughness, the effective surface area for subsequent polyelectrolyte adsoption was higher. Thus, the adsorbed mass would also increase and finally lead to a super-linear growth. This explanation is plausible in some cases, where surface roughness was effectively shown to be increased. However, it could not be valid for most polypeptides and polysaccharides films, as their surface roughness tended, instead, to decrease when the number of layer pairs was increased (Picart et al. 2001). For (PLL/HA) films, it increased only in the first 8 layer pairs. In fact, these films grow by the progressive coalescence of droplets of polyelectrolytes deposited on the surface.

Another mechanism had thus to be proposed. The diffusion of the polypeptide PLL was anticipated from optical waveguide spectroscopy measurements (OWLS) (Picart et al. 2001) and was visualized by confocal laser scanning microscopy (CLSM) using a fluorescently labeled PLL (Picart et al. 2002; Lavalle et al. 2004) (**Figure 1.4**). In (PLL/HA) films, when the 19th PLL layer was replaced with PLL^{FITC} (Fluorescein isothiocyanate, green label) and 19th HA layer was replaced by HA^{TR} (Texas red, red label), the green color distributed throughout the whole film thickness while the red color was restricted in the place where HA^{TR} was deposited. These results clearly demonstrated that PLL chains can diffuse "in" and "out" of the film but HA chains did not in this condition.

In fact, various types of molecules, such as PLL and Poly(L-glutamic acid) (PGA) as polypeptides (Picart et al. 2002; Lavalle et al. 2004), chitosan (CHI) as polysaccharide (Richert et al. 2004) and some synthetic polyelectrolytes such as poly(ethylene imine) (PEI) (Zacharia et al. 2007) can diffuse "in" and "out" of the film. In this case, these polyelectrolytes can diffuse in the film during the deposition step and can partially diffuse out of it during the deposition step of the next layer, by interaction with the incoming polyelectrolyte.

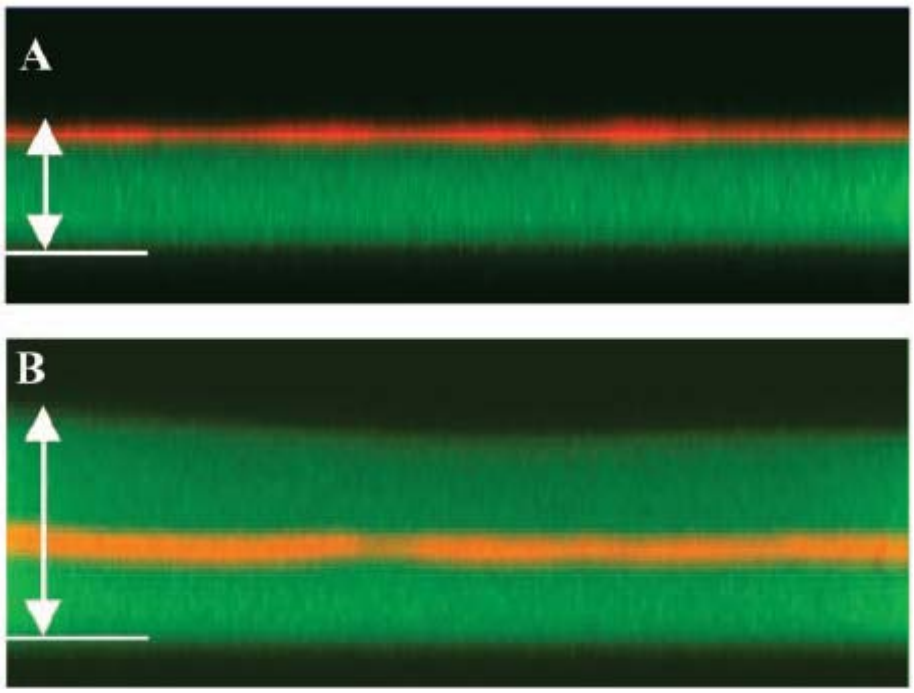

Figure 1.4 Vertical sections through different film architectures containing labeled polyelectrolytes (HA^{TR}, red; PLL^{FITC}, green) obtained from CLSM observations. The borosilicate substrate (bottom of the chamber) is indicated with a white line. (A) $(PLL/HA)_{19}$-PLL multilayer containing two labeled layers, PLL_{19}^{FITC} and HA_{19}-TR. The image size is 26.2 µm × 8.4 µm. Green fluorescence (corresponding to PLL^{FITC}) is visible over a total thickness of around 4 µm (white arrow). (B) $(PLL/HA)_{25}$ multilayer containing two labeled layers, PLL_{19}^{FITC} and HA_{19}^{TR}. The image size is 36.6 µm × 14.4 µm. Green fluorescence is visible over a total thickness of around 8.0 µm (white arrow). (Reproduced from (Picart et al. 2002))

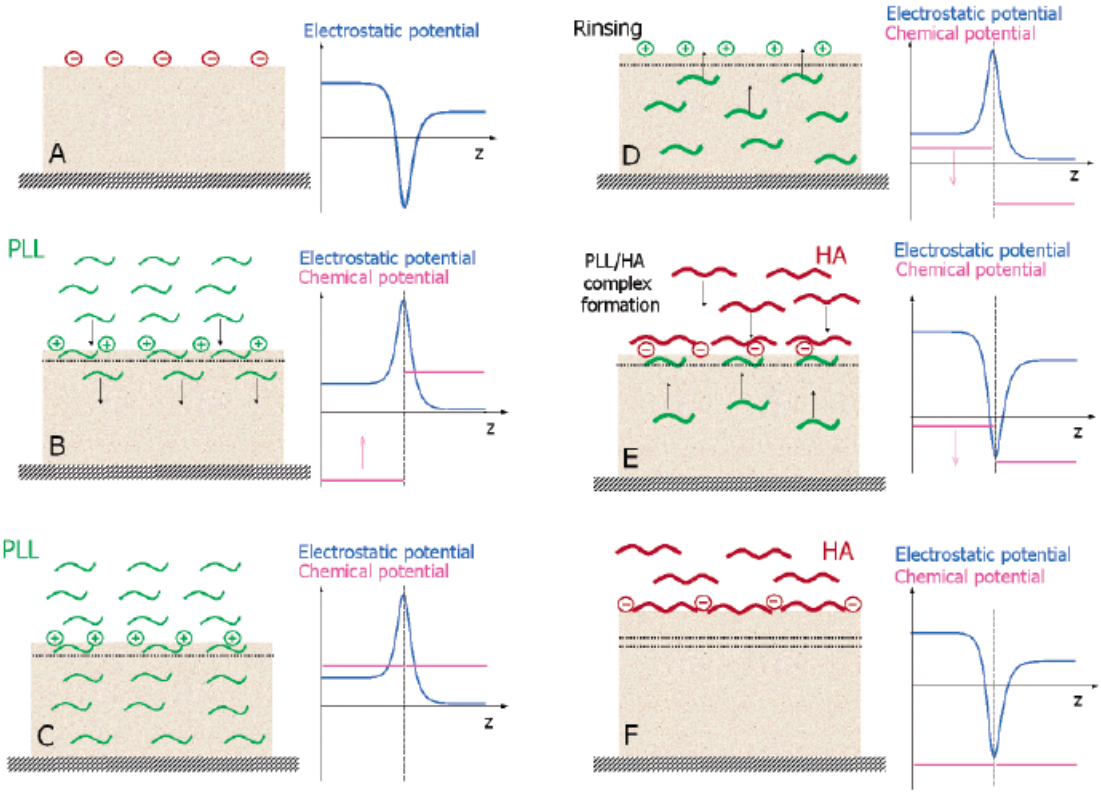

Figure 1.5 Proposed scheme for the buildup mechanism of a (PLL/HA) film. (A) At the end of a HA deposition step, the top of the film has a negative electrostatic potential. (B) PLL interaction with the surface renders it positive; PLL chains can cross the energy barrier and diffuse into the film. As they diffuse into the film, the chemical potential of free PLL chains increases and (C) diffusion stops when the chemical potential of the free PLL chains in the film is equal to that of the PLL chains in the solution. (D) During the rinsing phase with pure buffer, the free PLL chains can cross the electrostatic energy barrier in the reverse direction and diffuse out of the film. During this process, the chemical potential of these chains decreases as well. (E) When this film is further brought in contact with a HA solution, HA chains interact with the outer PLL layer to form PLL/HA complexes, which form the new outer layer of the film. The positive electrostatic barrier totally disappears. The remaining free PLL chains can thus diffuse out of the film. (F) The diffusion process stops when all the free PLL chains inside of the film have diffused out of it. (Reproduced from (Richert et al. 2004))

The proposed mechanism of diffusion is recapitulated in **Figure 1.5** (Richert et al. 2004). For a HA-ending films (**Figure 1.5A**), the surface charge is negative and the electrostatic potential is also negative. When the film is put in contact with PLL solution, PLL molecules firstly interact with the HA on surface (**Figure 1.5B**) and turn the surface electrostatic potential to be positive. Then, the PLL molecules diffuse into the "bulk" of the film until the equilibrium of the chemical potential is reached (**Figure 1.5C**). The diffusion of PLL is concentration dependent and some PLL molecules that have diffused into the film remain as "free" PLL chains. After the rinsing step (**Figure 1.5D**), the loosely-bound PLL are removed and part of the "free" PLL diffuse out. When the film is immersed in the HA solution, free PLL molecules complex with the incoming HA molecules. The surface electrostatic potential becomes negative (**Figure 1.5E**). On the next deposit cycle, as the film is thicker, more PLL molecules can diffuse in the film and more HA can subsequently be deposited. Polyelectrolyte

diffusivity and the capacity of the film to act as reservoir are two key parameters for exponentially growing films.

1.1.2 Quantification of diffusion and effect of physico-chemical parameters

Recently, the exponential growth mechanism has seen significant developments. Quantification of the translational diffusion coefficients has been obtained based on fluorescence recovery after photo-bleaching (FRAP) (Picart et al. 2005; Nazaran et al. 2007; Crouzier et al. 2009) or after pattern photo-bleaching (FRAPP) measurements (Jourdainne et al. 2008). In FRAP measurements, CLSM was used to photo-bleach a circular area of several tens of µm on the film and to record the evolution of the fluorescence profile along a diameter of the bleached zone during a certain time. By assuming that the fluorescent molecules exhibit a Brownian motion, the molecular diffusion coefficient can be calculated. The FRAPP technique allows to detect more precisely different diffusion coefficients in case one population of the polyelectrolyte diffuses at a high speed and another population at a lower speed in the same film (Jourdainne et al. 2008).

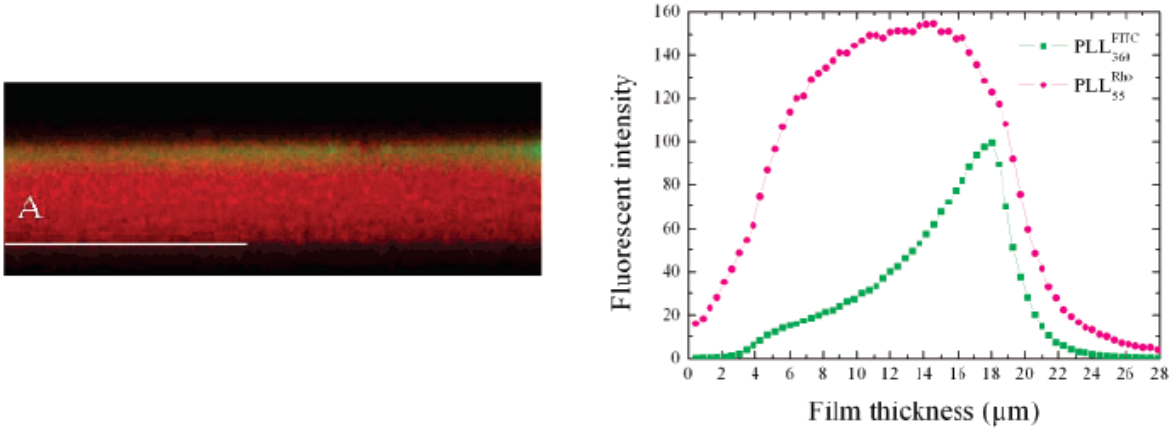

Figure 1.6 CLSM observations of vertical sections of PEI-$(HA_{400}/PLL_{360})_{80}$-$HA_{400}/PLL_{360}^{FITC}$-$HA_{400}/PLL_{55}^{Rho}$ observed 1 hr after the deposition of PLL_{55}^{Rho} with polyelectrolyte solution concentrations of 3×10^{-3} M in monomer units (image size 76.8 µm × 27.9 µm). The white bar indicates the position of the glass slide. The fluorescent intensity profiles for both PLL_{360}^{FITC} and PLL_{55}^{Rho} are given on the right. (Reproduced from (Porcel et al. 2007))

The diffusion coefficient is low for a system that is in a linear growing manner, such as (PSS/PAH), at less than 5×10^{-4} $\mu m^2/s$ (Nazaran et al. 2007). In contrast, the mean diffusion coefficient of PLL in (PLL/HA) films (0.15 M NaCl, neutral pH) that grow exponentially is about three orders of magnitude larger (around 0.2 $\mu m^2/s$) (Picart et al. 2005). Besides the type of polyelectrolyte, molecular structure and conformation of the polyelectrolyte, i.e. linear, branched or star have an impact on diffusion (Zacharia et al. 2007; Choi et al. 2011). Also, molecular weight seems to be another important parameter for controlling chain diffusivity (Porcel et al. 2007; Sun et al. 2007; Zacharia et al. 2007). For instance, Porcel et al. (Porcel et al. 2007) found that the PLL chains with molecular weight of 55 000 Da or smaller could diffuse throughout the whole film thickness (more than 20 μm) in a few minutes, while PLL chains of high molecular weight (360 000 Da) were only found in the top 4 μm of the film even after 1 hr of deposition (**Figure 1.6**).

The diffusivity of the molecules that is capable to diffuse can further be tuned by the environmental conditions, such as pH of the solution, temperature of the experiment and applied voltage. Below are given three examples for each parameter.

pH. Related to the diffusion of a film component is the exchange of polyelectrolytes within the film, when the film is in contact with a solution of a third type of polyelectrolyte. Exchange can be followed by using Fourier transform infrared spectroscopy (FTIR) to trace the specific chemical signature of each polyelectrolyte (Hübsch et al. 2005). Zacharia and co-workers (Zacharia et al. 2007) investigated the interdiffusion and exchange of a series of polyamines with pre-assembled multilayer films. They found that the polyamines at much lower pH (i.e. fully charged or with high ionization degree) in dilute aqueous solutions was unable to diffuse through the multilayer film, whereas increasing the solution pH (i.e. decreasing the ionization of the polyamines) increased the mobility of the polycations, as illustrated in **Figure 1.7**.

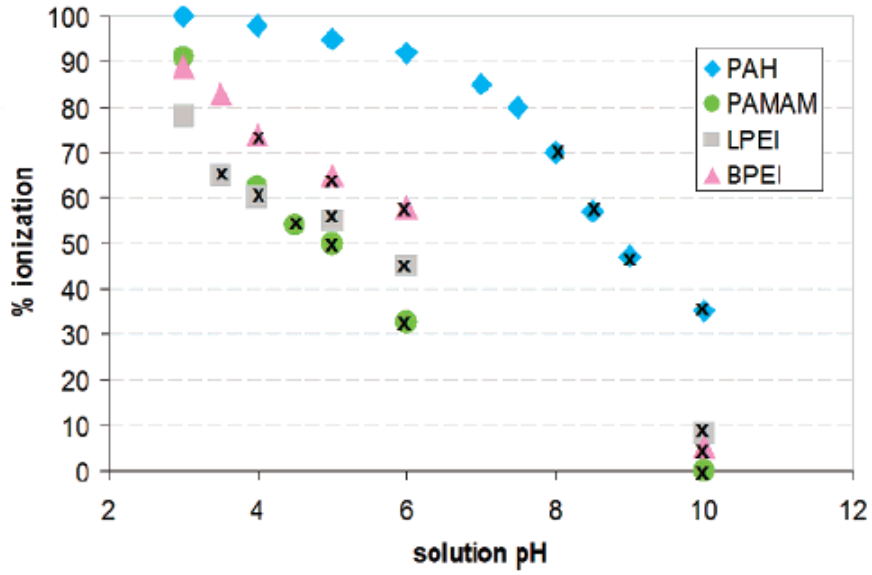

Figure 1.7 Degree of ionization of various polyamines as a function of the solution pH. The conditions of pH where exchange of the polyamine with PXV (in the $(PXV/PAA)_{25}$ multilayer) occurred, are marked by an *x*. For each polycation, there seems to be a degree of ionization above which exchange cannot take place. In the case of PAMAM, the dendrimer, this critical degree of ionization is lower, probably due to PAMAM's geometry and high charge density, which makes it more likely to adsorb to a charged surface. (Reproduced from (Zacharia et al. 2007))

Temperature. As molecular diffusion is energy dependent, increasing temperature can enhance the molecular mobility. Salomaki et al. (Salomaki et al. 2005) demonstrated that (PSS/Poly(diallyldimethylammonium chloride), PSS/PDDA) and (PSS/PAH) films, which grew linearly under room temperature, showed an exponential growth behavior when the temperature was increased (**Figure 1.8**).

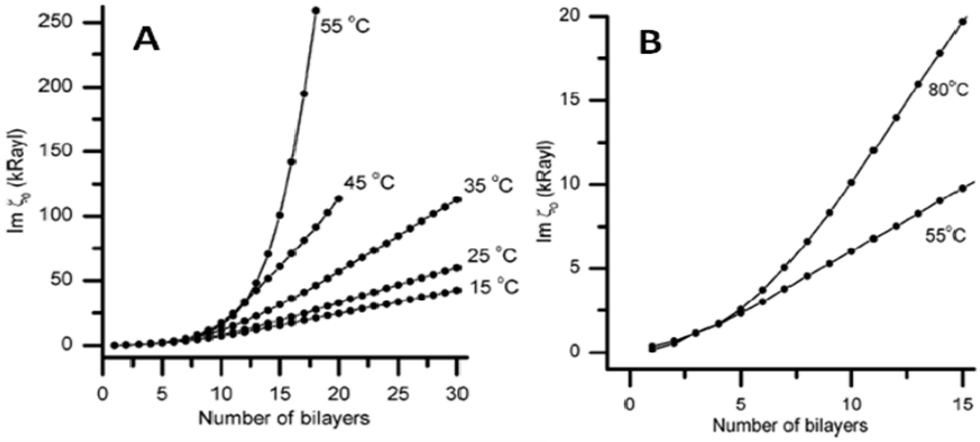

Figure 1.8 (A) (PSS/PDDA) multilayers deposited in 0.1 M NaBr at different temperatures. (B) (PSS/PAH) multilayers deposited in 1 M NaCl at 55 ℃and 80 ℃. (Reproduced from (Salomaki et al. 2005))

Applied voltage. The polyelectrolyte mobility in solution as well as in the films can also be tuned by applying a voltage. Ngankam and Tassel (Ngankam et al. 2005) investigated *in situ* the kinetics of the formation of LbL films under an applied voltage by using OWLS. They found that the PLL deposit amount in (PLL/Dextran sulfate, PLL/DXS) film increased when the applied voltage increased from 0 to 2 V (**Figure 1.9**).

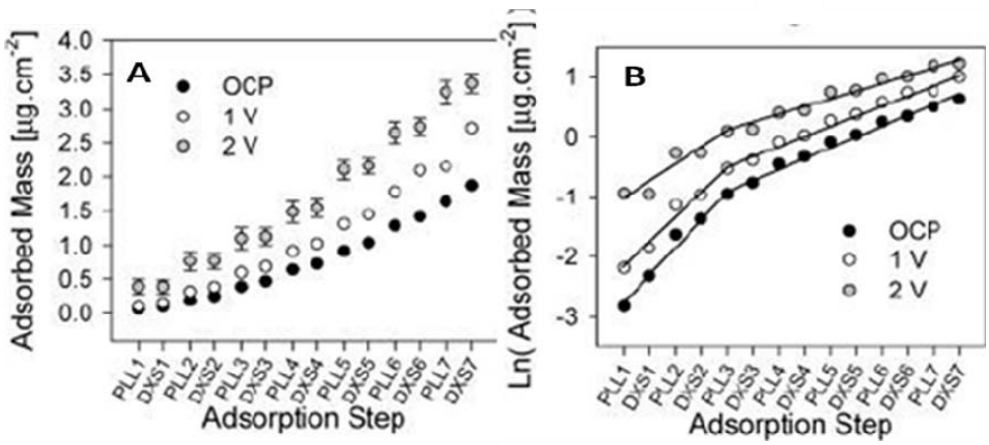

Figure 1.9 (A) Adsorbed mass of polyelectroytes during the buildup of a (PLL/DXS) film, as a function of the adsorption step : at open circuit potential and under voltage. Mass was determined by OWLS. Error bars represent the standard deviation of two measurements. (B) Logarithmic plot of (PLL/DXS) film mass versus adsorption step number (the lines represent best linear fits to data before and after the 5th step). (Reproduced from (Ngankam et al. 2005))

1.1.3 pH effect on layer-by-layer film growth and film morphology

Layer-by-layer assembly can be easily adjusted by changing the deposit conditions or performing a post treatment. Several parameters can have a considerable effect on layer-by-layer film growth as well as on the film structure formed. Two major parameters have been already largely varied and studied by different groups: ionic strength (McAloney et al. 2001; Ren et al. 2005) and pH (Yoo et al. 1998; Mendelsohn et al. 2000). Controlling pH is a powerful tool especially in the case of weak polyelectrolytes and of hydrogen bonded films (Sukhishvili et al. 2002).

For weak polyelectrolytes, the ionization degree as well as molecular conformation is largely dependent on the solution pH. PAA was among the first examples whose ionization degree under different pH was thoroughly studied. Choi and Rubner (Choi et al. 2005) calculated the ionization degree of PAA in solution under different pH by casting PAA films from solutions of PAA at different pH. FTIR spectroscopy was used for this purpose since COOH and COO^- groups have very different signature in FTIR spectrum and their peaks can be quantified.

As shown in **Figure 1.10A**, the pKa of PAA in solution was ~6.5 from FTIR study (Choi et al.

2005), this value being in very good accordance with the results obtained by other groups from titration measurements (Philippova et al. 1997; Bromberg 1998; Petrov et al. 2003). It was also noticed that the pKa of weak polyelectrolytes may change once they were assembled into multilayer films, due to interaction with polyelectrolytes of opposite charge (Fery et al. 2001; Park et al. 2001; Mendelsohn et al. 2003; Choi et al. 2005). For instance, it was found that the ionization degree of PAA in the layer-by-layer films increased compared to the ionization degree of PAA in solution (**Figure 1.10B**).

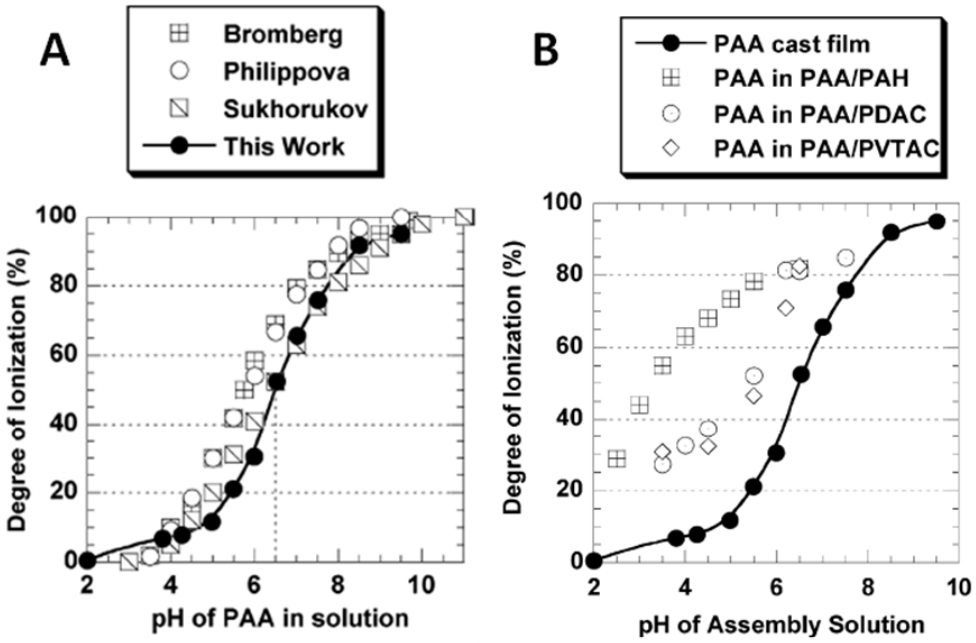

Figure 1.10 (A) Estimated degree of ionization of PAA in solution as a function of pH. Data from other studies are also plotted for comparison. Broken line indicates the pH at which 50% of the PAA units are charged (pH = 6.5). (B) Estimated degree of ionization of PAA within multilayers of (PAA/PAH), (PAA/PDAC), and (PAA/PVTAC) as a function of assembly pH. The degree of ionization of PAA in solution is also plotted for comparison. (Reproduced from (Choi et al. 2005))

pH effect on layer-by-layer film growth. Thus, the pH of the polyelectrolyte solution can have a significant effect on layer-by-layer film growth when weak polyelectrolytes are involved. This was first noticed and extensively studied in (PAA/PAH) films by Rubner and co-workers. Although the films still grow linearly at different pH condition (Yoo et al. 1998), their results evidenced that a small pH change in deposit solution can lead to a significant difference in the thickness of one layer pair (Shiratori et al. 2000). As shown in **Figure 1.11**, the thickness of a "bilayer" increased from less than 20 angstrom to 120 angstrom when the pH of PAH solution changed from 7.5 to 8.5. Over a pH range of 2.5 to 9, the pH of PAA solution seemed to have a predominant effect on film growth. Much larger layer pair thicknesses were obtained when the pH of PAA was lower than 5. At high pH, significant differences only appeared when the pH of PAH was equal or higher than 8.5. There was one exception when both PAA and PAH

were at very high pH of 9, which leaded to a very large thickness increment. This result can be explained by the effect of pH on charge density and molecular conformation of polyelectrolyte in solution (Shiratori et al. 2000; Park et al. 2002). At pH lower than 5, the PAA (pKa = 6.5) molecules were in coiled state with low charge density. Thus, compared to higher pH where PAA molecules were highly or fully charged, more PAA molecules were needed to compensate and reverse the surface charge of the film. Conversely, for PAH molecules (pKa = 9) only changed their conformational state at pH close to or higher than 9. Thus, tuning the pH toward the pKa values of the polyelectrolytes was found to lead to significant changes in the thickness of one layer pair.

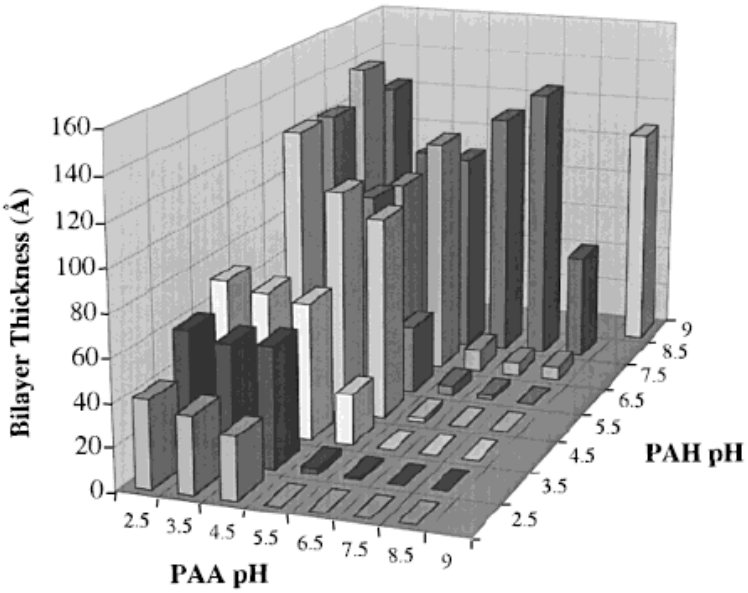

Figure 1.11 Complete pH matrix showing the average incremental thickness contributed by a (PAH/PAA) layer pair as a function of dipping solution pH. (Reproduced from (Shiratori et al. 2000))

The modulation of layer-by-layer assembly by changing the assembly pH of the polyelectrolytes was also observed for exponentially growing films. The initial conditions for building exponentially growing films corresponded to the same pH used for both polyanion and polycation. The pH effect on a typical exponentially growing film (PGA/PLL), in which both polyelectrolytes can diffuse, was studied by Richert and co-workers (Richert et al. 2004).

As shown in **Figure 1.12**, either increasing the deposit pH from 7.4 to 10.4 or decreasing the pH from 7.4 to 4.4 resulted in a considerable acceleration of film growth and the acceleration could be further amplified as the deposit cycles went on due to the exponential growth nature.

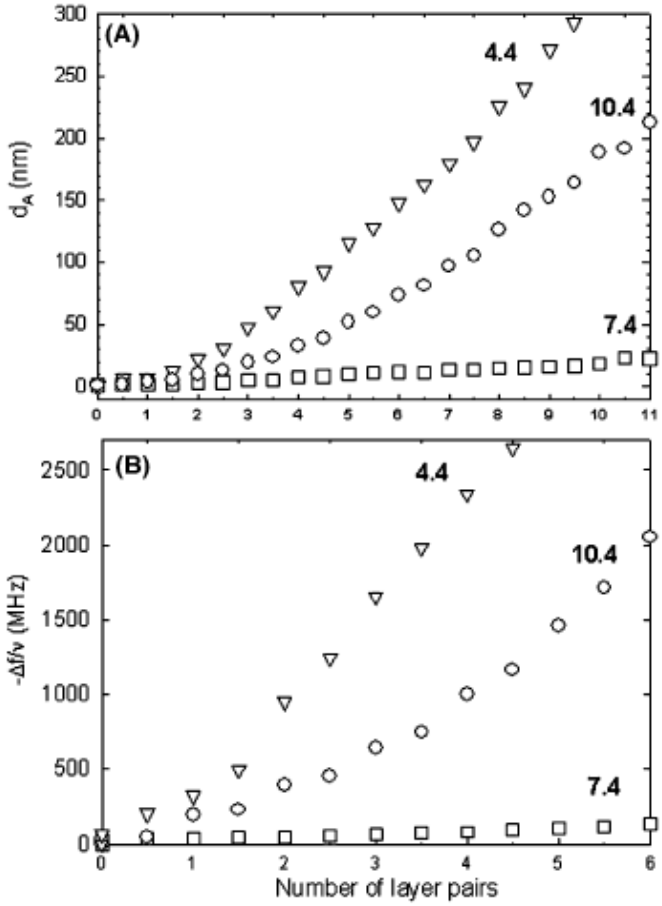

Figure 1.12 (A) Thickness d_A (nm) of PEI-(PGA/PLL)$_i$ films built at pH = 4.4 (△), 7.4 (□) and 10.4 (○) as a function of the number of layer pairs *i* in the film, as measured by the OWLS technique. (B) Frequency shift measured for the same films by QCM-D as a function of *i*. For clarity, only the signal obtained at 15 MHz is represented. (Reproduced from (Richert et al. 2004))

For (Linear poly(ethylene imine)/PAA, LPEI/PAA) films, different phenomena were found. In the pH rang of 3.0 to 5.0 the film growth rate decreased when the deposit pH decreased (Yoo et al. 2008). As illustrated in **Figure 1.13**, the film grew linearly at pH 3.0 and showed very limited exponentially growth at pH 3.5. Above pH 4.0, the exponential growth was predominant and became even more pronounced when the pH increased. This is because LPEI was not able to diffuse under low pH (< 3.5) and its diffusivity increased when the solution pH increased (with a much lower charge density). Here, the importance of molecular diffusivity in exponentially growing film was again evidenced.

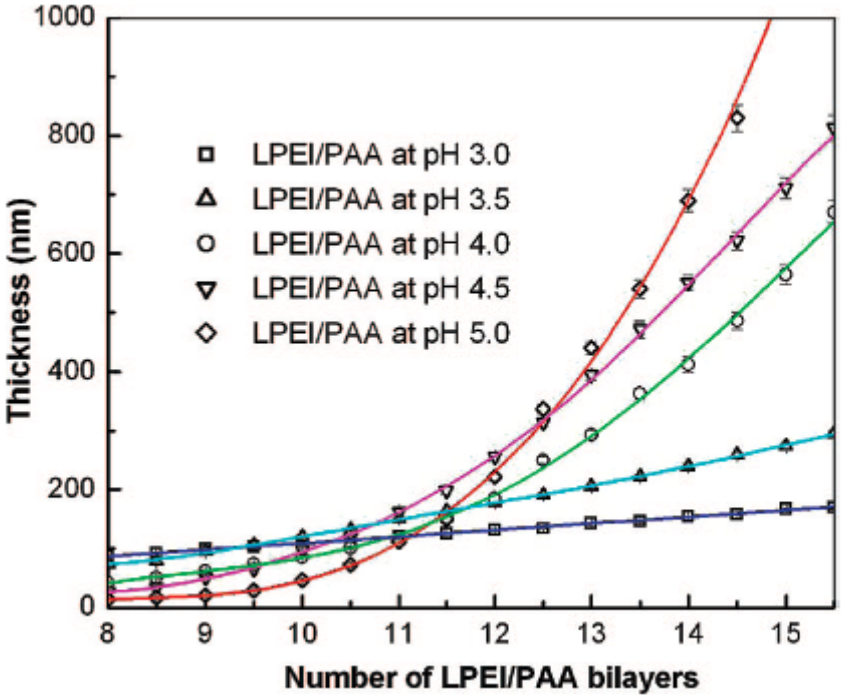

Figure 1.13 Ellipsometric observations of the film thickness growth with increasing the number of deposition in (LPEI/PAA) multilayers at different pH condition ranging from 3.0 to 5.0. Films are linearly growing below pH 3.5. Through the transition period at pH 4.0, films are exponentially growing above pH 4.5. Solid lines are linear fit lines or exponentially fit curves depending on growth characteristics. Error bars indicate standard deviations. (Reproduced from (Yoo et al. 2008))

When a pH shift was introduced into the exponentially growing system, for example (PEI/PAA), a significant different film growth behavior was observed (Fu et al. 2009). To clarify, the notation of $(PAx/PBy)_i$ means the multilayer film was built from polymer-A under pH x and polymer-B under pH of y, and the film is composed of *i* layer pairs.

As demonstrated in **Figure 1.14**, film growth was largely amplified when the pH of PAA was decreased and that of PEI was increased. A film thickness of 3.25 μm for a (PEI/PAA) film made of 7 layer pairs was found. A thickness of 1.5 μm was obtained for the 7^{th} layer pair, in the case where the pH of PAA was 2.85 and that of PEI was 9.0. The fast film buildup can be attributed to the amplified diffusion "in" and "out" of PEI chains throughout the whole film. CLSM evidenced that even in very low pH of 2.85, the PEI chains was still able to diffuse in the film (**Figure 1.15**). The extraordinary diffusivity of PEI chains in pH-amplified (PEI/PAA) system may come from two reasons: (i) the strong ionic attraction and repulsion in the film upon pH change and (ii) the loose bulk structure obtained in such fast buildup film.

The pH-amplified film growth was also found in typical and well studied exponentially growing (PLL/HA) system (Wang et al. 2009). The film growth was incredibly amplified by increasing the PLL deposit pH to 9.5 and lowering the HA deposit pH to 2.9. Of note, when the pH of PLL was even higher than 9.5, unstable film growth can happen.

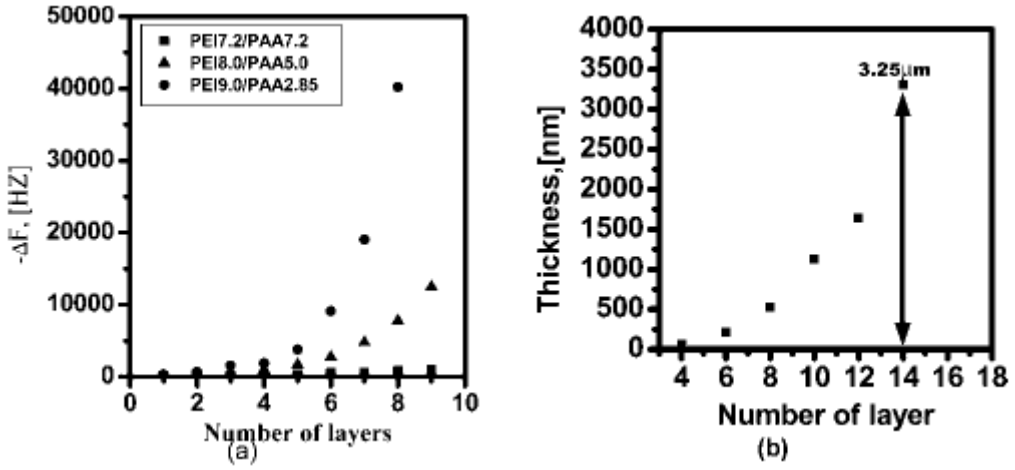

Figure 1.14 (a) QCM frequency shifts of multilayer films assembled at different pH: (PAA7.2/PEI7.2) (■), (PAA5.0/PEI8.0) (▲), and (PAA2.85/PEI9.0) (●). (b) Thickness of the multilayer films prepared at pH pair of (PAA2.85/PEI9.0) as determined by SEM of the film cross sections. (Reproduced from (Fu et al. 2009))

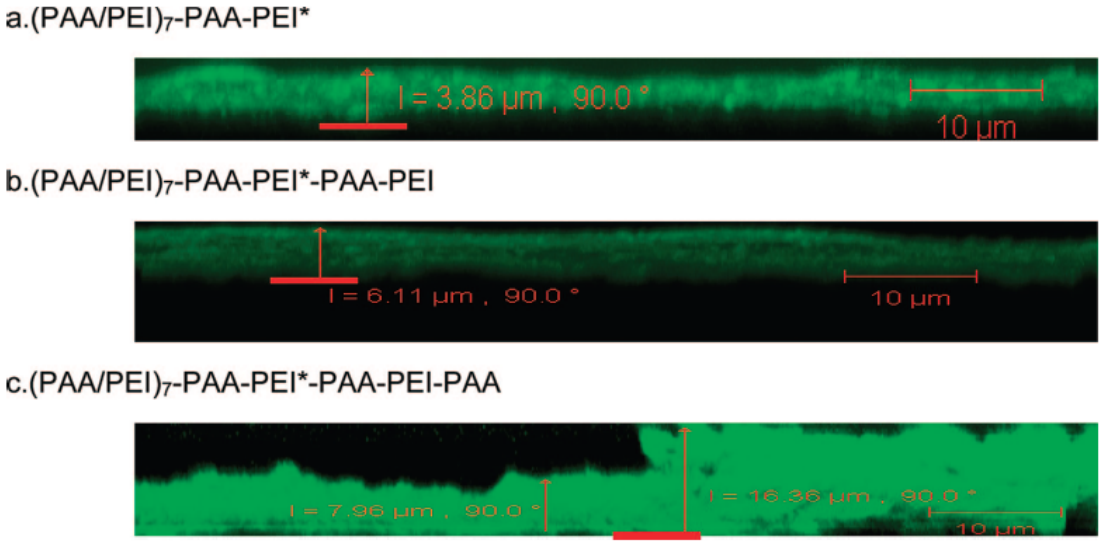

Figure 1.15 Vertical sections through different (PEI9.0/PAA2.85) multilayer films containing PEI^{FITC} obtained from CLSM. For all of the multilayer films, PEI^{FITC} was assembled in 16^{th} layer. PEI* means PEI labeled by FITC. The glass substrate is indicated by the red line. (Reproduced from (Fu et al. 2009))

pH effect on film surface morphology. Morphology and wettability are fundamental properties for solid surfaces as they can have a great impact on the adsorption of protein, adhesion of cells and microorganisms as well as other contaminants. Functional surfaces with special wettability have aroused numerous interests because of their great advantages in various applications (Feng et al. 2002; Hajicharalambous et al. 2009; Detry et al. 2010; Bhushan et al. 2011; Liu et al. 2011). For example, superhydrophobic surfaces with a water contact angle larger than 150° and a sliding angle less than 10° exhibit superexcellent water-repellent properties and known as self-cleaning or anti-adhesive (Feng et al. 2002), while hydrophilic surfaces can absorb water and water soluble moieties easily. Wettability and

surface morphology are related. Roughening the surface can make a hydrophobic surface even more hydrophobic while turning a hydrophilic surface even more hydrophilic (Sun et al. 2004). It was shown that a superhydrophobic surface is a combination of micro-nano hierarchical structures with a coating by a low surface energy compound (Cebeci et al. 2006).

The surface properties of LbL films made of pH-sensitive polyelectrolytes can be modified by post-treatments (Mendelsohn et al. 2000; Fery et al. 2001; Nolte et al. 2007). Techniques to introduce microporosity in polyelectrolyte multilayers based on a low-pH solution treatment were first suggested by Mendelsohn et al. on (PAA/Polyallylamine) film(Mendelsohn et al. 2000). Since then similar techniques were used to induce micro and nanoporosity in a number of films including (PAA/PAH) (Hiller et al. 2002), (PSS/PAH) (Zhai et al. 2004) and (PAA/PEI) (Lutkenhaus et al. 2008) multilayers.

Itano and co-workers (Itano et al. 2005) studied the surface morphology change upon immersion in solutions of different pH of the films containing PAH. **Figure 1.16** displays *in situ* AFM images of (PAH/PSS) films recorded during treatment cycles of pH 2.0 and pH 10.5. The as-prepared dry film was relatively featureless with a low RMS (root mean square) roughness of 1 nm. Upon immersion of the as-prepared film in a pH 10.5 solution, the film morphology and roughness remained essentially unchanged. However, immersion into the first pH 2.0 solution produced a change in morphology towards globular structures with a RMS roughness that was more than an order of magnitude larger than the as-prepared film. Repeated cycling in the pH 2.0 and pH 10.5 solutions shifted the surface between globular morphology with high RMS (at pH 2.0) and wormlike morphology with low RMS (at pH 10.5). Of note, the surface morphology change and its degree as well as the recovery ability also depended on the deposit pH during film buildup.

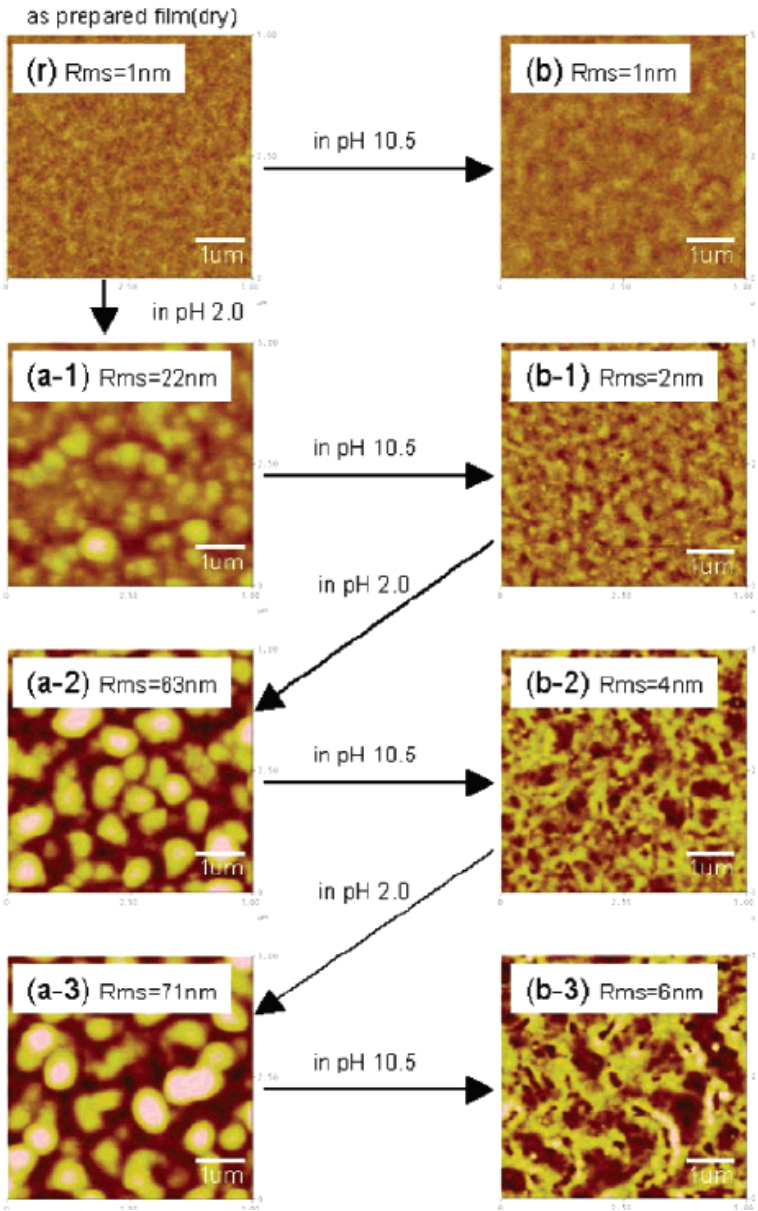

Figure 1.16 *In situ* AFM images of (PAH9.3/PSS9.3) films during treatment cycles of pH 2.0 and pH 10.5: (r) the as prepared film in the dry state, (b) a pH 10.5 immersion of the as-prepared film, (a-1) the first pH 2.0 immersion, (b-1) the first pH 10.5 immersion, (a-2) the second pH 2.0 immersion, (b-2) the second pH 10.5 immersion, (a-3) the third pH 2.0 immersion, and (b-3) the third pH 10.5 immersion. AFM images were recorded 3 min after immersion. All films started with a dry thickness of 50 ± 5 nm. (Reproduced from (Itano et al. 2005))

A more precise study on the morphology change upon post treatment at low pH on (PAH/PAA) films was realized by Sun et al. (Sun et al. 2011). **Figure 1.17** shows a series of SEM images of the film morphology after incubation for 1 hr in aqueous solution at different pH. The film immersed in solution of pH 3.5 kept the original surface morphology. Decreasing the solution pH introduced porosity in the film and the size of the pores decreased from 10 µm to 0.3 µm when the solution pH was even lower. The post treatment of the film in pH 1.5 showed wormlike structures and a considerable decrease in film thickness was noticed. Immersing the film in solution of pH 1.0 was found to erase the film totally from silicon substrate.

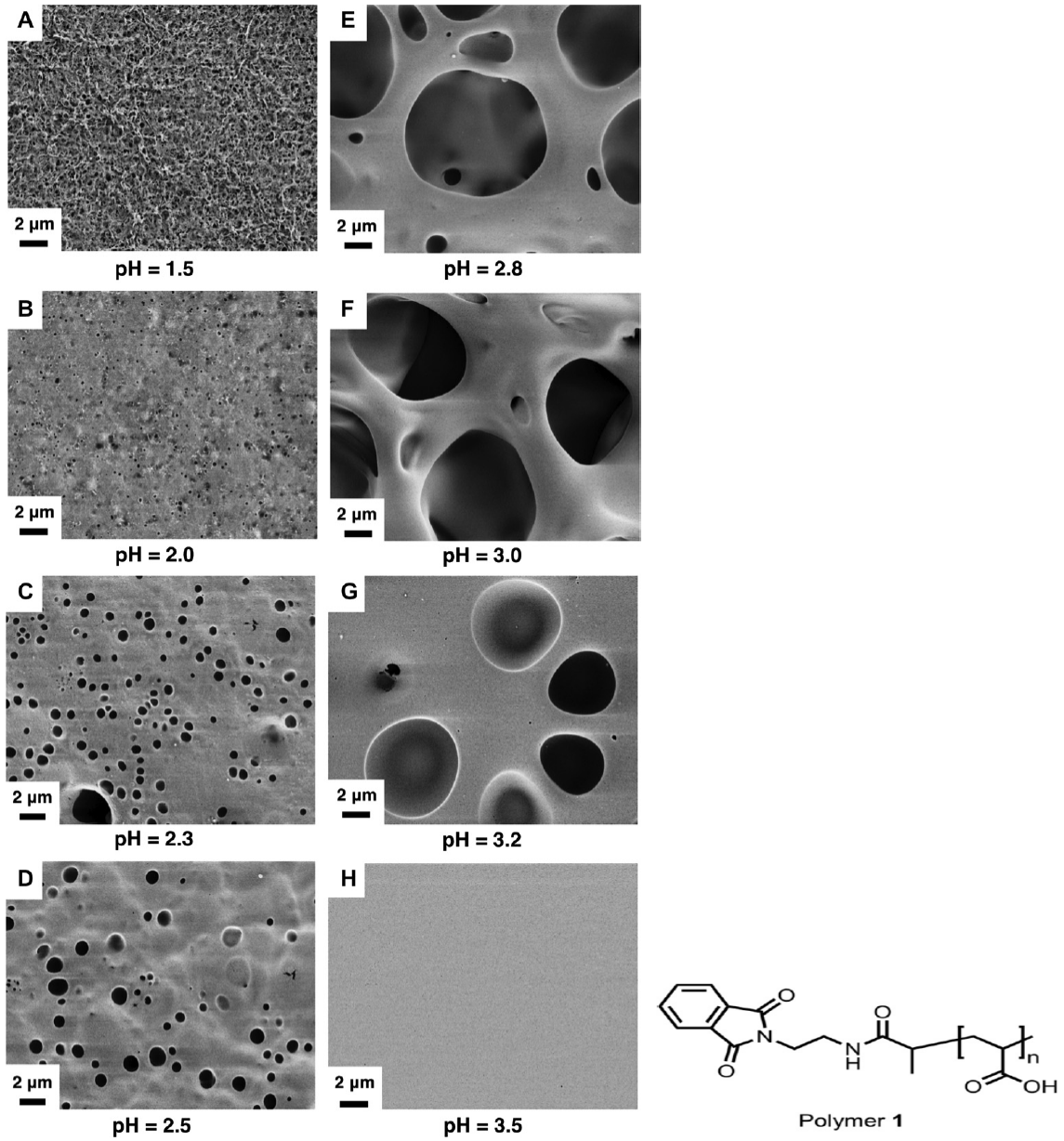

Figure 1.17 SEM images showing top-down views of eight multilayered $(PAH/1)_{20}$ films after immersion in aqueous solutions adjusted to eight different pH values (ranging from 1.0 to 3.5) for 1 hr. (Reproduced from (Sun et al. 2011))

Based on the fact that post low pH treatment can induce micro scale porosity into (PAH/PAA) films, Zhai and co-workers (Zhai et al. 2004; Zhai et al. 2006) constructed stable superhydrophobic films by combining the micro scale porosity with nanoparticle deposition. Firstly, they performed a combination of two low pH treatment (2 hrs in pH 2.7 followed by 4 hrs in pH 2.3) to create a porous surface with the pore size at 440 nm (**Figure 1.18A**). Then they deposited a layer of silica nanoparticles after a thermal cross-linking to obtain micro-nano hierarchical structured surface (**Figure 1.18B**). Finally they coated the surface with low surface energy compound (semifluorinated silane) via chemical vapor deposition and the superhydrophobic surface was successfully fabricated.

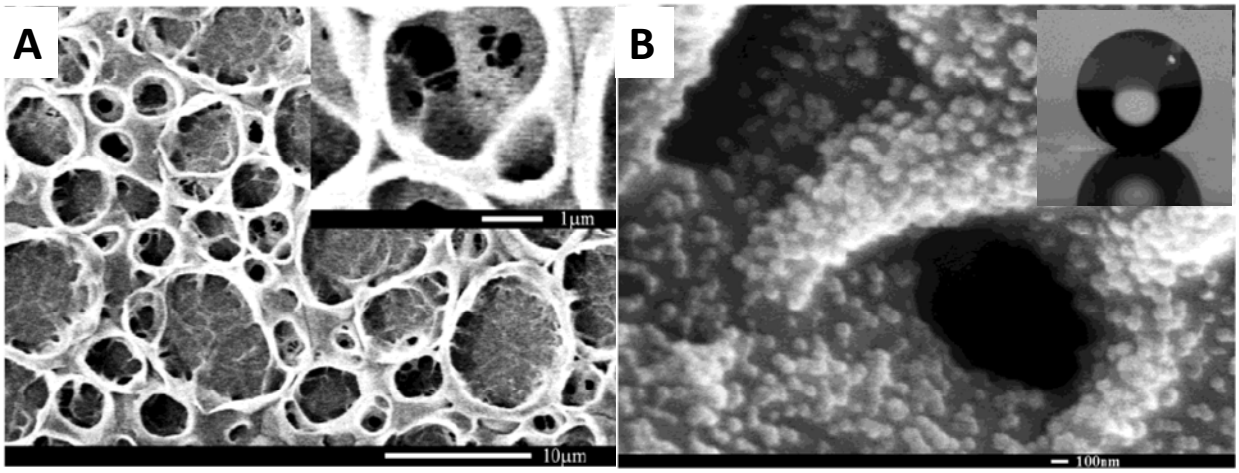

Figure 1.18 SEM images for surface morphology of (A) $(PAH8.5/PAA3.5)_{100.5}$ film after 2 hrs incubation at pH 2.7 and another 4 hrs incubation at pH 2.3 and (B) film in A after silica nanoparticle deposition and low surface energy compound chemical vapor deposition. The insertion in B shows a water droplet on this superhydrophobic surface. (Reproduced from (Zhai et al. 2004))

The surface morphology can also be regulated directly by controlling the deposit pH. In the pH-amplified exponentially growing (PEI/PAA) system, the film surface morphology from different deposit pH were also studied (Fu et al. 2009). As demonstrated in **Figure 1.19**, a progressive increase in the roughness of the films was observed with increasing pH differences of the dipping solutions. Films prepared at pH 7.2 were flat and featureless with a slight granular structure. A more globular structure emerged in the multilayer films prepared from deposit PEI at pH 8.0 and PAA at pH 5.0. More interestingly, by further increasing PEI deposit pH to 9.0 and decreasing PAA pH to 2.85, the obtained multilayer films exhibited hierarchical structures with distinct features on the micro- and nanometer length scales: vermiculate patterns of 500-1500 nm as well as micropores on the order of 10 μm were observed. A magnification of the vermiculate patterns showed nanowrinkles of 100-200 nm. The (PEI9.0/PAA2.85) film with hierarchical structure can be turned to be superhydrophobic after coating with a low surface energy compound. In this case, no nanoparticle deposition was need.

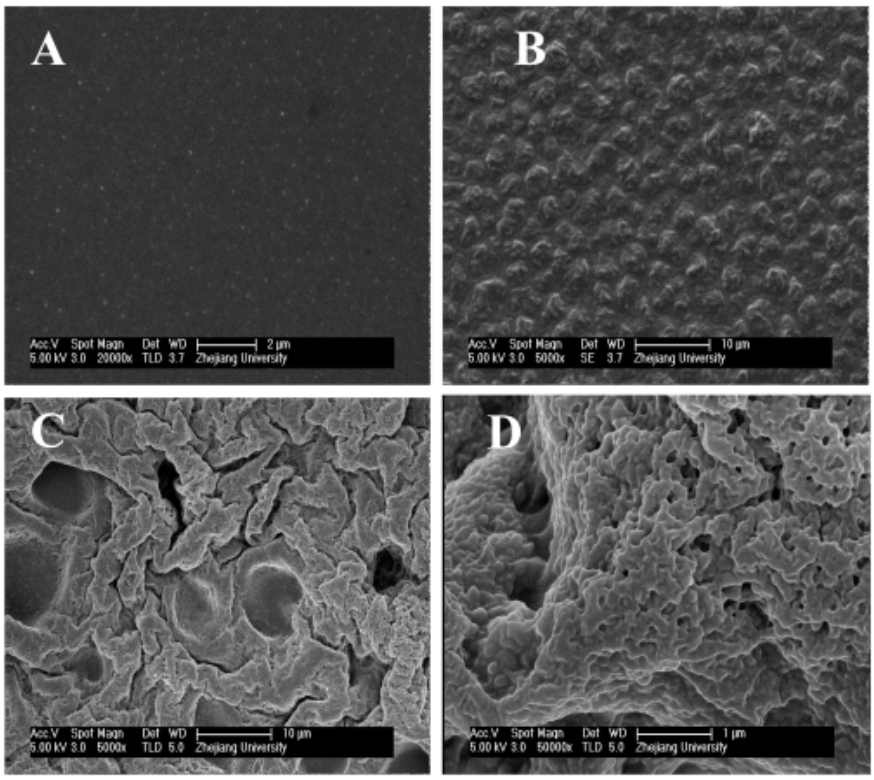

Figure 1.19 SEM images of a (PAA/PEI) films made of 7.5 layer pairs constructed at different pH values: (A) (PAA7.2/PEI7.2), (B) (PAA5.0/PEI8.0), and (C) (PAA2.85/PEI9.0). Image D is an enlargement of image C. (Reproduced from (Fu et al. 2009))

For the same (PEI/PAA) system, more different surface morphologies can be obtained via carefully controlling the deposit pH (Cao et al. 2010). As shown in **Figure 1.20**, when the pH of PAA was kept at 2.89, varying the pH of PEI solution from 5.0, 6.5, 7.5 to 9.0, similar surface structures but with different texture sizes of 600, 1100, 1600 and 2300 nm, respectively, were obtained. These surfaces are mimicking the morphology of the skin of a pilot whale *Globicephala melas*, and were used to study the self-cleaning abilities based on nano-roughness. It was found that the settlement of zoospores of *Ulva* was strongly influenced by the size of the features present on the surfaces. The lowest level of settlement was observed for structures of the order 2 μm, the same size as features on the skin of *Globicephala melas.* The strength of adhesion of settled spores was lowest on the surface with the sub-micrometer-sized features. This may be related to the inability of the adhered spores to thoroughly bind to the entire surface area beneath them.

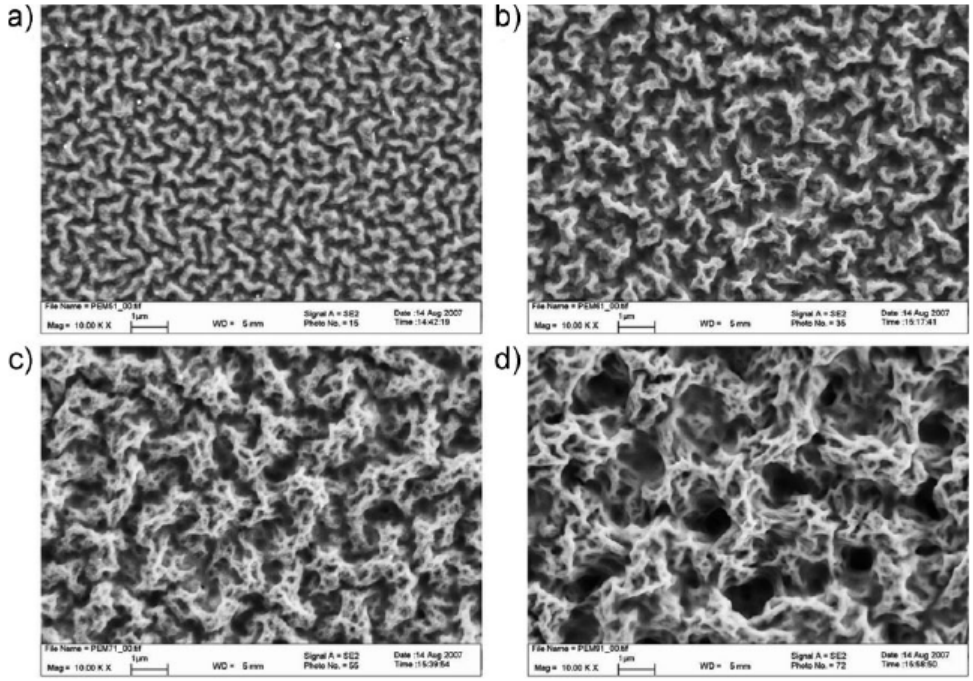

Figure 1.20 SEM topographic images of (PAA/PEI) multilayer films prepared by using polyelectrolyte solutions at different pH values: a) PAA pH 2.89/PEI pH 5.0; b) PAA pH 2.89/PEI pH 6.5; c) PAA pH 2.89/PEI pH 7.5; d) PAA pH 2.89/PEI pH 9.0. (Reproduced from (Cao et al. 2010))

1.1.4 Incorporation of bioactive molecules in exponentially growing film

Compared to linearly growing films, exponentially growing films show very different properties such as fast film buildup and loose film bulk structures. These properties make the exponentially growing film a good candidate for reservoirs to incorporate bioactive molecules (Vodouhe et al. 2006; Volodkin et al. 2011).

Crouzier and Picart (Crouzier et al. 2009) studied the ion pairing in polyelectrolyte multilayer films containing polysaccharide and PLL using QCM-D and attenuated total internal reflectance infrared spectroscopy (ATR-FTIR). Their results showed that the monomer ratio of anion in the polysaccharide over lysine in the obtained films tends to 0.5 as the films buildup went on. Only about half of the amino groups on PLL chains interacted with carboxylate groups from HA chains in (PLL/HA) film. That means that the exponentially growing (PLL/HA) film is a good container (reservoir) for PLL chains as 50% of the PLL chains are incorporated but are free to move, i.e. they are not tightly interacting with HA chains. Thus, the (PLL/HA) film may be a good reservoir for negatively charged ions or polyelectrolytes, thanks to the excess positively charged amine groups that are presented in the film.

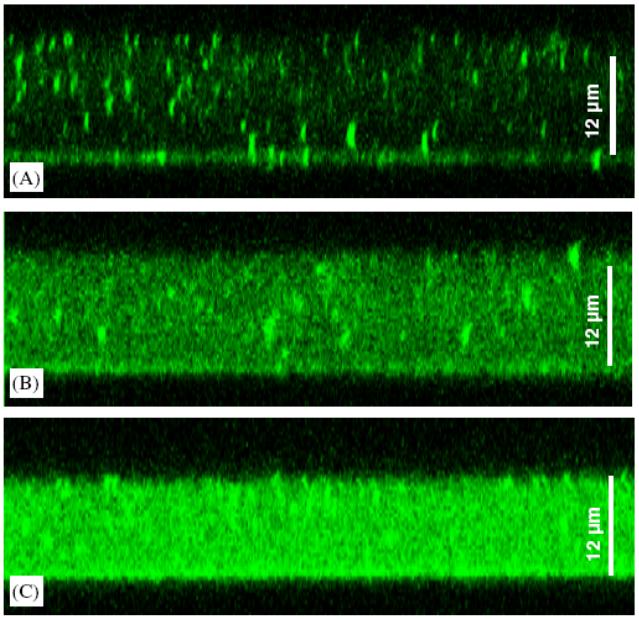

Figure 1.21 CLSM images of $(PLL/HA)_{60}$/paclitaxel$^{Green\ 488}$ film sections. Paclitaxel$^{Green\ 488}$ was adsorbed from solutions at 10 µg mL^{-1} (A), 50 µg mL^{-1} (B) and 200 µg mL^{-1} (C). Image sizes are 76.8×23.9 μm^2. All CLSM settings are identical for the three images. (Reproduced from (Vodouhe et al. 2006))

Indeed, Lavalle and co-workers found that an antiproliferative agent paclitaxel can be loaded in (PLL/HA) films (Vodouhe et al. 2006). As demonstrated in **Figure 1.23**, paclitaxel molecules distributed homogenously throughout the whole film thickness (~ 12 µm). More interestingly, the paclitaxel local concentration in the film can achieve up to 50 times of the concentration in the solution for absorption.

Much bigger molecules such as proteins can also be loaded into (PLL/HA) films. For instance, a growth factor (i.e. a protein) of 27 000 Da, which belongs to the family of Bone morphogenetic proteins (BMP-2), has been loaded into (PLL/HA) films (Crouzier et al. 2009) and in composite films made of (PLL/HA-HEP) (Crouzier et al. 2010). As shown in **Figure 1.22**, thicker film adsorbed more rhBMP-2 molecules than the thinner ones. The overlay of the green and red channels for films containing 12 layer pairs indicated that rhBMP-2 diffused throughout the entire $(PLL/HA)_{12}$ film and thus distributed homogenously in the film containing 12 layer pairs. As for $(PLL/HA)_{24}$ film, rhBMP-2 seemed to accumulate in the upper part of the film with a limited diffusion within the film. Strikingly, the rhBMP-2 local concentration in the film was increased up to 500-fold when compared to its initial solution concentration (Crouzier et al. 2009).

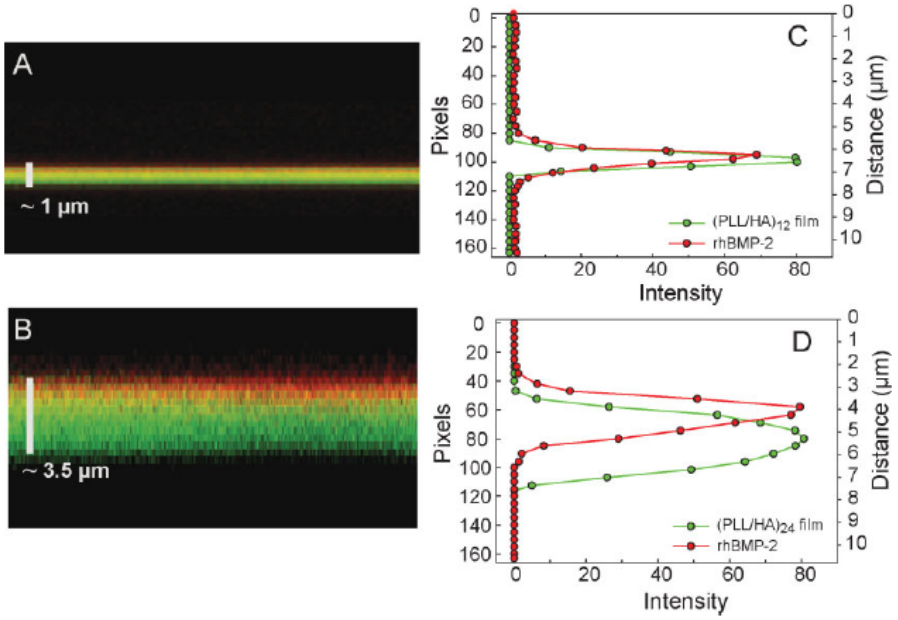

Figure 1.22 (A,B) CLSM observations in HEPES/NaCl buffer (pH 7.4) of cross-linked $(PLL/HA)_i$-PLL^{FITC}-HA multilayer films loaded with rhBMP-2; (A) i=12 and (B) i=24. PLL^{FITC} was used to visualize the whole film and rhBMP-2^{Rhod} was adsorbed at 20 µg mL^{-1} (in 1mM HCl) and rinsed for 7 h in HEPES/NaCl buffer (pH 7.4) before observation. (C,D) The corresponding z-intensity profiles are given along with the film thickness (left y axes) for rhBMP-2^{Rhod} (red) and for PLL^{FITC} (green). (Reproduced from (Crouzier et al. 2009))

The film growth can be further enhanced by introducing a pH shift. For example, increasing the PLL solution pH and decreasing the HA solution pH can largely amplify the (PLL/HA) film growth. A film made of 5 layer pairs of (PLL9.5/HA2.9) can reach a wet thickness of 4 µm (Wang et al. 2009). Trans-activating transcriptional factor peptide (TAT) can diffuse into the whole film and are distributed homogenously in the film. Besides, the pH-amplified (PLL/HA) film showed superiority over traditional (PLL/HA) film (built at neutral pH) in loading of a third part agent, such as TAT. As illustrated in **Figure 1.23**, the $(PLL6.5/HA6.5)_5$ film can load 0.12 µg/cm^2 TAT at pH 6.5 whereas the $(PLL9.5/HA2.9)_5$ film can achieve a loading of 15 µg/cm^2 of TAT in the same conditions. Further increasing the pH of TAT to 9.5 allowed to reach a loading amount of almost 30 µg/cm^2 (Wang et al. 2009).

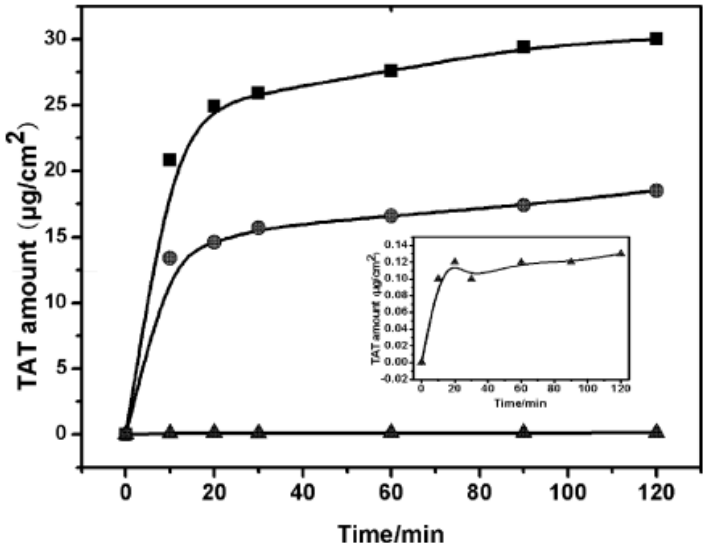

Figure 1.23 Amount of TAT loaded into the films with time: TAT at pH 9.5 loaded into $(PLL9.5/HA2.9)_5$ film (■); TAT at pH 6.5 loaded into $(PLL9.5/HA2.9)_5$ film (●); TAT at pH 6.5 loaded into $(PLL6.5/HA6.5)_5$ multilayer (▲). The inset at bottom right corner also shows TAT at pH6.5 loaded into $(PLL6.5/HA6.5)_5$ multilayer. (Reproduced from (Wang et al. 2009))

Besides post-loading, the bioactive molecules, such DNA (Lvov et al. 1993; Shi et al. 2002), RNA (Recksiedler et al. 2006), vascular endothelial growth factor (VEGF) (Van den Beucken et al. 2007), bone morphogenetic proteins (BMP-2) (Van den Beucken et al. 2006) have also been incorporated into the LbL films by direct assembly. Here again, the pH-amplified LbL assembly showed great advantages not only in achieving a large loading amount but also in realizing a tunable polycation/polyanion ratio. Wang et al. (Wang et al. 2011) investigated the (PLL/DNA) system under pH-amplified buildup condition. DNA is commonly used as a model gene in gene therapy. DNA loading amount and DNA complex size after disassembly from the multilayers are two important factors for gene therapy efficiency. It was proved that by increasing the PLL deposit pH and decreasing the DNA deposit pH, DNA loading amount as high as 121.2 $\mu g/cm^2$ was achieved within a (PLL10.0/DNA4.6) film made of 7.5 layer pairs. Moreover, the N/P ratio in the film can be tuned in a large range thus resulted in tunable DNA complex sizes.

1.2 Free-standing films based on layer-by-layer assembly

A free-standing film made by layer-by-layer assembly is a film that is first made on a supported substrate and subsequently detached from this substrate. Free-standing films usually refer to ultrathin membranes that can sustain their shapes and properties in air or liquid with no or little assistant from their substrates (Mamedov et al. 2000; Jiang et al. 2006).

Ultrathin free-standing film has attracted lots of interests due to its unique properties on glass transition (Mattsson et al. 2000), molecular motion, transport (Huang et al. 2004; Neyertz et al. 2008; Bason et al. 2011) and mechanical properties (Vendamme et al. 2006), as compared to bulk polymer blends or supported films. For example, Forrest et al. established that free-standing poly(styrene) (PS) films exhibit a reduction in their T_g for films thinner than 60 nm (Forrest et al. 1997). Similar phenomena were also found for other polymers, such as Poly(methyl methacrylate), Poly(4-tert-butylstyrene), Poly(α-methylstyrene), and Poly(2-vinylpyridine) (Paeng et al. 2011). The substrate can also have some effect on the molecular motion and glass transition temperature of the supported film (Torres et al. 2000). As shown in **Figure 1.24**, free-standing films showed lower glass transition temperature than the supported films (built on a strong or weak surface energy substrate) when the film thickness was less than 30 nm.

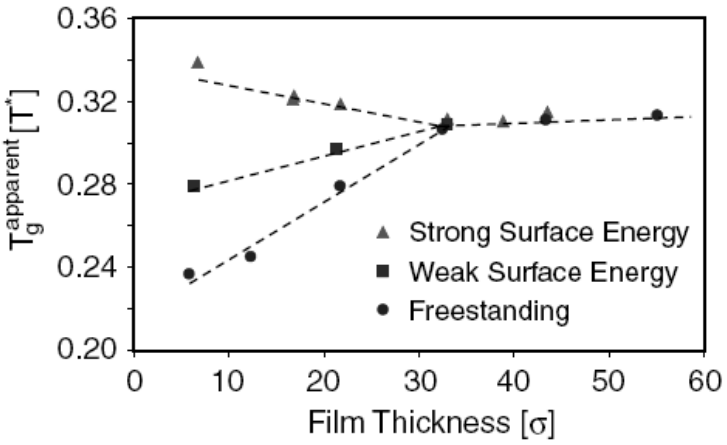

Figure 1.24 Apparent glass transition temperature *vs* film thickness for films built on a strong surface energy (or weak surface energy) substrate, as compared to free-standing films. The estimated uncertainty in simulated T_g's is approximately four times the size of the symbols. (Reproduced from (Torres et al. 2000))

Layer-by-layer assembly has proved itself as a good technique to construct free-standing films (Mamedov et al. 2000; Dubas et al. 2001; Mamedov et al. 2002; Tang et al. 2003; Jiang et al. 2004) as it is a versatile and inexpensive technique. Composite films can be easily prepared by incorporating different kinds of charged and uncharged species, including inorganic nanoparticles. Besides, layer-by-layer film can be built on almost any kind of substrate, which may facilitate the film release after buildup.

Although many techniques have been developed to follow the layer-by-layer film buildup on a supported substrate and to characterize their physico-chemical properties (adsorbed mass, conformation of polyelectrolytes), some parameters such as thermal properties or mechanical properties are easier to measure once the film is detached from the substrate. After forming a

free-standing membrane based on LbL films, Hammond and co-workers (Lutkenhaus et al. 2005; Lutkenhaus et al. 2007) were among the first to carry out differential scanning calorimetry (DSC) and dynamic mechanical analysis (DMA) tests on free-standing films. These films were made of 100 layer pairs, and had a thickness of 8 μm and covered a surface of 4 cm^2, so as to provide films with enough mass and dimension for performing DSC and DMA tests.

1.2.1 Methods to release film from substrate

Getting the films released from the supporting substrate is the key step in fabricating a free-standing film. Several methods to release films from their substrates have been developed until now. Of note, the integrity of the film is quite important for film release. The key point in the release step is that the interaction between molecules in the film should be far stronger than the interaction between the film and the substrate.

Erosion of the substrate. This method has often been used in early studies for preparing TEM samples for layer-by-layer films. Harsh solution or solvent were used. For example, hydrofluoric acid (HF) was always used for silica substrates (Chia et al. 2008) and tetrahydrofuran (THF) was usually used for plastic substrates (Lavalle et al. 2005). As the harsh solution or solvent may destroy the film structure, this method can only be applied to very resistant films. Furthermore, care has to be taken to make sure that the film structure has not been drastically changed after the detachment procedure.

Introduction of a sacrificial layer. In this method, a sacrificial layer is deposited or is cast on the substrate before the layer-by-layer assembly takes place. The films are released by dissolving the sacrificial layer. Cellulose acetate (Mamedov et al. 2000; Tang et al. 2003), which is stable in water and can be dissolved quickly in acetone was often used. pH-responsive multilayer films have also been introduced as a sacrificial layer recently (Ono et al. 2006; Gui et al. 2009). Ono and Decher (Ono et al. 2006) introduced a new strategy to obtain ultrathin free-standing polyelectrolyte multilayer membranes at physiological conditions. As demonstrated in **Figure 1.25**, on the surface of a substrate, a hybrid film structure composed of two compartments, (1) a pH-responsive film segment formed via hydrogen bonds and (2) a polyelectrolyte multilayer film on top of 1, was assembled. Finally, the pH-responsive polymer multilayer segments disintegrated at a neutral pH and the free-standing polyelectrolyte multilayer films was thus released.

Introduction of on-off binding sites. Ma et al. (Ma et al. 2007) found that Cu^{+} ions at pH 2 could break the ionic interaction between PAA and PDDA while reinforcing the interaction between PAA and PAH. Based on this finding, they used $CuCl_2$ solution of pH 2 as the exfoliate solution to get (PAA/PAH) free-standing films when PDDA was deposited as the first layer on the substrate.

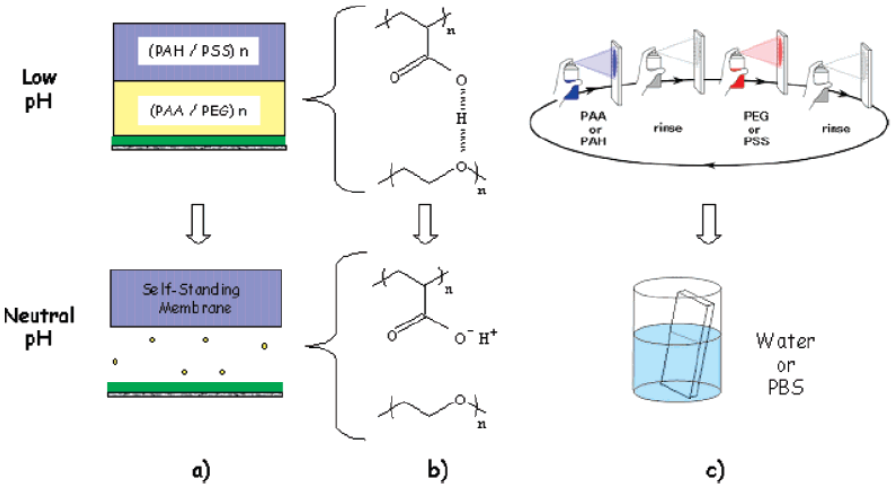

Figure 1.25 Scheme of the principle for preparing free-standing membranes using disintegration of a pH-responsive multilayer film as a sacrificial base. (a) Top: a hybrid structure composed of two components: a pH-responsive multilayer film segment and an electrostatically assembled polyelectrolyte film. Bottom: release of the free-standing membrane (b) pH response of hydrogen bonds between PAA and PEG by dissociation of carboxylic acid (-COOH) groups to carboxylate ions ($-COO^{-}$) of PAA. (c) The layer-by-layer alternating spray depositions of hydrogen donor/acceptor or polycation/polyanion (top) and immersion of the substrates in a solution of neutral pH (bottom). (Reproduced from (Ono et al. 2006))

Using hydrophobic substrate. Hydrophobic substrates like Teflon show poor interactions with the film in dry state, thus the films can be released easily when the films are dried (Lutkenhaus et al. 2005). In case the film is dried after buildup, it is a good way to keep the original properties of the film by peeling it away from hydrophobic substrate directly without any post-processing steps.

Using liquid or gas as template. If the films are built at air/liquid interface (**figure 1.26**), it is possible to get the free-standing film directly after film buildup (suspended in liquid or air). In this case, no substrate removal was needed (Ferri et al. 2005; Ferri et al. 2006).

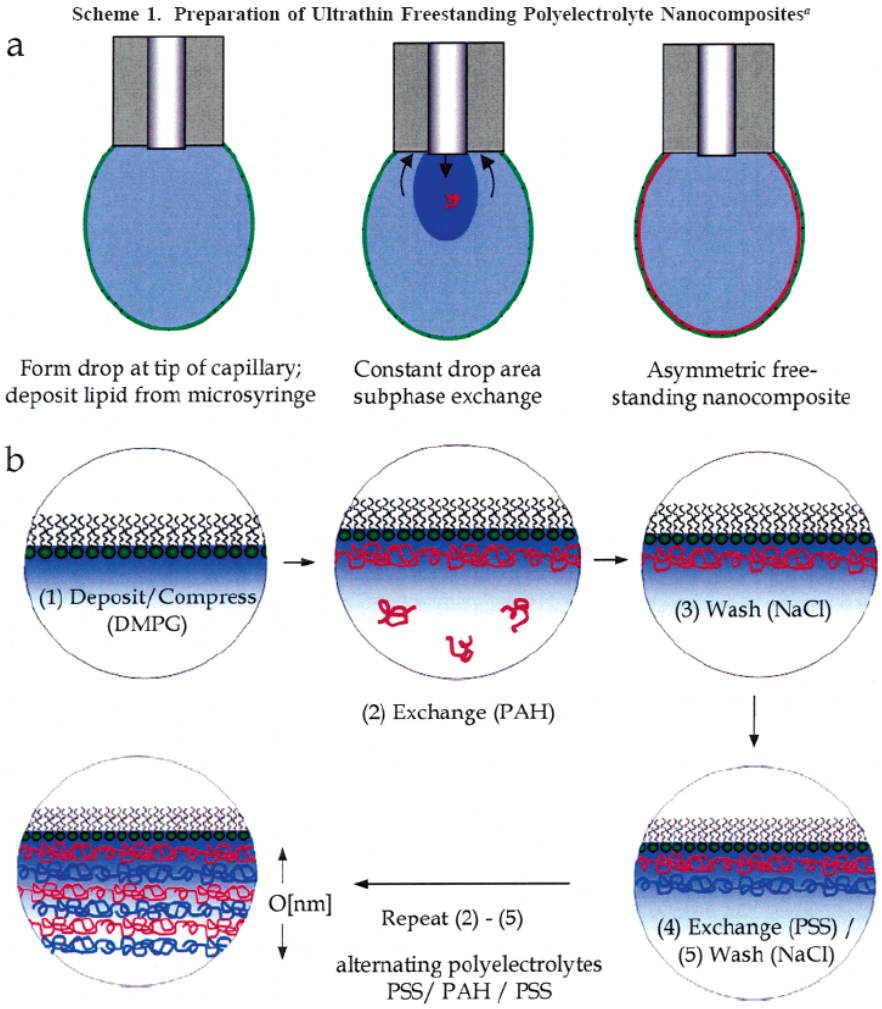

Figure 1.26 Scheme for the preparation of ultrathin freestanding polyelectrolyte nanocomposites: (a) polyelectrolyte adsorption onto a lipid monolayer by subphase exchange in a pendant drop; (b) schematic of the multilayer assembly process at the air-water interface. (Reproduced from (Ferri et al. 2005))

1.2.2 Free-standing films based on polypeptides and polysaccharides

Ultrathin membranes are potentially interesting for applications in wound healing, in arterial repairs and as dermal substitute (Fujie et al. 2009; Okamura et al. 2009; Larkin et al. 2010). For such applications, biocompatibility, biodegradability and bioactivity should be considered. Free-standing films based on polypeptides and/or polysaccharides were constructed in this purpose as these polyelectrolytes are components of natural tissues. They could be used to mimic the properties of these tissues, especially their hydration and softness. The first trial was carried out by Lavalle and co-workers (Lavalle et al. 2005; Bernsmann et al. 2008). The multilayer films consisting of PLL and HA were deposited on glass slides or on polystyrene substrates. Two different methods were applied for detaching the films from the underlying

substrates. For film built on a PS substrate, THF was used to dissolve the polystyrene substrate and lead to a membrane possessing micrometric holes. For films built on a glass substrate and chemically cross-linked by 1-Ethyl-3-(3-dimethylaminopropyl) carbodiimide (EDC) and N-hydroxysulfo-succinimide (sNHS), a dipping step in 0.1 M NaOH solution allowed to detach the film and to produce a non-porous and very smooth membrane (**Figure 1.27**). The free-standing (PLL/HA) film were found to preserve the bioactivity of alkaline phosphatase, which was loaded after film detachment, for at least one week after incorporation (Lavalle et al. 2005). However, this method was not convenient in collecting free-standing film after detachment. The released film could adhere again to the collecting substrate when it is dried. Besides, large dimension films are not easy to obtain in this way.

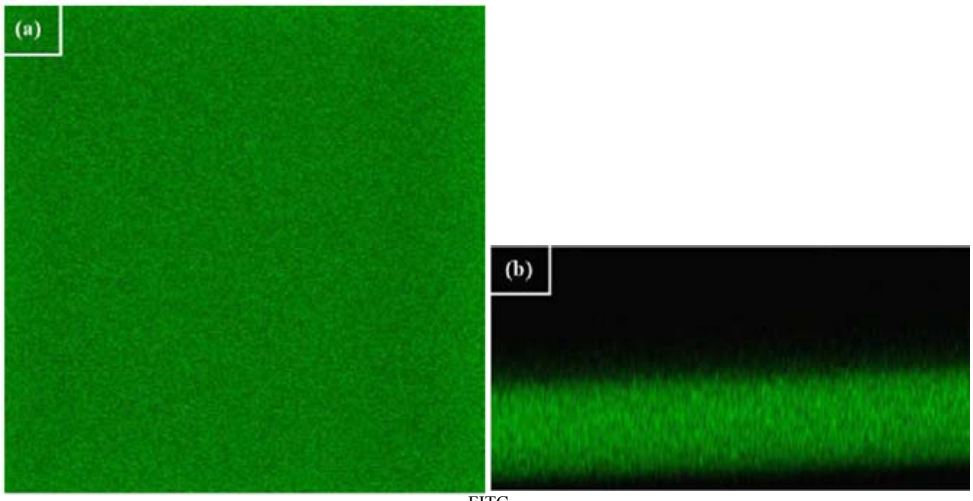

Figure 1.27 CLSM image of a $(PLL/HA)_{68}$-PLL^{FITC} membrane. The polyelectrolyte multilayer film, built on a glass slide, was cross-linked with EDC/sNHS before being detached from the substrate by dipping it in a 0.1 M NaOH solution for 30 min. The floating membrane has been re-deposited on a glass slide before observation in pure water: (a) (x, y) top view of free-standing membrane (image size 76.8 µm×76.8 µm) and (b) (x, z) cross section view (image size is 72.5 µm×37.5 µm). The total thickness of the membrane is about 15 µm. (Reproduced from (Lavalle et al. 2005))

Larkin et al.(Larkin et al. 2010) studied the detachment of (CHI/HA) films in dry state with much larger dimension on an inert polypropylene (PP) substrate, which facilitated the multilayer film release without any post-processing step. In this case, detachable and robust films were obtained from films made of 50 layer pairs with thickness around 3 µm (**Figure 1.28**). The Young's modulus of these films was found to be in the range of 300-400 MPa after cross-linking, as measured by nanoindentations. The response of BALB/c 3T3 fibroblasts was also tested. The authors found that fibroblast adhered well on the multilayer films and colonized the entire surface over a six day period.

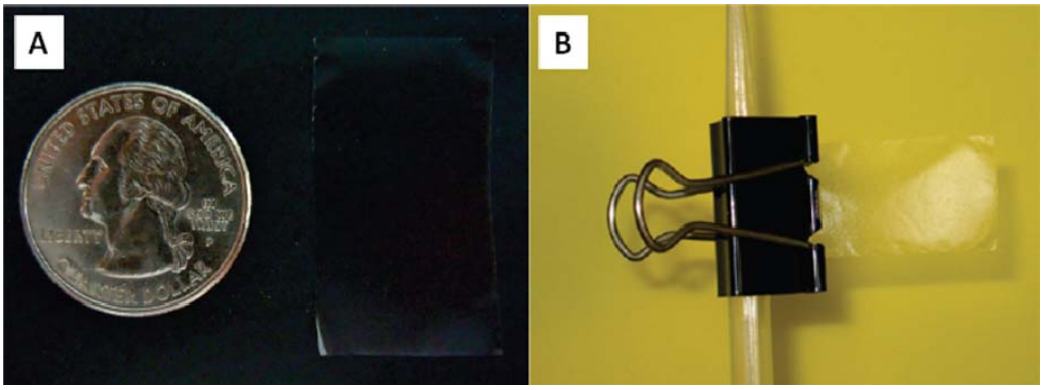

Figure 1.28 Detachable $(CHI/HA)_{50}$ polyelectrolyte multilayer film. (Reproduced from (Larkin et al. 2010))

In general, large dimension free-standing films obtained by releasing from inert hydrophobic substrate require a dry thickness up to 3 μm, in case of polysaccharide multilayers such as (CHI/HA). However, by using spin-assisted LbL technique and with the assistant of a water-soluble sacrificial membrane, polysaccharide free-standing films with large surface but sub-micron thickness was also made. Polysaccharide nanosheet with a thickness of less than 100 nm, known as a "nano-adhesive plaster", and in the dimension of approximately 4 cm^2 (**Figure 1.29**) was constructed by Fujie and co-workers. They used CHI and ALG as building blocks and employed the convenient manipulation of the polymer nanosheet involving ubiquitous transfer from the liquid-solid interface to the air-solid interface using a water-soluble sacrificial membrane (Fujie et al. 2007). The mechanical property of the nanosheet was tested via bulging test (Nolte et al. 2005; Fujie et al. 2009). The elastic modulus of the polysaccharide nanosheet was of the order of 1 GPa for 35 nm thick films. Similar values were obtained for (PSS/PAH) films having the same thickness (Jiang et al. 2004). The elastic modulus of the polysaccharide nanosheet increased to ~ 10 GPa when the film thickness reached 70 nm. This value is close to the typical elastic modulus of 1 μm thick cellulose films, which is also polysaccharide. Further increase the thickness of the nanosheet did not change their ultimate tensile strength and the elastic modulus (Fujie et al. 2009). These results were in good agreement with those reported by Rubner and co-workers (Nolte et al. 2005), where the elastic modulus of ultrathin films composed of PAH and PSS reached a plateau value when the thickness was close to 70 nm. Besides, the polysaccharide nanosheet can be transferred to almost any kind of surface including organ and shows extraordinary nano-adhesion ability. The polysaccharide nanosheet was proved to be stable for at least 24 hrs on human skin, despite perspiration from the skin and the risk of being rinsed away by washing with soap. Due to the good mechanical properties, nano-adhesive ability, good biocompatibility and ease in manipulation, the ultrathin polysaccharide nanosheet has found

potential application in tissue defect repair (Fujie et al. 2009; Fujie et al. 2010).

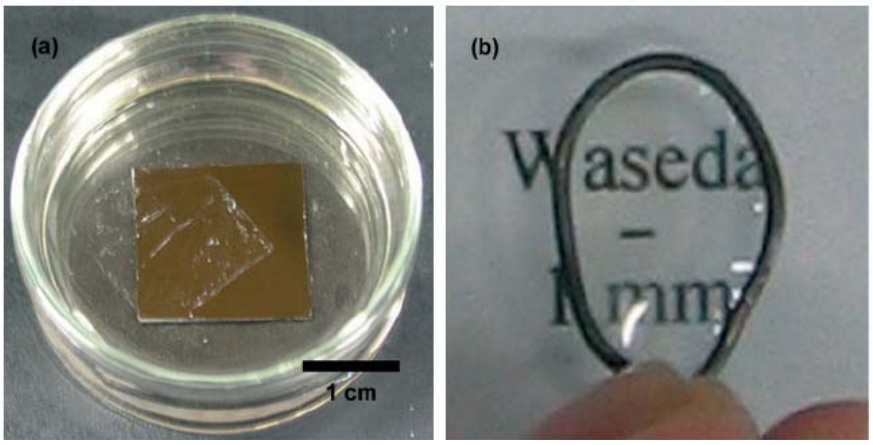

Figure 1.29 Images of a polysaccharide nanosheet: (a) detached from the substrate and floating in acetone and (b) supported by a wire loop and observed in air. (Reproduced from (Fujie et al. 2007))

To further increase the mechanical property of polyelectrolyte multilayer free-standing films, inorganic nanoparticles were usually incorporated (this part will be discussed in section 1.3). Indeed, study has shown that the mechanical properties of silk matrices can be greatly enhanced by incorporationg inorganic nanoparticles (Kharlampieva et al. 2010; Kharlampieva et al. 2010). Up to 6-fold and 8-fold increase in elastic modulus and toughness, respectively, were found.

1.2.3 Application of layer-by-layer free-standing films

Free-standing films prepared by the LbL technique have seen significant development in the last decades due to advantages of the LbL fabrication method, including low cost, ease of functionalization and tunability of film components. The free-standing multilayered films have found applications in the fields of sensors (Jiang et al. 2004), capacitors (Byon et al. 2011), conductors (Shim et al. 2010; Zhu et al. 2011), electrodes (Shim et al. 2007; Hammond 2011), membranes for pervaporation (Von Klitzing et al. 2004; Yin et al. 2010; Zhao et al. 2010; Bolto et al. 2011), cantilevers (Hua et al. 2004) as well as in biomedical fields (Kim et al. 2008; Fujie et al. 2010).

Sensors. Highly sensitive sensor arrays are in high demand for prospective applications in remote sensing and imaging. Ultrathin, flexible membranes and microcantilevers are emerging as critical elements in various sensing devices, such as acoustic, chemical, pressure and thermal sensors (Rogalski 2003). Layer-by-layer assembly provides an easy way to

fabricate flexible and light weight ultrathin membrane for sensors by incorporating sensitive components, of which the amount and position (Jiang et al. 2004) as well as alignment (Correa-Duarte et al. 2005) can be easily and precisely controlled.

A generation of membrane-based sensor arrays with extraordinary sensitivity and tremendous dynamic range was fabricated by Jiang and co-workers (Jiang et al. 2004; Jiang et al. 2005; Jiang et al. 2005). The membrane composed of two $(PAH/PSS)_n$ films sandwiched a gold nanoparticle layer. As shown in **Figure 1.30**, the membranes show very good linear relationship between temperature/pressure and deflection in a large range and the sensitivity is far better than silicon membrane. The free-standing organic/inorganic films are extremely strong, robust, have a long life, are highly sensitive, and show an unprecedented ability to recover from deflection. A free-standing film that has been deflected by high pressure and long loading time can recover to a flat shape in a few seconds. Interestingly, this deflection-recovery cycle can be repeated for several hundred times. The detection parameters can further expand to acoustic, chemical, and so on (Jiang et al. 2004).

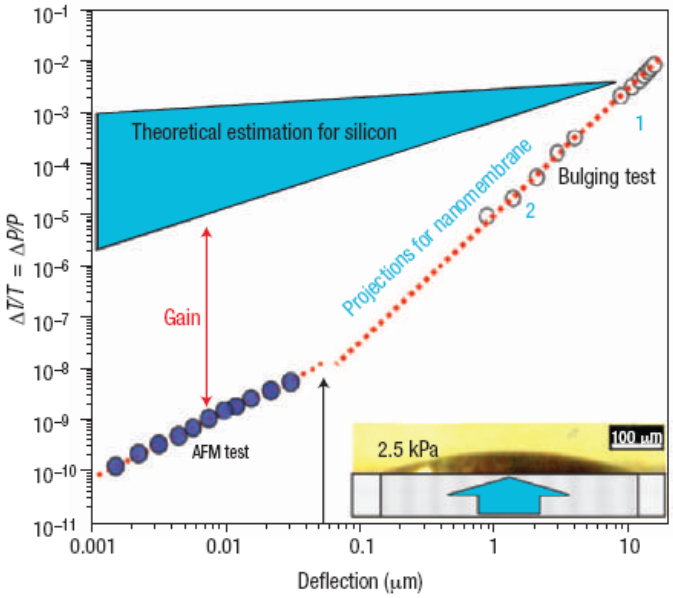

Figure 1.30 Pressure–temperature sensitivity of freely suspended $((PAH/PSS)_9PAH\text{-}Au\text{-}PAH(PSS/PAH)_9)$ membrane of 600 µm diameter in comparison with a silicon membrane of the same diameter. The relative variation of pressure is equivalent to relative variation of temperature (T) for the isochoric regime. The results of two independent bulging tests (1 and 2) (open circles) for high deflections and AFM distributed-pressure results for nanoscale deflections (filled circles) are used to estimate the overall behaviour. The black arrow shows the membrane thickness. The insert shows a side-view of a deflected membrane. (Reproduced from (Jiang et al. 2004))

Battery related. Batteries are an ideal mode to store excess energy produced from alternative means (*e.g.* electronic cells, fuel cells, solar cells). Extensive works have been carried out by the group of Professor Hammond, who is working toward the elaboration of light batteries, ultra thin and flexible electrodes and electrolytes, taking advantage of the layer-by-layer technique (DeLongchamp et al. 2004; Nam et al. 2006; Ashcraft et al. 2010; Hammond 2011).

To achieve efficient electrochemical processes within multilayer thin films, ion transport must be possible within the multilayer thin films. Multilayer assembly is actually the ideal approach for tuning both electron and ion transport in thin films because of the ability to control these properties at the nanometer level and to create complex composite systems. Layer-by-layer films, either ionic bonded or hydrogen bonded, have been proved to act as a solid-state electrolyte (DeLongchamp et al. 2004; Lutkenhaus et al. 2007; Argun et al. 2008; Lutkenhaus et al. 2008; Argun et al. 2010). Fast ion-conduction was achieved within (LPEI/PAA) and (LPEI/Poly(acrylamidosulfonic acid), LPEI/PAMPS) films as well as (PEG/PAA) multilayer thin films.

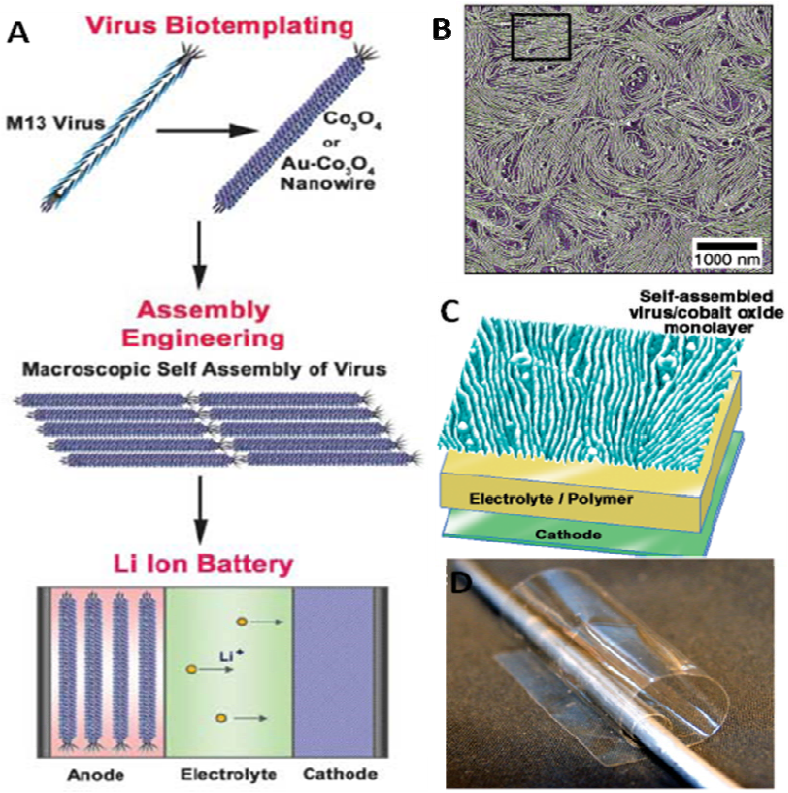

Figure 1.31 (A) Schematic diagram of the virus-enabled synthesis and assembly of nanowires as negative electrode materials for Li ion batteries. Rationally designed peptide and/or materials-specific peptides identified by biopanning were expressed on the major coat p8 proteins of M13 viruses to grow Co_3O_4 and Au-Co_3O_4 nanowires. Macroscopic ordering of the engineered viruses was used to fabricate an assembled monolayer of Co_3O_4 nanowires for flexible, lightweight Li ion batteries. (B) Phase mode AFM image of macroscopically ordered monolayer of Co_3O_4 coated viruses. Z-range is 30°. (C) A lithium battery using Co_3O_4 nanowires assembled atop (LPEI/PAA) multilayers. The LbL film also acts as the polymer electrolyte. (D) Digital camera image of a flexible and transparent free-standing film of $(LPEI/PAA)_{100.5}$ on which Co_3O_4 viral nanowires are assembled into nanostructured monolayer with dimensions of 10 cm by 4 cm. (Reproduced from (Nam et al. 2006))

A very original approach was developed by the group of professor Hammond in collaboration with the group of professor Belcher (both at MIT). They investigated the insertion of rigid M13 viruses as a third component in (LPEI/PAA) films (Yoo et al. 2008). They evidenced that the interdiffusion present in these exponentially growing films favored virus ordering at the

film surface. Virus ordering and the distance between them could be controlled by manipulating the deposit pH of the underlying polyelectolyte multilayers. More importantly, the patterned M13 virus on (LPEI/PAA) film surface can be used as heterostructured templates and are suitable for the growth of monodisperse, highly crystalline nanowires such as cobalt oxide (Nam et al. 2006). As shown in **Figure 1.31**, a light-weight and flexible Li battery was obtained using the patterned nanowires assembled atop (LPEI/PAA) multilayer film as anode, where the layer-by-layer film also acts as the polymer electrolyte (Nam et al. 2006; Lutkenhaus et al. 2007).

Biocompatible Patch. Layer-by-layer ultrathin free-standing film has also found applications in the biomedical field, such as drug delivery (Lavalle et al. 2005; Kim et al. 2008) and wounding dressing (Fujie et al. 2007; Fujie et al. 2009; Fujie et al. 2009; Fujie et al. 2010). Fujie and co-workers constructed biodegradable 75 nm (CHI/ALG) polysaccharide free-standing films for wound sealing (Fujie et al. 2009). As illustrated in **Figure 1.32**, a water soluble polyvinyl alcohol (PVA) layer was casted atop (CHI/ALG) multilayer to facilitate the manipulation of the nanosheet after detachment. When the film was used for wound healing, water or PBS was added to dissolve the PVA layer when the nanosheet adhered on the defect.

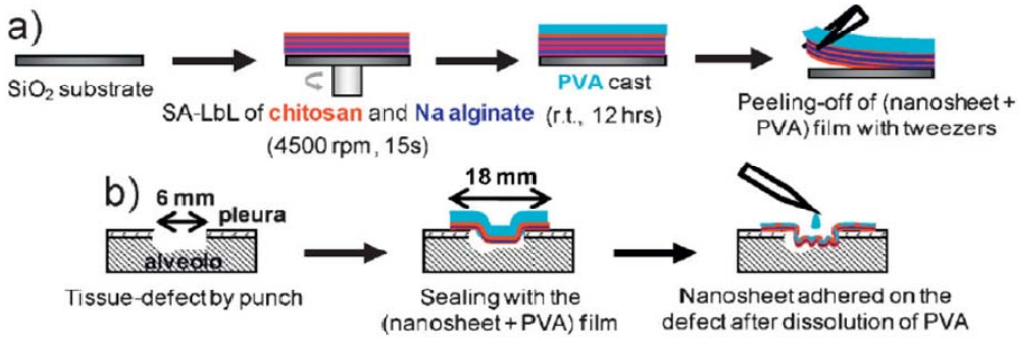

Figure 1.32 Schematic representation of the polysaccharide nanosheet integrated for tissue-defect repair. a) Fabrication method for a free-standing polysaccharide nanosheet using a Spinning Assisted layer-by-layer method and a water-soluble supporting PVA film. b) Schematic explanation of tissue-defect repair using a polysaccharide nanosheet. (Reproduced from (Fujie et al. 2009))

The nanosheets show tremendous adhesion onto the organs. The bursting pressure of the nanosheet in visceral pleural defect repair was 30 cm H_2O immediately after operation and increased to 60 cm H_2O after 24 hrs, which is the same as the bursting pressure of fibrin nanosheet. The high flexibility of the polysaccharide nanosheet ensured the well attachment and densely overlapping to the defect site without any air leakage. The good attachment combined the biocompatibility finally facilitated the fast wound healing (**Figure 1.33**).

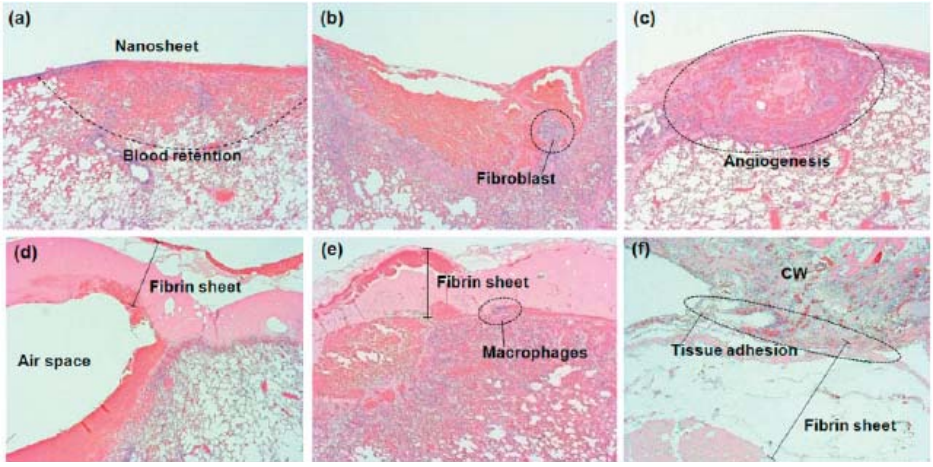

Figure 1.33 Representative histological findings at different time points after repair (hematoxylin-eosin staining, magnification 4×) using the polysaccharide nanosheet or the fibrin sheet. Upper and lower panels correspond to the polysaccharide nanosheet and the fibrin sheet, respectively, at 3 hrs (a, d), 3 days (b, e) and 7 days (c, f) after repair. At 7 days, angiogenesis occurred in the polysaccharide nanosheet groups while strong adhesion between the fibrin sheet and the chest wall (CW) was observed. (Reproduced from (Fujie et al. 2009))

1.3 Organic/inorganic nanocomposite made by Layer-by-Layer assembly

Inorganic nanoparticles, including carbon nanotubes (Yu et al. 2000; Mamedov et al. 2002), montmorillonite (MTM) platelets (Kotov et al. 1998; Manevitch et al. 2004), and metal nanoparticles (NPs) (Wang et al. 2002; Jiang et al. 2004), are of great interest for adjusting the mechanical, optical and other properties of polymer materials when they were used as fillers. Inorganic NPs/polyelectrolyte composites are used in an increasingly large number of biomedical applications in the field of biotechnology, sensing (Anker et al. 2008; Sepulveda et al. 2009; Iost et al. 2011), bioimaging (Agarwal et al. 2011), and drug and gene delivery (Volodkin et al. 2009; Volodkin et al. 2009), due to their interesting mechanical, optical and electrical properties.

During the past years, many studies have focused on the introduction of inorganic NPs into organic matrix to form organic/inorganic hybrid nanomaterials. The polymer matrix can stabilize the NPs and keep them from aggregation. Meanwhile, the NPs can provide organic materials with special functionality such as high mechanical properties (Mamedov et al. 2002), particular optical properties (Goulet et al. 2005), or selective permeability (Van Ackern et al. 1998; Struth et al. 2001).

Layer-by-layer assembly technique provides a versatile approach for constructing

organic/inorganic nanocomposite, as this technique allows the incorporation of modified and unmodified NPs and polyelectrolytes in a controlled way.

1.3.1 Incorporation versus *in situ* synthesis

Organic/inorganic nanocomposites are synthesized via two major strategies. The first consists in assembling prefabricated inorganic NPs with polymers, either by chemical grafting or by adsorption of the polymer onto the particles. Assemblies of NPs and polyelectrolytes can be built in a layer-by-layer fashion to control the number and position of NPs (Fendler 1996; Hao et al. 2000; Mamedov et al. 2000; Eckle et al. 2001; DeRocher et al. 2011). This has been the most widely employed method to construct nanocomposites based on LbL assembly.

The second and less common strategy uses an organic solution (or "matrix") as a template to nucleate and grow *in situ* inorganic NPs, usually for metal NPs (Wang et al. 2002). This is most often achieved directly by adding precursor ions into the polymeric solution or polyelectrolyte multilayer films. These ions are usually positively charged (such as Ag^+) or negatively charged (tetrachloroaurate ions, $AuCl_4^-$), thus can be anchored by charged groups via ionic interaction. Moreover, polymers bearing primary, secondary or tertiary amine groups are able to form complexes with a wide variety of transition metal cations (Belfiore et al. 2000). For instance, uncharged amine groups can coordinate with Ag^+. The reduction of metal NPs from their precursors can be realized via several ways, including photoreduction (UV light) (Eustis et al. 2005), thermal reduction (Dai et al. 2002) and chemical reduction (Sohn et al. 2001). In this latter case, the reduction is performed by using a strong reducing agent such as sodium tetrahydroborate ($NaBH_4$), Ascorbic Acid and so on.

In case of the *in situ* synthesis of NPs, layer-by-layer films show great advantages as templates for precursor loading: (i) phase separation can be totally avoided in LbL films; (ii) charged groups, such as carboxylate and amine which show specific affinity to the precursors, can be introduced and their amount and distribution can be precisely controlled down to a molecular level. Thus, the amount, position, homogeneity and even alignment of the inorganic components can be precisely controlled when keeping them well separated.

Table 1.1 and **Table 1.2** summarize the typical works concerning construction of hybrid nanocomposites based on layer-by-layer assembly, either by directly assembling the as

prepared NPs (**Table 1.1**) or by synthesizing nanoparticles *in situ* (**Table 1.2**). Of note, other NPs, including TiO_2 (Kim et al. 2002; Dontsova et al. 2011), SiO_2 (Bravo et al. 2007), Quantum Dots (Komarala et al. 2006), Magnetite NPs (Mamedov et al. 2000; Pichon et al. 2011) were also introduced into LbL films in direct incorporation as layers in the film.

Table 1.1 Overview of studies dealing with the design of nanocomposite films based on layer-by-layer assembly of NPs with polyelectrolytes.

Inorganic NPs	PEM	Main findings	Ref
Carbon Nanotube	((PEI/PAA) $(PEI/SWNT)_5)_n$	High CNT loading, Extremely high mechanical properties	(Mamedov et al. 2002)
	(PVA/SWNT)	Homogeneity, optimized electrical, mechanical, and optical properties.	(Shim et al. 2007)
	(Poly(aniline)/ CNT)	Strain and corrosion processes tracing	(Loh et al. 2007)
	(Polypyrrole/ MWNTs)	Electron transfer enhancement, higher bioactivity carrier	(Korkut et al. 2008)
	Chitosan/ MWNTs/ glucose oxidase	Rapid response, good reproducibility, long-term stability	(Zou et al. 2008)
	Antimicrobial lysozyme/ SWNT	Large scale, significant antimicrobial activity, high Young's Modulus, controlled SWNT orientation	(Nepal et al. 2008)
MTM clay	PDDA/MTM	Unusual high strength, flexibility, resistance to crack Surface roughness tuned by PDDA concentration	(Kotov et al. 1998; Duffel et al. 1999)
	Styrene-poly(di-allylammonium-chloride)/MTM	Film roughness reduced, barrier functionality improved	(Vuillaume et al. 2002)
	Chitosan/MTM	Decreased interfacial interaction, decreased toughness	(Podsiadlo et al. 2007)
	PEI/PAA/ PEI/MTM	Exponential growth, exfoliate the short stacks of MTM into single lamella	(Podsiadlo et al. 2008)
	Poly(vinyl alcohol)/MTM	Record-high mechanical properties, high transparency	(Podsiadlo et al. 2007)
	Silk/MTM	All-natural, transparent, enhanced mechanical properties	(Kharlampieva et al. 2010)
	$(PSS/PAH)_6$-MTM-$(PSS/PAH)_6$	Hindered ion diffusion	(Struth et al. 2001)
Au NP	PDDA/PAA/ PDDA/Au NPs	Interaction between the NPs in adjacent layers studied	(Malikova et al. 2002)
	$(PSS/PAH)_n$-Au-$(PAH/PSS)_n$	High mechanical properties, flexibility	(Jiang et al. 2004)
	Polyaniline/Au NPs	Electrocatalyst, DNA detection	(Tian et al. 2004)
	Polyviologen derivative/Au	Different NP deposition times lead to different NP morphology: very long time caused aggregation	(Terzi et al. 2009)
	Glucose oxidase /Au NPs	Enzyme activity increased with the increase of layer number	(Hoshi et al. 2007)
	Au NPs on (PLL/HA) film	Au NPs aggregated on film surface, near IR triggered DNA release	(Volodkin et al. 2009)

Ag NP	Poly(propylene-imine)/AgNPs	Surface enhanced Raman scattering	(Goulet et al. 2005)
	$(PAH/PSS)_n$-Ag-$(PAH/PSS)_n$	Mechanical property enhancement	(Gunawidjaja et al. 2006)
	Chitosan/Ag NPs	Improved hydrophilicity, antibacterial activity, hemocompatibility, cytocompatibility	(Yu et al. 2007)
	(PDDA/MTM) (PDDA/Ag)	Excellent structural stability, antibacterial activity	(Podsiadlo et al. 2005)

Table 1.2 Studies on the *in situ* synthesis of NP using LbL films as templates.

Inorganic nanoparticles	PEM	Main findings	Ref
Ag NP	$[(PAH/PAA)_n (PSS/PDDA)_m]_l$	Silver NPs synthesized in (PAH/PAA) region, refractive index tunable	(Wang et al. 2002)
	Chitosan/ heparin	Antibacterial, NP size controlled by the assembly pH and loading pH	(Yuan et al. 2010)
	PDDA/PSS	Silver NP amount and size adjusted by the salt concentration	(Zan et al. 2009)
	HA/PDDA	The Ag NP amount and antibacterial ability tuned by layer number	(Cui et al. 2008)
Au NP	$(PLA-PEI/PAA)_8$, $(PEI/PLA)_8$, $(PVPON/PLA)_8$	Au NPs served as probe for optical reporting of biodegradation process	(Orozco et al. 2010)
	(PAH/PAA), (PAH/PSS)	Au NP loading, size and distribution tuned by loading pH	(Chia et al. 2008)
	$(PAH-PSS)_2PAH$-silk fibroin	Au NP size controlled by silk secondary structure	(Kharlampieva et al. 2009)

1.3.2 Importance of charged groups

The charged groups, such as carboxylate and amino groups are important in stabilizing and positioning the metal NPs especially when the metal NPs are incorporated by *in situ* synthesis, because they can anchor the precursors via electrostatic interactions. For example, carboxylate groups can interact with positively charged metal ions like Ag^+ (Wang et al. 2002) and Pb^{2+} (Joly et al. 2000). Amino groups show specific association with negatively charged metal ion complex like $AuCl_4^-$ (Leff et al. 1996; Sohn et al. 2001). Moreover, some groups such as amino are important in the stabilization and positioning of the reduced metal NPs as they can interact with the NPs via coordination.

Thanks to the association between silver ions and negatively charged carboxylate groups, the *in situ* synthesis of silver NPs, whose precursor is positively charged, is possible in LbL films. For example, Wang et al. (Wang et al. 2002; Nolte et al. 2004) reported the fabrication of one-dimensional photonic structure based on the combination of layer-by-layer assembly of

polyelectrolytes and *in situ* silver nanoparticle synthesis. The periodic $(PAH/PSS)_n$ $(PAH/PAA)_m$ films were constructed as the template to load silver ions for further reduction and offered precise control over layer thicknesses. Meanwhile, the *in situ* silver NP synthesis facilitated the tuning of refractive index within specific region (**Figure 1.34**) as silver ions associated with carboxylate groups but not sulfite. Furthermore, the refractive index can be controlled by varying *in situ* synthesis cycles because the negatively charged carboxylate groups were regenerated once silver NPs were synthesized, and were capable to interact with silver ions again.

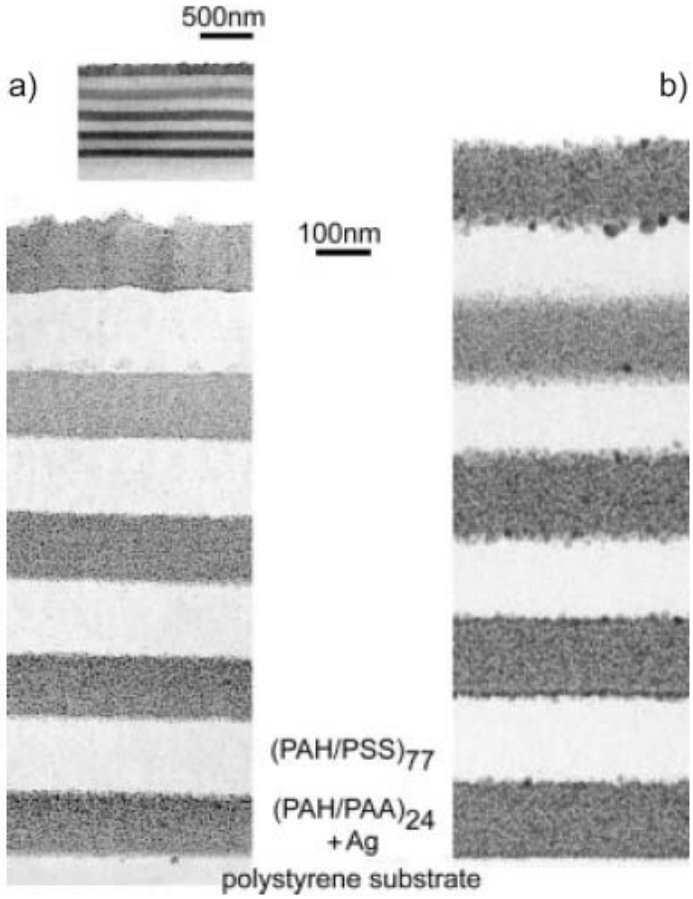

Figure 1.34 Cross-sectional TEM images of a 4.5 period Brag stack after a) one cycle of Ag NP synthesis and b) five cycles of NP synthesis. In (a), the high index strata (dark contrast) have average thickness of 120 ± 4 nm and the low index strata (light contrast) have average thickness of 137 ± 6 nm. In (b), after five cycles of NP synthesis, the average thickness of the high index stratum is 167 ± 7 nm (containing ~ 19 vol. % Ag) and of the low index stratum is 148 ± 9 nm. Note that the surface imperfections at the top of the stack resulted from damage caused by ultramicrotomy; RMS surface roughness of < 10 nm was measured by profilometry. (Reproduced from (Wang et al. 2002))

In situ synthesis of silver NP approach was also employed in (PAH/PAA) (Li et al. 2006; Agarwal et al. 2010), (CHI/HEP) (Yuan et al. 2008; Yuan et al. 2010) and (HA/PDDA) (Cui et al. 2008) films to constructed anti-bacterial coatings. Agarwal and co-workers(Agarwal et al. 2010) used (PAH/PAA) multilayer film as template to load silver ions and then reduce them *in situ* to form silver NPs (**Figure 1.35**). The amount of Ag NPs embedded in the film can be

controlled by adjusting the deposit pH, or by repeating the silver ions loading and reduction steps. This provides the film with a capacity to kill bacteria effectively while, at the same time, supporting mammalian cell growth.

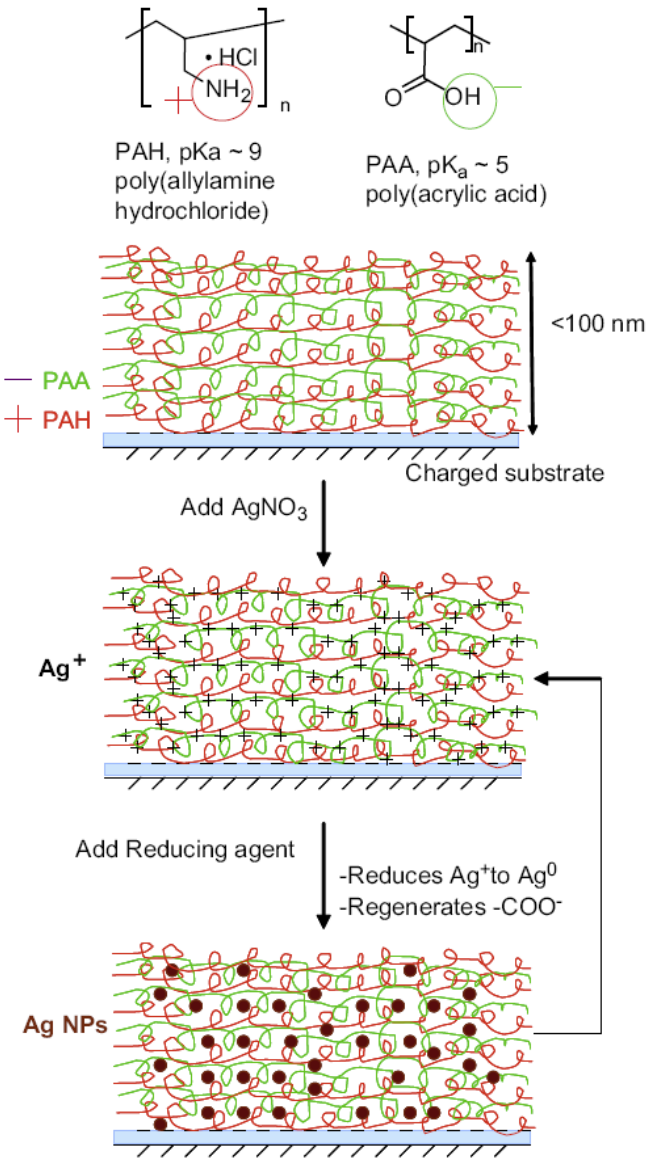

Figure 1.35 Schematic illustration of the layer-by-layer deposition of multilayers of (PAH/PAA) on a charged substrate. Post-assembly, the multilayer super-lattice is incubated with a solution of $AgNO_3$ in order to promote the exchange of the silver ions with protons of the carboxylic acid groups of PAA within the film. Subsequently, silver ions within the film are reduced to silver NPs by a chemical reducing agent ($NaBH_4$). Chemical reduction of the silver ions to silver NPs also regenerates the carboxylic groups within the film. (Reproduced from (Agarwal et al. 2010))

Gold NPs are particularly interesting due to their non-toxicity, biocompatibility, photothermal properties, ease of imaging and versatility of surface chemistry. In the preparation of gold NPs, amino group were shown to be very important both for anchoring aurochlorate precursors and for stabilizing the resultant gold nanoparticles. By controlling the organization of specific

groups, such as amine, the control of the aggregation state of gold NPs can be achieved either in solution or on a surface.

Sardar et al. (Sardar et al. 2008) used poly(allylamine) solution as template to synthesize gold NPs of 3 nm in diameter. They observed the reversible organization of the NPs upon changing of solution pH. In this way, the synthesized Au NPs were good "dyes" to visualize the poly(allylamine) conformation in solution, because the Au NPs were tightly bonded to amino groups (**Figure 1.36**). At high pH theNPs were in aggregated states showing coiled and compact conformation of poly(allylamine), whereas in low pH the well separated NP formation indicating stretched and lined conformation of poly(allylamine) chains.

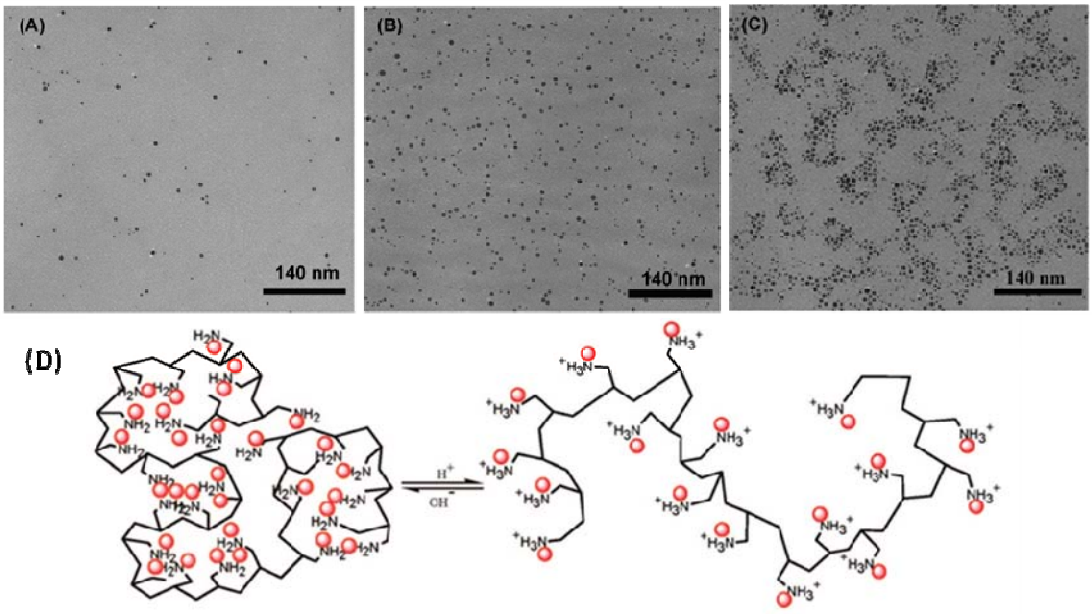

Figure 1.36 TEM images of PAH stabilized Au NPs at pH of (A) 1.5, (B) 3.5, and (C) 12.5. (D) Schematic illustration of reversible changes in pH-dependent nanocomposite organization. (Reproduced from (Sardar et al. 2008))

To avoid harsh solvent or agent, redox active peptides or proteins, like Silk fibroin, were used by Tsukruk and co-workers as template to synthesize gold NPs (Kharlampieva et al. 2009). They found that the gold NP size can be controlled by protein secondary structures. The presence of β-sheet in silk facilitated tyrosine (an amino acid that has redox-active properties) ordering thereby resulting in well-dispersed, uniform NPs with diameters of less than 6 nm, whereas the random structure in silk resulted in much larger and inhomogeneous NP formation.

1.3.3 Mechanical property of layer-by-layer hybrid films

The mechanical properties and stability of layer-by-layer films are essential for several applications. Different strategies can be used to enhance mechanical properties, which rely usually on chemical or physical stiffening. For instance, films can be chemically cross-linked by carbodiimide chemistry (Richert et al. 2004), by photo-cross-linking (Kadi et al. 2009) or by natural cross-linking agents (Hillberg et al. 2009). Alternatively, the incorporation of inorganic NPs such as MTM clay, carbon nanotube and metal nanoparticles is a good mean to enhance film mechanical properties.

Inorganic NPs like MTM clay (with the in-plane modulus of elasticity on the order of ~270 GPa (Manevitch et al. 2004)) and carbon nanotube (with toughness up to 300 GPa (Yu et al. 2000)) are always used as reinforcing fillers for enhancing the mechanical properties of commercial plastics. A significant enhancement of strength, elastic modulus and toughness has been observed upon addition of just a few volume percentages of the inorganic filler. However, above the few percentiles, the mechanical properties begin to deteriorate due to strong tendency of inorganic fillers to phase segregate and aggregate, thus creating fatal defects (Podsiadlo et al. 2009). The layering of the NPs with polyelectrolyte show an interesting promise for overcoming these problems thanks to a number of advantages: (i) the nanocomposite are constructed by alternating deposit nanometer thick layers of polyelectrolyte and NP, thus allowing for nanometer-level control of preparation; (ii) alternating the layers of inorganic NP with few-nanometer-thick layers of polymers translates into volume fractions upwards to 50 vol%; (iii) the colloidal self-assembly process restricts adsorption of NPs to well-exfoliated ones; and (iv) sandwiching of the NPs between polymer layers and strong interfacial bonding prevent phase segregation of the nanofillers.

Supported films. For supported layer-by-layer films, researchers were more concerned about the film stability. It was thus shown that the incorporation of inorganic clay in the film improved crack resistance of the film (Kotov et al. 1998).

Several research groups subsequently aimed at precisely measuring the film mechanical properties for organic/inorganic nanocomposite films. To this end, nanoindentation and nanoscratch techniques (Olek et al. 2006) were employed. It was found that the interaction between inorganic filler and polyelectrolyte was important for enhancing film mechanical properties, especially when carbon nanotube was incorporated (Olek et al. 2006). Yeom et al.

(Yeom et al. 2006) studied the effect of interfacial adhesion on the mechanical properties of organic/inorganic hybrid nanolaminates. They found that, in the case of formation of strong interfacial adhesion between the organic and the inorganic layers, the fracture toughness and the crack resistance of hybrid multilayer films were significantly improved. According to them, this may from the redistribution of stress concentration and from the dissipation of fracture energy by the plasticity of the organic polyelectrolyte layers. On the other hand, samples with relatively low interfacial adhesion between the organic and the inorganic layers had little effect on the improvement of fracture toughness of the hybrid films.

Free-standing films. The mechanical property of layer-by-layer free-standing films has often been measured by tensile or bulge test (Nolte et al. 2005) or point-load nanodeflection (Markutsya et al. 2005) depending on film dimension and mechanical properties. For films composed of pure polyelectrolytes, the elastic modulus is ~ 1 GPa for 35 nm thick films (*e.g.* (PSS/PAH), (CHI/ALG) films) (Jiang et al. 2004; Fujie et al. 2009). Increasing the film thickness resulted in an increase in the elastic modulus up to ~ 10 GPa (Nolte et al. 2005; Fujie et al. 2009). To further increase the mechanical properties, inorganic NPs, like metal NPs, MTM clay, carbon nanotubes, were usually incorporated into layer-by-layer free-standing films (Mamedov et al. 2002; Jiang et al. 2006; Podsiadlo et al. 2009; Podsiadlo et al. 2009; Podsiadlo et al. 2009).

Tsukruk and co-workers (Jiang et al. 2004; Jiang et al. 2004; Jiang et al. 2005) constructed nanocomposite membrane via embedding a layer of gold NPs (12.7 ± 1 nm in diameter) between two spin assisted layer-by-layer $(PAH/PSS)_n$ films. The mechanical properties from bulging test show that the elastic modulus of the free-standing film increased from 1.5 to 9.6 GPa by incorporating 3.9% of gold NPs (Jiang et al. 2004).

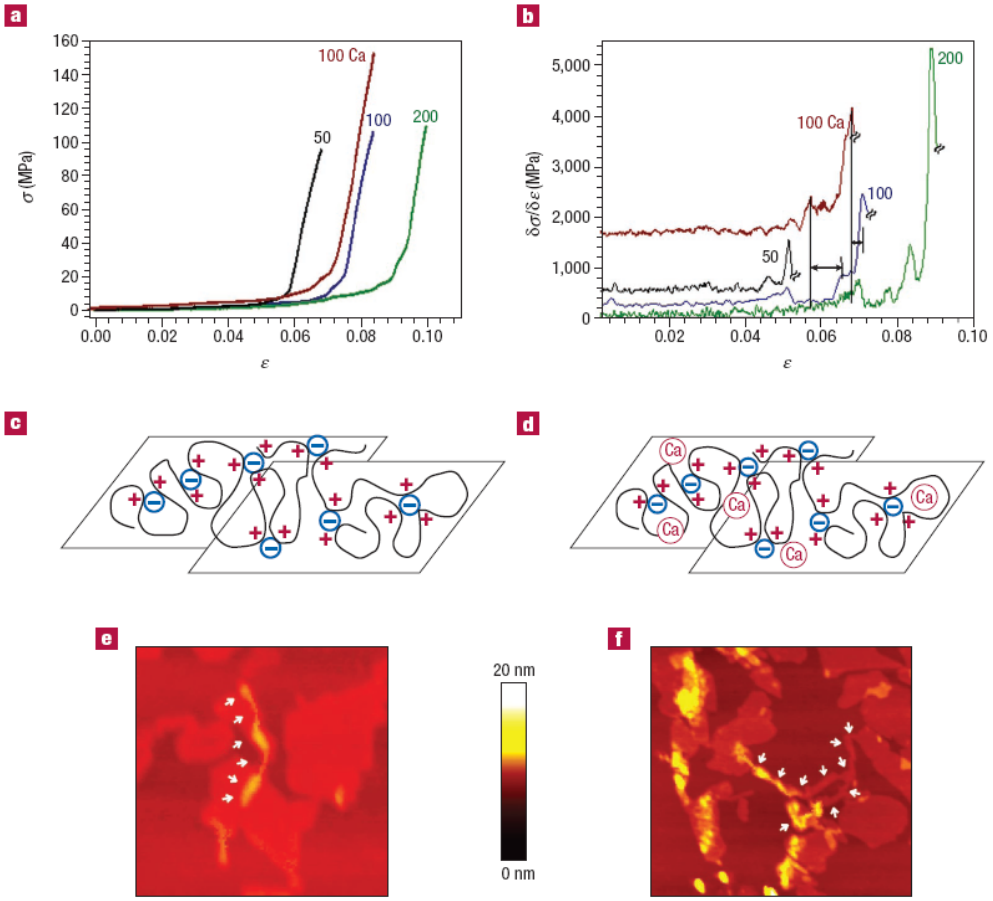

Figure 1.37 (a) Mechanical properties of $(PDDA/MTM)_n$ films. Stress (σ) versus strain (ε) curves of free-standing films made from $(PDDA/MTM)_{50}$, $(PDDA/MTM)_{100}$, $(PDDA/MTM)_{200}$ and $(PDDA/MTM)_{100}$ ion-exchanged with 1M $Ca(NO_3)_2$ for 24 h. (b) The derivatives of the stretching curves in (a) in the low- and intermediate-stress regions revealing the saw-tooth pattern. $(PDDA/MTM)_{50}$, $(PDDA/MTM)_{100}$, $(PDDA/MTM)_{200}$ and $Ca(NO_3)_2$ ion-exchanged $(PDDA/MTM)_{100}$ curves were shifted along the δσ/δε axis for clarity with baselines being 550, 250, and 1 600 MPa, respectively. The saw-tooth patterns for stretching macroscopic samples are not as pronounced as for single-molecule experiments due to averaging over a large ensemble of polymer molecules, which necessitates using the differential coordinates. The data were obtained at a relative humidity of 32%, T=25 ℃. (c, d) Polyelectrolyte folding and PDDA- MTM clay ion-pair formation with and without Ca^{2+} ion exchange. (e, f) Topographic AFM images of PDDA molecules adsorbed between the clay platelets. Elevated areas of irregular shape represent PDDA coils adsorbed to MTM platelets. Arrows track the partially decoiled macromolecules stretched between the clay platelets. (Reproduced from (Tang et al. 2003))

The incorporation of MTM platelets into the layer-by-layer free-standing films was studied by Tang et al. (Tang et al. 2003; Podsiadlo et al. 2007; Podsiadlo et al. 2007) to replicate nacre and bone structures. By assembling negatively charged MTM with PDDA in a layer-by-layer fasion, free-standing films with thicknesses of 1.2, 2.4 and 4.9 μm were obtained for 50, 100 and 200 layer pairs, respectively. A tensile test was carried out to measure the mechanical properties of the free-standing films (**Figure 1.37a**). The ultimate strength and modulus were found to be 100 ± 10 MPa and 11 ± 2 GPa, respectively. The material was stronger and stiffer than some of the strongest commercial plastics and the enhancement of strength and stiffness

over the base PDDA polymer was nearly 10× and 50×. After initial plastic deformation under fairly low stress, films revealed abrupt hardening on further stretching and exhibited a characteristic step pattern of the stress-strain curves. The non elasticity of the materials can be seen even more clearly in the differential form of the stretching curves, which showed clear saw-tooth-like patterns (**Figure 1.37b**). The pattern was attributed to a successive opening of polymer intra-chain loops formed from different polymer segments connected by ionic linkages, which are sequentially broken when extending the macromolecule. These sacrificial bonds were found to be the molecular basis of the mechanical toughness of biocomposites, which help to effectively dissipate the stretch energy. High-resolution AFM images (**Figure 1.37e and f**) obtained for PDDA adsorbed on clay platelets confirm the extensive coiling of the polyelectrolyte which leads to the formation of loops with macromolecular segments linked together by van der Waals and ionic interactions. The ionic interactions are probably brought about by negative surface charges on the clay surface and negative counter ions. It was also found that introduction of Ca^{2+} ions resulted in a competition for binding, and the loss of some polycation-clay contacts (Tang et al. 2003).

The polyelectrolyte molecular coiled nature and its strong interaction with MTM clay were confirmed to be critical for the high strength and toughness of the polyelectrolyte/MTM clay nanocomposite free-standing films. Methods that can reinforce the interaction between polyelectrolyte chains and MTM clay can dramatically enhance the mechanical property of the nacre replica. It is found even a small amount of L-3,4-dihydroxyphenylalanine (DOPA) (Waite et al. 1981), the marine adhesive of mussels, has a dramatic effect on the mechanical properties: the ultimate strength increased 2× and the toughness by 8× (Podsiadlo et al. 2007).

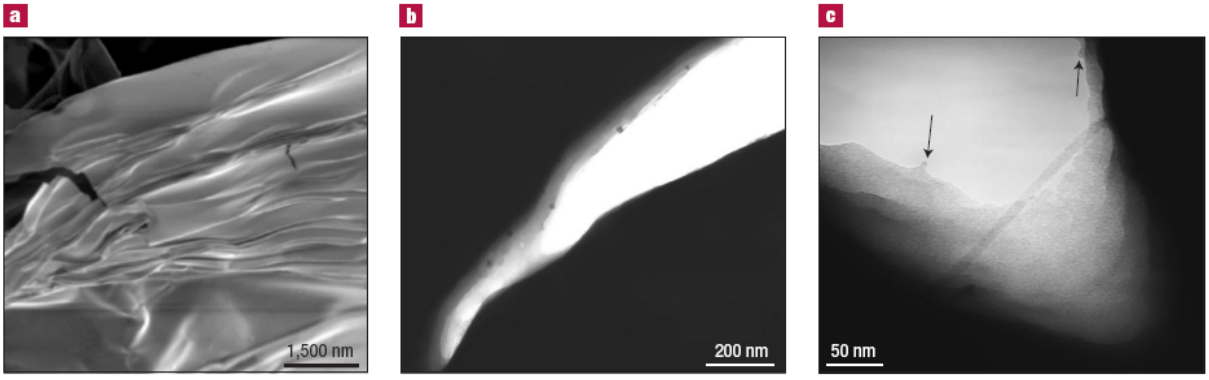

Figure 1.38 (a) SEM image of the surface and broken edges of $((PEI/PAA)(PEI/SWNT)_5)_8$. (b, c) TEM images of ruptured areas of the free-standing films. The arrows indicate the possible positions of the stubs of the broken nanotube bundles. They were identified as such because the diameter of both of them is similar to that of the actual SWNT bundle bridging the gap, and their mutual positioning presents an almost perfect match with the expected location of the ends of a bundle broken during gap opening. (Reproduced from (Mamedov et al. 2002))

Even high strength (220 MPa) and elastic modulus (35 GPa) were obtained for layer-by-layer free-standing film containing single wall carbon nanotubes (SWNT) (Mamedov et al. 2002; Shim et al. 2009). Mamedov and co-workers constructed nanometer-scale uniform and defect-free composite free-standing films with SWNT loading as high as 50 wt%. The film was constructed by layering negatively charged (COO^-) SWNT with PEI into $((PEI/PAA)(PEI/SWNT)_5)_8$ multilayer and sequential thermal cross-linking. The good dispersion of SWNT in the whole film and the strong interaction between the polymer chains and SWNT are key parameters in achieving high strength and modulus. TEM examination of the initial stages of rupturing showed that virtually no fiber pullout occurred in the LbL multilayers (**Figure 1.38b**). For many TEM images obtained in different areas of the free-standing films, the authors were able to observe only one SWNT bundle bridging the break region (**Figure 1.38c**).The same image also shows two broken carbon fiber stubs imbedded in the walls of the crack (marked by arrows in **Figure 1.38c**). These results indicate that there is an efficient load transfer in the LbL composite. For multiwall carbon nanotubes (MWNT), the structure and morphology of the MWNT are important for the mechanical properties of the resultant composite films (Olek et al. 2004).

1.4 Objective of the thesis

Previous works in the group of Professor Ji at Zhejiang University have demonstrated that the exponential growth of films made of weak polyelectrolytes can be enhanced by increasing the deposit pH of the polycation and decreasing the deposit pH of the polyanion. This is the so-called pH-amplified LbL assembly (Fu et al. 2009; Wang et al. 2009). My thesis takes advantages of the newly explored pH-amplified layer-by-layer assembly.

One aim was to investigate the potential applications of this amplified growth mode.

Two different systems were used: the first one involves poly(ethylene imine) (PEI) and poly(acrylic acid) (PAA), a largely studied exponentially growing synthetic polyelectrolyte pair. The second one concerns poly(L-lysine) (PLL) and hyaluronic acid (HA) films, one of the most studied exponentially growing systems based on natural polymers.

For (PEI/PAA) multilayer films, the aim was to construct two kinds of asymmetric free-standing films:

The first one possesses a top surface that is superhydrophobic and a bottom surface that is hydrophilic, to form a humidiy sensor (chapter 2.1).

The second membrane is to be used as anti-bacterial dressing (chapter 2.2). It contains silver ions that can be essentially released by the bottom surface, which is hydrophilic and possesses a top surface that is self-cleaning.

For (PLL/HA) multilayer films, the first aim was to investigate the effect of the molecular weight of HA on film growth and to get insight into the mechanism of the accelerated growth of (PLL/HA) film under pH amplified condition (Chapter 3).

In the subsequent step, we explored the possibility of using these exponentially-growing films, which are rich in amine and carboxylic groups, as a template to synthesize NPs *in situ* and to constructing hybrid films. To this end, two types of NPs were synthesized: silver NPs (chapter 4.1) and gold NPs (chapter 4.2). Both silver NP and gold NP were synthesized within the bulk of (PLL/HA) film in mild conditions using UV photoreduction to reduce their precursor ions.

Chapter 2 Asymmetric free-standing (PEI/PAA) multilayered films

2.1 Humidity Responsive asymmetric free-standing multilayered film

2.1.1 Summary

Introduction

Biomimetic is a big and interesting topic in material designing. Stimuli-responsive behavior, which is an intrinsic property of living systems, has become a key guidance for developing new materials and devices. The bending/unbending responsive materials are of great interests as the movement can be easily observed by naked eyes. For materials able to bend/unbend under various stimuli, the asymmetric response to the applied stimuli is crucial. One example of such stimuli-responsive material is modulated gels also called bigels.(Hu et al. 1995) Such gels consist of a controlled layer that is responsive to the environmental stimuli and a nonresponsive substrate layer. A 10-fold change in volume can be reached for the control layer as a consequence of a thermally induced abrupt change in the gel microstructure. The drastic swelling and shrinking of the control layer guarantees that the bigel strip bends uniformly upon heating to form an arch and recovers to the strip upon cooling. Of note, as the membranes' sensitivity relies on film thickness, thinner membranes will be more sensitive. A metal/polymer composite bilayered film with a thickness at the micrometer scale was prepared(Ma et al. 2009) in which 10% of absorbed water within the polymeric layer was enough for the bilayered film to exhibit such bending/unbending movement upon humidity changes.

In this work, we constructed a free-standing polyelectrolyte multilayered film with asymmetric wettability, superhydrophobic *vs* hydrophilic. The bending/unbending movement of the asymmetric free-standing film under humidity change was studied.

Results and discussion

Teflon plate was alternately immersed into poly(ethylene imine) (PEI, 1 mg/mL) at pH 9.0 and poly(acrylic acid) (PAA, 3 mg/mL) at pH 2.9 (for 15 min each) to form 20-bilayer multilayer films. After thermal cross-link and chemical deposition of low surface energy silane, the films can be easily peeled away from the Teflon plate to yield a free-standing film. The pH shift in (PEI/PAA) film build-up process resulted not only in the amplified film growth but also in roughening of film surface morphology. The top surface of the film, which was previously facing air, showed micro-nano hierarchical structures and got a water contact angle as high as 161.2° with a low surface energy silane coating; the surface morphology of the bottom surface of the free-standing film, which was facing the substrate before detachment, was relatively smooth with only micrometer scale structures and the water contact angle on the bottom surface declined rapidly to 25.6°.

The sharp differences on wettability of the two surfaces brought asymmetric responses upon water or vapor for the two surfaces and thus leaded to bending/unbending movement of the free-standing film. The film was in the state of rolling bottom surface inside at low humidity, when the film was then shifted to high humidity it first extended and then rolled up and wrapped the upper surface inside. In case the humidity changed from high to low, the opposite unbending/bending transition was observed.

Conclusion

A facile method for creating asymmetrical free-standing films has been demonstrated in this work based on the alternated deposition of PEI at high pH and PAA at low pH on a Teflon substrate. After coating with a layer of a low surface energy compound, the released free-standing films with asymmetric surface morphology and wettability can exhibit reversible humidity-induced shape transitions.

2.1.2 Article

Humidity responsive asymmetric free-standing multilayered film

L.Shen, J. Fu, K. Fu, C. Picart, and J. Ji, Langmuir. 2010, 26(22), 16634–16637.

Humidity responsive asymmetric free-standing multilayered film

Liyan Shen, Jinhong Fu, Ke Fu, Catherine Picart, and Jian Ji,

Abstract

A humido-responsive free-standing film has been created using layer-by-layer assembly technique. Polyethylenimine (PEI) at high pH was assembled with poly(acrylic acid) (PAA) at low pH on a Teflon substrate to yield a micro-nano structured surface that can be made superhydrophobic after being coated with a low surface energy compound. The resulting asymmetric freestanding film with one surface being superhydrophobic while the other is hydrophilic after detachment from the substrate can undergo reversible bending/unbending shape transitions when the environmental humidity is changed. The bending/unbending movement of the free-standing film can be ascribed to the different responses of these two surfaces to humidity.

Stimuli-responsive behavior is an intrinsic property of living systems that has become a key guidance for developing new materials and devices. Smart polymeric materials, such as hydrogels,[1,2] capsules,[3,4] and multilayers,[5] can respond with a considerable change in their volume, shape, or other properties to even small changes in the environment. Materials that exhibit reversible shape transitions such as bending/unbending hold great promise in applications such as artificial muscles,[6,7] cantilevers,[8] sensors,[9] actuators,[10,11] and so on. For materials able to bend/unbend under various stimuli, the asymmetric response to the applied stimuli is crucial. One example of such stimuli-responsive material is modulated gels also called bigels.[12] Such gels consist of a controlled layer that is responsive to the environmental stimuli and a nonresponsive substrate layer. A 10-fold change in volume can be reached for the control layer as a consequence of a thermally induced abrupt change in the gel microstructure. The drastic swelling and shrinking of the control layer guarantees that the bigel strip bends uniformly upon heating to form an arch and recovers to the strip upon cooling.[12] Wang and co-workers synthesized polyaniline asymmetric membranes with integral skin.[11] The asymmetric volume expansion/ contraction because of the presence/ absence of counterions makes the membrane undergo bending/unbending movement. It has to be noted that, as the membranes' sensitivity relies on film thickness, thinner membranes will be more sensitive. A metal/polymer composite bilayered film with a thickness at the micrometer scale

was prepared by Sun and Ma,[13] in which 10% of absorbed water within the polymeric layer was enough for the bilayered film to exhibit such bending/unbending movement upon humidity changes.

Wettability is a fundamental property of a solid surface, which plays an important role in the adhesion of proteins, cells, microorganisms as well as other contaminants on surfaces. Functional surfaces with controlled wettability have raised great interest because of their great advantages in various applications.[14-17] For example, superhydrophobic surfaces with a water contact angle larger than 150° and a sliding angle less than 10° exhibited excellent water-repellent properties, while hydrophilic surfaces can absorb water and water-soluble moieties easily. Such superhydrophobic surfaces are known as self-cleaning or anti-adhesive. It would be interesting to design an ultrathin film with asymmetric wettability, since the opposite surfaces may respond unequally to water.

The layer-by-layer (LBL) assembly (also called multilayer assembly) provides a simple, versatile, and robust tool for constructing ultrathin films with different functionalities.[18-22] The sensitivity of the LbL film toward the environmental parameters (including pH, ionic strength, etc.) further provides the possibility to modulate the layered nanostructure at will. Recently, the facial LBL technique has become an attractive way to fabricate free-standing films.[23-33] Many efforts have been devoted to both improve mechanical properties[25-28] and explore novel functionalities[29-32] of LbL free-standing films. Although the LbL assembly provides an approach to fabricate asymmetric films since the top and the underlying layer can be easily made of different polyelectrolytes with different structures and functionalities, only few studies[23,33] have paid attention to the asymmetric properties of free-standing films. Herein, we report the facial fabrication of a free-standing LbL multilayer film with asymmetric topography, which further exhibits an asymmetric wettability, namely, superhydrophobic and hydrophilic. We found that the free-standing film with asymmetric topography and wettability presents extraordinary shape-transition properties based on reversible humidity changes.

The approach is based on our previously published method to develop hierarchical micro- and nanostructured surfaces by the alternating deposition of the polycation at high pH and the polyanion at low pH.[34] Following the method initially reported by Lutkenhaus et al.[23] of preparing a free-standing film after deposition of the film onto a low surface energy substrate, we immersed a Teflon plate alternately into polyethylenimine (PEI, 1 mg/mL) at pH 9.0 and poly(acrylic acid) (PAA, 3 mg/mL) at pH 2.9 (for 15min each) to form multilayers. The films were then thermally crosslinked following an established procedure for the heat-induced amide formation of the carboxylate-ammonium complexes.[35] This was achieved in a sealed chamber in the presence of a low surface energy silane (tridecafluoroctyl)-triethoxysilane, which was employed here to reduce the film's surface energy to render it superhydrophobic. The treatment was performed at 130 ℃ for 2.5 h. Finally, the free-standing film with opposite wettability was obtained by peeling it away from the substrate. As shown in our previous study,[34] the pH shifts during the assembly of the weak polyelectrolytes PEI and PAA lead to a drastic change in the ionization degree of the polyelectrolytes in the multilayer. This enhances

PEI diffusion into and out of the films and hence increases the deposited mass per cycle. The synergetic action of the pH-dependent charge density and diffusivity of the weak polyelectrolytes provided a facile method to rapidly fabricate multilayers. The film build-up process was monitored by quartz crystal microbalance (QCM), and its thickness was estimated by scanning electron microscopy (SEM) after performing a cross section (Figure 1). The film grows exponentially and rapidly as the number of deposited layers increases.

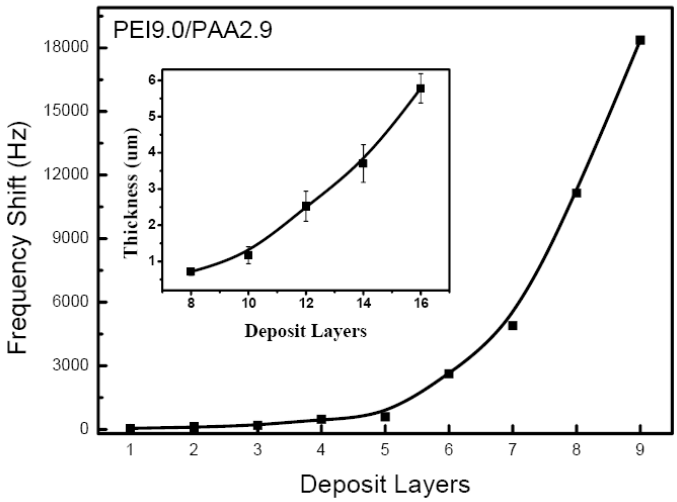

Figure 1. *QCM data of the PEI/PAA film growth on a QCM crystal. Insert: film thickness of PEI/PAA film deposited on silicon and measured by SEM.*

A film made of nine layers leads to a frequency shift of ~18 500 Hz, which corresponds to a mass of 126.8 μg/cm^2 according to Sauerbrey's equation. A 16-layer film reached a thickness of 5.6 μm as observed by SEM cross-sectional measurements. Although the films on Teflon substrate grew much more slowly due to poor initial absorption onto the substrate, the free-standing $(PEI/PAA)_{20}$ film reached a thickness of 11.6 μm (Figure 2A), as can be observed by SEM. The enlarged diffusion "in" and "out" of PEI due to the pH shift not only resulted in the amplified exponential growth but also in the roughening of the film surface. Figure 2B shows that the surface initially facing the substrate (indicated as bottom surface) was relatively smooth while the upper surface ending with PAA was very rough (Figure 2C), with wormlike features of 5-10 μm in size, in which many granular nanostructures and nanopores can be observed (Figure 2D). The detachment of the films from the hydrophobic substrate did not change the morphology of the upper surface. The film thermal crosslinking was confirmed by infrared spectroscopy (Supporting Information Figure S1). The disappearance of the amine band around 3380 cm^{-1} and emergence of an amide A band around 3000 cm^{-1} indicated amide formation. The peaks corresponding to COOH and COO^- groups did not change much because of the large number of COOH and COO- groups compared to amino groups in the films terminated by PAA as the outermost layer. Silane can be grafted to the film by reacting with the free amino groups on the film surface[17] (see Supporting Information Scheme S2). X-ray photoelectron spectroscopy data confirmed the successful deposition of the silane (Supporting Information Figure S2).

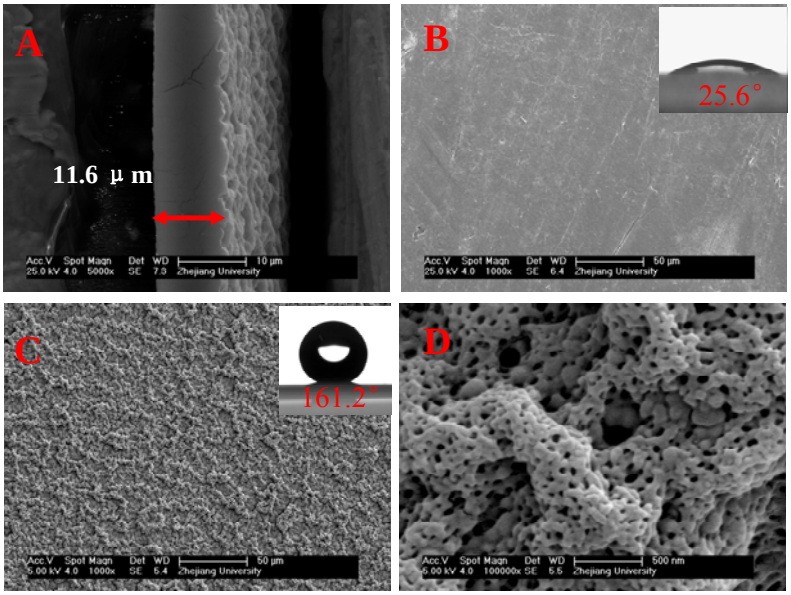

Figure 2. *SEM images of the free-standing films after detachment from the Teflon substrate. A) Cross-section of free-standing (PEI/PAA)$_{20}$ film, which is 11.6 μm thick. B) Surface morphology of the bottom surface which was facing the Teflon substrate before detachment. C) Surface morphology of the upper surface. D) Magnified image of C). The insets in B) and C) show the corresponding water contact angle measurements. The contact angle was high (161.2°) on the upper surface, while it rapidly decreased to 25.6° on the bottom surface.*

The film with an asymmetric surfacemorphology here provides a platform to construct a free-standing film with asymmetric wettability. After coating with a layer of a low surface energy silane and thermally crosslinking the films, the water contact angle of the upper surface reached 161.2° (Figure 2 C inset), indicating that it was superhydrophobic. Conversely, the water contact angle of the bottom surface was relatively low at 25.6°. This sharp difference in wettability leads to a very different behavior of these two surfaces when put in contact with water.

Indeed, this leads to extraordinary shape transitions induced by humidity changes. Figure 3 shows the shape changes that can be observed upon variation in the relative humidity (RH) of the environment. The film initially equilibrated at RH 75% under 20 ℃ was rolled bottom surface inside (Figure 3A). When the film was exposed to higher humidity (95% at 20 ℃), it first extended (Figure 3B) and then rolled up and wrapped the upper surface inside (Figure 3 C). Such shape transition occurred in about 1 min. When the film thereafter was put back to a lower humidity (75% at 20 ℃), it behaved exactly the inverse way (Figure 3D-F and Supporting Information 3). It first relaxed to be flat from the upper surface inside situation and then rolled down and wrapped the bottom surface inside. This phenomenon was totally reversible over 50 cycles.

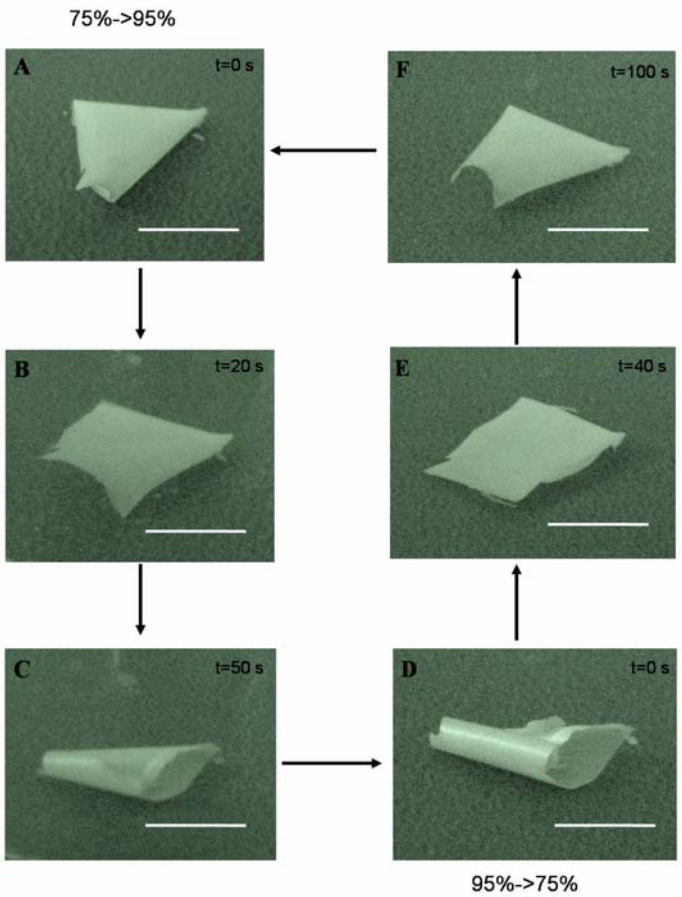

Figure 3. *Time lapse images of shape transitions of an asymmetric free-standing $(PEI/PAA)_{20}$ film after changing the relative humidity of the environment. The upper surface of the film is superhydrophobic. Left: the RH was increased from 75% to 95% (from A to C); right: the RH was set back to 75% and the shape changes were observed (from D to F). The experiments were performed at room temperature (20 °C). Scale bar is 1 cm.*

Hydrodynamic shape transition of LbL related film has been investigated by Fujie et al.[36] A free-standing film consisting of thermoresponsive 47 nm thick pNIPAM polymer brushes on a 41 nm thick polysaccharide nanosheet was constructed by the combination of spin-coating-assisted layer-by-layer assembly and atom transfer radical polymerization (ATRP). The film was found to exhibit reversible structural color changes when the temperature changes. However, the film fabrication process was relatively complex and the stimuli responsive ability mainly came from the relatively thick pNIPAM polymer brushes and not the LbL film. In fact, previous works have reported that multilayer films can respond to environmental stimuli such as humidity changes and undergo water absorption and desorption coupled with dimension expanding or shrinking.[13,37,38] For example, Kleinfeld and Ferguson found that PDDA/hectorite multilayered films adsorbed water rapidly and reversibly upon cycling repeatedly between dry and wet atmospheres. The ellipsometric thickness of a $(PDDA/hectorite)_{25}$ film increased from 67.2 nm at RH 0.5% to 82.1 nm at RH 87%.[37] Here, we found the relative mass of $(PEI/PAA)_{20}$ free-standing films changes reversibly when cycling between high RH and low RH (see Supporting Information Figure S3). More interestingly, we show that, by introducing an asymmetric wettability into two surfaces of an ultrathin film, the shape changes can be significantly amplified and be coupled to a curvature

transition. The asymmetric free-standing film with a superhydrophobic upper surface and a bottom hydrophilic surface which is water absorbable converts the small volume and/or dimension changes to a noticeable shape and curvature transition.

After thermal crosslinking, the mass of the film decreased by 10% (0.0262 g out of 0.26 g initially for the whole film), indicating some water was expelled out of the film during the crosslinking procedure and evaporated in the sealed chamber. We estimate that the increase in water vapor pressure during the crosslinking process leads to a 13% increase in RH (see the Supporting Information), which may explain why the film appears flat at RH ~ 85%. Our hypothesis is that the film may "memorize" the shape it had at the end of the crosslinking process.

This humidity can be considered as the critical point. Figure 4 D to F represents schematically the different shapes of the asymmetric free-standing films upon different humidity. When the humidity is increased from 85% to 95% (at 20 ℃), the bottom surface absorbs more water and expands in length. However, the upper surface is water resistant and remains at its original size.

The mismatch between the two surfaces leads to a film bending upward and coiling of the superhydrophobic surface inside (Figure 4 A and D). This coiled shape was obtained in 30 s and maintained under the atmosphere of high humidity (95% at 20 ℃). When the humidity is decreased, the film loses water from the bottom surface and its length decreases. When the humidity is lower than the "memorized" point (85% at 20 ℃ in this case), for example, at RH 75%, the bottom surface contracts and the film bends down to the bottom side (Figure 4 C and F). It takes around 80 s for the film to coil the hydrophilic surface inside. This appears reasonable and is indeed in accordance with the results reported elsewhere,[36] because the water desorption from the film is much slower than adsorption by the film.

The superhydrophobicity obtained from the combination of micro-nano hierarchical surface structures and low surface energy coating of the upper surface is crucial for the reversible humido induced shape-transition. Two other asymmetric free-standing films were also constructed (see Supporting Information Scheme S1): One is of asymmetric topography; that is, the upper surface is micro-nano hierarchical structured but without low surface energy coating. In this case, the water contact angle on the upper surface is 90°; the other one has a flat upper surface (see Supporting Information Figure S4) and is coated with a low surface energy compound, which provides it with asymmetric wettability (water contact angle of the upper surface is 107.5°). The fact that the upper surfaces were hydrophobic, not superhydrophobic, limited the humido-response of the films, resulting in weakening or even loss of their ability to sustain reversible shape transitions. The rough/flat asymmetric free-standing film always wrapped the bottom surface inside at high, low, and intermediate RH; and the hydrophobic/hydrophilic asymmetric free-standing film rolled irregularly and irreversibly when exposed to higher humidity (data not shown).

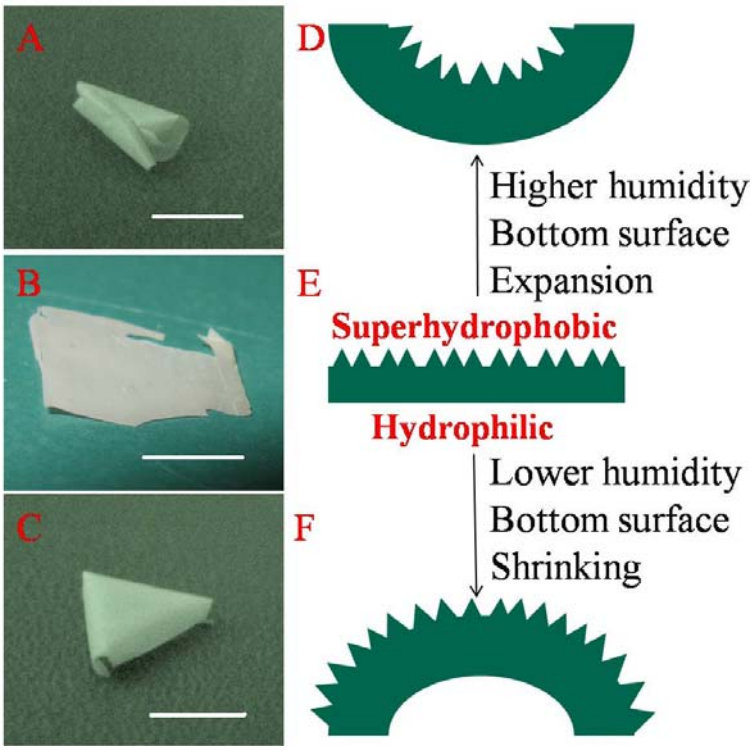

Figure 4. *Left: Images of the steady-state shapes of a $(PEI/PAA)_{20}$ free-standing film under different RH (T = 20 ℃). A) at 95% RH, the upper surface is rolled inside, B) at 85% RH, the film is almost flat, C) at 75% RH, the bottom surface is rolled inside. Right: Schematic illustration of shape transitions of an asymmetric free-standing film towards humidity changes. The upper surface is superhydrophobic and the lower surface is hydrophilic (E). The bottom surface can either shrink (F) or expand (D) leading to different shape transitions. Scale bars show 1 cm.*

All together, these data indicate that asymmetries in topography as well as in wettability are both required to achieve the optimal effects. The fast and pronounced responses combined with robustness of the free-standing film make it a good candidate for applications as a sensor or detector. Modulation of the crosslinking conditions may provide an additional way to further tune the relative humidity range over which the film can respond.

In conclusion, we have demonstrated a facile method for creating an asymmetrical free-standing film by the alternated deposition of PEI at high pH and PAA at low pH on a Teflon substrate. After coating with a layer of a low surface energy compound, the released free-standing films with asymmetric surface morphology and wettability can exhibit reversible humidity-induced shape transitions. The concept of asymmetric functionalization may largely expand the fundamental research area and broaden the application fields of the free-standing films. Other functionalities and associated properties originating from the asymmetry of free-standing films will be investigated in future studies.

Acknowledgment.

Financial support from the Natural Science Foundation of China (20774082, 50830106), National Science Fund for Distinguished Young Scholars (51025012), Open Project of State Key Laboratory of Supramolecular Structure and Materials (SKLSSM200911), the

Fundamental Research Funds for the Central Universities (2009QNA4039), Ph.D. Programs Foundation of Ministry of Education (No. 20070335024), NSFC-ZJ (Y4080250), as well as the FrenchMinistry of Foreign and European Affairs (Egide, Eiffel Scholarship to L.S.) are gratefully acknowledged.

Supporting Information Available:

Description of experimental and calculation details (Supporting Information 1) and two videos showing the shape transition when the film was taken to RH 75% from RH 95% and the shape transition when the film was taken to RH 95% from RH 75% (Supporting Information 2 and 3, respectively). This material is available free of charge via the Internet at http://pubs.acs.org.

REFERENCES

[1] Ulijn R. V., Bibi N., Jayawarna V., Thornton P. D., Todd S. J., Mart R. J., Smith A. M., Gough J. E. *Mater. Today* **2007**, *10*, 40.

[2] Tokarev I., Minko S. *Soft matter* **2009**, *5*, 511.

[3] (a) Peyratout C. S., Dähne L. *Angew. Chem. Int. Ed.* **2004**, *43*, 3762, (b) Wang Y., Xu H., Zhang H, X. *Adv. Mater.* **2009**, *21*, 2849.

[4] Sukhishvili S. A. *Curr. Opin. Colloid Interface Sci.* **2005**, *10*, 37.

[5] Tokarev I., Minko S. *Adv. Mater.* **2009**, *21*, 241.

[6] Osada Y., Okuzaki H., Hori H. *Nautre* **1992**, *355*, 242.

[7] Ikeda T., Mamiya J., Yu Y. *Angew. Chem. Int. Ed.* **2007**, *46*, 506.

[8] Hua F., Cui T., Lvov Y. M. *Nano. Lett.* **2004**, *4*, 823.

[9] Singamaneni S., McConney M. E., LeMieux M. C., Jiang H., Enlow J. O., Bunning T. J., Naik R. R., Tsukruk V. V. *Adv. Mater.* **2007**, *19*, 4248.

[10] Yu Y., Nakano M., Ikeda T. *Nature***, 2003,** *425***,** 145

[11] Wang H.-L., Gao J., Sansinena J.-M., McCarthy P. *Chem. Mater.* **2002,** *14*, 2546.

[12] Hu Z., Zhang X., Li Y. *Science* **1995**, *269*, 525.

[13] Ma Y., Sun J. *Chem. Mater.* **2009**, *21*, 898.

[14] (a) Sun T. L., Feng L., Gao X. F., Jiang L. *Account of Chemical Research,* **2005**, *38***,** 644, (b) Xia F., Jiang L. *Adv. Mater,* **2008**, *20*, 2842, (c) Feng L., Zhang Z. Y., Mai Z. H., Ma Y. M., Liu B. Q., Jiang L., Zhu D. B. *Angew. Chem. Int. Ed.* **2004**, *43*, 2012, (d) Shi F., Wang Z. Q., Zhang X. *Adv. Mater.* **2005**, *17*, 1005.

[15] (a) Wang R., Hashimoto K., Fujishima A., Chikuni M., Kojima E., Kitamura A., Shimohigoshi M., Watanabe T. *Nature* **1997**, *388*, 431, (b) Blossey R. *Nat. Mater.* **2003**, *2*, 301, (c) Lahann J., Mitragotri S., Tran T. N., Kaido H., Sundaram J., Choi I. S., Hoffer S., Somorjai G. A., Langer R. *Science* **2003**, *299*, 371.

[16] (a) Soeno T., Inokuchi K., Shiratori S. *Tran. Mater. Res. Soc. Jpn.* **2003**, *28*, 1207, (b) Jisr R. M., Rmaile H. H., Schlenoff J. B. *Angew. Chem. Int. Ed.* **2005**, *44*, 782, (c) Aulin C., Yun S.

H., Wågberg L., Lindström T. *ACS Appl. Mater. Interfaces* **2009**, *1*, 2443, (d) Wang L., Peng B., Su Z. *Langmuir*, **2010**, *26*, 12203.
[17](a) Zhai L., Cebeci F. C., Cohen R. E., Rubner M. F. *Nano Lett.* **2004**, *4*, 1349, (b) Ma M. L., Gupta M., Li Z., Zhai L., Gleason K. K., Cohen R. E., Rubner M. F., Rutledge G. C. *Adv. Mater.* **2007**, *19*, 255.
[18] (a) Decher G., Eckle M., Schmitt J., Struth B. *Curr. Opin. Colloid. Interface Sci.* **1998***, 3,* 32, (b) Leguen E., Chassepot A., Decher G., Schaaf P., Voegel J.-C., Jessel N. *Biomol. Eng.* **2007***, 24,* 33.
[19] (a) Han Y., Radziuk D., Shchukin D., Moehwald H. *Macromol. Rapid. Commun.* **2008**, *29*, 1230, (b) Dronov R., Kurth D. G., Moehwald H., Scheller F. W., Lisdat F. *Angew. Chem. In. Ed.* **2008**, *47*, 3000.
[20](a) Picart C. *Curr. Med. Chem.* **2008**, *15*, 685, (b) Boudou T., Crouzier T., Ren K., Blin G., Picart C. *Adv. Mater.* **2009**, *21*, 441.
[21](a) Ariga K., Hill J. P., Ji Q. *Phys. Chem. Chem. Phys.* **2007**, *9*, 2319, (b) Ariga K., Hill J. P., Ji Q. *Macromol. Biosci.* **2008**, *8*, 981.
[22] (a) Li X., Zhou Y., Zheng Z., Yue X., Dai Z., Liu S,, Tang Z. *Langmuir* **2009,** *25***,** 6580, (b) Liu M., Yue X., Dai Z., Ma Y., Xing L., Zha Z., Liu S., Li Y. *ACS Applied Materials&Interfaces* **2009**, *1*, 113.
[23]Lutkenhaus J. L., Hrabak K. D., McEnnis K., Hammond P. T. *J. Am. Chem. Soc.* **2005**, *127*, 17228.
[24]Jiang C., Tsukruk V. V. *Adv. Mater.* **2006**, *18*, 829.
[25]Mamedov A. A., Kotov N. A., Prato M., Guldi D. M., Wicksted J. P., Hirsch A. *Nat. Mater.* **2002**, *1*, 190.
[26]Tang Z., Kotov N. A., Magonov S., Ozturk B. *Nat. Mater.* **2003**, *2*, 413.
[27]Olek M., Ostrander J., Jurga S., Mo1hwald H., Kotov N., Kempa K., Giersig M. *Nano Lett.* **2004**, *4*, 1889.
[28]Podsiadlo P., Qin M., Cuddihy M., Zhu J., Critchley K., Kheng E., Kaushik A. K., Qi Y., Kim H.-S., Noh S.-T., Arruda E. M., Waas A. M., Kotov N. A. *Langmuir*, **2009**, *25*, 14093.
[29]Lin Y.H., Jiang C., Xu J., Lin Z.Q., Tsukruk V.V. *Soft Matter.* **2007**, *3*, 432.
[30]Fujie T., Okamura Y., Takeoka S. *Adv. Mater.* **2007**, *19*, 3549.
[31]Fujie, T. Okamura Y., Takeoka S. *Colloids Surf., A: Physicochem. Eng. Aspects* **2009**, *334*, 28.
[32]Okamura Y., Kabata K., Kinoshita M., Saitoh D., Takeoka S. *Adv. Mater.* **2009**, *21*, 4388.
[33](a) Lutkenhaus J. L., McEnnis K., Hammond P. T. *Macromolecules* **2008**, *41*, 6047, (b) Kim B. S., Park S. W., Hammond P. T. *ACS Nano* **2008**, *2*, 386, (c) Seo J., Lutkenhaus J. L., Kim J., Hammond P.T., Char K. *Langmuir,* **2008**, *24*, 7995.
[34] (a) Ji J., Fu J. H., Shen J. C. *Adv. Mater.* 2006, 18, 1441 (b) Fu J., Ji J., Shen L., Küller A., Rosenhahn A., Shen J., Grunze M. *Langmuir* **2009**, *25*, 672.
[35] Harris, J. J.; DeRose, P. M.; Bruening, M. L. *J. Am. Chem. Soc.* **1999**, *121*, 1978.
[36]Fujie T., Park J. Y., Murata A., Estillore N. C., Tria M. C. R., Takeoka S., Advincula R. C.

ACS Appl. Mater. Interfaces **2010**, *2*, 1404.
[37] Kleinfeld E. R., Ferguson G. S. *Chem. Mater.* **1995**, *7*, 2327.
[38] Kügler R., Schmitt J., Knoll W. *Macromol. Chem. Phys.* **2002**, *203*, 413.

Supporting information 1

Free-standing film fabrication:

PEI/PAA multilayer films were constructed using 1 mg/mL PEI (pH 9.0) and 3 mg/mL PAA (pH 2.9) aqueous solutions on the hydrophobic Teflon substrates. The multilayer films were built by first immersing Teflon plate into the PEI solution for 15 min followed by rinsing with pure water (with an pH of approximately 5.5) for three times and blowing dry with a gentle stream of nitrogen; The substrates were then immersed into PAA solution for 15min followed by washing three times with pure water and nitrogen blowing dry. The adsorption, washing and drying steps were repeated until 19.5 layer pairs (for PEI outermost films) and/or 20 layer pairs (for PAA outermost films) were obtained. The films were then thermally crosslinked by heating at 130°C for 2.5 hours in a sealed chamber with (for superhydrophobic/hydrophilic and hydrophobic/hydrophilic asymmetric films, Scheme S1 (A) and (C)) or without (for rough/flat asymmetric film, Scheme S1 (B)) (tridecafluoroctyl)triethoxysilane. (Tridecafluoroctyl)triethoxysilane is used here as a low surface energy compound to obtain very low surface energy surfaces via chemical vapor deposition. Finally, the multilayered films were peeled away from the hydrophobic substrate using tweezers.

The superhydrophobic/hydrophilic asymmetric free-standing film Scheme S1 (A) was reported in the paper gaining humido-responsive ability. The other two free-standing films were made to confirm the importance of superhydrophobicity of the upper surface for humido-responsive capability.

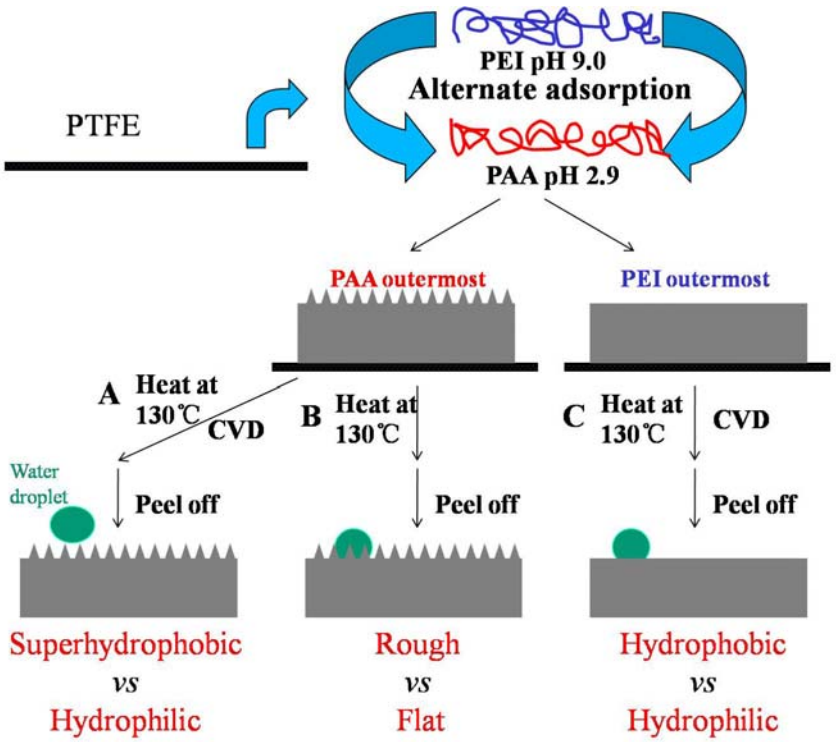

Scheme S1: Schematic illustration for the fabrication of three kinds of asymmetric free-standing films.

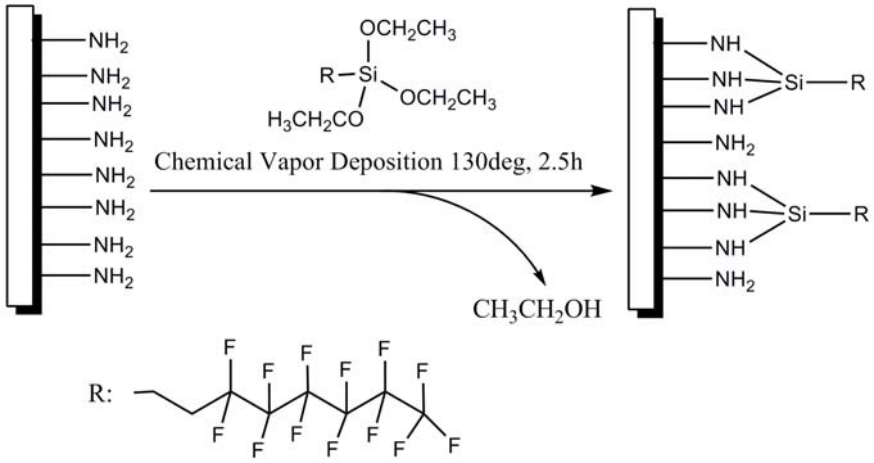

Scheme S2: Schematic illustration of the reaction between silane and amino groups on PEI/PAA film when chemical vapor deposition of silane occurred.

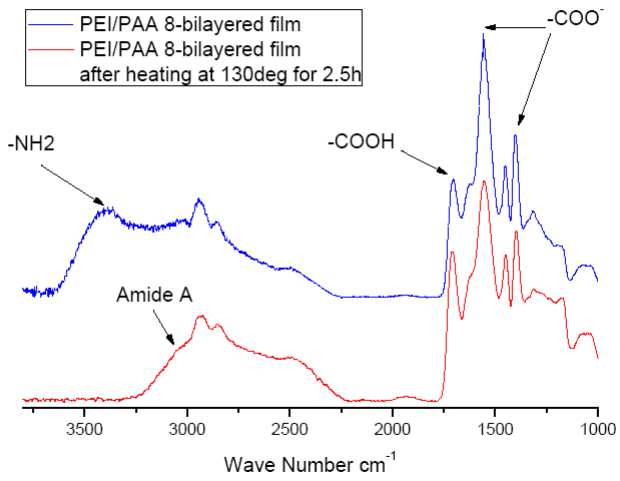

Figure S1: Infrared spectrum of $(PEI/PAA)_8$ film before (blue) and after (red) thermal crosslinking. The films were built on silicon wafer and the spectra were collected in transition mode.

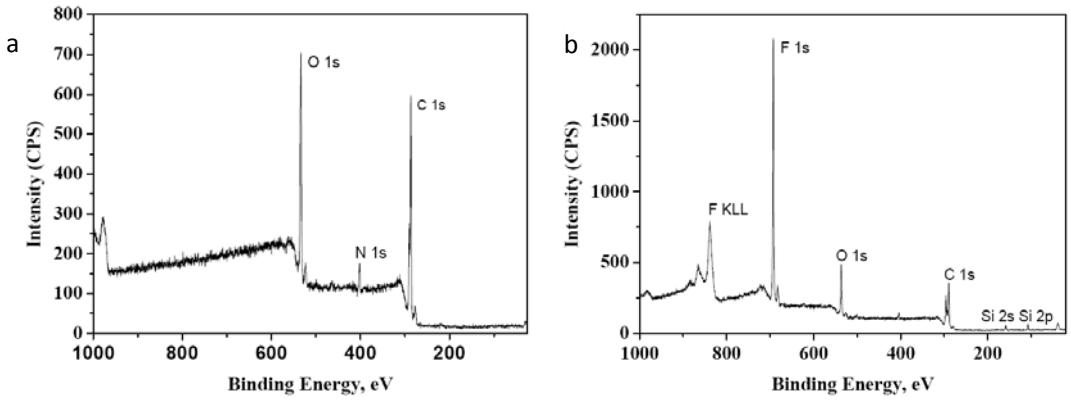

Figure S2: XPS data of a $(PEI/PAA)_8$ film before (a) and after (b) silane deposition. The films were built on silicon wafer.

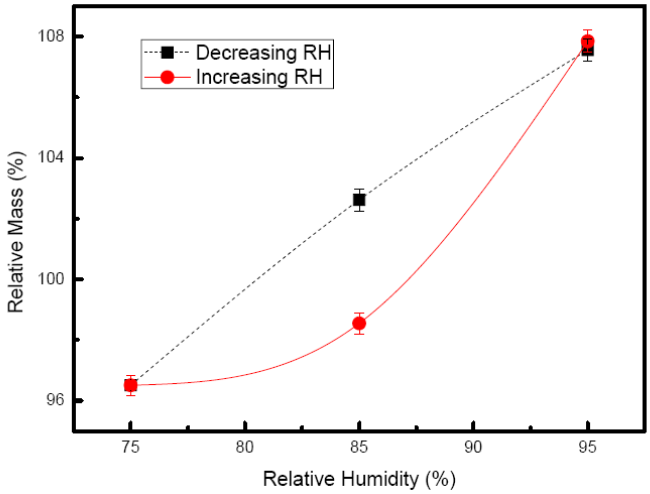

Figure S3: Relative mass of $(PEI/PAA)_{20}$ free-standing film as a function of relative humidity. The square (dash line) corresponds to a decrease in RH while the circle (solid line) corresponds to an increase in RH. The mass of $(PEI/PAA)_{20}$ free-standing film after thermally crosslinking was used as reference. Measurements performed at room temperature, T=25 ℃ by electronic balance.

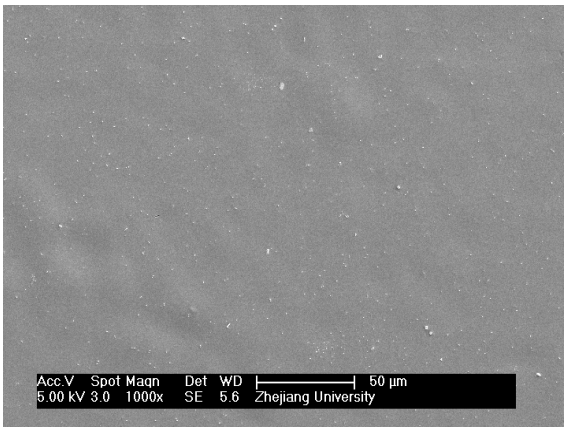

Figure S4: SEM image of PEI outermost upper surface. The surface morphology of PEI ending film is flat and featureless with a slight granular structure. The water contact angle after being coated with a low surface energy (tridecafluoroctyl)-triethoxysilane is 107.5°.

Water vapor pressure increment calculation: When the film was heated in a sealed chamber, water adsorbed on the film can go out of the film and increase water pressure in the chamber. According to Clapeyron equation for ideal gas

$PV=nRT$

Where P is the pressure increment of the gas of interest, V is the volume the gas filled, n is the mole of gas, R is the gas constant (8.314472 L·kPa·K·mol) and T is the absolute temperature (293.15 K).

The water vapor pressure increment at a given temperature can be estimated by knowing the volume of the chamber (12 L) and the mass decreased for a film after crosslink, which was caused by water evaporation (0.0262 g in this case). The water vapor pressure increment was calculated to be 295.5 Pa, which can be easily transformed to relative humidity at a given temperature. For example, the saturated water vapor pressure at 20°C is 2337.8 Pa, so 295.5 Pa corresponds to an increase of 13% of the relative humidity. Considering the relative humidity in the lab is around 75%, the water vapor pressure at the end of crosslink equals to about RH 85% at 20°C.

2.2 Asymmetric Free-Standing Film with Multifunctional Anti-Bacterial and Self-Cleaning Properties

2.2.1 Summary

Introduction

Free-standing films have aroused numerous research interests due to their unique properties compared to bulk materials, such as transparency, flexibility, selective permeability, adhesiveness and so on. Recently, free-standing film has also found application in biomedical fields as membrane for defect repair (Fujie et al. 2009).

Multifunctionality can be needed in some cases such as for wound dressing (Boateng et al. 2008). Infection is one of the big problems after surgery as well as for burning defects, for this reason, antibacterial activity is demanded for wound dressing materials; to promote wound healing, semi-permeation of the membrane is required for keeping water and useful moieties in contact with the wound but getting away the smelling gas; and the wound dressing membrane should protect the defect from the outer environment.

Layer-by-layer assembly is a suitable technique to construct ultrathin coatings or films with multifunctionality as this method allows the incorporation of multiple functional components and can control their deposition in a nanometer level. Meanwhile, previous work has already proved the successful fabrication of asymmetric free-standing film via layer-by-layer assembly.

In this work, a silver nanoparticles loaded free-standing film with one surface surperhydrophobic and the other surface being hydrophilic was created via amplified layer-by-layer assembly. The anti-adhesive and self-cleaning properties of the superhydrophobic surface and the bactericidal activity of the hydrophilic surface which extensively releases silver ions were studied.

Results and discussion

Teflon substrate (or PET) was alternately dipped into poly(ethylene imine)-Ag^{+} complex (PEI-Ag^{+}) solution and Poly(acrylic acid) (PAA) solution for 15 min respectively to form multilayers. After thermal cross-linking and chemical vapor deposition of low surface energy

silane, the free-standing film with one surface hierarchically structured and superhydrophobic (CA=168.2°) and the other surface being flat and hydrophilic (CA=52.7°) was obtained. Of note, the asymmetric free-standing film embedded with silver nanoparticles, which were reduced from silver ions on the thermal cross-linking step.

Silver ions were found to release one-directionally from the bottom surface due to the anti-wetting properties of the superhydrophobic top surface, and ensured the film with high antibacterial activity. Meanwhile, the superhydrophobic surface showed extraordinary self-cleaning and anti bacterial adhesion abilities.

Conclusion

An easy way to construct asymmetric free-standing film loaded with silver nanoparticles by amplified layer-by-layer assembly was reported. The solid isolated free-standing films have asymmetric surface morphology, which resulted in asymmetric wettability of superhydrophobic *vs* hydrophilic. The superhydrophobic surface was proved to limit bacterial adhesion and to be self-cleaning, while the hydrophilic surface can extensively deliver bactericidal silver ions.

2.2.2 Article

Asymmetric Free-Standing Film with Multifunctional Anti-Bacterial and Self-Cleaning Properties

L. Shen, B. Wang, J. Wang, J. Fu, C. Picart, J, Ji,

submitted to *ACS Applied Materials & Interfaces*

Asymmetric Free-Standing Film with Multifunctional Anti-Bacterial and Self-Cleaning Properties

Liyan Shen, Bailiang Wang, Jinlei Wang, Jinhong Fu, Catherine Picart, Jian Ji

ABSTRACT:

A superhydrophobic/hydrophilic asymmetric free-standing film has been created using layer-by-layer assembly technique. Poly(ethylene-imine)-Ag^+ complex (PEI-Ag^+) at pH 9 was assembled with poly(acrylic acid) (PAA) at pH 3.2 on a Teflon substrate to yield a micro-nanostructured surface that can be turned to be superhydrophobic after being coated with a low surface energy compound. Silver nano-particle loaded free-standing film with one surface being superhydrophobic while the other surface is hydrophilic was then obtained after detachment from the substrate. The superhydrophobicity enabled the upper surface with anti adhesion and self-cleaning properties and the hydrophilic bottom surface can release silver ions as antibiotic agent. The broad-spectrum antimicrobial capability of silver ions released from the bottom surface coupled with superhydrophobic barrier protection of the upper surface may make the free-standing film a new therapy for open wound.

KEYWORDS: Asymmetric, superhydrophobic, free-standing films, anti adhesion, drug release, layer-by-layer assembly

INTRODUCTION

Free-standing films can sustain their shape and other properties in air or liquid after been released from the substrates.[1] Thin free-standing films have aroused great interest because they exhibit dramatically different behavior when compared to bulk materials, with changes in properties such as glass transition,[2-4] transport,[5-7] and stress to failure.[8,9] Meanwhile, free-standing films have found great potential use as sensors,[10,11] barrier materials,[12] reflectors,[13] and electronic films.[14,15] Due to their unique properties including high flexibility,

non-covalent adhesiveness, transparency and large aspect ratio, free-standing films have found new use in the biomedical field.[16-23] Fujie et al.[16-18] reported the fabrication of a polysaccharide free-standing film via a spin-coating assisted layer-by-layer method, using alternating deposition of oppositely charged polysaccharides through electrostatic interactions. The polysaccharide free-standing films were proved to be capable to tightly and firmly repair a pleural injury/defect after thoracic surgery so as to prevent air leakage and postsurgical adhesion.[17] Recently, attention has been paid to the asymmetric properties, such as wettability and morphology, for the two surfaces of free-standing films. Lutkenhaus and co-workers[24] fabricated an asymmetric membrane with a fine porous skin layer and a thick microporous underlying layer via acidic postassembly treatment of a linear poly(ethylene-imine)/PAA (LPEI/PAA) multilayer. The same authors[25] also pointed out the possibility of constructing free-standing films with asymmetric wettability just after detachment of Poly(ethylene oxide)/PAA (PEO/PAA) LBL multilayer from substrates. The LBL assembly technique actually provides its attractive advantage to fabricate asymmetric free-standing films since the top and the underlying layer can be easily made of different polyelectrolytes with different structures and functionalities. Multifunctionality is desired for several applications. For example, the cure for wound dressing should be on one hand antibacterial and on the other hand keep the wound from the outer environment. We have previously constructed a humidity responsive free-standing (PEI/PAA) film via pH-amplified layer-by-layer assembly.[26] We showed that the film exhibited a fast and reversible humidity responsiveness, which originated from its asymmetric superhydrophobic/hydrophilic wettability. Indeed, we believe that the asymmetric wettability can be explored as more functionality since surface wettability plays a pivotal role in the contact of liquids with solids and in surface adhesion as well. A surperhydrophobic surface is known to be water-repellent and self-cleaning.[27] It provides a barrier to prevent water molecules from penetrating the film and protect it from the outer environment. In addition, the superhydrophobic barrier may also keep water and other moieties from leakage via diffusion, while water and water soluble moieties can be absorbed and/or desorbed by the hydrophilic surface easily.

In this work, a free-standing film loaded with silver nanoparticles with one surperhydrophobic surface and the other being hydrophilic was created via amplified layer-by-layer assembly on hydrophobic polytetrafluoroethylene (PTFE, name here Teflon). The LBL film was subsequently released from the substrate. The anti adhesive and self-cleaning properties of the superhydrophobic upper surface and the bactericidal activity of the hydrophilic surface which extensively release silver ions were studied.

EXPERIMENTAL SECTION

Fabrication of Free-standing films. PEI-Ag/PAA multilayer films were built by firstly immersing the Teflon substrate into PEI-Ag^+ solution (1 mg/mL, pH 9.0, Ag^+ 1.6 mM) for 15 min followed by three rinsing with pure water (with pH of approximately 5.5) and dried in a stream of N_2. The substrate was then immersed into PAA solution (3 mg/mL, pH 3.2) for 15

min followed by three washes with pure water and drying. The adsorption and washing steps were repeated until 40 layers were obtained. Chemical vapor deposition of triethoxy-tridecafluoro-n-octylsilane was performed on the films to obtain surfaces with very low surface energy. The multilayer films were placed in a sealed chamber together with triethoxy-tridecafluoro-n-octylsilane, the sealed chamber was placed in an oven at 130°C for 2.5 hrs. Then, the samples were withdrawn from the chamber, and placed in an oven at 180°C for 1.5 hrs to remove unreacted silane molecules. The thermal crosslinking, ie thermally-induced imide formation, and the reaction with silane and amino groups during chemical vapor deposition have been already established in our previous work.[26] Finally, the multilayer film was peeled away from the hydrophobic substrate using tweezers. For the studies on supported films, PET (polyethylene terephthalate) was always used as substrate.

Scanning Electron Microscopy (SEM). The surface morphology of both upper and bottom surfaces as well as the cross-section of the $(PEI\text{-}Ag/PAA)_{20}$ free-standing film was imaged using a field emission scanning electron microscope (FESEM; FEI, SiRion100).

Water Contact Angle. Surface wettability for both free-standing and supported films was determined via sessile drop contact angle (CA) measurements taken with a KRUSS DSA 100-MK2 contact angle system at ambient temperature. At five different positions, a 4 μL water droplet was dispensed onto the substrate and the average CA was measured and averaged for each sample.

Inductively Coupled Plasma Mass Spectrometry (ICP-MS). Silver ions release was carried out by immersing pieces of 5x5 mm^2 free-standing $(PEI\text{-}Ag/PAA)_{20}$ films in to 50 mL PBS at 37°C. For PET supported films, $(PEI\text{-}Ag/PAA)_{19}$-PEI-Ag or $(PEI\text{-}Ag/PAA)_{20}$ films with or without silane coating were studied in the same conditions. The Ag^+ concentrations at different release times were measured using ICP-MS PQ3 (X II, Thermo Scientific). To measure the total Ag NPs loading amount, a 5x5 mm^2 piece of film was dissolved in 1 mL HNO_3 and diluted to 50 mL, then the silver ion concentrations were determined by ICP-MS.

Bacteria Initial adhesion. The bacterial strain used herein was *Escherichia coli* (*E. Coli* BL21). The PET supported films were immersed in a bacterial suspension (10 ml) of 10^6 cells per mL in a sterile test tube. The test tube was then shaken at 37 °C for 4 h. After that the samples were taken out and washed three times with sterile PBS. The bacteria were then fixed in 3% glutaraldehyde for 30 min followed by step dehydration using 25%, 50%, 70%, 95% v/v water/ethanol mixture and finally pure ethanol. The samples were imaged by a field emission scanning electron microscopy (FESEM; FEI, SiRion100) after sputtering a thin gold layer. The number of *E. Coli* adhered on the samples were counted from the SEM images taken at magnification X5000. At lease 6 images were counted to give an average number for each sample.

Bactericidal Activity of the films. The bactericidal activity of the silver NPs incorporated films was tested using a Kirby-Bauer assay.[28] Briefly, the solid slabs of agar made from Cation-adjusted Mueller Hinton Broth II (CMHB) media and BactoAgar were used for

bacterial culturing. 1000 cells were planted on each plate, on which free-standing film bottom surface as well as PET supported films were placed film upside down. The plates were incubated at 37 °C overnight and then the inhibition zones were measured. All experiments were done in triplicate.

Digital camera images and videos were captured by Sony digital camera (SONY-H 9).

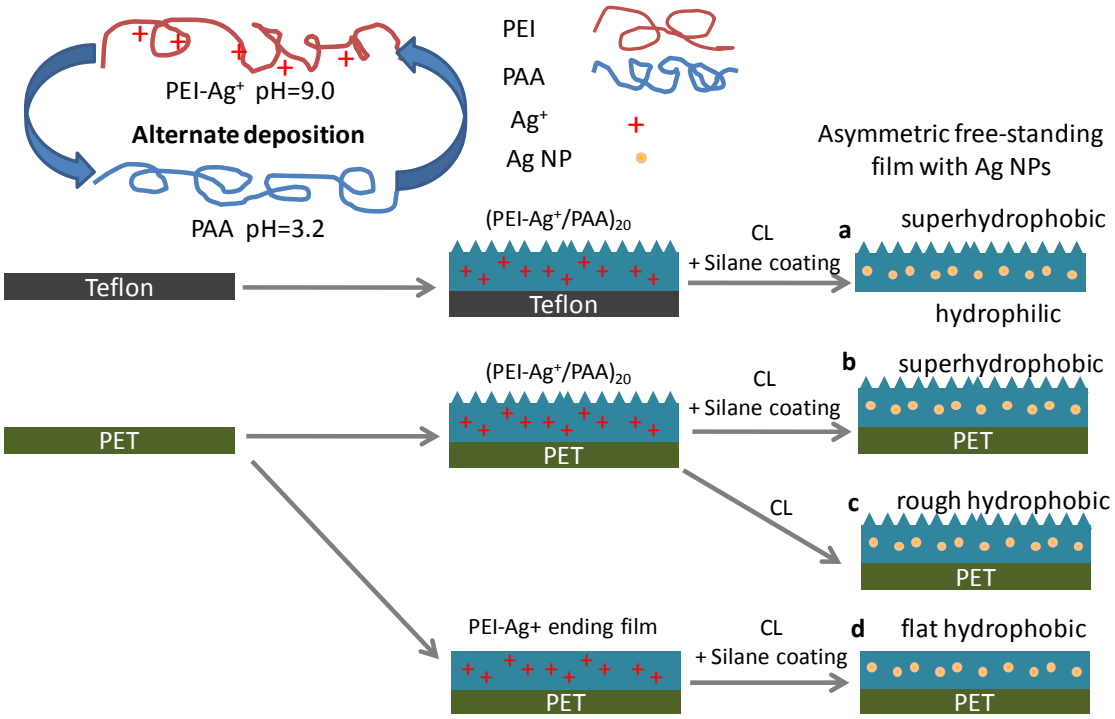

Scheme 1. *Schematic illustration of the fabrication of free-standing (a) and supported (b, c, d) films. Teflon substrate was used to construct free-standing film and PET substrate was used for the supported films. First, the substrates were alternately immersed in PEI-Ag$^+$ (pH=9.0) and PAA (pH=3.2) solutions to form 20 (a, b, c) or 19.5 (d) bilayered films (PAA-ending films or PEI-Ag+-ending films). Then, the films were heated in a sealed chamber to be thermally crosslinked (CL) in the presence (a, b, d) or absence (c) of an additional silane coating. Finally, free-standing film with top surface superhydrophobic and bottom surface hydrophilic (a) was obtained from Teflon substrate, and supported superhydrophobic film (b), supported hydrophobic rough film (c) and supported hydrophobic flat film (d) were obtained on PET substrate.*

RESULTS AND DISCUSSION

We have previously reported the construction of superhydrophobic multilayered films via silver ion amplified exponential growing layer-by-layer deposition.[28,29] Here we employed the same protocol while slightly increased the pH of PAA deposition solution, so that part of silver ions can still be captured in the films (see Table SI1). As shown in the scheme, the substrate (Teflon or PET) was alternately dipped into poly(ethylene imine)-Ag$^+$ complex (PEI-Ag$^+$) solution and poly(acrylic acid) (PAA) solution for 15 min respectively to form multilayers. The films were then cross-linked by heating and coated with triethoxy-tridecafluoro-n-octylsilane to reduce surface energy via chemical vapour deposition. Meanwhile, the silver ions incorporated were reduced to be silver nanoparticles[31,32] which can serve as the source for Ag$^+$ release.[33] Finally, the free-standing films with inverse wettability

were obtained by peeling them away from the Teflon substrates with tweezers. When the PET substrate was used, supported films with either flat or rough surface morphology depending on the outermost layer were constructed.

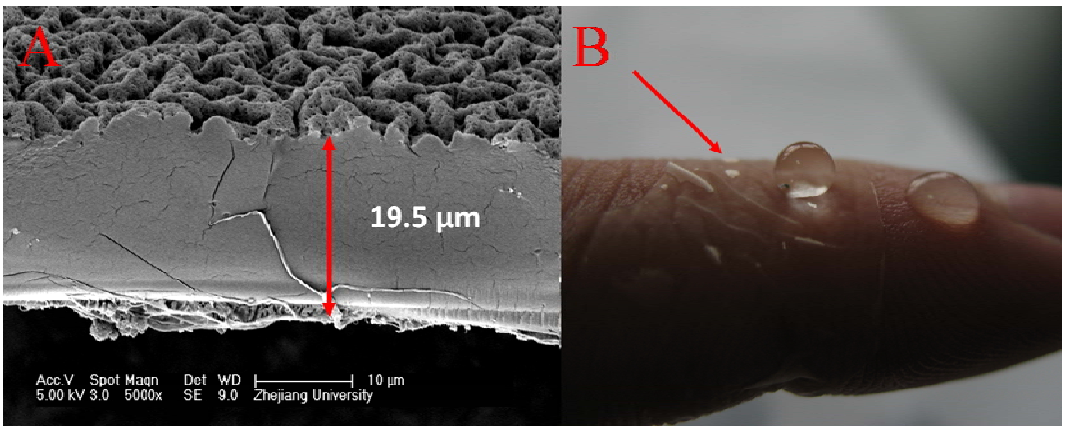

Figure 1. *(A) SEM image of the cross-section of free-standing $(PEI\text{-}Ag/PAA)_{20}$ film. (B) Digital photo of a free-standing $(PEI\text{-}Ag/PAA)_{20}$ film deposited on skin of finger. The top surface is superhydrophobic and the film is transparent.*

The thickness of a (PEI-Ag/PAA) film made of 20 layer pairs was of 19.5 ± 1.6 µm after peeling off from the Teflon substrate, as indicated in Figure 1 A. The free-standing film can be transferred to most liquid/air or solid/air interface including the human tissues easily, especially in wet state. As shown in figure 1 B, the free-standing film was flexible and attached easily to human skin. SEM was also applied to monitor the surface morphology for both top and bottom surfaces of free-standing film (see supporting information figure SI 1). The surface previously attached to the substrate (indicated as the bottom surface) was relatively smooth with some micro scale structures (figure SI 1 A) while the other surface which was far away from substrate (indicated as top surface) exhibited micro and nano-hierarchical topography (figure SI 1 B and C). These micro- and nano- structures combined with a low surface energy coating by a silane (triethoxy-tridecafluoro-n-octylsilane) ensured the superhydrophobicity of top surface. If the film was ending with PEI-Ag, quite flat surface morphology[26] with silver nanoparticles was observed (figure SI 1 D).

Water contact angles for PET-supported films and for free-standing films were measured. They are listed in table 1. The water contact angle on the hierarchically structured surface of the free-standing film was as high as 168.2°, indicating it was superhydrophobic whereas that of the bottom surface was relatively low at 52.7°. The sharp difference on wettability leads to very different behaviors of the two surfaces when set in contact with water. Two pieces of free-standing films were put on water, one with its top surface facing air (the left one in Supporting information 2) and the other with the bottom surface facing air (the right piece in Supporting information 2). Both films were well spread at the air-water interface. When water droplets were deposited onto the films, the water droplet on the top (superhydrophobic) surface remained a sphere for a long time, as anticipated, whereas a water droplet on the

bottom surface was gradually absorbed into the film. After ~ 16 s, the 15 µL droplet disappeared on the bottom surface.

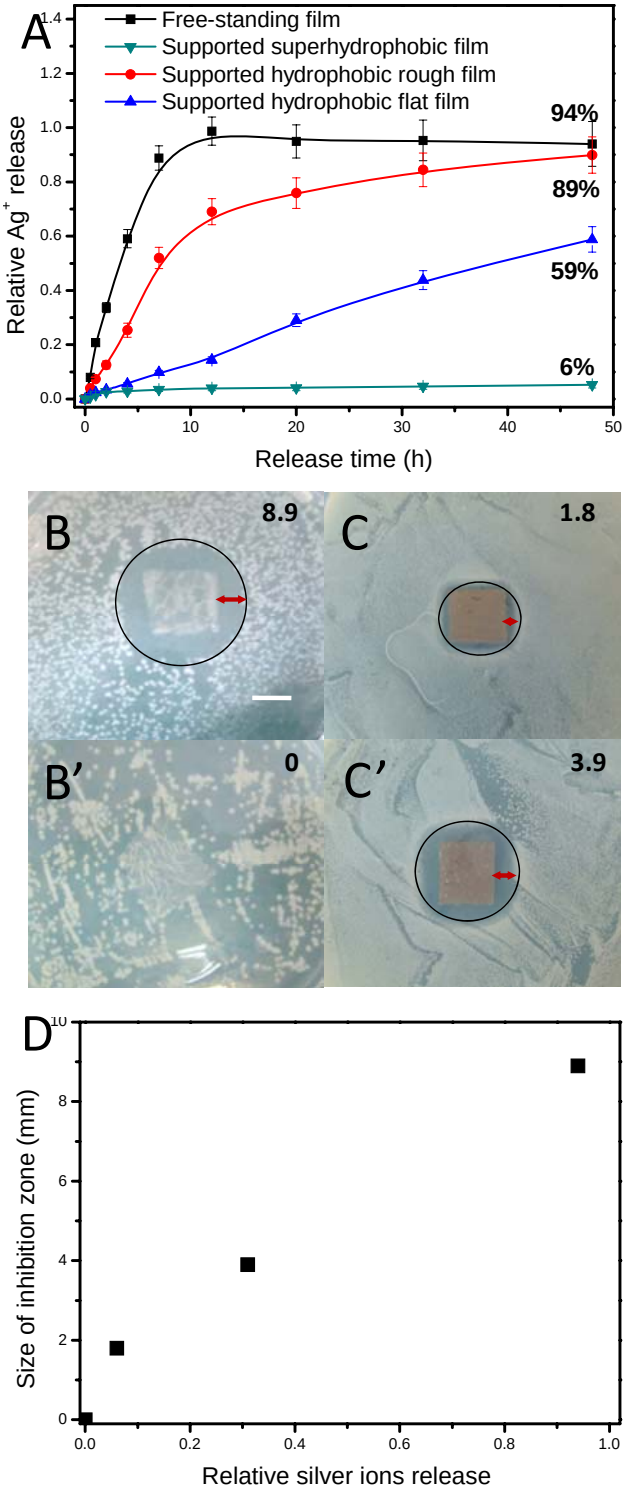

Figure 2. *(A) Silver ion release in percentage for different films including free-standing $(PEI\text{-}Ag/PAA)_{20}$ film (■), $(PEI\text{-}Ag/PAA)_{20}$ film adhering to PET without silane (●) and with silane (▼), PET supported $(PEI\text{-}Ag/PAA)_{19}$-PEI-Ag film with silane (▲). (B, B', C and C') E. Coli inhibition zone on agar nutrition with the bottom (hydrophilic) surface of a free-standing $(PEI\text{-}Ag/PAA)_{20}$ film (B) and a free-standing $(PEI/PAA)_{20}$ film (B'), PET supported $(PEI\text{-}Ag/PAA)_{20}$ film (C) and $(PEI\text{-}Ag/PAA)_{19}$-PEI-Ag film (C') with silane. The sizes of inhibition zone were 8.9, 0, 1.8 and 3.9 mm for B, B', C and C', as indicated in the right top corner of the images, respectively. (D) Plot of the inhibition zone sizes against relative silver ions release. Scale bar in B is 1 cm.*

Table 1 *Water contact angles for supported and free-standing films. Supported films are made of 40 layers for PAA-ending films, or of 39 layers for PEI-ending films.*

	(PEI-Ag/PAA) film on PET		**$(PEI\text{-}Ag/PAA)_{20}$ free-standing film**
	Thermal crosslinking	**Thermal crosslinking + silane coating**	**Thermal crosslinking + silane coating**
PAA-ending	126.2±1.3°	169.2±3.5°	168.2±2.5°[a] , 52.7±5.7°[b]
PEI-ending	98.6±0.8°	112.1±1.9°	

[a] measured on the top surface of $(PEI\text{-}Ag/PAA)_{20}$ free-standing film; [b] measured on the bottom surface of $(PEI\text{-}Ag/PAA)_{20}$ free-standing film

The amount of Silver NPs loaded in the free-standing $(PEI\text{-}Ag/PAA)_{20}$ film was 2.17 ± 0.08 μg/cm^2 determined by ICP-MS. The silver nanoparticles here provided a good source for Ag^+ release, to act as antibacterial agent [34]. The silver ions release behavior of both supported and free-standing films was tested. As demonstrated in figure 2 A, the free-standing film released silver ions rapidly and most of its silver ions were released in the first 12 hrs. In contrary, for PET supported superhydrophobic $(PEI\text{-}Ag/PAA)_{20}$ film, only 6% of the total silver was released in 48 hrs. These differences between free standing film and supported film clearly demonstrated that most of the Ag^+ in free-standing film was released from the bottom (hydrophilic) surface. To further understand the Ag^+ entrapment, the silver ions release behavior was also investigated for PET-supported hydrophobic films with rough (PAA-ending without silane coating) or flat (PEI-ending with silane coating) surfaces. As shown in figure 2 A, silver ions released quickly from the rough film (PAA-ending without silane coating). Indeed, this film released 89% of its Ag^+ content in 48 hrs. Compared to the lowest release for the PET supported superhydrophobic film (PAA-ending with silane coating), which released only 6% of silver ions, it is clearly demonstrated that the silane coating was important for Ag^+ entrapment. However, the micro-nano structure of the surfaces also contributed to the entrapment of Ag^+. The PET supported hydrophobic flat film, which is PEI-Ag^+ ending and coated with silane, can still release silver ions but in a much more gradually motion (~ 59% release in 48 hrs). Wetting plays a very important role in the release of water soluble moieties embedded within the film, such as Ag^+ here. For the bottom (hydrophilic) surface of free-standing film, water can diffuse in the film and this facilitated the ion release process. In contrary, for the top (superhydrophobic) surface, as water could not wet it, the release of Ag^+ was greatly inhibited.

Of note, neither the micro-nano structure on film surface alone (eg PAA-ending film without silane, CA=126.2°) nor a low surface energy coating alone (eg PEI-Ag-ending film with silane, CA=112.1°) can effectively prevent the release of Ag^+ ions. But combining micro-nano structure with silane coating could effectively prevent silver ions from releasing. Therefore, the asymmetric film with inverse superhydrophobic/hydrophilic wettability delivered Ag^+ one-directionally from the bottom surface.

Silver ions are known as a wide-spectrum anti-bacterial agent.[34] The bactericidal activity of the silver NPs loaded films was examined by a Kirby-Bauer assay[28] using *E. Coli*. As indicated in figure 2, inhibition zones were found for samples with Ag NPs but no inhibition zone was observed for film without Ag NPs (figure 2 B'). While a big inhibition zone of 8.9 mm was found when the bottom surface of $(PEI\text{-}Ag/PAA)_{20}$ free-standing film was turned up (figure 2 B), the inhibition zone decreased drastically to 1.8 mm on the PET supported superhydrophobic $(PEI\text{-}Ag/PAA)_{20}$ film which is supposed to be similar as the up surface of $(PEI\text{-}Ag/PAA)_{20}$ free-standing film (Figure 2C). It is not difficult to understand the results if we consider the relationship between the inhibition zone and the amount of relative released silver ion of different samples (Figure 2 D). And the results of the Kirby-Bauer assay confirmed again the asymmetric release rate of Ag^+ from the asymmetric free-standing film, which will led to asymmetric anti-bacterial ability.

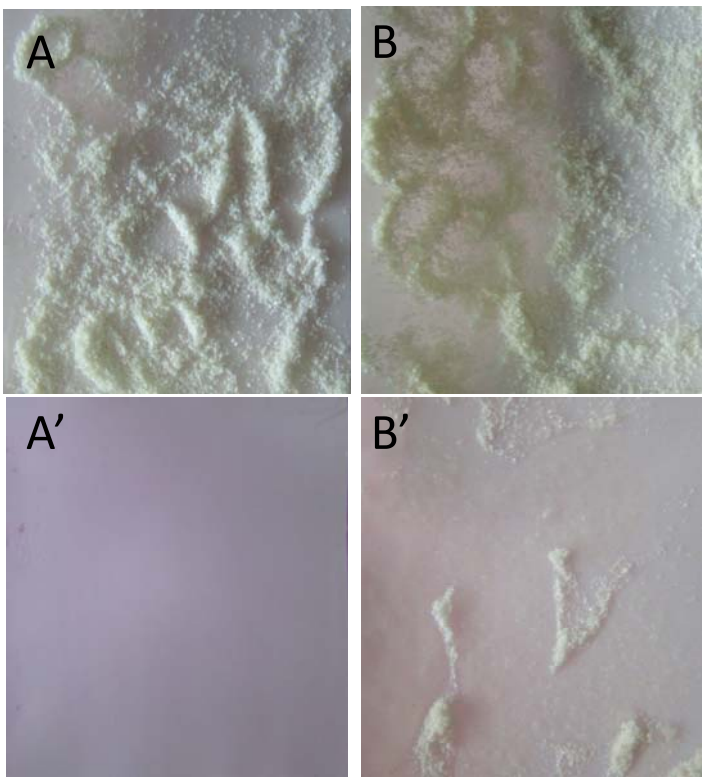

Figure 3. *Digital images of superhydrophobic $(PEI\text{-}Ag/PAA)_{20}$ film on PET (A, A') and PTFE (B, B') with dust (A, B) and after adding 3 mL (A') and 7 mL (B') of water dropwise.*

Superhydrophobic surfaces are also well known as anti-adhesive or self-cleaning[27] like lotus leaves, which can get rid of dusts in the presence of water droplets. The self-cleaning property of PET supported suprhydrophobic $(PEI\text{-}Ag/PAA)_{20}$ film was examined. The hydrophobic Teflon substrate, which is a commercially available self-cleaning material, was chosen here as control. The substrates were initially covered with dusts (figure 3 A and B). When water was added dropwise on the film, the droplet rolled down from the film surface and took away the dusts on its path. After adding 3 mL water, all the dusts on the film surface had been taken away (figure 3 A'). In comparison, for the Teflon substrate, water droplet slid down on the surface and could not remove the dusts. Even after addition of 7 mL water, the

dusts were still on Teflon surface (figure 3 B'). (Video was shown in supporting information 3)

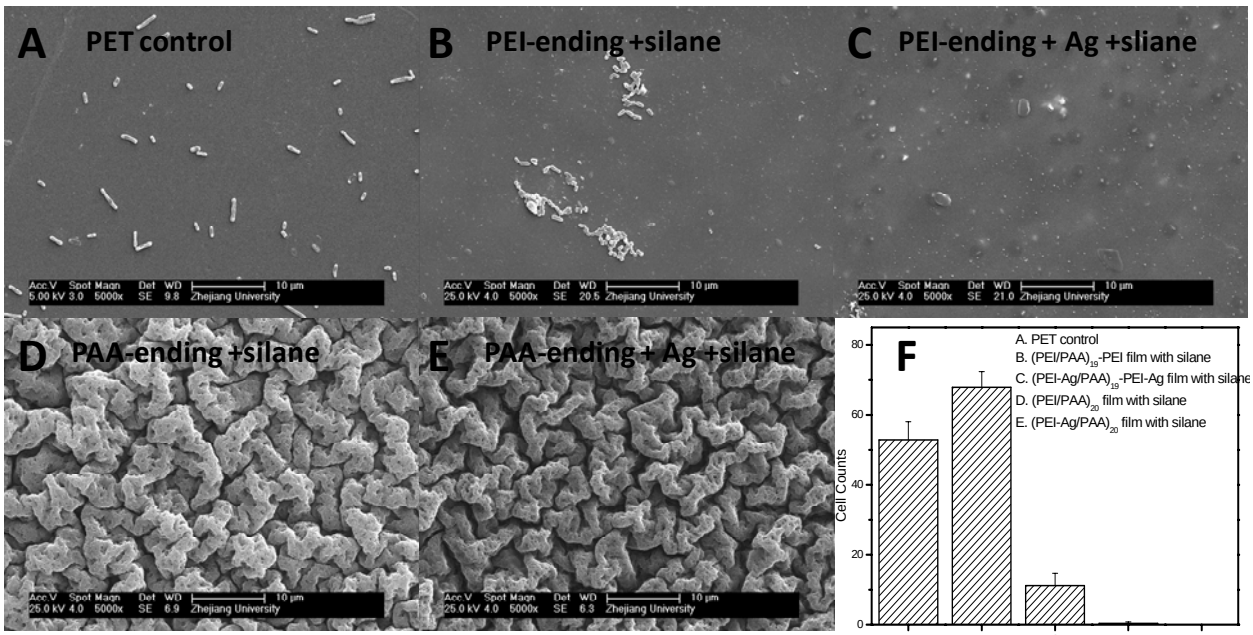

Figure 4. *SEM images of PET supported (PEI/PAA) films after incubation in E.Coli solution for 4 h. (A) PET control; (B) $(PEI/PAA)_{19}$-PEI film with silane deposition; (C) $(PEI\text{-}Ag/PAA)_{19}$-PEI-Ag film with silane deposition, (D) $(PEI/PAA)_{20}$ film with silane deposition, (E) $(PEI\text{-}Ag/PAA)_{20}$ film with silane deposition. (F) Corresponding bacterial counts on the different samples, averaged from 6 images for each sample.*

Furthermore, the superhydrophobic surface exhibited anti-adhesive properties for microorganism. Thus, the initial *E. Coli* adhesion on PET supported and silane coated films with either PAA-ending or PEI-ending was tested. As illustrated in figure 4, *E. Coli* adhered separately on PET substrate but aggregated on $(PEI/PAA)_{19}$-PEI surface (figure 4 B). When *E.Coli* was incubated with $(PEI\text{-}Ag/PAA)_{19}$-PEI-Ag film (figure 4 C), less bacteria were found on the surface compared to $(PEI/PAA)_{19}$-PEI film, and the bacteria were not in a normal shape. This may be because the bacteria were killed by the released silver ions. Interestingly, almost no *E. Coli* was be found on the PAA-ending films with silane coating containing or no Ag^+ ions (figure 4 D, E). The excellent anti-adhesion ability may come from the combination of micro- nano structure and superhydrophobicity. Indeed, Cao et al. have revealed that the settlement of zoospores of *Ulva* was strongly influenced by the size of the features present on the surfaces.[35] The lowest level of settlement was observed for structures of the order of 2 μm, a size similar to that of the spores of *Ulva*. Furthermore, the lowest settlement strength was on the surface with the sub-micrometer-sized features. This may be explained by the inability of the adhesive to thoroughly bond to the entire surface area provided. Here, we prove that the combination of micro-nano hierarchical structure and superhydrophobicity can lead to anti bacteria adhesion. Of note, the size of micro-structure on the PAA-ending film here was ~2-5μm, close to the size of *E. Coli*.

CONCLUSIONS

In conclusion, we have demonstrated a facile method for creating asymmetrical free-standing films via amplified layer-by-layer assembly. The free-standing films have asymmetric surface morphology, which resulted in asymmetric wettability: the upper surface being superhydrophobic while the lower one being hydrophilic. The superhydrophobic surface was proved to limit bacterial adhesion and to be self-cleaning, while the hydrophilic surface could extensively deliver bactericidal silver ions. Importantly, the film can be transferred to another interface, such as human skin. Therefore, these asymmetric, multifunctional films may be of great potential for use as patches for open wound, as well as in the area of barrier, separation, transportation or drug delivery.

ACKNOWLEDGMENTS.

CP thanks the "Institut Universitaire de France" and the European Research Council for financial support (ERC StG 259370). LS thanks the French government for financial support through a "Eiffel Doctorat" fellowship, the Rhône-Alpes region through a CMIRA fellowship, and the French Embassy in China. JJ thanks the financial support from the NSFC-50830106, The National Basic Research Program of China (2011CB606203) and China National Funds for Distinguished Young Scientists (51025312).

Supporting Information Available:

Supporting information include film EDX data and SEM images for film surface morphology (supporting information 1) and two videos showing wettability of top surface (left) and bottom surface (right) of free-standing film (supporting information 2) and self-cleaning of superhydrophobic surface (supporting information 3), respectively. The material is available free of charge via the Internet at http://pubs.acs.org.

REFERENCES

(1) Jiang, C. Y.; Tsukruk, V. V. *Advanced Materials* **2006**, *18*, 829.

(2) Bohme, T. R.; de Pablo, J. J. *Journal of Chemical Physics* **2002**, *116*, 9939.

(3) Torres, J. A.; Nealey, P. F.; de Pablo, J. J. *Physical Review Letters* **2000**, *85*, 3221.

(4) Guerin, G.; PruD'Homme, R. E. *Journal of Polymer Science Part B-Polymer Physics* **2007**, *45*, 10.

(5) Huang, J. J.; Keskkula, H.; Paul, D. R. *Polymer* **2004**, *45*, 4203.

(6) Huang, Y.; Paul, D. R. *Journal of Membrane Science* **2004**, *244*, 167.

(7) Lutkenhaus, J. L.; McEnnis, K.; Hammond, P. T. *Macromolecules* **2007**, *40*, 8367.

(8) Jiang, C. Y.; Markutsya, S.; Tsukruk, V. V. *Advanced Materials* **2004**, *16*, 157.

(9) Markutsya, S.; Jiang, C. Y.; Pikus, Y.; Tsukruk, V. V. *Advanced Functional Materials* **2005**, *15*, 771.

(10) Jiang, C. Y.; Markutsya, S.; Pikus, Y.; Tsukruk, V. V. *Nature Materials* **2004**, *3*, 721.

(11) Mitsuishi, M.; Ishifuji, M.; Endo, H.; Tanaka, H.; Miyashita, T. *Molecular Crystals and Liquid Crystals* **2007**, *471*, 11.

(12) Letendre, M.; D'Aprano, G.; Lacroix, M.; Salmieri, S.; St-Gelais, D. *Journal of Agricultural and Food Chemistry* **2002**, *50*, 6017.

(13) DeCorby, R. G.; Ponnampalam, N.; Nguyen, H. T.; Clement, T. J. *Advanced Materials* **2007**, *19*, 193.

(14) Shim, B. S.; Tang, Z. Y.; Morabito, M. P.; Agarwal, A.; Hong, H. P.; Kotov, N. A. *Chemistry of Materials* **2007**, *19*, 5467.

(15) Park, J.; Kim, J.; Lee, S.; Bang, J.; Kim, B. J.; Kim, Y. S.; Cho, J. *Journal of Materials Chemistry* **2009**, *19*, 4488.

(16) Fujie, T.; Okamura, Y.; Takeoka, S. *Advanced Materials* **2007**, *19*, 3549.

(17) Fujie, T.; Matsutari, N.; Kinoshita, M.; Okamura, Y.; A. Saito, Takeoka, S. *Advanced Functional Materials* **2009**, *19*, 2560.

(18) Fujie, T.; Kinoshita, M.; Shono, S.; Saito, A.; Okamura, Y.; Saitoh, D.; Takeoka, S. *Surgery* **2010**, *148*, 48.

(19) Okamura, Y.; Kabata, K.; Kinoshita, M.; Saitoh, D.; Takeoka, S. *Advanced Materials* **2009**, *21*, 4388.

(20) Okamura, Y.; Fukui, Y.; Kabata, K.; Suzuki, H.; Handa, M.; Ikeda, Y.; Takeoka, S. *Bioconjugate Chemistry* **2009**, *20*, 1958.

(21) Okamura, Y.; Utsunomiya, S.; Suzuki, H.; Niwa, D.; Osaka, T.; Takeoka, S. *Colloids and surfaces A: Physicochemical Engineering Aspects* **2008**, *318*, 184.

(22) Mattoli, V.; Pensabene, V.; Fujie, T.; Taccola, S.; Menciassi, A.; Takeoka, S.; Dario, P. *Procedia Chemistry* **2009**, *1*, 28.

(23) Podsiadlo, P.; Qin, M.; Cuddihy, M.; Zhu, J.; Critchley, K.; Kheng, E.; Kaushik, A. K.; Qi, Y.; Kim, H.-S.; Noh, S. –T.; Arruda, E. M.; Waas, A. M.; Kotov, N.A. *Langmuir* **2009**, *25*, 14093.

(24) Lutkenhaus, J. L.; McEnnis, K.; Hammond, P. T. *Macromolecules* **2008**, *41*, 6047.

(25) Lutkenhaus, J. L.; Hrabak, K. D.; McEnnis, K.; Hammond, P. T. *Journal of the American Chemical Society* **2005**, *127*, 17228.

(26) Shen, L.; Fu, J.; Fu, K.; Picart, C.; Ji, J. *Langmuir* **2010**, *26*, 16634.

(27) Feng, L.; Li, S.; Li, Y.; Li, H.; Zhang, L.; Zhai, J.; Song, Y.; Liu, B.; Jiang, L.; Zhu, D. *Advanced Materials* **2002**, *14*, 1857.

(28) Bauer, A. W.; Kirby, W. M.; Sherris, J. C.; Turck, M. *The American Journal of Clinical Pathology* **1966**, *45*, 493.

(29) Ji, J.; Fu, J. H.; Shen, J. C. *Advanced Materials* **2006**, *18*, 1441.

(30) Fu, J.; Ji, J.; Shen, L.; Küller, A.; Rosenhahn, A.; Shen, J.; Grunze, M. *Langmuir* **2009**, *25*, 672.

(31) Yuan, W.; Fu, J.; Su, K.; Ji, J. *Colloids and Surfaces B: Biointerfaces* **2010**, *76*, 549.

(32) Taylor, P. L.; Omotoso, O.; Wiskel, J. B.; Mitlin, D.; Burrell, R. E. *Biomaterials* **2005**, *26*, 7230.

(33) Agarwal, A.; Weis, T. L.; Schurr, M. J.; Faith, N. G.; Czuprynski, C. J.; McAnulty, J. F.; Murphy, C. J.; Abbott, N. L. *Biomaterials* **2010**, *31*, 680.

(34) Feng, Q. L.; Wu, J.; Chen, G. Q.; Cui, F. Z.; Kim, T. N.; Kim, J. O. *Journal of Biomedical Materials Research* **2000**, *52*, 662.

(35) Cao, X.; Pettitt, M. E.; Wode, F.; Sancet, M. P. A.; Fu, J.; Ji, J.; Callow, M. E.; Callow, J. A.; Rosenhahn, A.; Grunze M. *Advanced Functional Materials* **2010**, *20*, 1984.

Supporting information 1

Table SI1. Element ratio of films at various deposition layers for (PEI-Ag^{+}(9.0)/PAA(3.2)) films. The concentration of silver nitrate is 1.6 mM.

Element content	PEI-Ag^{+}(9.0)/PAA(3.2)			
	C_K	N_K	O_K	Ag_L
9 layers	54.59	17.07	28.08	0.26
10 layers	61.43	13.93	24.52	0.12
11 layers	61.75	13.64	24.19	0.42
12 layers	63.64	13.25	22.90	0.21

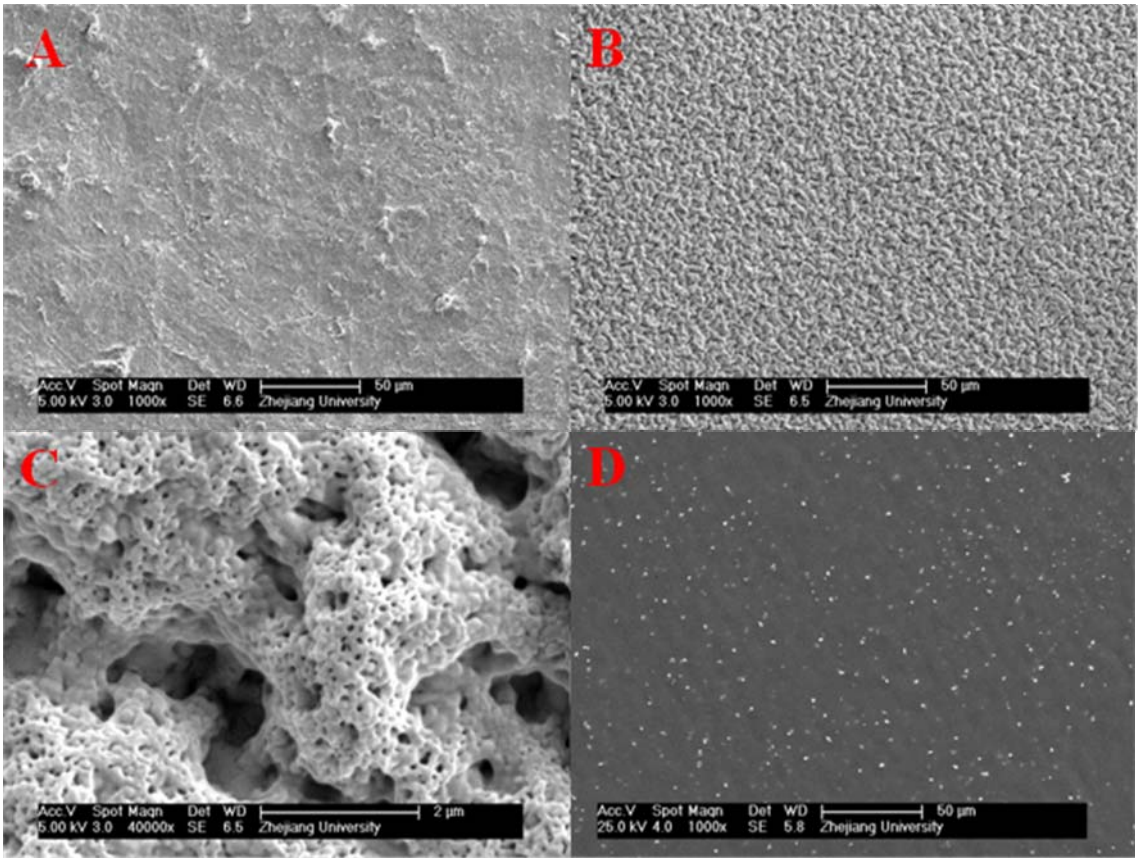

Figure SI1. SEM images for surface morphology of the bottom surface (A) of free-standing film and top surface (B, C) of free-standing film as well as the surface of supported PEI-Ag ending film. Scale bar was 50 μm for A, B and D and 2 μm for C.

Chapter 3 pH-Amplified Multilayer Films Based on Hyaluronan: Influence of HA molecular weight and concentration on film growth and stability

3.1 Summary

Introduction

Layer-by-layer assembly has seen great development since it has been introduced by Decher et al. The internal composition and growth properties of polyelectrolyte multilayers are an intensive field of research. Differences in growth modes, i.e. linear versus exponential, have been evidenced depending on the buildup conditions and on the polyelectrolyte intrinsic properties. Physico-chemical parameters such ionic strength of the suspending medium or pH of the polyelectrolytes solutions during deposition will influence the growth mode. Recently, the pH-amplified exponential growth for weak polyelectrolytes pairs was reported, where the lowering of polyanion pH and the increasing of polycation pH can significantly accelerate film growth.

In addition to pH and ionic strength variation, the nature of the polyelectrolyte itself, its structure, flexibility as well as its molecular weight, may provide additional ways to modulate film growth and film properties. However, up to now, the influence of polyelectrolyte molecular weight on film growth is less well understood and there are only few available studies.

In this work, we would like to see the influence of the molecular weight of HA on (PLL/HA) film growth, for films built in pH-amplified conditions with intermediate drying steps. Quartz crystal microbalance with dissipation monitoring was used to obtain information on the

deposited mass and Fourier Transformed Infrared spectroscopy was employed to analyze the structure of PLL in the films as well as follow film growth. Furthermore, the behavior and the stability of these films in a physiological buffer were also investigated.

Results and discussion

Three HA with different molecular weight were used in this research, namely HA200 (MW=200 kDa), HA400 (MW=400 kDa) and HA1300 (MW=1300 kDa).

The film growth was followed by QCM-D in dry state step-by-step. It was demonstrated that film growth behavior depended strongly on the molecular weight of HA, with a much more rapid growth when the molecular weight of HA was increased. (PLL/HA1300) grew steadily and rapidly exhibiting a clear exponential trend, whereas in the growth of (PLL/HA400) and (PLL/HA200) slightly decreases in ($\Delta f_3/3$) occurred upon PLL deposit steps. Similar growth modes were confirmed by monitoring the film growth with FTIR.

The film stability in PBS was investigated and found it relied on film ending layer as well as HA molecular weight. PLL-ending films were more stable than their HA-ending counterparts and films with HA of higher molecular weight showed better stability.

FTIR was also used to investigate PLL secondary structures in the film as well as in solutions of different pH. Although the β-sheet structures can be observed for PLL at pH 9.5 in solution, they turned to random structures when layered with HA of low pH. HA ionization degree in the film was estimated from the FTIR spectra. It was shown that HA1300 at pH 2.9 in solution got an ionization degree around 15%, this ionization degree increased when HA was assembled into (PLL/HA) multilayer and kept increasing when the layer number increased.

The surface morphology of dried films was imaged by SEM. The films made of HA200 were very smooth. The films built with HA400 displayed the highest surface roughness followed by those built from HA1300. Both PLL-ending film and HA-ending film showed similar surface features. PLL diffusion in different films were quantified by FRAP, and found PLL showed higher diffusivity when layered with much higher molecular weight HA.

The effect of HA1300 concentration on film growth was also studied by QCM-D. The results showed that, at low concentration the films grew irregularly; when in the range of 0.5 to 2 mg/mL, the film growth increased significantly as the concentration increased; at even higher concentration, films growth tended to be in a steady stage.

Finally, a scheme was proposed to explain the differences in (PLL/HA) film growth with HA

of different molecular weight. The interaction between PLL and HA in each assembly step as well as inter and intra molecular interactions of HA chains were highlighted.

Conclusion

The influence of hyaluronan molecular weight and of its concentration on the growth and structure of PEM films fabricated from PLL at high pH and HA at low pH has been extensively investigated. It is found that the film thickness of the high molecular weight HA increased exponentially and much more rapidly than for HA of lower molecular weight. In addition, HA concentration in solution had an important effect on film growth. These films also contained numerous hydrogen bonds and exhibited inter and intra molecular associations between HA chains. Furthermore, films ending by PLL were much more stable and PLL diffusion was found to be significantly faster in the films made of higher molecular weight HA. Overall, HA molecular weight, HA concentration and the nature of the outermost layer of the films are all important parameters contributing to film growth, internal cohesion and stability in a physiological medium.

3.2 Article

pH-Amplified Multilayer Films Based on Hyaluronan: Influence of HA Molecular Weight and Concentration on Film Growth and Stability

L,Shen, P, Chaudouet, J, Ji, and C, Picart, Biomacromolecules, 2011, 12, 1322-1331

pH-Amplified Multilayer Films Based on Hyaluronan: Influence of HA Molecular Weight and Concentration on Film Growth and Stability

Liyan Shen, Patrick Chaudouet, Jian Ji, and Catherine Picart

ABSTRACT:

In this study, we investigate the growth and internal properties of polyelectrolyte multilayer films made of poly(L-lysine) and hyaluronan (PLL/HA) under pH-amplified conditions, that is, by alternate deposition of PLL at high pH and HA at low pH. We focus especially on the influence of the molecular weight of HA in this process as well as on its concentration in solution. Film growth was followed by quartz crystal microbalance and by infrared spectroscopy to quantify the deposited mass and to characterize the internal properties of the films, including the presence of hydrogen bonds and the ionization degree of HA in the films. Film growth was significantly faster for HA of high molecular weight (1300 kDa) as compared with 400 and 200 kDa. PLL was found to exhibit a random structure once deposited in the films. Furthermore, we found that PLL-ending films are more stable when they are placed in PBS than their HA counterparts. This was explained on the basis of more cohesive interactions in the films for PLL-ending films. Finally, we quantified PLL^{FITC} diffusion into the films and observed that PLL diffusion is enhanced when PLL is paired with the HA of high MW. All together, these results suggest that besides purely physicochemical parameters such as variation in pH, the molecular weight of HA, its concentration in solution, and the possibility to form intermolecular HA association play important roles in film growth, internal cohesion, and stability.

INTRODUCTION

Polyelectrolyte multilayer films made by self-assembly of polyelectrolytes onto solid substrates[1] have received considerable interest because of their versatility[2] and large potential applications in fields as diverse as optical devices,[3] biomaterials coatings,[4] electrochemistry or

biosensors.[5]

The internal composition and growth properties of polyelectrolyte multilayers (PEMs) are an intensive field of research since the past decade.[2,6-8] Differences in growth modes, that is, linear versus exponential, have been evidenced depending on the buildup conditions and on the polyelectrolyte intrinsic properties.[9-11] Physico-chemical parameters such as ionic strength of the suspending medium[12] or pH of the polyelectrolytes during deposition will influence the growth mode.[13,14] Studies mostly concern films based on synthetic polyelectrolytes, which offer a large working range of chemistries, structure, and charge densities.[15] Poly(allylamine hydrochloride)/ poly(acrylic acid) (PAH/PAA) films made of two weak polyelectrolytes have probably been the most investigated films[13,16] with respect to pH variations. Significantly different polymer adsorption behaviors were observed when the charge density of weak polyelectrolytes was varied over a very narrow pH range. By controlling pH, Rubner and coworkers have shown that it is possible to vary the thickness of an adsorbed polycation or polyanion layer from < 1 nm to almost 10 nm.[13] More recently, one of us evidenced that film growth can be drastically amplified by a large shift of pH during assembly of the polyelectrolytes.[17] Thus, in the case where PAA at low pH was assembled with PEI at high pH, a nonlinearity in film growth became much more pronounced with increasing pH difference.[17] In addition to pH and ionic strength variation, the nature of the polyelectrolyte itself, its structure, flexibility as well as its ability to form secondary interactions such as hydrogen bonds can all greatly influence film growth. Variation in the polyelectrolyte molecular weight may be an additional way to modulate film properties.[18] However, up to now, the influence of polyelectrolyte molecular weight on film growth is less well understood,[19] and there are only a few available studies.

Films made of natural polyelectrolytes such as polysaccharides or polypeptides have more recently begun to be investigated.[8,10,20] These films, which can be viewed as a novel kind of biomimetic self-assemblies, offer numerous possibilities for the design of biofunctional coatings.[21,22] For such biopolymeric films, which are most often built at constant deposit pH, the exponential character of their initial growth is now becoming a more and more common feature.[8,20,23] This growth results from the diffusion “in” and “out” of the films of at least one of the polyelectrolytes constituting the multilayer.[11] Exponentially growing films are indeed now advantageously used as reservoirs for bioactive molecules[24] or loading nanoparticles.[25]

Among the exponentially growing films based on biopolymers, the poly(L-lysine)/ hyaluronan system has become one of the most studied “model systems”.[11,26-28] These films offer several advantages as they become rapidly thick (on the order of micrometer) after deposition of a few layer pairs. In addition, they offer the possibility to visualize and quantify PLL diffusion easily by means of several different optical techniques.[11,28] Schaaf and coworkers employed PLL/HA films built at neutral pH to focus on the linear regime that is reached after the initial exponential growth.[26] They evidenced that the film thickness increment per deposition step in the linear growth regime was fairly independent of the molecular weight of the polyelectrolytes. In a recent study, one of us investigated the effect of

pH shifts on (PLL/HA) films growth[29] and employed these films for loading an oligo-peptide. Interestingly, exponential film growth was further amplified by depositing PLL at high pH and HA at low pH.

In this work, our aim was to study the influence of the molecular weight of HA on (PLL/HA) film growth for films built in pH-amplified conditions with intermediate drying steps. We employed Quartz crystal microbalance with dissipation monitoring to obtain information on the deposited mass and Fourier transform infrared (FTIR) spectroscopy to analyze the structure of PLL in the films as well as follow film growth. Furthermore, we investigated the behavior and the stability of these films in a physiological buffer and measured the diffusion coefficient of PLL in these assemblies.

MATERIALS AND METHODS

Preparation of Polyelectrolyte Multilayer Films. Poly(L-lysine) hydrobromide (PLL, *Mw* 47.9 kDa) and FITC-labeled poly(L-lysine) (PLL-FITC, *Mw* 68.3 kDa) were purchased from Sigma-Aldrich (Saint Quentin Fallavier, France). Hyaluronan (HA) of three different molecular weights, 200 (HA200), 400 (HA400), and 1300 kDa (HA1300), were purchased from Lifecore (Chaska, MN) and Fluka.

The films were built on gold-coated crystals (QSX 301 quartz crystals, Q-sense), 12 mm diameter glass slides (VWR Scientific), or silicon wafers previously cleaned with 2% (v/v) HELLMANEX II (Hellma GmbH, KG, Germany) aqueous solution at 70 ℃ for 15 min, then rinsed thoroughly with water and dried with a stream of nitrogen.

PLL/HA films were built layer-by-layer using PLL at 1 mg/mL (pH 9.5) and HA at 3 mg/mL (pH 2.9) unless indicated. The pH of the polyelectrolyte solution was adjusted by using HCl or NaOH. The substrates were first dipped in PLL for 10 min then rinsed in water (pH 9.5) three times before being dried under a stream of nitrogen. Similarly, they were then immersed in HA solution for 10 min, followed by dipping in water (pH 2.9) three times and drying. The same procedures were repeated until the desired number of layer pairs was reached to prepare $(PLL/HA)_i$ films (with $i = 8$ typically). In the following, we will denote the films $(PLLx/HAy)_i$ with x being the pH of PLL, y being that of HA, and *i* being the number of layer pairs.

Quartz Crystal Microbalance with Dissipation Monitoring (QCM-D). The film buildup process on gold-coated quartz crystals was monitored by a quartz crystal microbalance (QCM-D, D300, Q-sense). The frequency shifts Δf were measured in air on dried films after deposition of each layer. The same crystal was used for monitoring the whole build-up of the multilayer. The layer was deposited on the crystal, which was then rinsed and dried under nitrogen flow before being mounted for the measurements (three independent measurements for each layer). The crystal was then unmounted for depositing the subsequent layer and mounted again for measurements. Δf was used to estimate the mass adsorbed after each deposit step, which was calculated using the Sauerbrey equation[30]

$$\Delta m = - C \Delta f / v$$

where C is the mass sensitivity constant (17.7 ng· cm^{-2} Hz^{-1} at 5 MHz) and v is the overtone number.

Experiments for each type of HA were performed in triplicate. QCM-D was also employed to investigate film stability in phosphate-buffered saline (PBS). To this end, $(PLL9.5/HA2.9)_7$-PLL9.5 or $(PLL9.5/HA2.9)_8$ films were immersed in PBS for a given time period; then, the crystals were briefly rinsed with water to remove salt and dried in a stream of nitrogen before the frequency changes were recorded.

Fourier Transform Infrared Spectroscopy. Film buildup on a silicon wafer was investigated by FTIR spectroscopy in transmission mode with a Vertex 70 spectrophotometer (BrukerOptic Gmbh, Ettlingen, Germany) equipped with an MIR detector. The spectrum from the bare Si surface coated with one PEI layer (20 min of immersion in 5 mg/mL, salt-free PEI solution, followed by water rinsing and blow drying) was taken as reference. After each polyelectrolyte layer deposit and rinsing step, a single-channel spectrum from 1024 interferograms was recorded between 400 and 4000 cm^{-1} with a 2 cm^{-1} resolution using Blackman-Harris three-term apodization and the standard Bruker OPUS/IR software v6.5 (Bruker OpticGmbh). The different peaks characteristic of the polyelectrolytes and of the films are identified in Table 1.[31,32] The characteristic peaks of saccharide rings on HA were visible in the 960-1200 cm^{-1} region, with the most intensive peak at 1045 cm^{-1}.This polysaccharide band was composed of five main saccharide peaks at 995, 1045, 1080, 1105, and 1155 cm^{-1}, which were deconvoluted using the Opus Software after residual water removal and baseline correction. We assumed all bands to be Gaussian.

TABLE 1. *Attribution of the main bands of HA and PLL in $(PLL/HA)_8$ dried films analyzed by FTIR in transmission mode.*

Chemical bond	**Wavenumber (cm^{-1})**
$\nu_{C\text{-}OH}$ (hydrogen-bonded O-H groups of HA)	3400
$\nu_{N\text{-}H}$ (hydrogen-bonded N-H groups of HA and PLL)	3275
$\nu_{C\text{-}H}$ methylene C-H stretching of HA and PLL	2936, 2862
$\nu_{C=O}$ of COOH groups of HA	1735
Amide I : β-sheet structure of PLL	1694, 1623
Amide I : random structure of PLL and HA	1650
$\nu_{C\text{-}O}^{-}$ of COO^{-} of HA	1605
$\nu_{C\text{-}OH}$...of alcool (H-bonded) and $\nu_{C\text{-}O\text{-}C}$ ring mode of HA	1078
$\nu_{C\text{-}OH...}$of alcool in HA (possibly H-bonded)	1045

For film cross-linking, 1-ethyl-3-(3-dimethylaminopropyl)carbodiimide hydrochloride (EDC) and N-hydroxysulfosuccinimide (sNHS) were dissolved in water at pH 5.5 with the final concentration of 50 and 11 mg/mL, respectively. The film-coated substrates were put in contact with the freshly prepared EDC/sNHS solution overnight at 4 ℃, followed by three rinses in water (pH 5.5) and air drying.

Scanning Electron Microscopy (SEM). For SEM observations, the films of either

HA-ending (8 layer pairs) or PLL-ending (7.5 layer pairs) with the different MW HA were prepared on silicon wafer following the procedure described above. The morphology of these dried films was visualized using an S-4500 SEM (Hitachi, Tokyo, Japan) after sputtering a thin layer of carbon on the samples (Emscope-TB500 apparatus, Elexience, Verriere le Buisson, France).

Confocal Laser Scanning Microscopy (CLSM) and Fluorescence Recovery after Photobleaching (FRAP). For CLSM observations, the films made of 7.5 ((PLL9.5/HA2.9)$_7$-PLL9.5 FITC) or 8 layer pairs (PLL9.5/HA2.9)$_7$-PLL9.5^{FITC}/ HA2.9 were built on glass slides and observed with an LSM510 confocal microscope (Carl Zeiss, Germany, 25 mW argon laser) as previously described.[33] Images were acquired in air or in PBS. For FRAP experiments, the PLL-ending films were photobleached over a 56 μm circular region with the laser at 15% laser power, and time-lapse microscopy was subsequently performed by acquiring the images every 30 s over a 5 min period. The images were analyzed using the LSM software. Because the exact determination of the diffusion coefficient requires a complex simulation procedure, we used a simplified form of the full equation given in Picart et al.,[33] which can be approximated in the case where $\tau=(4Dt)/(a^2) <1$ (where D is the diffusion coefficient in $\mu m^2/s$ and *a* is the bleached diameter in μm)[34]

$$\frac{c(t)}{c_0} = \alpha + (1-\alpha)\frac{\sqrt{4Dt}}{a\sqrt{\pi}}\left(1 - \frac{Dt}{4a^2}\right) \qquad (1)$$

When t tends to 0, this can be approximated by

$$\frac{c(t)}{c_0} \rightarrow \alpha + b\sqrt{t} \qquad (2)$$

Thus, α and *b* were easily deduced from the linear regression obtained by plotting $c(t)/c_0 = f((t)^{1/2})$.

From the slope *b*, a first approximation of D can be deduced

$$D = \frac{\pi a^2 b^2}{4(1-\alpha)^2} \qquad (3)$$

Of note, D estimated here is a mean coefficient measurement obtained by assuming that all of the molecules are diffusing.

RESULTS AND DISCUSSION

Buildup of Multilayer Films. (PLL9.5/HA2.9) multilayer films were fabricated under pH-amplified conditions, that is, with PLL at high pH (pH 9.5) and HA at low pH (pH 2.9) with no added salt in the polyelectrolyte solutions. These deposit conditions are typically followed by intermediate drying steps. We first investigated the effect of HA molecular weight on film growth for HA of increasing MW (200, 400, and 1300 kDa, respectively). Step by step film growth was monitored by QCM-D for PLL at 1 mg/mL and HA at 3 mg/mL

(Figure 1A). We observed that film growth depended strongly on the MW of HA, with a much more rapid growth when the molecular weight of HA was increased. Film growth with HA1300 exhibited a clear exponential trend (y = 116 exp(0.438x), where x is the number of layers and y is the QCM-signal at 15 MHz). For comparison, film growth entirely in PBS solution (no pH shifts) was drastically slower, and a 10-fold difference was noted in the frequency shifts (~2200 Hz for buildup in PBS as compared with ~22 300 for buildup in water) for a film made of eight layer pairs. It is indeed known that weakly charged polymers tend to take more of a globular shape in solution and adsorb to surfaces in a conformation reach in loop and tails with fewer ionic links to the surface per chain.

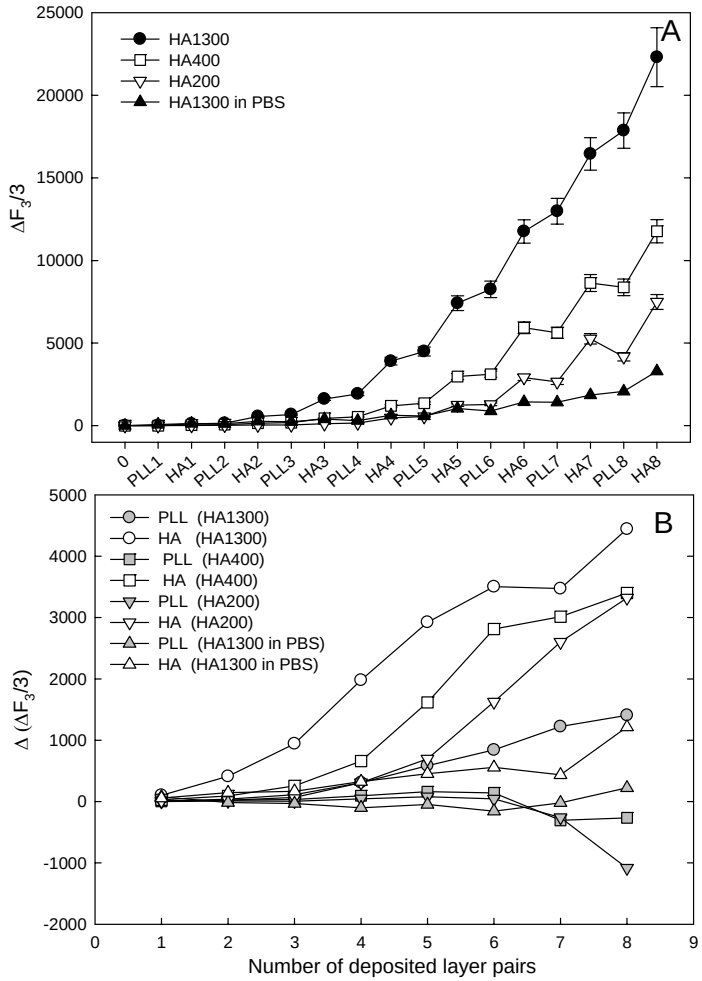

FIGURE 1. *Film growth followed by QCM-D. (A) Differences in the frequency shifts (Δf/ν) measured at 15 MHz at the end of each polycation and polyanion deposition for* $(PLL_{9.5}/HA_{2.9})_8$ *films with HA1300 (●), HA400 (□), HA200 (▽), in comparison to* $(PLL_{7.4}/HA_{7.4})$ *films built in PBS (▲). (B). Increment in frequency shift per layer Δ(Δf/ν) plotted for PLL layers (gray symbols) and for HA layers (open symbols) for the same films as in (A). The symbols for the HA of different MW were kept identical to (A) for more clarity.*

The differences in frequency shifts emerged more clearly by plotting the differences in frequency shifts ($\Delta(\Delta f_3)$)/3 as a function of the number of deposited layer pairs (Figure 1B). When HA layers were deposited (open symbols), the frequency shifts were always positive, and they increased when the molecular weight of HA increased. Conversely, the frequency

shifts were very low or even negative for PLL layers. Notably, the increment in PLL paired with HA1300 was always positive and was steadily increasing, whereas that of PLL paired with the low- MW HA was decreasing when the number of deposited layer pairs increased. This suggests that there may be some polyelectrolyte desorption during the PLL deposition steps when PLL is paired to HA200 and 400. This decrease may also be related to a densification of the films via repulsion of water molecules out of the films.[8]

Because QCM-D gives information on the film mass including solvent molecules,[35] we employed infrared spectroscopy as a complementary technique to probe the chemical signature of the polyelectrolytes in the film. FTIR is known to sense the "dry film mass". Figure 2A shows the spectra acquired during a (PEI/HA2.9) $(PLL9.5/HA2.9)_6$-PLL9.5 film buildup (with HA1300), which were obtained in air after each deposition step. Three main regions were revealed in these spectra: a broad and intense band in the 3700 to 3000 cm^{-1} region, corresponding to hydroxyl O-H and amide N-H stretching and which is mostly representative of H-bonds in the film associated with N-H and O-H. The first peak at 3400 cm^{-1} can tentatively be attributed to O-H of alcohols engaged in hydrogen bonds and to watermolecules.[31] It is maximal for HA-ending films (Figures 2A and 3A). The second peak at 3275 cm^{-1}, which is maximal for PLL-ending films (Figures 2A and 3A), can be attributed to hydrogen-bonded amide N-H groups.[32] The presence of these very large and steadily increasing bands indicates that a large number of H bonds are present in these LbL assemblies.

The second intense region contains the amide I (~1650 cm^{-1}) as well as the carboxylate (1605 cm^{-1}) and carboxylic acid (1735 cm^{-1}) peaks; the third main region between 960 and 1200 cm^{-1} includes the characteristic peaks of saccharide rings.[36] The intensity of the most intense saccharide peak at 1045 cm^{-1} was used to compare the absorbance values of the different films during film buildup (Figure 2B).

For film made of HA1300, the intensity steadily increased for each HA deposit. The slight intensity increase upon PLL deposition may be due to slight changes in the pH of the film, which may affect the hydration degree of the alcohol H-bonded groups.[31] For films made of HA400 and HA200, the absorbance increased to a less extent and a slight decrease may potentially be observed.

PLL Structure in the Film and HA Ionization Degree. Beside film growth, FTIR can be employed to get information on PLL conformation in the film[37] as well as on the degree of ionization of the carboxylate groups in the films.[7] Spectra of PLL-ending and HA-ending films were compared with spectra of pure PLL (pH 9.5) or HA (pH 2.9) droplets dried after deposition (Figure 3A,B). The H-bond associated with the O-H group is particularly visible for HA at pH 2.9 and for films ending by HA (Figure 3A). The N-H bond vibration at 3275 cm^{-1} is particularly visible for PLL at pH 9.5 and can also be seen in PEM films. This band is indeed slightly higher for PLL-ending films. The peak at 3100 cm^{-1} can be attributed to the Fermi resonance of N-H bond. Other peaks characteristic of CH_2 groups are also emerging at 2862 and 2936 cm^{-1}.

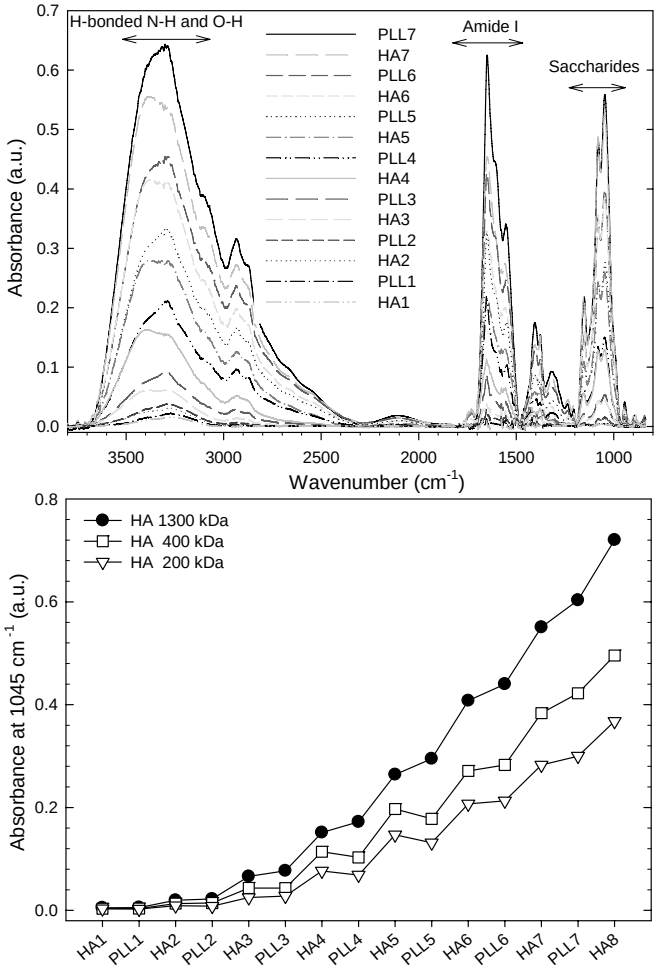

FIGURE 2. *(A) FTIR spectra acquired after the deposition of each layer during the buildup of a (PEI/$HA_{2.9}$) ($PLL_{9.5}$/$HA_{2.9}$)$_6$-$PLL_{9.5}$ film with HA1300. (B) Absorbance at 1045 cm^{-1} (most intense saccharide peak) after each layer deposit for HA of different MW: HA1300 (●), HA400 (□) and HA200 (▽).*

At basic pH, PLL is known to form secondary structures such as β sheets in solution or in films.[32,38] The β-sheet structures can indeed be observed for PLL at pH 9.5, with two clear peaks centered at 1694 and 1623 cm^{-1}. However, once engaged with HA in the (PLL9.5/HA2.9) films, the β-sheet structure of PLL was totally lost as no peak emerged at these wavenumbers. In contrary, a new amide I band appeared at~1650 cm^{-1}, which corresponded to random structures.

For HA in solution at pH 2.9, both carboxylic acid and carboxylate groups were identified at 1735 and 1605 cm^{-1}, respectively. From the integration of these two peaks, the ionization degree of HA dried from solution at pH 2.9 was estimated at ~15%. However, in (PLL/HA) films made of eight layer pairs, the carboxylic acid band was absent for PLL-ending films or very weak for HA-ending films. This is the first indication that the carboxylic group has a high degree of ionization in the films.

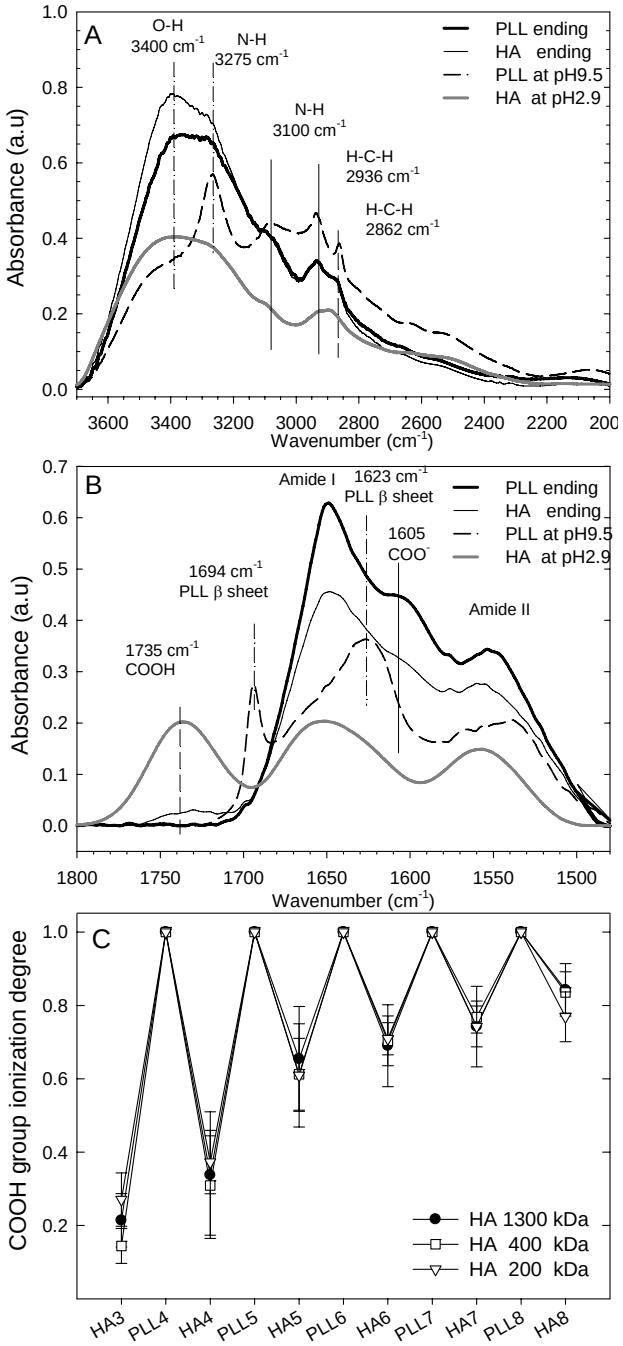

FIGURE 3. *FTIR spectra acquired for a PLL-ending $(PLL_{9.5}/HA_{2.9})_7$-PLL film (thick plain line), a HA-ending $(PLL_{9.5}/HA_{2.9})_8$ film (plain line) as well as for PLL in solution at pH 9.5 (dashed line) and HA in solution at pH 2.9 (gray line): (A) 3650-2000 cm^{-1} region, (B) 1800-1450 cm^{-1} region. (C) Degree of ionization of the carboxylic groups in the films as a function of the deposited layers.*

Using COOH and COO^- bands, we calculated the ionization degree of HA in the films at each deposition step (Figure 3C). The procedure based on the quantification of the specific peaks in ATR-FTIR spectra has already been employed to estimate the ionization degree of carboxylic groups in various other PEM films.[7,39,40] We always found a 100% ionization degree for PLL ending films, as can be seen from the absence of a peak at 1735 cm^{-1} in the PLL-ending spectrum (Figures 3B and 2A). For HA-ending films, the ionization degree increased significantly with the number of deposit cycles from 20 to 85%, an upper value that

was reached for films made of eight layer pairs. Thus, the pairing of HA with PLL forces the COOH groups to ionize in the films. In a previous study, Barrett et al. reported a decrease in acid strength of HA and base strength of PLL when (PLL/HA) was assembled at pH 7.[41] They hypothesized that a certain degree of secondary conformational ordering was present in such films to compensate for this decrease. In the present work, we find that HA ionization is increased during buildup and that PLL does not form β-sheets in the pH-amplified (PLL9.5/HA2.9) film.

SEM Observation of the Film Surface. The surface morphology of dried films was imaged by SEM (Figure 4). Unlike the films built under physiological conditions (neutral pH, 0.15 M ionic strength, and no intermediate drying step) that have a typical roughness of a few nanometers,[8] the films built under pH-amplified condition exhibited a much higher roughness. The films made of HA200 were very smooth. The films built with HA400 displayed the highest surface roughness, followed by those built from HA1300. Of note, both PLL-ending film and HA-ending film showed similar surface features (data not shown). Unfortunately, the very high roughness of the HA1300 and HA400 films did not enable us to image them by AFM over a large area (50 μm × 50 μm) because of the limits in the z-displacement of the piezoelectric ceramic, but the roughness of 1 μm × 1 μm images of (PLL/HA1300) films was on the order of 10 nm (data not shown).

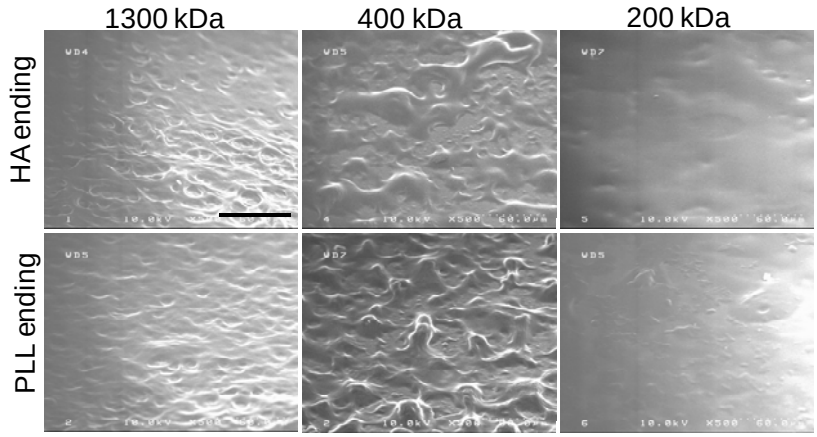

FIGURE 4. S*canning electron microscopy images of HA-ending films made of 8 layer pairs and of PLL-ending films made of 7.5 layer pairs (bottom row) for the HA of different MW. Scale bar is 60 μm.*

Stability of the Films in PBS. Because these films are built in a solution containing no added salt and with intermediate drying steps after each layer deposit, we further investigated their stability in a physiological medium (PBS, 0.15 M NaCl, pH 7.4). QCM measurements of film mass after immersion for different time periods in PBS are shown in Figure 5. For all films, a mass loss of 20-50% occurred within the very first hours (typically 3-5 h); then, the mass remained constant over several days (Figure 5A). The remaining film mass after 1 day of immersion in PBS (single immersion without medium change) is also represented in Figure 5B. As a general trend, we found that PLL-ending films were all more stable than HA-ending ones, whatever the MW of HA. In addition, HA-ending film stability was also increased when the MW of HA was higher (~50 to ~78%).We observed that film stability was slightly higher

when the film was dipped only once in PBS. This systematically higher stability of PLL-terminated films may be explained by the fact that (i) the film is more stitched because HA is fully ionized in such films (Figure 3C) and (ii) the pH jump from 9 to 7.4 (PBS) is less drastic than that between 2.9 (HA-ending films) and 7.4, a transition during which HA can swell.

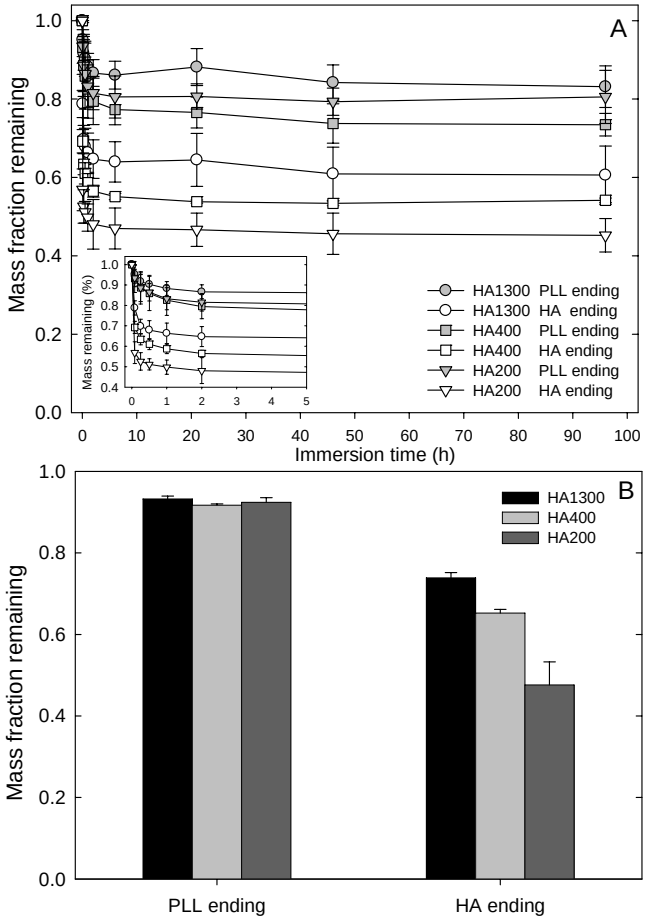

FIGURE 5. *Stability of the pH-amplified films in PBS measured by QCM. (A) Fraction of the initial mass of the films after immersion in PBS for given time periods. Gray symbols correspond to PLL-ending films made of 7.5 layer pairs and open symbols correspond to HA-ending films made of 8 layer pairs. Data are shown for HA1300 (circles), HA400 (squares), and HA200 (triangles). (B) Fraction of the initial mass remaining after immersion for 24 h in PBS for PLL-ending films (left) as well as HA-ending films (right).*

CLSM Imaging of Film Swelling in PBS and Quantification of PLL Diffusion. Because HA is known to have a very high water retention capacity,[42] we further probed the swelling capacity of the films once introduced in PBS as well as their morphology. Indeed, previous studies on PAH/HA films[43] as well as PLL/HA films built at pH 5 or 9[41] have shown that these films can greatly take up water and swell by ~800% depending on the pH of the LbL assembly.

Top view and z-section images in dried and wet state obtained by CLSM are shown in Figure 6. The film built with HA200 appeared very thin. The HA400 kDa film seemed to be

the most heterogeneous with uncontinuous features, which confirmed the SEM observations. On the contrary, $(PLL9.5/HA2.9)_8$ films built with HA1300 were homogeneous with a dry thickness of 2.8 µm. The immersion of the films in PBS induced a notable swelling, and hydrated thicknesses ranged from a few micrometers to ~25 µm. The swelling ratios, which were measured for each condition, are gathered in Table 2. They were similar for the three PLL ending films at ~400%. A greater hydrated thickness and swelling was found for the HA-ending film (HA1300) with a swelling of 600%. Of note, fluorescence distribution in the (PLL9.5/HA2.9) film (HA1300) also exhibited differences depending on the outermost layer. A homogeneous fluorescence in the z-direction was observed for the PLL^{FITC}-ending film (Figure $6C_2$), indicating that PLL chains were diffusing homogeneously throughout the whole films. Conversely, for HA-ending films, the fluorescence was heterogeneous and mostly localized at the film surface, with large patches of fluorescence (Figure $6D_2$). These observations indicate that when placed in PBS, PLL molecules interacted more strongly with HA and were distributed more homogenously in PLL-ending films as compared with HA-ending ones. This confirms that PLL-ending films are more stable.

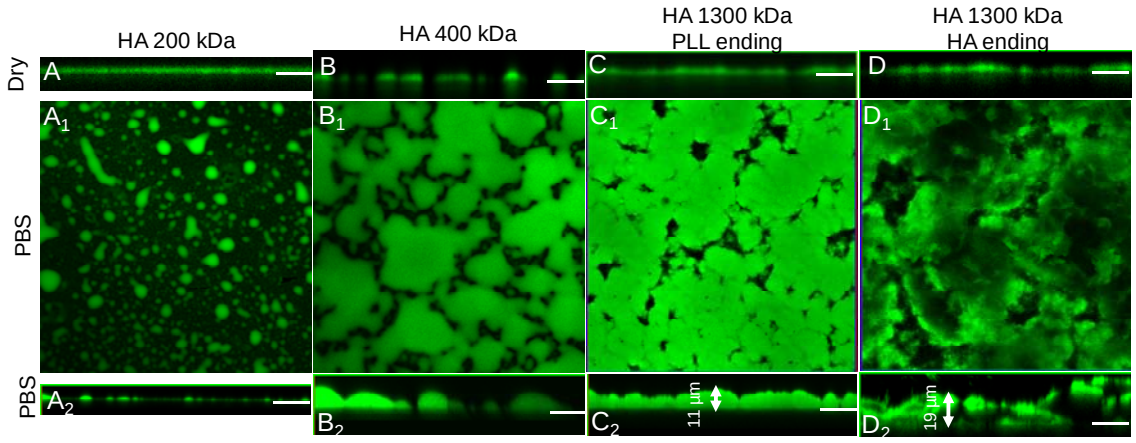

FIGURE 6. *Confocal images of the films made of HA of different MW observed in dry (upper row, A to D) and wet states (middle and bottom row). From the left to the right, PLL-ending films made of HA200 (A), HA400 (B) and HA1300 (C) as well as a HA-ending film with HA1300 (D). For each conditions in the wet state, a (X,Z) section is shown (X=142.8 µm and Z scales are respectively 8 µm for A, and 12 µm for B, C and D). For each condition in the hydrated state, a (X,Y) top view is shown (142.8 µm x 142.8 µm) as well as a (X,Z) section (X=142.8 µm and Z scales are respectively of 15.7 µm for A_2, 38 µm for B_2, 37.5 µm for C_2 and 45 µm for D_2).*

TABLE 2. *Comparison between the $(PLL/HA)_8$ films built from HA of different MW.*

	HA1300 HA-ending	HA1300 PLL-ending	HA400 PLL-ending	HA200 PLL-ending
Mass(mg/cm^2)[a]	0.395	0.316	0.148	0.074
Dry Thickness (µm) [a]	3.3	2.7	1.2	0.6
Wet thickness (µm) [b]	~18-25	~10-12	~5	~2
Swelling (%)	~600	~400	~400	~300

[a]Mass and dry thickness were calculated from QCM data. The film density was assumed to be 1200 kg/m^3. [b]Wet thickness was measured by CLSM on films immersed in PBS

To quantify PLL diffusion in hydrated films ending by PLL^{FITC}, we performed FRAP. The normalized intensity ratio of the bleached area is plotted as a function of the recovery time (Figure 7A), from which the PLL diffusion coefficient was calculated (Figure 7B). Interestingly, the diffusion coefficient of PLL was found to depend on the MW of HA. The higher the MW was, the greater the diffusion. Thus, PLL mobility was about three times significantly higher in the (PLL9.5/HA2.91300) films than in HA400-based films and ~15-fold higher as compared with HA200 films.

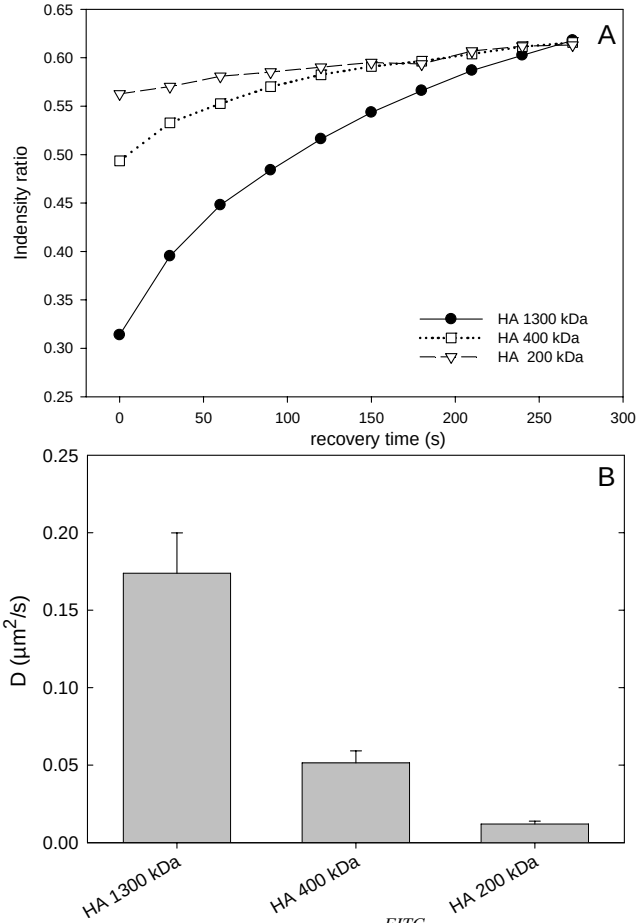

FIGURE 7. *FRAP experiments on $(PLL_{9.5}/HA_{2.9})_7$-PLL^{FITC} films made of the different HA. (A) The fluorescence intensity ratio in the bleached area is represented for each type of film as a function of the time; (B) PLL diffusion coefficients deduced from these curves (means ± standard deviation on three independent measurements). The diameter of the bleached circular area was 56 µm.*

Influence of HA Concentration and Intermolecular Associations between HA Molecules. Because HA1300-based films appeared to be the thickest, most homogeneous (Figure 6), and most stable assemblies (Figure 5), we decided to investigate further whether the concentration of HA plays a role in film growth and whether intra- and intermolecular associations of HA are present in such films. Figure 8 shows film growth, followed by QCM for different concentration of HA (Figure 8A) as well as FTIR spectra obtained for $(PLL9.5/HA2.91300)_8$ films for HA at two different concentrations (Figure 8B). We observed a striking effect of HA concentration on film growth (Figure 8A). Films grew slowly and almost linearly in the 0.5 to

1 mg/mL region, whereas the exponential growth became prominent when HA concentration was ≥2 mg/mL. For these films, FTIR spectra also showed, besides the increase in the amide (1700-1600 cm^{-1}) and saccharide bands (960-1200 cm^{-1}), a strong increase in the H-bond associated to O-H and N-H bands when HA concentration was changed from 1 to 3 mg/mL. This indicates that the number of all different types of H-bonds is much higher for these latter films. Of note, the H-bonded O-H peak at 3400 cm^{-1} is dominant in the film fabricated from HA at 3 mg/mL, whereas the H-bonded N-H stretching is more intense in the film from HA at 1 mg/mL.

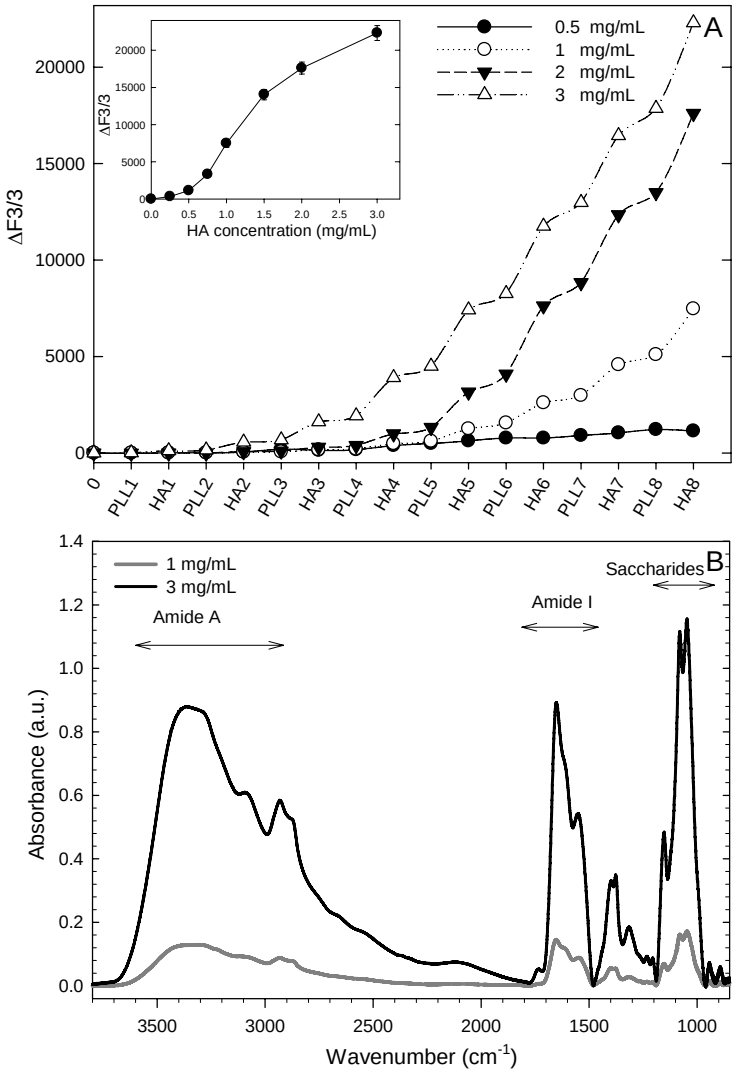

FIGURE 8. *(A) Film growth followed by QCM-D for $(PLL_{9.5}/HA_{2.9})_8$ films with HA1300 at different concentration of HA : 0.5 mg/mL (●), 1 mg/mL (○), 2 mg/mL (▼) and 3 mg/mL (Δ). The differences in the frequency shifts (Δf/ν) measured at 15 MHz are given for each deposited layer. Insert: frequency shifts (Δf/ν) measured at 15 MHz for $(PLL_{9.5}/HA_{2.9}1300)_8$ films built HA at different concentrations. (B) FTIR spectra of $(PLL_{9.5}/HA_{2.9}1300)_8$ films obtained for films built with HA at 1 mg/mL (gray line) and at 3 mg/mL (black line).*

To investigate whether intermolecular associations of HA were present in such multilayer films, we applied a cross-linking protocol using EDC as cross-linker. The basic idea was to characterize the type of bonds present in the (PLL9.5/HA2.9) films after cross-linking. If HA molecules are preferentially interacting with PLL, then covalent amide bonds are expected to form between ammonium and carboxylic groups. This is indeed what has already been shown for (PLL7/HA7) films built under physiological conditions.[44] However, if HA is self-associating or tightly packed, then other bonds such as ester bonds are expected to form. It is also known that HA gels can be cross-linked with EDC.[45] In this case, not only amide bonds but also ester bonds can be formed. Such bonds involve ester formed by the reaction of hydroxyl and carboxylic groups of HA or acid anhydride formed by the reaction between two carboxylic groups. Indeed, it has already been evidenced that ester bonds can be formed in layer-by-layer made of polysaccharides (chitosan and hyaluronan).[46]

Figure 9 shows the differences between the spectra obtained after and before cross-linking for HA at 1 and 3 mg/mL. The highest differences in the values of peak absorbance emerged for HA1300 at 3 mg/mL. Several bands decreased, especially the C-O-H stretching at 1078 cm^{-1} as well as the carboxylic peaks (at 1600 and 1410 cm^{-1}, respectively). Concomitantly, the intensity of several other bands increased: the C-O-C anhydrate band at 1050 cm^{-1}, the C-O ester band in the 1180-1300 cm^{-1} region,[45,46] the amide I and II bands (in the 1630-1700 cm^{-1} region and in the 1500-1580 cm^{-1} region, respectively), the C=O ester bands at 1740 and 1720 cm^{-1}, and C=O anhydrate bands at 1783 and 1806 cm^{-1}. As anticipated, the decrease in the carboxylic peaks of HA and the concomitant increase in the amide bands proves the reaction between the corresponding chemical groups and the ammonium groups of PLL. The disappearance of the characteristic saccharide peaks and the appearance of ester bands at ~1238 and at 1740 cm^{-1} suggest the formation of ester bonds. Here the reaction presumably occurs between hydroxyl and carboxylic groups of HA or between two COO^- groups of HA. This proves the intermolecular association of HA molecules. To quantify this further, we plotted the intensity ratio between the ester band (at 1740 cm^{-1}) and the methylene bands (at 2936 cm^{-1}), which is attributed to CH_2 vibrations and can be used as reference.[34,42] We found a higher intensity ratio in the case of HA1300 at 3 mg/mL than for HA at 1 mg/mL (0.71 versus 0.57). This indicates that intra- and intermolecular associations between HA molecules are favored under this condition. Of note, similar findings were found for HA of different MW: the intra/intermolecular associations are higher for HA1300 as compared with HA400 and HA200 (ratio of, respectively, 0.71, 0.51, and 0.47).

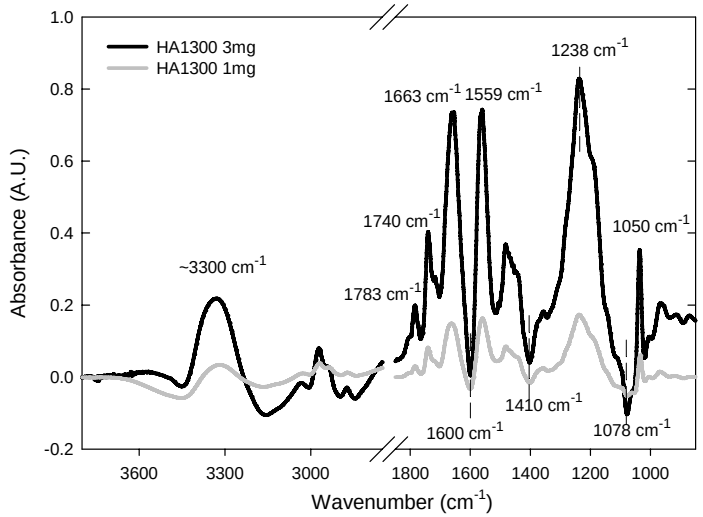

FIGURE 9. *FTIR differences of spectra obtained after and before crosslink for* $(PLL_{9.5}/HA_{2.9}1300)_8$ *films corresponding to HA concentration of 1 mg/mL (gray line) and 3 mg/mL (black line).*

General Discussion. We investigate in this study the influence of HA molecular weight and of HA concentration on the buildup, stability, and internal properties of pH-amplified (PLL/HA) films. In solution, both PLL (pH 9.5) and HA (pH 2.9) are partially ionized and in a coiled conformation, which allows thicker layers to be deposited than when both polyelectrolytes are deposited at neutral pH.[29] Indeed, this had first been evidenced for linearly growing poly(allylamine hydrochloride)/ poly(acrylic acid) (PAH/PAA) films built with polyanions and polycations solutions set at the same pH13 and more recently for exponentially growing poly(ethylene imine)(PEI)/PAA films.[17] Importantly, besides pH shift, other parameters such as MW of HA and its concentration in solution are also key parameters. We found a drastic enhancement of film growth, which was particularly striking for the HA of high MW(Figure 1). The effect of HA MW of (CHI/HA) films growth had already been highlighted by Winnik et al.,[47] who found that the larger film thickness was attributed to an earlier onset of the step exponential growth phase in the case of the high-molecular-weight pair. In our case, the effect of MW is much more pronounced and impacted not only the film growth rate but also the film homogeneity, swelling (Figure 6), stability (Figure 5) as well as PLL diffusion within the film (Figure 7). Importantly, we also found that the concentration of HA has a drastic effect on the presence of H-bonds in the films (Figure 8B) as well as on intermolecular associations between HA molecules (Figure 9). We hypothesize that the important role of the MW of HA and of its concentration on film growth are revealed because HA is deposited at low pH (2.9), close to the value of 2.42, where concentrated HA solutions (at 10 mg/mL) exhibited a sol/gel transition.[48] Because hyaluronan local concentration in the film is much higher than its concentration in the deposit solution (3 mg/mL), one may expect that the confinement of HA chains in the films leads to the formation of nano or microgels. Such intermolecular interactions between HA chains are favored by chain length, which is ~6 times longer for a molecule of HA1300 as compared with HA200 as well as by the concentration of chains. Interestingly, a noticeable effect of the concentration of HA was recently evidenced on the formation of poly(allylamine)/HA films on a $CaCO_3$ template.[49] It

was indeed shown that films formed with HA at 5 mg/mL better resisted the dissolution step to form a hollow polyelectrolyte microcapsule.

Of note, PLL in such pH-amplified PLL/HA films adopted a random structure, in contrast with what has been observed for other polypeptide-based films such as PLL/Poly(glutamic acid) films.[37] Furthermore, PLL diffusion also depended on the molecular weight of HA (Figure 7). The ionization degree of HA in the films was maximum when PLL was the outermost layer in the films (Figure 3C) and such PLL-ending films were indeed found to be the most stable ones (Figure 5) with an homogeneous repartition of PLL^{FITC} in the films (Figure 6). Hydrogen bonds appeared to be numerous in the pH-amplified PLL/HA films, especially for the HA of high molecular weight at high concentration.

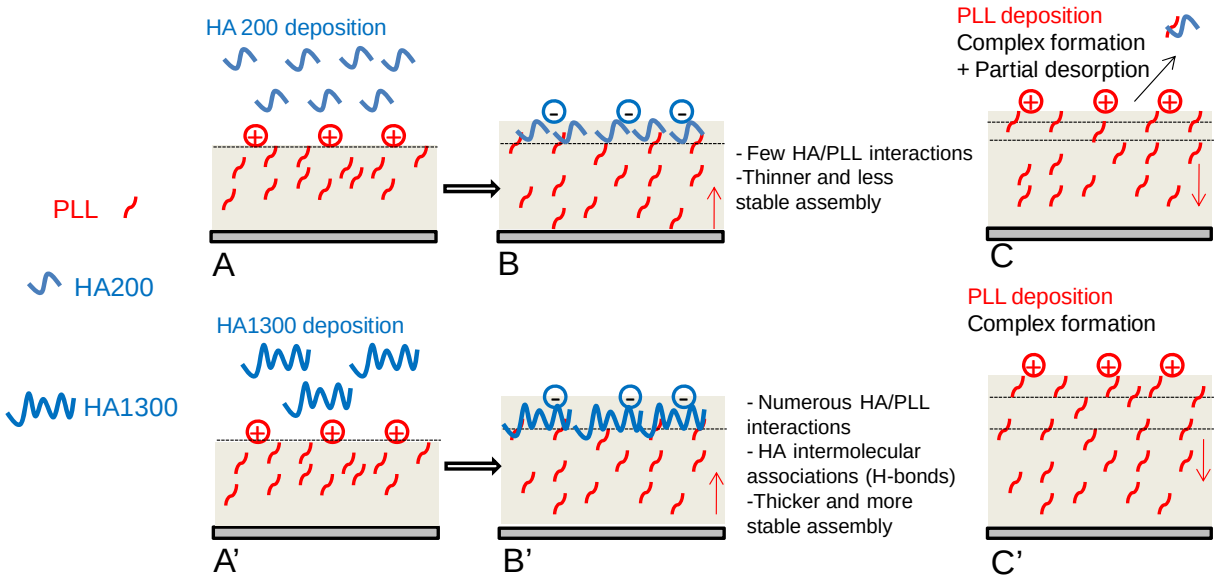

FIGURE 10. *Schematic drawing of the buildup mechanism of a (PLL/HA) multilayer films with HA at different MW: HA of low MW (upper row) and HA of high MW HA (lower row). (A,A') starting with a PLL ending layer, the film is put in contact with the HA solution at different MW. (B,B') some HA200 chains interact with PLL and adsorb onto the film. In the case of HA1300, which contains a 6-fold higher number in chains, interactions are more numerous and there are also a large number of HA intermolecular associations. (C,C') after rinsing PLL assembly followed, which diffuses into the films and adsorbs onto the films. For HA of low MW, (PLL/HA) complex formation is associated to partial desorption whereas HA of high MW forms more numerous interactions with PLL, leading to an enhanced stabilization of the film.*

Altogether, these results suggest that the superior properties of the pH-amplified films built with HA1300 may be a combination of an accumulation of higher amounts of HA during HA deposit, enhanced PLL diffusion, and enhanced stability of the films due to secondary interactions (hydrogen bonds) and intermolecular associations. The scheme presented in Figure 10 highlights the major differences between films built with HA of low molecular weight (HA200) and those built with HA1300. We start here with a PLL-ending layer (Figure 10A, A'). At pH 2.9, PLL in the film is almost fully charged, whereas HA in solution is partially charged with an ionization degree of ~15%. Therefore, the numbers of charges for

PLL (MW 47.9 kDa), HA200 (MW 200 kDa), and HA1300 (MW 1300 kDa) at pH 2.9 are 230, 75, and 450 per molecule, respectively. So, when HA deposits on PLL-ending film at pH 2.9, one HA 1300 molecule can interact with two or even more PLL chains, whereas one HA 200 molecule may interact with only one PLL chain. That is to say HA200 will establish only few interactions with PLL molecules, whereas HA1300 will establish both interactions with PLL molecules and intermolecular association between HA chains via H-bonds. The resulting films contain more HA in the case of HA1300 than for HA200 (Figure 10B, B'). The increase in HA chain length and of HA concentration in solution are thus both contributing to strengthen the whole cohesion of the film. Upon subsequent PLL deposition (Figure 10C, C'), two phenomena are likely to occur simultaneously:[8] (i) diffusion of PLL chains inside the film and (ii) complexation between the incoming PLL chains and the HA molecules at the film-liquid interface to promote film growth. Because there is less HA-PLL interaction and few HA intermolecular associations in films ending with HA200, a partial desorption of some (PLL/HA) complexes occurs for HA of low MW. This does not occur in the case of the HA of high MW.

In summary, we have investigated the influence of hyaluronan molecular weight and of its concentration on the growth and structure of PEM films fabricated from PLL at high pH and HA at low pH. We observed striking differences depending on HA MW. We found that the thickness of the high MW HA increased exponentially and much more rapidly than that for HA of lower MW. In addition, HA concentration in solution had an important effect on film growth. Structural insights obtained by FTIR revealed that PLL had a random conformation in such films and that the degree of COOH ionization, which increased upon film growth, was higher for PLL-terminated films. These films also contained numerous hydrogen bonds and exhibited intermolecular associations between HA molecules. Furthermore, the extent of film swelling in PBS was of the order of 400-600%, and notably, films ending by PLL were much more stable. PLL diffusion was found to be significantly faster in the films made of higher MW HA. Overall, HA molecular weight, HA concentration, and the nature of the outermost layer of the films are all important parameters contributing to film growth, internal cohesion, and stability in a physiological medium.

ACKNOWLEDGMENT

C.P. is a Junior Member of the "Institut Universitaire de France", whose support is gratefully acknowledged. L.S. thanks the French government of financial support through an "Eiffel Doctorat" fellowship. J.J. thanks the financial support from the NSFC-50830106 and China National Funds for Distinguished Young Scientists (51025312).

REFERENCES

(1) Lvov, L.; Haas, H.; Decher, G.; Moehwald, H.; Mikhailov, A.; Mtchedlishvily, B.; Morgunova, E.; Vainshtein, B. Langmuir 1994, 10, 4232–4236.

(2) Decher, G. Science 1997, 277, 1232–1237.
(3) Hiller, J.; Mendelsohn, J. D.; Rubner, M. F. Nat. Mater. 2002, 1, 59–63.
(4) Werner, S.; Huck, O.; Frisch, B.; Vautier, D.; Elkaim, R.; Voegel, J. C.; Brunel, G.; Tenenbaum, H. Biomaterials 2009, 30, 2291–2301.
(5) Tang, Z.; Wang, Y. l.; Podsiadlo, P.; Kotov, N. A. Adv. Mater. 2006, 18, 3203–3224.
(6) Ladam, G.; Schaad, P.; Voegel, J.-C.; Schaaf, P.; Decher, G.; Cuisinier, F. J. G. Langmuir 2000, 16, 1249–1255.
(7) Sukhishvili, S.; Granick, S. Macromolecules 2002, 35, 301–310.
(8) Picart, C.; Lavalle, P.; Hubert, P.; Cuisinier, F. J. G.; Decher, G.; Schaaf, P.; Voegel, J.-C. Langmuir 2001, 17, 7414–7424.
(9) McAloney, R. A.; Sinyor, M.; Dudnik, V.; Goh, M. C. Langmuir 2001, 17, 6655–6663.
(10) Lavalle, P.; Gergely, C.; Cuisinier, F.; Decher, G.; Schaaf, P.; Voegel, J.-C.; Picart, C. Macromolecules 2002, 35, 4458–4465.
(11) Picart, C.; Mutterer, J.; Richert, L.; Luo, Y.; Prestwich, G. D.; Schaaf, P.; Voegel, J.-C.; Lavalle, P. Proc. Natl. Acad. Sci. U.S.A. 2002, 99, 12531–12535.
(12) Dubas, S. T.; Schlenoff, J. B. Macromolecules 1999, 32, 8153– 8160.
(13) Shiratori, S. S.; Rubner, M. F. Macromolecules 2000, 33, 4213– 4219.
(14) von Klitzing, R. Phys. Chem. Chem. Phys. 2006, 8, 5012–5033.
(15) Schoeler, B.; Kumaraswamy, G.; Caruso, F. Macromolecules 2002, 35, 889–897.
(16) Yoo, D.; Shiratori, S. S.; Rubner, M. F. Macromolecules 1998, 31, 4309–4318.
(17) Fu, J.; Ji, J.; Shen, L.; Kuller, A.; Rosenhahn, A.; Shen, J.; Grunze, M. Langmuir 2009, 25, 672–675.
(18) Sui, Z. J.; Salloum, D.; Schlenoff, J. B. Langmuir 2003, 19, 2491–2495.
(19) Sun, B.; Jewell, C. M.; Fredin, N. J.; Lynn, D. M. Langmuir 2007, 23, 8452–8459.
(20) Elbert, D. L.; Herbert, C. B.; Hubbell, J. A. Langmuir 1999, 15, 5355–5362.
(21) Dimitrova, M.; Arntz, Y.; Lavalle, P.; Meyer, F.; Wolf, M.; Schuster, C.; Haikel, Y.; Voegel, J.-C.; Ogier, J. Adv. Funct. Mater. 2007, 17, 233–245.
(22) Benkirane-Jessel, N.; Schwint_e, P.; Falvey, P.; Darcy, R.; Haaïkel, Y.; Schaaf, P.; Voegel, J.-C.; Ogier, J. Adv. Funct. Mater. 2004, 14, 174–184.
(23) Tezcaner, A.; Hicks, D.; Boulmedais, F.; Sahel, J.; Schaaf, P.; Voegel, J. C.; Lavalle, P. Biomacromolecules 2006, 7, 86–94.
(24) Crouzier, T.; Ren, K.; Nicolas, C.; Roy, C.; Picart, C. Small 2009, 5, 598–608.
(25) Podsiadlo, P.; Michel, M.; Lee, J.; Verploegen, E.; Kam, N. W. S.; Ball, V.; Lee, J.; Qi, Y.; Hart, A. J.; Hammond, P. T.; Kotov, N. A. Nano Lett. 2008, 8, 1762–1770.
(26) Porcel, C.; Lavalle, P.; Ball, V.; Decher, G.; Senger, B.; Voegel, J. C.; Schaaf, P. Langmuir 2006, 22, 4376–4383.
(27) Porcel, C.; Lavalle, P.; Decher, G.; Senger, B.; Voegel, J. C.; Schaaf, P. Langmuir 2007, 23, 1898–1904.
(28) Jourdainne, L.; Lecuyer, S.; Arntz, Y.; Picart, C.; Schaaf, P.; Senger, B.; Voegel, J. C.; Lavalle, P.; Charitat, T. Langmuir 2008, 24, 7842–7847.
(29) Wang, X.; Ji, J. Langmuir 2009, 25, 11664–11671.

(30) Sauerbrey, G. Z. Phys. 1959, 155, 206–222.
(31) Haxaire, K.; Marechal, Y.; Milas, M.; Rinaudo, M. Biopolymers 2003, 72, 10–20.
(32) Rozenberg, M.; Shoham, G. Biophys. Chem. 2007, 125, 166–171.
(33) Picart, C.; Mutterer, J.; Arntz, Y.; Voegel, J. C.; Schaaf, P.; Senger, B. Microsc. Res. Tech. 2005, 66, 43–57.
(34) Crouzier, T.; Picart, C. Biomacromolecules 2009, 10, 433–442.
(35) Vörös, J. Biophys. J. 2004, 87, 553–561.
(36) Etienne, O.; Schneider, A.; Taddei, C.; Richert, L.; Schaaf, P.; Voegel, J.-C.; Egles, C.; Picart, C. Biomacromolecules 2005, 6, 726–733.
(37) Boulmedais, F.; Ball, V.; Schwinte, P.; Frisch, B.; Schaaf, P.; Voegel, J.-C. Langmuir 2003, 19, 440–445.
(38) Boulmedais, F.; Bozonnet, M.; Schwinte, P.; Voegel, J.-C.; Schaaf, P. Langmuir 2003, 19, 9873–9882.
(39) Kharlampieva, E.; Sukhishvili, S. A. Langmuir 2003, 19, 1235–1243.
(40) Zacharia, N. S.; DeLongchamp, D. M.; Modestino, M.; Hammond, P. T. Macromolecules 2007, 40, 1598–1603.
(41) Burke, S. E.; Barrett, C. J. Biomacromolecules 2003,4, 1773–1783.
(42) Leach, J. B.; Bivens, K. A.; Collins, C. N.; Schmidt, C. E. J. Biomed. Mater. Res., Part A 2004, 70, 74–82.
(43) Burke, S. E.; Barrett, C. J. Biomacromolecules 2005,6, 1419–1428.
(44) Richert, L.; Boulmedais, F.; Lavalle, P.; Mutterer, J.; Ferreux, E.; Decher, G.; Schaaf, P.; Voegel, J.-C.; Picart, C. Biomacromolecules 2004, 5, 284–294.
(45) Tomihata, K.; Ikada, Y. J. Biomed. Mater. Res., Part A 1997, 37, 243–251.
(46) Picart, C.; Schneider, A.; Etienne, O.; Mutterer, J.; Egles, C.; Jessel, N.; Voegel, J.-C. Adv. Funct. Mater. 2005, 15, 1771–1780.
(47) Kujawa, P.; Moraille, P.; Sanchez, J.; Badia, A.; Winnik, F. M. J. Am. Chem. Soc. 2005, 127, 9224–9234.
(48) Gatej, I.; Popa, M.; Rinaudo, M. Biomacromolecules 2005, 6, 61–67.
(49) Szarpak, A.; Pignot-Paintrand, I.; Nicolas, C.; Picart, C.; Auzely-Velty, R. Langmuir 2008, 24, 9767–9774.

Chapter 4 Metal NP *in situ* synthesis in pH-Amplified (PLL/HA) films

4.1 Construction of Silver nanoparticles loaded (PLL/HA) free-standing films

4.1.1 Introduction

The elaboration of free standing films based on the Layer-by-layer technique has seen significant development in the last decades due to the versatility and low cost of this deposition method. Free-standing films made of polysaccharides and/or polypeptides have recently been shown to exhibit potential applications in wound healing, in arterial repair and as dermal substitutes (Fujie et al. 2009; Larkin et al. 2010).

As an ultrathin membrane, the mechanical property is quite important for manipulation in further applications. The elastic modulus and ultimate tensile strength of (CHI/ALG) free-standing films are E=1.1 GPa, σ_{max}=51 MPa for 35 nm thick film and E=8.1 GPa, σ_{max}=123 MPa for films that thicker than 75 nm, respectively (Fujie et al. 2009). One common way to enhance the mechanical properties of polyelectrolyte multilayers is to incorporate nanometer-size inorganic compounds such as clays (Tang et al. 2003), carbon nanotubes (Mamedov et al. 2002) and metal nanoparticles (Jiang et al. 2004). Many works have been done to construct inorganic/organic hybrid multilayer films (either supported or free-standing) with high toughness and ultimate strength. However, such approach has barely been used for films made of polypeptide and/or polysaccharide, the mechanical properties are most commonly tuned by chemical cross-linking (Richert et al. 2004; Boudou et al. 2009). Very recently, Kharlampieva and co-workers constructed all-natural and robust nanoscale free-standing films by layering silk fibroin matrix with montmorillonite (MTM) clay (Kharlampieva et al. 2010) or silica nanoparticles with silsesquioxane cores (POSS) (Kharlampieva et al. 2010). They found the incorporation of inorganic nanoparticles coupled with cross-linking can largely enhance the mechanical properties of the silk matrix.

Furthermore, they reported that the mechanical properties of the hybrid films fabricated from a single-solution approach gained more enhancement than those from LbL way, due to the homogenous dispersion of inorganic components (Kharlampieva et al. 2010).

Beside direct assembly of inorganic nanoparticles with polymeric components, *in situ* synthesis of nanoparticles in a polymeric template provides another way to control nanoparticle size, shape, organization and distribution in the film. (PLL/HA) film is amongst the most investigated layer-by-layer coating to tune cell behavior and to serve as a drug delivery vehicle, due to its excellent biocompatibility. In chapter 3, we have shown that a large amount of HA is incorporated in pH amplified (PLL/HA) multilayer films. The numerous COO^- groups of HA may be used to trap Ag^+ ions, thus making the loading of a large amount of silver ions possible.

The aim of this work was: firstly, to investigate whether it is possible to synthesize silver NPs *in situ* in pH amplified (PLL/HA) film. This hypothesis was based on the fact that the number HA contain COO^- groups for the binding of Ag^+; second, to investigate whether it is possible to control NP size and distribution via the loading method and concentrations of silver ion and via the outermost layer (PLL versus HA); finally, to study the mechanical properties of free-standing films made of these nanocomposite films.

4.1.2 Materials and methods

Preparation of multilayer films and silver NP in situ synthesis. Poly(L-lysine bromide) (PLL, MW=68.3 kDa) and silver nitrate (99.0%) were purchased from sigma and hyaluronic acid (HA, MW=1 300 kDa) from Fluka.

The substrates, 14 mm diameter glass slides (VWR Scientific, France) or silicon wafers (SILTRONIX SAS ARCHAMPS, France), were cleaned with 2% (v/v) HELLMANEX® II (Hellma GmbH&Co. KG, Germany) aqueous solution at 70 ℃ for 15 min, then rinsed thoroughly with water, and dried with a stream of nitrogen. Teflon was cleaned via ultrasonicating in acetone, ethanol, and water for 15 min each and dried under nitrogen stream.

The film was built via immersing the substrate alternately in PLL solution (1 mg/mL) at pH 9.5 and HA (3 mg/mL) at pH 2.9 with intermediate rinse in water of according pH and blowing dry until predetermined layer were obtained. Either 7.5 layer pairs PLL-ending or 8 layer pairs HA-ending films were used in this work. To load silver ions, PLL-ending or HA-ending films were immersed into silver nitrate solution ($AgNO_3$) at different

concentrations from 1 to 10 mM for 15 min, followed by three water rinse, then dried in air at 37 ℃ for about half an hour. The largest concentration of 10 mM was chosen according to literature (Cui et al. 2008; Yuan et al. 2010). The pH of freshly prepared silver nitrate is about 6. Meanwhile, the silver ions were also introduced into the film via pre-complexation where silver nitrate was added to PLL solution before film buildup and PLL-Ag^+ complex solution (Dai et al. 2002) (with $AgNO_3$ concentration of 2 mM) was used instead of PLL solution for layer-by-layer assembly. *In situ* nanoparticle reduction was carried out by irradiating with UV lamp (VL-215.LC, France, Power=30 W) at a distance of ~1 cm for 35 hours. The reduction light used here is with λ= 254 nm.

For the preparation of free-standing films, Teflon substrate, coated with $(PSS/PDDA)_8$ multilayer to turn the surface from hydrophobic to hydrophilic, was used as substrate. The same film buildup procedure as mentioned above was performed and the resulted free-standing films were peeled off from the Teflon substrate with tweezers without any post-proceeding steps.

UV-visible spectrometry. Films were built on 14 mm diameter glass slides and their UV-visible spectra were taken using a UV-visible microplate reader (Tecan Infinite M1000, Australia) at predetermined time intervals to follow the reduction process. The wavelength ranges from 230 nm to 800 nm with 1 nm step size. The bandwidths for 230 to 300 nm and 301 to 800 nm are 2.5 nm and 5 nm respectively.

Inductively Coupled Plasma Mass Spectrometry. Ag nanoparticle loading amount in the films were determined by an Inductively Coupled Plasma Mass Spectrometry (ICP-MS, Thermo Corporation Inc, USA). Films embedded with Ag nanoparticle of a certain surface (around 5 × 4 mm^2) were put into 1 mL HNO_3 for 10 min to turn Ag^0 to Ag^+ ions. Finally, the solutions were diluted to 200 mL and the Ag^+ concentrations were quantified by ICP-MS.

Scanning electron microscopy. For SEM observations, the films of either HA-ending (8 layer pairs) or PLL-ending (7.5 layer pairs) embedded with silver nanoparticles were prepared on silicon wafer following the procedure described above. The surface morphology as well as cross-section of the nanoparticle embedded films was visualized by using a FEG 250 SEM (QUANTA FEG 250, FEI, Czech Republic). The vCD mode was used to enhance the element contrast to better identify the silver nanoparticles.

Atomic force microscopy. The surface morphology of films with silver nanoparticles was imaged by a Veeco AFM (Technical Manufacturing Corporation, Peabody, MA, USA). The final images were treated with Gwyddion software version 2.22.

Transmission electron microscopy. The cross-section morphology of the silver nanoparticle embedded films and Ag NP distribution in film Z-direction were monitored by TEM. Transmission electron microscopy and High Resolution TEM were carried out with a JEM-2010 TEM (ELECTRON MICROSCOPE, JEOL, Japan) operating at 200 kV with a 0.19 nm point to point resolution. Cross-section samples preparation was realized by the tripod polishing method (Ayache et al. 1995). The specimen was prepared in the form of a silicon-film with Ag NP-resin sandwich to get a cross-section. The specimen was glued onto the glass stub of the tripod polisher. Samples were polished on both sides using a series of plastic diamond lapping films, with grains of decreasing sizes (30µ, 15µ, 6µ, 1µ, 0.5µ). One side was planar polished. In the second stage the specimen was removed from the glass stub support with polished side stuck back. Polishing on the other side was performed with a tilt angle of 0.3-0.6° adjusted with the micrometer screws. Further polishing was achieved with identical steps as on the first side. An optical inverted microscope was used to check frequently the residual specimen thickness so as to obtain less than 10 µm thick. Finally, the specimen was removed by dissolving in acetone from the glass stub and glued onto a one-hole TEM grid. Low-angle ion beam milling was used for final perforation of the samples to be sure to have a large electron transparent area.

Tensile test. The mechanical properties of the free-standing film with and without silver nanoparticles were characterized via stress-strain curves measured by a mechanical strength microtest (Deben, U.K.). The stress where the film break was taken as ultimate stress and the elastic modulus was deduced from the linear part of the stress-strain curve. 10 tests were carried out for each sample.

4.1.3 Results and discussion

Silver nanoparticle in situ reduction follow-up. Two methods were applied to load silver ions (silver nitrate): complexing silver nitrate with PLL in solution before LBL assembly or post-diffusion of silver nitrate into (PLL/HA) films.

The *in situ* reduction of silver nanoparticle was triggered by UV irradiation (UV irradiation condition: λ=254 nm, power=30 W, distance=~1 cm) and UV-visible spectrometer was used to follow the *in situ* reduction of the nanoparticle (**Figure 4.1**). Upon UV irradiation, the plasma resonance peak of silver emerged in the UV-visible spectra. For pre-complexed films, two broad peaks centered at λ=398 nm and λ= 530nm were be observed, suggesting two populations of silver nanoparticles with different sizes were synthesized in the films

(Soltwedel et al. 2010). The reduction time was about 35 hrs. For post-loaded films, the absorbance was relatively low. The main peaks are around λ=450 nm, with a shoulder at around λ=500 nm. But for HA-ending film, the shoulders were not so visible, especially after a reduction time of 8 hrs. Silver ions were completely reduced in about 2 hrs.

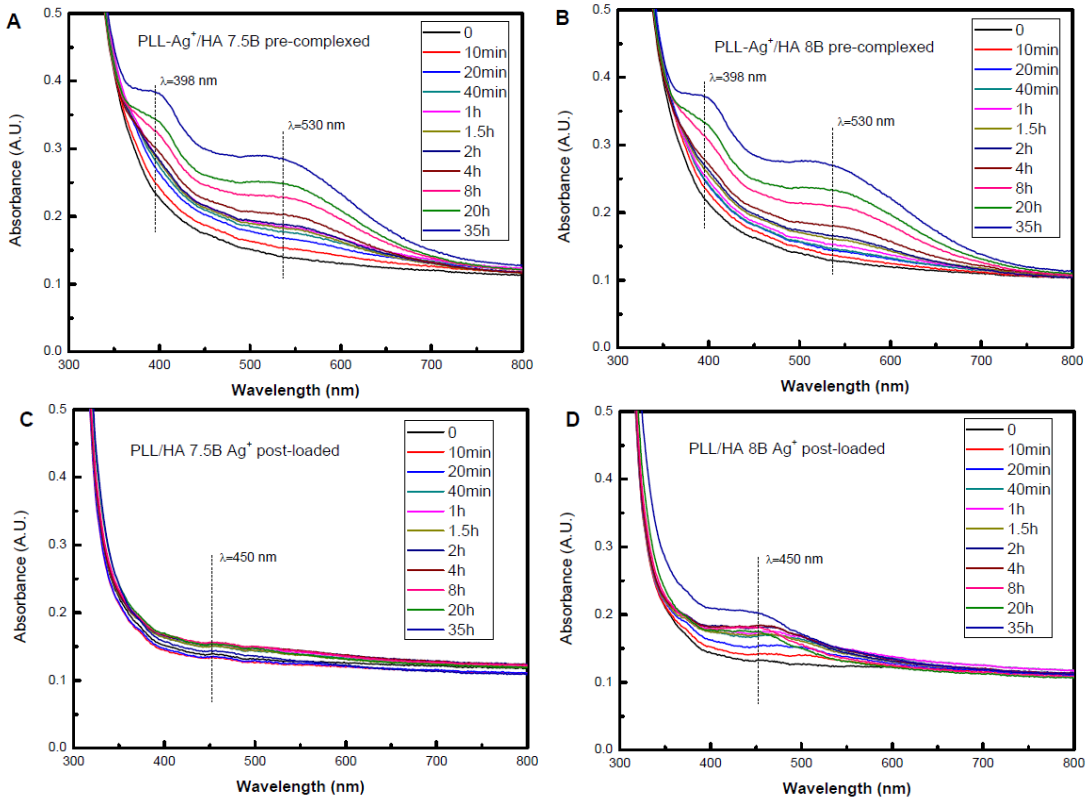

Figure 4.1 UV-visible spectra of silver nanoparticle *in situ* reduction in (PLL/HA) films at different UV irradiation time for pre-complexed films with PLL-ending (A) and HA-ending (B) and post-loaded films with PLL-ending (C) and HA-ending (D). UV irradiation condition: λ=254nm, power=30W, distance= ~1cm. The $AgNO_3$ post loading concentration was 10 mM.

The silver NPs loading amount in the films were determined by first dissolving silver NPs in HNO_3 then measuring the silver ion concentration by ICP-MS (**Figure 4.2**). For post-loaded samples, HA-ending films load more Ag NPs than the PLL-ending counterparts. Increasing $AgNO_3$ concentration from 1 mM to 10 mM did not change the final Ag NPs loading in PLL-ending films but drastically increased the Ag NPs loading amount in HA-ending films. We may tentatively attribute these differences to the presence of some free COO- groups in HA-ending films. In contrary, for PLL-ending film, the silver ion loading was almost saturated when the post loading concentration is 1 mM; whereas for HA-ending film more loading amount can be achieved by increasing the concentration of $AgNO_3$ solution.

Slighly more Ag NPs were found in pre-complexed PLL-ending film than its HA-ending counterpart, indicating part of the silver ions may diffuse into HA solution upon HA deposit step.

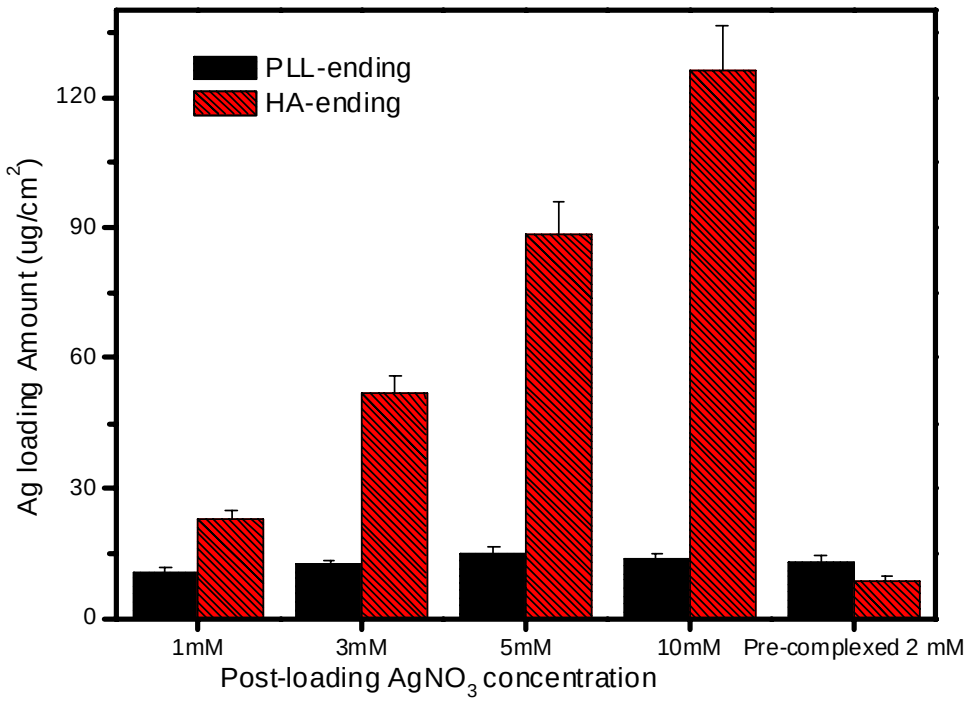

Figure 4.2 Silver NPs loading amount in different films.

To further study the nanoparticle size and distribution on film surface as well as in film bulk structure, SEM, AFM and TEM were performed.

Surface morphology and silver NP distribution of (PLL/HA) films with Ag^+ introduced via Pre-complexation. Surface morphology as well as cross-section of the silver nanoparticle loaded films was observed by SEM. The silver nanoparticles were not homogeneous in size and in vertical direction in the pre-complexed films. As can be observed in **Figure 4.3**, the diameters of particles on film surface ranges from less than 50 nm to almost 200 nm, suggesting nanoparticle aggregated during synthesis in the film. This is in accordance with UV-visible spectra data which had two absorption peaks. In Z-direction, most of the silver particles were found aggregated on the film surface for PLL-ending film, but there were only few silver particles on HA-ending film surface. Of note, lots of charges accumulated on HA-ending film surface (**Figure 4.3B**) due to the poor conductivity caused by lack of NPs, this makes the imaging on film surface difficult especially in a much higher magnification. At high magnification, only images of the HA-ending surface with NP were obtained (**Figure 4.3B'**).

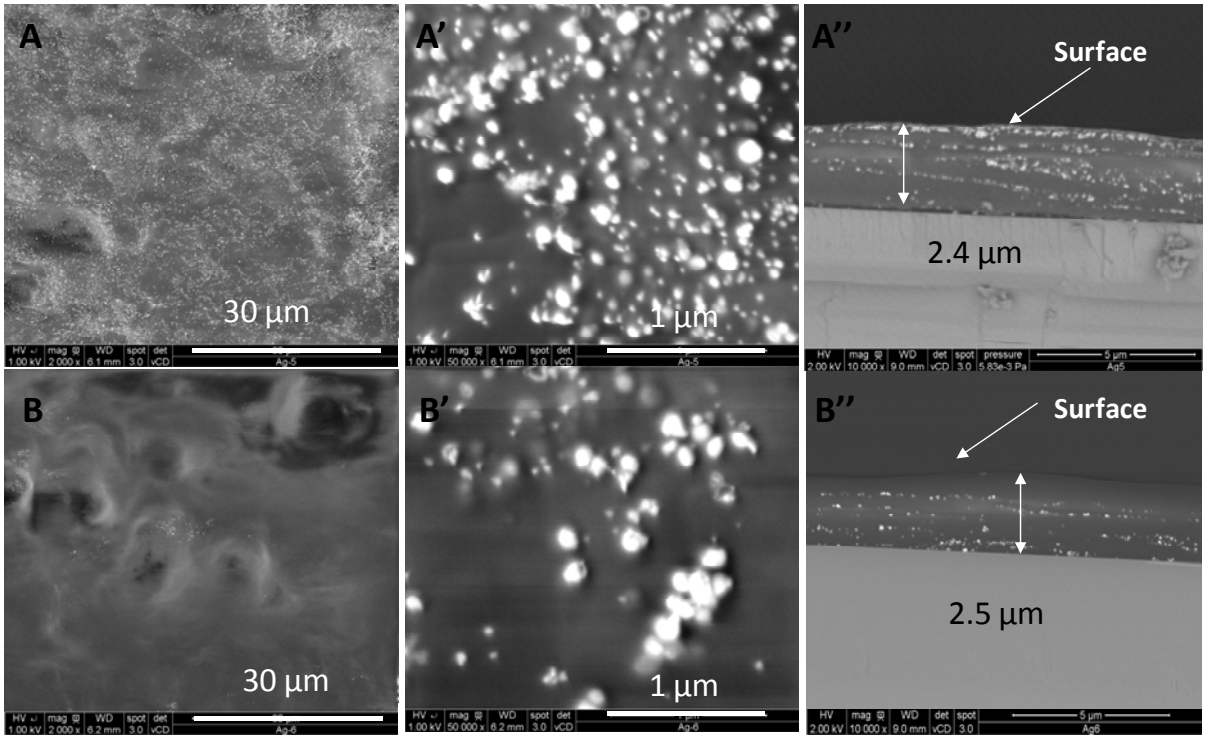

Figure 4.3 SEM images of surface morphology (A, A', B, B') and cross-section (A'' and B'') for silver nanoparticle pre-complexed (PLL/HA) films with PLL-ending (A) and HA-ending (B). A' and B' were the magnified images for A and B, respectively.

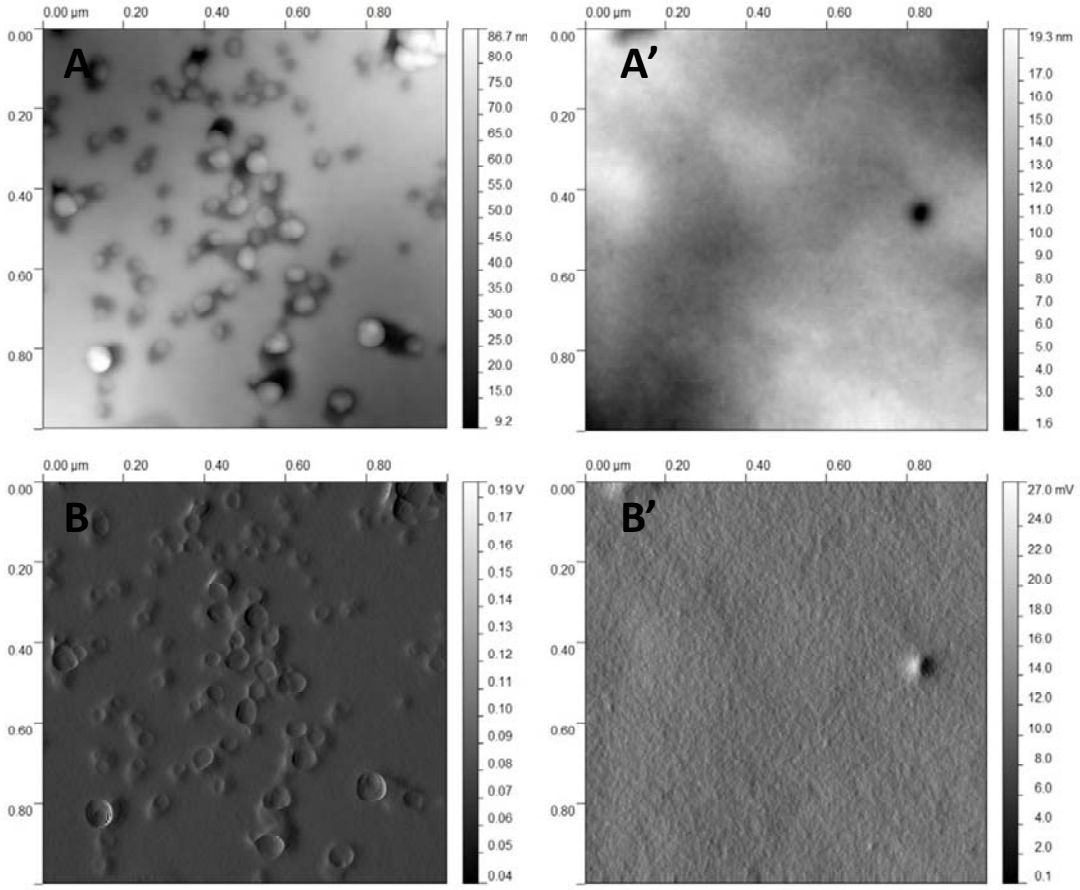

Figure 4.4 AFM images of both height images (A, A') and amplitude images (B, B') for silver nanoparticle pre-complexed (PLL/HA) films with PLL-ending (A, B) and HA-ending (A', B').

Film surface morphology was further confirmed by AFM images. As shown in **Figure 4.4**, almost no nanoparticles were found on HA-ending film surface, whereas a large number of nanoparticles with sizes of 50 nm to 200 nm can be observed on PLL-ending films. Of note, holes sized bigger than 50 nm appeared on HA-ending film surface (**Figure 4.4A', B'**), these holes may caused by the contraction of the polymer when the underneath Ag nanoparticle was formed under UV irradiation.

The nanoparticle distribution in the Z-direction of the pre-complexed films could be clearly visualized in TEM images in **Figure 4.5**. The silver nanoparticles separated on the top and in the middle and at the bottom of the PLL-ending film (**Figure 4.5A**). At higher magnification (**Figure 4.5A' and A"**), two populations of silver nanoparticles with the diameters of ~ 16 nm and ~ 50 nm, respectively, were found in the bulk of the film. For the HA-ending film, most of the silver nanoparticles were settled at the bottom of the film, and also two populations of different sizes were observed.

In the pre-complexed films, the silver ions were added in PLL solution. On PLL-Ag^+ complex deposit steps, silver ions may interact with COO^- of HA chains in the film when PLL chains diffused into the film, thus after UV reduction the nanoparticles were formed on film surface as well as in the film bulk. When another HA layer was added at pH 2.9, the ionization degree of carboxyl acid in the film decreased. Thus, part of the COO^- groups were protonated to be COOH and released part of the silver ions in the film. Meanwhile, the HA chains in solution of pH 2.9 have low charge density, which may lead to a very low number of Ag^+ ions trapped. In this case, the HA-ending films in which $AgNO_3$ was pre-complexed lead to a formation of silver nanoparticles only at the bottom of the film, i.e. close to the film/silicon interface.

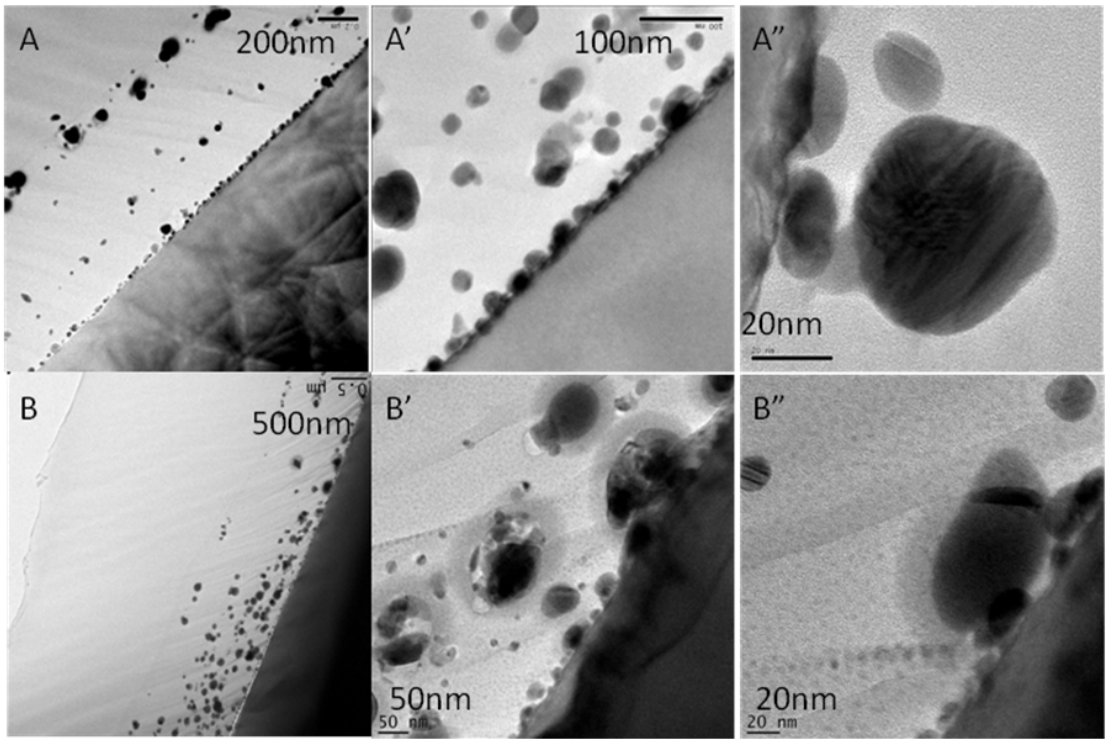

Figure 4.5 TEM cross-section images of silver nanoparticle pre-complexed (PLL/HA) films with PLL-ending (A-A") and HA-ending (B-B").

Surface morphology and silver NP distribution in (PLL/HA) films with Ag^+ introduced via post-loading. For the post-loaded films, the same techniques were used to analyze the morphology and distribution of reduced silver nanoparticles.

As demonstrated in **Figure 4.6**, the silver nanoparticles coverage on film surface was high, although the absorbance in UV spectra was low. The nanoparticle size was much smaller than that observed on pre-complexed films. Silver nanoparticle distribution at the surface of PLL-ending film was more homogeneous than on HA-ending film. Two different regions were observed on HA-ending films with domains of low amount of nanoparticles surrounded by large amounts of particle covered areas. This looks like a phase separation, as if silver ions could interact with negatively charged carboxylate groups on HA, the areas fully covered by particles can be ascribed to HA aggregations with high amount of negative charges. The low nanoparticle coverage domains might be HA-PLL complexes with less unpaired carboxylate groups. In the cross-section, PLL-ending film got a band near film surface embedded with more and larger sized nanoparticles. On the part close to silicon-film interface, the nanoparticles were less numerous and of smaller size. In the HA-ending films, a band with few nanoparticle just beneath the film surface was visible as well as a band with more homogeneous particles on the film surface. In the part of the film close to silicon-film interface, no silver nanoparticles could be observed at the magnification of 20 000. The band

with few nanoparticles beneath the film surface in HA-ending film cross-section may probably correspond to the HA-PLL complexed region with few free COO^- groups, which tended to disappear in the edge of **Figure 4.6B"**. Indeed, in some places of HA-ending film cross-section, no such band was observed.

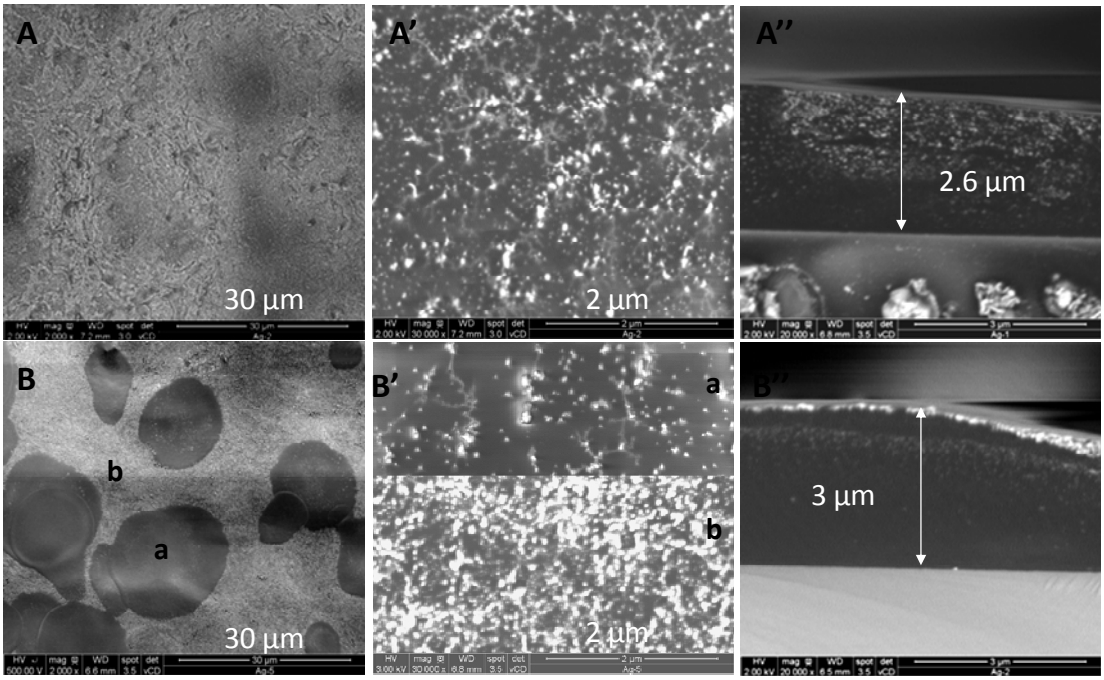

Figure 4.6 SEM images of surface morphology (A, A', B, B') and cross-section (A'' and B'') for silver nanoparticle post-loaded (PLL/HA) films with PLL-ending (A-A") and HA-ending (B-B"). A' and B' were the magnified images for A and B. The upper and lower part of B' corresponded to the magnification of different part in B, indicated as **a** and **b** respectively. The $AgNO_3$ loading concentration is 10 mM.

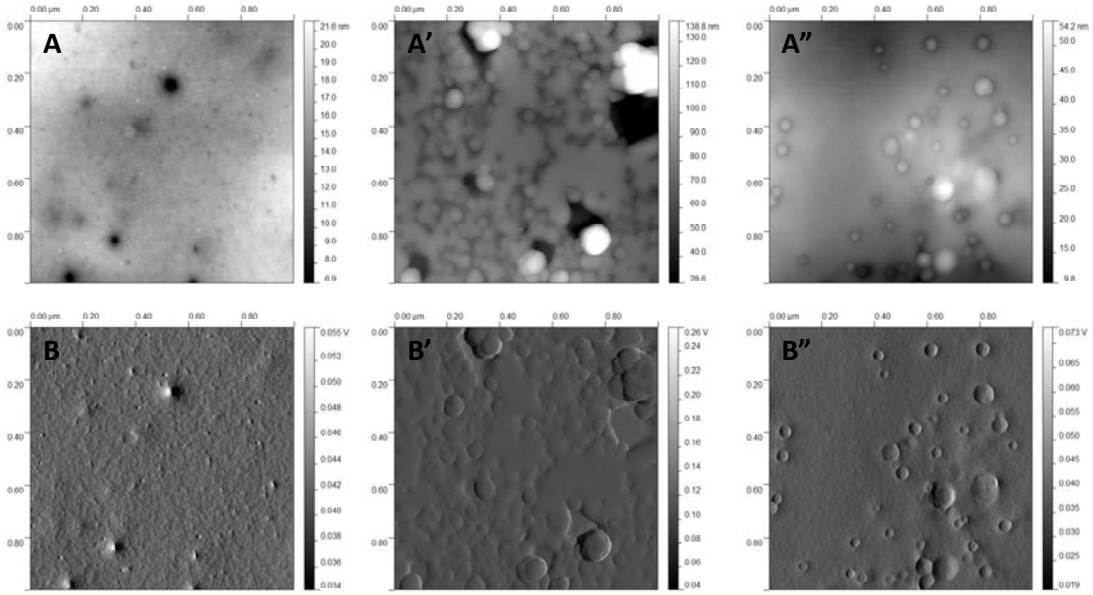

Figure 4.7 AFM images of both height images (A-A") and amplitude images (B-B") for silver nanoparticle post-loaded (PLL/HA) films with PLL-ending (A, B) and HA-ending (A', B', A" and B"). The $AgNO_3$ loading concentration is 10 mM.

AFM images gave more detail information about film surface morphology and particle size. As can be observed in **Figure 4.7**, only very small nanoparticles were found on PLL-ending film surface. Large and more numerous nanoparticles were observed on HA-ending films. As already shown in SEM images (**Figure 4.6B and B'**), the nanoparticles distribution on HA-ending surface was not homogenous. **Figure 4.7A' and A"** were taken at different places on HA-ending film surface, differences in Ag NPs amount can be noticed. Again, holes were found on PLL-ending film surface. The same as the case of HA-ending pre-complexed film, the holes may caused by the contraction of the polyelectrolyte when the underneath Ag nanoparticles were formed under UV irradiation.

Silver nanoparticle distribution in film Z-direction was confirmed in TEM images (**Figure 4.8**). As already found in SEM images, silver nanoparticles mostly located on the top of the PLL-ending film (**Figure 4.8A**). Only few and very small nanoparticles were found randomly separated in the bottom part of the film (**Figure 4.8A' and A"**). For the HA-ending film, a "vacuum" region with almost no Ag nanoparticles existed just beneath the film surface. Two layers of large nanoparticles were aligned at both sides of the "vacuum" region. More and smaller nanoparticles were found towards the film/silicon interface. Of note, the small Ag nanoparticles aligned in rows close to silica substrate, indicating layered structures in HA-ending films.

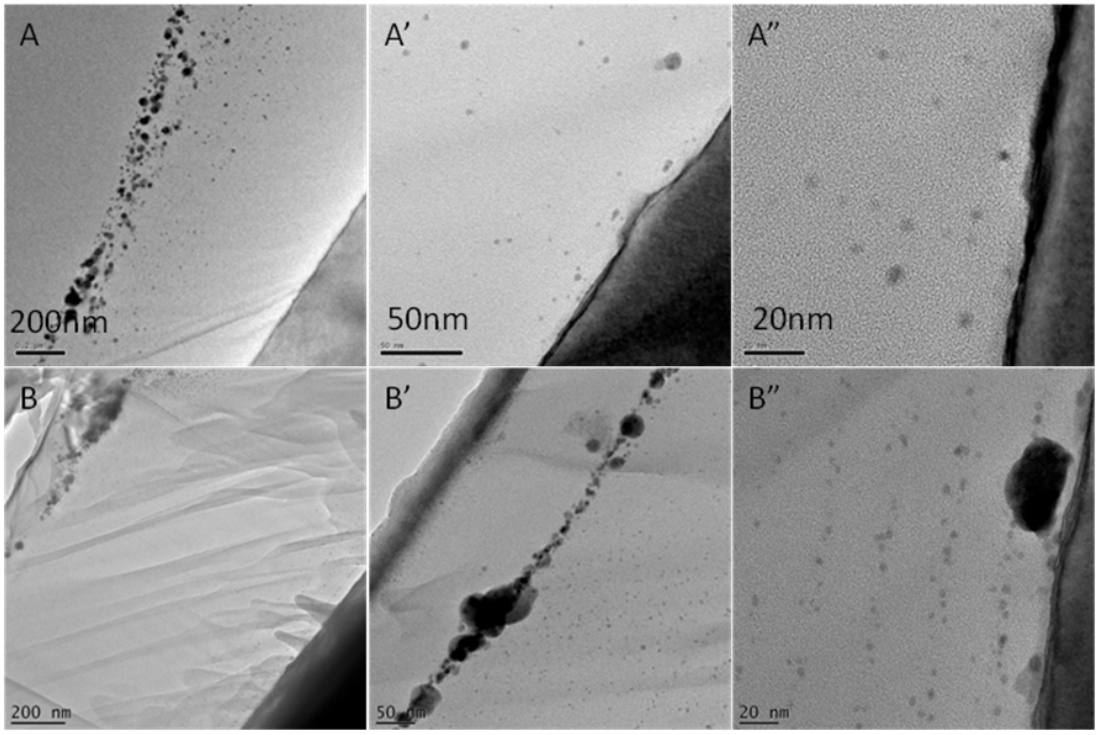

Figure 4.8 TEM cross-section images of silver nanoparticle post-loaded (PLL/HA) film with PLL-ending (A-A") and HA-ending (B-B"). The $AgNO_3$ loading concentration is 10 mM.

Mechanical properties of free-standing films. When Teflon was used instead of hydrophilic substrate, the films can be easily peeled away from substrate just after the films were dried in the air.

8 bilayers of (PDDA/PSS) was built on Teflon to turn the hydrophobic surface hydrophilic and promote (PLL/HA) film growth. After film build-up/ions loading and UV reduction, the films with silver nanopaticles can be easily and totally taken away from the substrate. As shown in **Figure 4.9** the released film got exactly the same size of the substrate.

Figure 4.9 Digital photo of $(PDDA/PSS)_8$-$(PLL\text{-}Ag/HA)_8$ free-standing film.

These free-standing films were cut into small pieces of 3×15 mm^2 and used for tensile microtest. The ultimate stress and elastic modulus for the different conditions are listed in **Table 4.1** in the form of absolute value as well as relative value in ratio compared with the film with no silver nanoparticles.

From **Table 4.1**, we can see the mechanical properties of the (PLL/HA) free-standing films are quite poor, the ultimate stress and elastic modulus are far less than the reported value for 75 nm (CHI/ALG) free-standing films (E=8.1 GPa, σ_{max}=123 MPa), even after reinforced by silver NPs. However, we can still find some trends that the nanoparticle loading amount, distribution, and its size can affect the reinforcement on (PLL/HA) multilayer when silver nanoparticles were inorporated.

Table 4.1 Mechanical properties of free-standing films averaged from at least 6 measurements.

Free-standing films	Ultimate Stress (σ_{max})		Elastic Modulus (E)		Ag loading amount ($\mu g/cm^2$)
	Absolute *(MPa)*	Relative In ratio	Absolute *(GPa)*	Relative In ratio	
$(PDDA/PSS)_8(PLL/HA)_8$	17±2	1	0.699±0.103	1	0
$(PDDA/PSS)_8(PLL\text{-}Ag/HA)_8$	17±2	1.0	0.734±0.123	1.05	8.68
$(PDDA/PSS)_8(PLL/HA)_8$-Ag 1 mM	19±1	1.1	0.923±0.137	1.32	23.15
$(PDDA/PSS)_8(PLL/HA)_8$-Ag 3 mM	19±2	1.1	0.922±0.118	1.32	51.87
$(PDDA/PSS)_8(PLL/HA)_8$-Ag 5 mM	21±2	1.2	0.925±0.078	1.32	88.59
$(PDDA/PSS)_8(PLL/HA)_8$-Ag 10 mM	28±2	1.6	1.115±0.170	1.64	126.16
$(PDDA/PSS)_8(PLL/HA)_7$ -PLL	12±1	1	0.465±0.081	1	0
$(PDDA/PSS)_8(PLL\text{-}Ag/HA)_7$ -PLL-Ag	20±4	1.7	0.958±0.159	2.06	13.09
$(PDDA/PSS)_8(PLL/HA)_7$ -PLL-Ag 10 mM	26±1	2.2	1.146±0.085	2.46	14.03

Compared the four different HA-ending post-loaded films, one can notice that no enhancement in mechanical properties was observed for films with low nanoparticle loading amount. A noticeable reinforcement in mechanical properties only happens when the nanoparticle amount reaches a certain level.

Nanoparticle distribution in the film is important for mechanical properties. Films with nanoparticles on surface, in the middle and at the bottom of the film (PLL-ending pre-complexed film, see **Figure 4.5A**) got an increase in ultimate stress and elastic modulus of the films compared to the pure (PLL/HA) film, whereas the films with nanoparticles only at the bottom of the film (HA-ending pre-complexed film, see **Figure 4.5B**) did not change the film mechanical properties.

Besides, the nanoparticle size can also have an effect on reinforcement of film mechanical properties. The PLL-ending pre-complexed film and the PLL-ending post-loaded film have similar nanoparticle loading amount, but much higher enhancement on stress and modulus was achieved in PLL-ending post-loading film (with much smaller nanoparticle size, see **Figure 4.8A**).

4.1.4 Conclusion

A nanocomposite film made of (poly(L-lysine)/Hyaluronan) and containing silver nanoparticles has been formed by *in situ* UV reduction of silver ions, which were loaded either by pre-complexation with PLL or by post-diffusion. Ag nanoparticle size synthesized in the film depended on the method for the loading of silver ions: pre-complexation method leads to much bigger and almost two populations of nanoparticles while post-load way resulted in much smaller nanoparticles.

Ag nanoparticle distribution on film surface as well as in the whole film thickness relies on the ending layer. For pre-complexed film, silver nanoparticles were mostly aggregated on the film surface for PLL-ending film, but there were only few at the surface of HA-ending films. PLL-ending film loaded more silver NPs than HA-ending counterpart. For post-loaded films, silver NP distributed evenly in PLL-ending film but unhomogeneously on surface as well as in bulk of HA-ending film. This suggested there are large HA aggregations in HA-ending film and the aggregations disappear when another PLL layer was added. Silver nanoparticles loading amounts did change in PLL-ending films when the $AgNO_3$ concentration was increased from 1 mM to 10 mM. While for HA-ending film, larger $AgNO_3$ concentration lead to a higher amount of Ag loaded.

Free-standing films made of (PLL/HA) and containing silver nanoparticles were obtained by peeling them away from Teflon substrate in dry state. Their mechanical properties were tested. The ultimate stress and elastic modulus of hybrid free-standing films depended on several parameters, including the loading amount of nanoparticle, their distribution and size.

4.2 *In situ* synthesis of gold nanoparticles in exponentially-growing layer-by-layer films

4.2.1 Introduction

Metal nanoparticles are used in an increasingly large number of biomedical applications (Liao et al. 2006) in the field of biotechnology, biosensing (Anker et al. 2008; Sepulveda et al. 2009), bioimaging (Murphy et al. 2008), and drug and gene delivery (Huang et al. 2007), due to their interesting optical and electrical properties. During the past years, several studies have focused on the directed assembly of metal nanoparticles into organic solutions to form organic-inorganic hybrid nanomaterials (Chen et al. 2010; Pastoriza-Santos et al. 2010). Hybrid nanocomposites are synthesized via two major strategies. The first consists in assembling prefabricated inorganic nanoparticles (NPs) with polymers, either by chemical grafting or by adsorption of the polymer onto the particles (Galyean et al. 2009). Assemblies of NPs and polyelectrolytes can be built in a layer-by-layer fashion to control the number and position of nanoparticles (Schrof et al. 1998; Dong et al. 2003; Lee et al. 2006), but the rinsing steps may possibly affect the stability of the assembly. The second uses an organic solution (or "matrix") as a template to nucleate and grow *in situ* inorganic NPs (Chia et al. 2008). This is most often achieved directly by adding precursor ions into the polymeric solution (Esumi et al. 1998). However, the chemical synthesis of metal nanoparticles, including platinum, silver or gold, often requires the use of harsh chemicals (i.e. detergents, solvents), which are undesirable for biomedical applications (Connor et al. 2005). In this respect, biomolecules such as peptides (Tan et al. 2010; Toroz et al. 2011), proteins, or polysaccharides (Cui et al. 2008) are interesting due to the presence of numerous charged groups in their chains. This enables them to interact with positively charged or negatively charged metal ions precursors, thereby stabilizing them (Richardson et al. 2006). Typically, anionic groups can interact with Ag^{+} (Cui et al. 2008) or Pb^{2+} ions (Joly et al. 2000) and cationic groups can interact with negatively charged ion complexes, such as gold aurochlorate ions ($AuCl_4^-$ or $AuCl_2^-$) (Sardar et al. 2008). Peptides can also contribute to the reduction of precursor ions by acting as electron donors (Tan et al. 2010). Moreover, peptides can act as stabilizer of the formed nanoparticles, as they can specifically bind to certain inorganic surfaces (Chen et al. 2010).

Gold nanoparticles are particularly interesting due to their non-toxicity (Connor et al. 2005),

biocompatibility, photothermal properties (Hu et al. 2006), ease of imaging and versatility of surface chemistry (Boisselier et al. 2009). Polymers containing amine groups have been widely used as binding sites for gold aurochlorate ions ($AuCl_4^-$) and as stabilizer of gold nanoparticles (Cho et al. 2005; Mei et al. 2005; Newman et al. 2006; Richardson et al. 2006). Natural biopolymers such as α-amino-acids are also emerging as versatile templates (Tan et al. 2010), due to their capacity to reduce gold ions and to bind to Au^0. Importantly, not only aromatic, amine or amide groups play a role in the synthesis of gold NPs, but other groups such as C-O-C and carboxylate have been shown to exhibit some reducing capacities (Mallick et al. 2005; Kar et al. 2010).

Of particular interest are the possibility offered by biopolymers to control nanoparticle sizes and morphologies (Tan et al. 2009), and also to work in mild conditions, i.e. at ambient temperature, in non-toxic solvents or even in aqueous medium. Typically, reduction of tetrachloroauric acid ($HAuCl_4$) can be achieved in a basic buffer such as sodium borate or by photo-chemical UV-irradiation (Pastoriza-Santos et al. 2010), which generates the necessary electrons to catalyze the reaction. This opens new perspectives for the "green" biomimetic synthesis of nanocomposites. So far, the majority of studies have focused on formation of NPs from solutions containing a mixture of the biomacromolecule and of the metallic ions (Mallick et al. 2005; Richardson et al. 2006; Sardar et al. 2008). However, controlling the spatial organization, nucleation and growth of monodisperse and non-aggregated NPs on material surfaces remains a challenge (Kharlampieva et al. 2008).

Polyelectrolyte multilayer films (PEM) constitute a versatile and easy system to build architectures whose properties can be tuned in terms of thickness, film internal structure and degree of ionization of the polyelectrolytes (Decher 1997; Yoo et al. 1998). Synthetic and/or biological polyelectrolytes that possess various functional groups, including carboxylic acid, amine, and amide, can be used as building blocks. Interestingly, PEM film thickness can grow linearly (Caruso et al. 1997) or exponentially (Picart et al. 2001; Picart et al. 2002), which leads to highly stitched films in the former case (Jaber et al. 2007) and to more swollen films in the latter case (Crouzier et al. 2009). PEM films made of synthetic polyelectrolytes have recently been used as a template for *in situ* reduction of gold precursors(Chia et al. 2008; Kharlampieva et al. 2008). Poly(L-tyrosine), a polyaminoacid, which was deposited as topmost layer on a poly(allylammine)/poly(styrene sulfonate) (PAH/PSS) film, was able to direct nanoparticle formation (Kharlampieva et al. 2008). However, the gold NPs were confined to the topmost polyaminoacid layer due to absence of diffusion of gold ions in the underlying stitched films. Beside its surface, the PEM film can potentially serve as

nanoreservoir to synthesize NPs in a spatially confined environment, i.e. in the “film bulk”. Rubner and coworkers performed the very first attempt to grow NPs in the entire depth of the film (Chia et al. 2008). They used the reducing properties of amine groups of PAH to synthesize gold NP within the bulk of polyacrylic acid/PAH (PAA/PAH) and (PAA/PSS) films. However, as these linearly growing films exhibit a high degree of ion pairing, they had to surpass the difficulties in introducing the gold chloride ions into them. To this end, they introduced a nanoporosity transition by soaking the film at very acidic pH (<2) to generate free ammonium groups.

In this context, exponentially growing films that are rich in unpaired amine groups and that contain other functional groups (i.e. carboxylic acid, hydroxyl), such as poly(L-lysine)/Hyaluronan (PLL/HA) films (Picart et al. 2001; Picart et al. 2002; Shen et al. 2011) may appear interesting for the loading of a high amount of gold ions as well as for their reduction. Furthermore, their tunable thickness over a large range (Richert et al. 2004) may allow a very large amount of NPs to be formed in such spatially-confined environment. We have recently studied the internal structure of pH-amplified (PLL/HA) films, with regards to their growth, presence of hydrogen bonds, ionization degree of HA and diffusive properties of PLL (Shen et al. 2011).

Here, we aim to use these pH-amplified (PLL/HA) films as template for *in situ* synthesis of gold NPs using UV-reduction. We demonstrate that the formation of NPs, especially their size and bulk density, can be controlled solely by varying the solution pH of the gold precursor solution from pH 3 to 9. Homogenous gold NPs were formed at varying pH, with diameter ranging from ~1.7 nm (high pH) to ~9 nm (low pH). Very interestingly, the gold NPs were homogeneously dispersed throughout the entire film depth over ~2.5 μm. To our knowledge, these results show for the first time the spatially-confined growth of a tunable amount of well-dispersed and homogeneous gold NPs, using a micrometer-thick PEM film as organic template.

4.2.2 Experimental section

Preparation of multilayer films. Poly(L-lysine) bromide (PLL, P2636, MW=68 kDa) and gold chloride trihydrate ($HAuCl_4 \cdot 3\ H_2O$, 99.9 % purity) were purchased from Sigma. Hyaluronic acid, (HA, MW=1 300 kDa) was a product of Fluka. 14 mm diameter glass slides (VWR Scientific, France) or silicon wafers (Siltronix SAS, Archamps, France) taken as

susbtrates were cleaned by soaking in 2% (v/v) Hellmanex® II (Hellma GmbH, Müllheim, Germany) aqueous solution at 70°C for 15 min, then rinsed thoroughly with water, and dried with a stream of nitrogen. The film was built by immersing the substrate alternately in PLL solution (1 mg/mL) at pH 9.5 and HA (3 mg/mL) at pH 2.9 with intermediate rinse in water of same pH and blowing dry. In this study, we built $(PLL9.5/HA2.9)_7$-PLL9.5 films (films made of 7.5 layer pairs, ending by PLL) and $(PLL9.5/HA2.9)_8$ (films made of 8 layer pairs, ending by HA).

Gold NP in situ synthesis. For gold salt loading, the PLL-ending or HA-ending films were immersed into 10 mM gold chloride salt solution for 15 min, followed by three water rinses, before being air dried in an incubator at 37 ℃ for 30 min. As the pH of the 10 mM gold chloride solution is ~2, NaOH was added drop wise until the desired pH was achieved. The gold-salt-loaded samples were irradiated with an ultra violet lamp (365 nm, VL-215.LC, France, Power = 30 W) at a distance of ~1 cm for 35 hrs, as described by others (Chia et al. 2008).

Fourier Transform Infrared Spectroscopy. Film structure was investigated by Fourier transform infrared (FTIR) spectroscopy in transmission mode using a Vertex 70 spectrophotometer (Bruker Optics GmbH, Ettlingen, Germany) equipped with a mid-infrared (MIR) detector. All the films were deposited on silicon wafers for these experiments. The spectrum from the bare Si was always taken as reference. A single-channel spectrum from 256 interferograms was recorded between 400 and 4000 cm^{-1} with a 2 cm^{-1} resolution, using Blackman-Harris three-term apodization and the standard Bruker OPUS/IR software v6.5 (Bruker Optics GmbH). The different peaks characteristic of the polyelectrolytes and of the pH-amplified (PLL/HA) films have identified in our previous work (Shen et al. 2011). Basically, there are three absorption regions in the FTIR spectra. The band from 3500 to 3000 cm^{-1} is mainly associated with hydrogen bonded N-H and O-H groups. The region from 1750 to 1350 cm^{-1} contains COOH (1735 cm^{-1}), amide I (1656 cm^{-1}, random), amide II (1560 cm^{-1}) and COO^- (1605 and 1400 cm^{-1}). The characteristic peaks of saccharide rings on HA are visible in the 960-1200 cm^{-1} region, with the most intensive peaks at 1045 and 1080 cm^{-1}.

UV-visible spectrometry. Films were built on 14 mm-diameter glass slides and their UV-visible spectra were taken using a spectrofluorimeter (Infinite M1000, Tecan, Australia) at predetermined time interval to follow the reduction process. The wavelength ranges from 230 nm to 800 nm with 1 nm step size. The bandwidth was of 2.5 nm over the range 230-300 nm and of 5 nm over the range 301-800 nm.

Inductively Coupled Plasma Mass Spectrometry (ICP-MS). The amount of Au nanoparticle loaded in the films was determined by an Inductively Coupled Plasma Mass Spectrometry (ICP-MS, X-series, Thermo Corporation Inc, USA). Films embedded with Au nanoparticle of a certain surface (around 5 x 4 mm^2) were put into 1 mL freshly prepared aqua regia (HNO_3: HCl *v*:*v* = 1:3) for 10 min to turn Au^0 to Au ions. Finally, the solutions were diluted to 200 mL and the Au ion concentrations were quantified by ICP-MS.

Scanning electron microscopy. For SEM observations, the PLL-ending (7.5 layer pairs) or HA-ending (8 layer pairs) films were prepared on silicon wafer following the procedure described above. The surface morphology and the cross-section of the NPs synthesized in the films were visualized by using a field emission gun (FEG) SEM (Quanta FEG 250, FEI, Czech Republic). The low voltage high contrast (vCD) detector mode was used to enhance the element contrast and better identify the gold NPs.

Atomic force microscopy. The surface morphology of films with or without gold NPs was imaged in tapping mode using a Veeco Di 3100 AFM (Veeco, France) with OMCT-240 tapping mode cantilevers (Olympus, France). The final images were treated with Gwyddion software version 2.22.

Transmission electron microscopy. The cross-section morphology of nanocomposite films was monitored by transmission electron microscopy (TEM) and high-resolution TEM (HR-TEM) using a JEM-2100 LaB6 (JEOL, Japan) operating at 200 kV with a 0.19 nm point-to-point resolution. Two pieces of film-coated silicon were embedded face-to-face in epoxy (M-bond 610) for 2 hrs at 150 ℃ such as to form a silicon-film-resin-film-silicon sandwich (~1.5 x 2 x 2.5 mm^3). This sandwich was further cut into 2-3 pieces before being polished by the tripod polishing method (Ayache et al. 1995). To this end, the specimen was glued onto the glass stub of the tripod polisher (model 590 TEM, South Bay Technology, San Clemente, USA). Samples were polished on both sides using a series of plastic diamond lapping films (Escil, Lyon, France), with grains of decreasing sizes (30 µm, 15 µm, 6 µm, 1 µm, 0.5 µm respectively). The first side of the sandwich was polished to achieve a 300-500 µm in thickness. Then, it was reverted to continue with the polishing of the second side, the sample being tilted at an angle ~ 0.6 °. An optical inverted microscope was used to check frequently the residual specimen thickness so as to obtain a thickness < 10-15 µm. Finally, the sample was removed from the glass stub and glued onto a TEM copper grid containing a central hole. Low-angle ion beam milling (Gatan, Colorado, USA) was used for the final precision polishing of the samples. The final thickness around the perforated area is <100 nm. Energy dispersive X-ray (EDAX) spectra were also collected perpendicular to the sample

surface.

Image analysis. Particle size was measured for each sample using Image J software v1.38x (NIH Bethesda, USA, http://rsbweb.nih.gov/ij/index.html) The reported particle sizes are the number average from at least 240 particles. The particle size distribution was also generated by Sigma Plot software (Systat, USA).

4.2.3 Results and discussion

In this work, we used a biocompatible polypeptide/polysaccharide made by alternating deposition of PLL at pH 9.5 and HA at pH 2.9 (i.e. a (PLL9.5/HA2.9) film) as template for *in situ* synthesis of gold NPs in mild conditions, i.e. in pure water. The films were built as described in our previous studies by alterning deposition of the polyelectrolytes followed by a water rinse and blow drying after each deposited layer (Richert et al. 2004; Shen et al. 2011). $(PLL9.5/HA2.9)_i$ films (i = 7.5 or 8, being the number of layer pairs) of typical thickness between 2-3 μm (Shen et al. 2011) have been used for all experiments. Aurochlorate ions were loaded as precursors by simple adsorption performed after film buildup. Here, we investigated the potentiality of these films to spatially confine the growth of gold NPs and to stabilize them. We focused on the effect of pH of the gold chloride solution, which is known to affect the stability of the Au-Cl-H_2O system (Richardson et al. 2006), on nanoparticle formation. We also studied the influence of the film ending layer (PLL versus HA). We have analyzed the effect of gold NP formation and film bulk structure by Fourier Transform infrared spectroscopy (FTIR). Furthermore, we have quantified the size of gold NPs and observed their distribution in the film cross-section by means of high resolution transmission electron microscopy (HR-TEM). Finally, the combination of UV-visible spectroscopy, FTIR and TEM data allows us to propose a mechanism for NP formation within the PEM film.

In situ synthesis of gold nanoparticles in the bulk of (PLL/HA) multilayer films

We loaded the gold aurochlorate ions into $(PLL9.5/HA2.9)_7$-PLL9.5 films by soaking the film in 10 mM gold chloride solutions under acidic, neutral or basic conditions, which correspond respectively to pH 3, 6 and 9. The films were then simply rinsed with water and air-dried before being analyzed by FTIR (**Figure 4.10**). **Figure 4.10A, A'** shows typical spectra for a PLL-ending film taken prior and after loading with the gold chloride solution at pH 6, as well as after UV-irradiation. Overall, the spectra look very similar over the whole range investigated (3700-900 cm^{-1}), which indicates at first sight that the film keeps its

integrity upon gold photo-reduction. Qualitatively similar spectra were obtained for HA ending films (see **Figure 4.11**). However, by plotting the differences between the spectra of PLL-ending films after loading with the gold precursors ion and after UV-reduction, as compared to the initial $(PLL9.5/HA2.9)_7$-PLL9.5 films, slight differences showed up for some specific peaks (**Figure 4.10B, B'**). We first noted in the band at ~3400 cm^{-1} a minor decrease of H-bonds associated with OH groups (Haxaire et al. 2003). It is already known that these bands can be easily affected by the presence of water molecules (Wolkers et al. 1998). Second, we observed that COO^- groups (at 1604 and 1400 cm^{-1}) as well as C-OH and C-O-C peaks from the saccharide groups (at 1047 and 1078 cm^{-1}) are slightly decreased. Conversely, the COOH peak at 1735 cm^{-1} is increased. Overall, these changes indicated a very slight change in the protonation state of the carboxylic acid and a change in H-bonds.

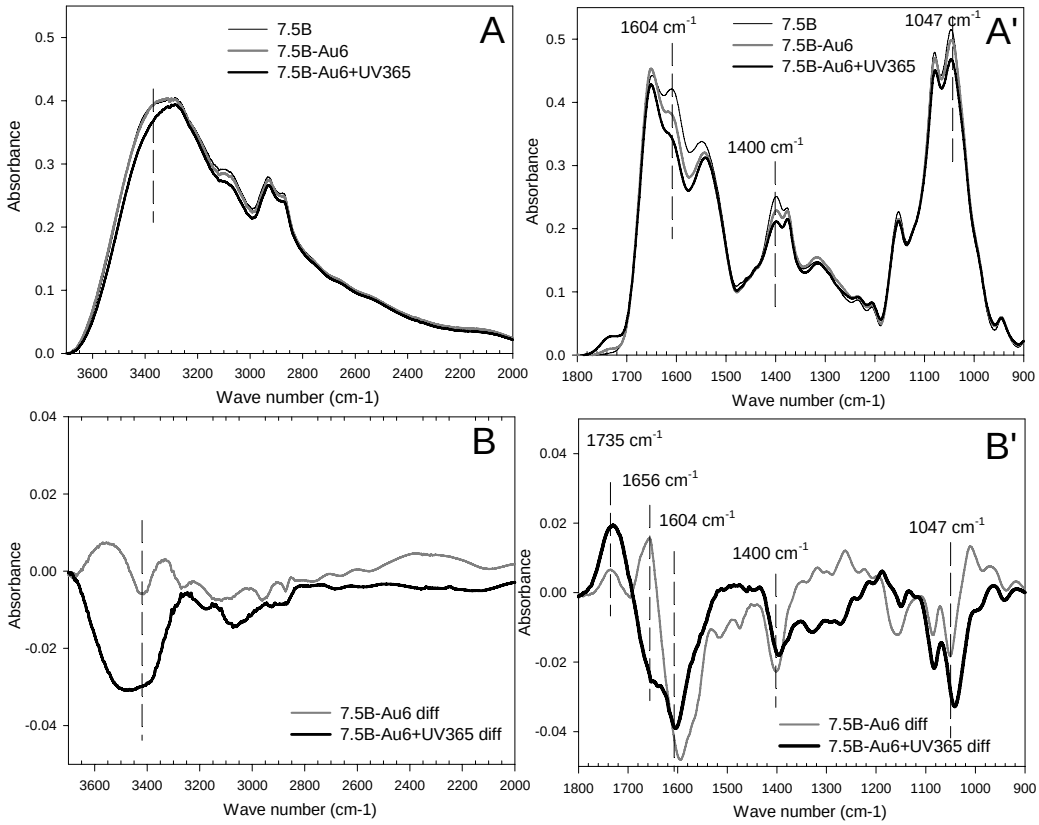

Figure 4.10. FTIR spectra of the films after gold chloride loading and UV-reduction. The gold chloride solution was adjusted to pH 6. (A,A') FTIR spectrum of a $(PLL9.5/HA2.9)_7$-PLL9.5 film built in pH-amplified conditions (pH = 2.9 for HA and pH = 9.5 for PLL deposition). The spectrum is shown over the range (A) 3600-2000 cm^{-1} and (A') 1800-900 cm^{-1}, respectively. (B, B') Differences between the FTIR spectra of the films taken after loading of the gold chloride solution (gray line) and after UV-irradiation (thick black line) over the same ranges as for A and A'.

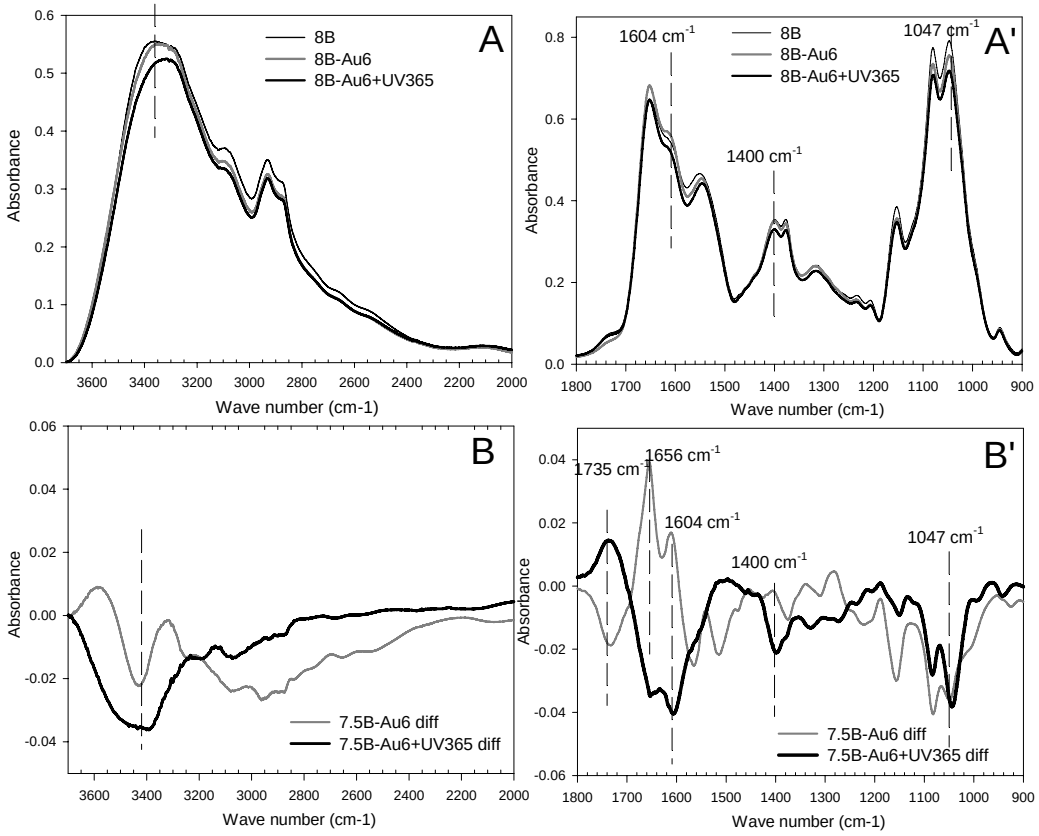

Figure 4.11. FTIR spectra of $(PLL9.5/HA2.9)_8$ (i.e. HA-ending) film after gold chloride loading and UV-reduction. The gold chloride solution was adjusted to pH 6. (A, A') FTIR spectrum of the film built in pH-amplified conditions (pH = 2.9 for HA and pH = 9.5 for PLL deposits). The spectrum is shown over the range (A) 3600-2000 cm^{-1} and (A') 1800-900 cm^{-1}, respectively. (B, B') Difference between the FTIR spectrum of the film taken after loading of the gold chloride solution (gray line) and after UV-irradiation (thick black line). Same ranges as for A and A'.

Next, we followed the *in situ* synthesis of gold NPs via UV-visible spectrometry (**Figure 4.12**) since it is well known that gold NPs exhibit a strong surface plasma resonance (SPR) band depending on the shape and size of nanoparticles (Link et al. 2000; Haes et al. 2004). **Figure 4.12** shows the spectra obtained over time for both PLL-ending (A-C) and HA-ending films (A'-C') immersed in gold chloride solutions at different pH. For all pH conditions, an absorbance peak emerged in the range of 500-550 nm. It is increased with the reduction time, which qualitatively indicated gold NPs were successfully synthesized (Eustis et al. 2006). The width of the peak of ~50 nm also indicated that the NPs were well-dispersed and rather spherical (Eustis et al. 2006). The reduction was completed in about 35 hrs. The maximum absorbance values for each condition were extracted and plotted as a function of the reduction time (**Figure 4.12D**). The films loaded with gold chloride at pH 3 exhibited the largest increase in absorbance, followed by those loaded with the precursor solution at pH 6. When the pH of the precursor solution was of 9, a small but steady increase was observed. Of note, the ending layer of the films did not appear to have a key role in the gold NPs formation

process as both PLL-ending and HA-ending films behaved very similarly. These results qualitatively indicated that the amount of gold NPs formed was directly dependent on the pH of the precursor solution: the lower it was the higher was the amount of NPs formed. Interestingly, these qualitative results were confirmed by quantitative measurement of gold mass using inductively coupled plasma mass spectrometry (ICP-MS) (**Table 4.2**).

Table 4.2. Quantification by ICP-MS of the mass of gold synthesized *in situ* in the PLL-ending and HA-ending films (respectively $(PLL9.5/HA2.9)_7$-PLL9.5 and $(PLL9.5/HA2.9)_8$) films as a function of the pH of the gold chloride solution. The mass is given in µg.

Total gold mass (µg)	**pH 3**	**pH 6**	**pH 9**
PLL-ending films	12.8 ± 0.4	8.5 ± 0.4	6.6 ± 0.2
HA-ending films	11.9 ± 0.3	7.6 ± 4.6	7.1 ± 0.1

Furthermore, we plotted the maximal wavelength (λ_{max}) of the SPR peak as a function of the pH of the precursor solution (**Figure 4.12E**). For PLL-ending as well as for HA-ending films, λ_{max} was found to decrease when the pH was increased, which qualitatively indicated that gold NPs size was smaller at high pH (Eustis et al. 2006). Of note, the wavelength shift was ~40 nm for 6 pH units of difference (from 3 to 9). These results qualitatively agreed with previous results showing that the size of NPs formed in bulk solutions of poly(allylamine) was slightly modulated by the pH, over a range from 1.5 to 12.5 (Sardar et al. 2008). However, in this case, the variation of λ_{max} was only of 6 nm. This suggests that the size of NPs formed in PEM films covers a broader range of diameters.

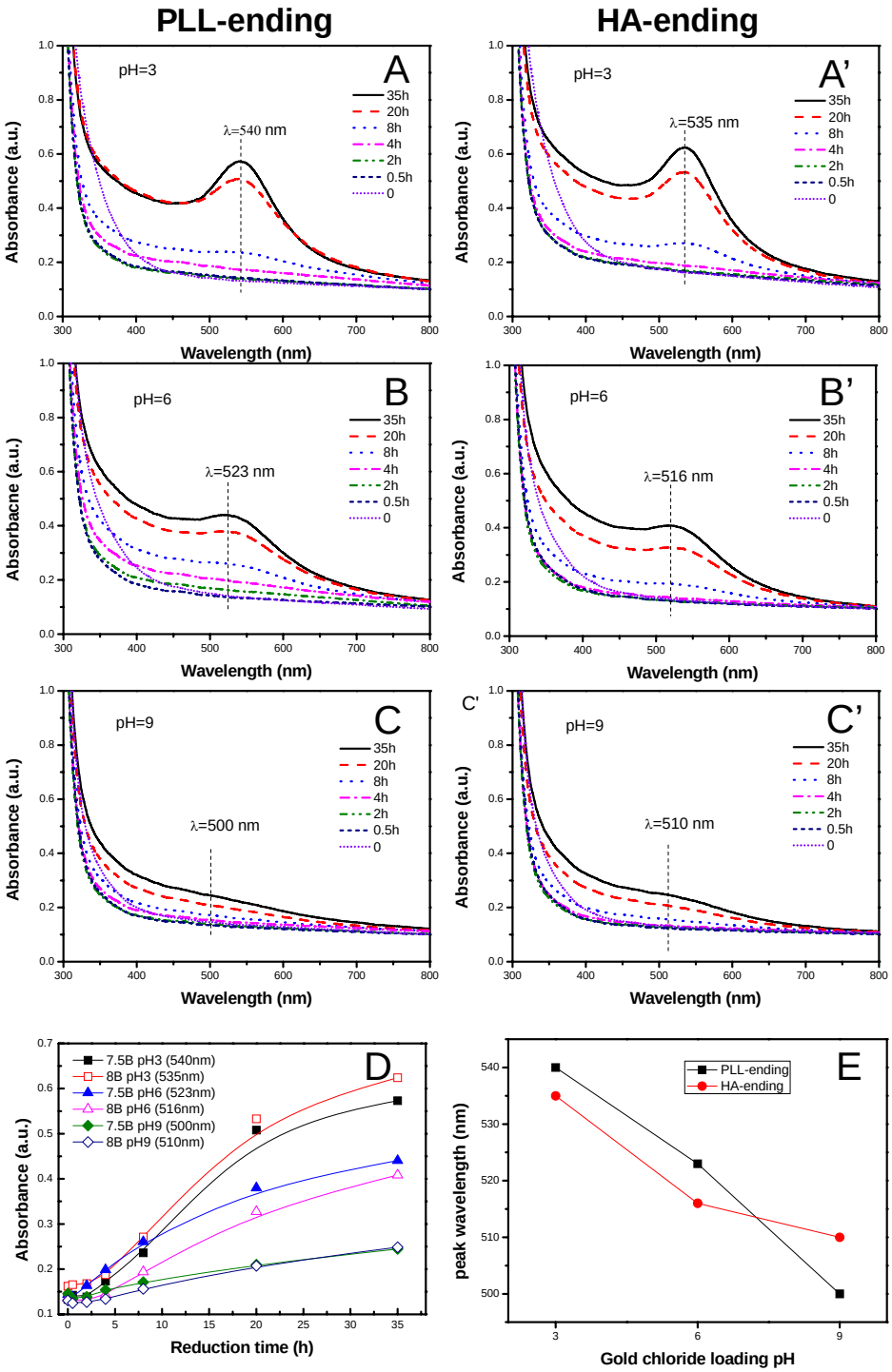

Figure 4.12. UV-visible absorption spectra acquired at different time points during UV-photoreduction in $(PLL9.5/HA2.9)_7$-PLL9.5 films (A, B, C) and $(PLL9.5/HA2.9)_8$ films (A', B', C'). Gold chloride was loaded at different pH: pH = 3 (A, A'), pH = 6 (B, B') or pH = 9 (C, C'). (D) Maximum of the SPR peak plotted as a function of the reduction time. (E) Wavelength of the maximum SPR peak, plotted as a function of the pH of the precursor solution.

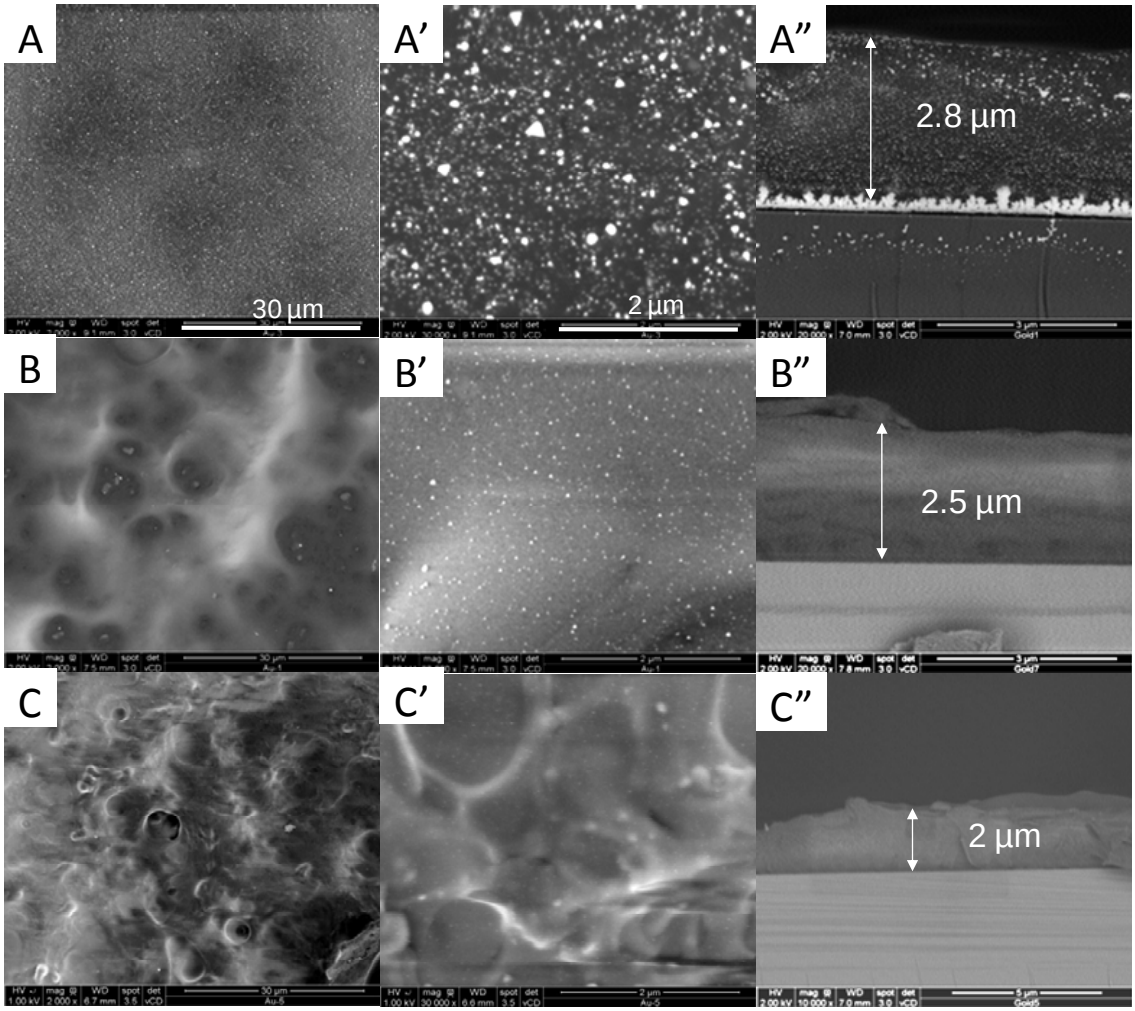

Figure 4.13. SEM images of gold nanoparticles synthesized *in situ* in $(PLL9.5/HA2.9)_7$-PLL9.5 films: surface morphology at different magnifications (left and middle columns) and cross-sections (right column). Gold chloride was loaded at pH 3 (A-A"), 6 (B-B"), and 9 (C-C"). The scale bars are 30 µm for (A, B, C) and 2 µm for (A', B', C').

After gold NP photoreduction, film surface morphology and cross-sections were visualized by scanning electron microscopy (SEM) using low voltage high contrast (vCD) detector to enhance element contrast (**Figure 4.13**). Drastic differences between the different samples emerged. When the precursors were loaded at pH 3, gold NPs homogenously covered the entire film surface and appeared as bright spots of various sizes (**Figure 4.13A, A'**). Furthermore, the gold NPs were distributed throughout the whole film thickness, over ~2.5 µm (**Figure 4.13A"**). As the loading pH increased to 6 (**Figure 4.13B, B'**), homogenously distributed gold NPs appeared on the film surface, but of smaller size than those observed at pH 3. However, no NPs could be visualized in the film cross-section at this magnification (**Figure 4.13B"**). We noted that the film prepared at pH 9 (**Figure 4.13C-C"**) was very difficult to observe. Some charges accumulated on the surface when observing this film, which may be due to the limited amount of gold NPs on the surface **(Figure 4.13 C'**) or to the

fact that the NPs were too small to release the accumulated charges. Here again, no NP were visualized in the cross-section at this magnification. Of note, large gold crystals were also formed in the film/silicon interface after loading gold chloride at pH 3. This may originate from the fact that the SiO_2 layer at the surface of the silicon substrate is positively charged at very low pH (Parks 1965). It may thus serve as nucleation site for gold chloride ions.

We noted that the surface and cross-section morphology of HA-ending films made of 8 layer pairs (**Figure 4.14**) were almost identical to their PLL-ending counterparts, except that the film thickness was about 0.5 µm thicker. Considering the very similar behavior of PLL-ending and HA-ending films regarding gold NP synthesis (**Figure 4.12**) and the minor changes in film structure change after UV irradiation **(Figure 4.10**), we now only focus on PLL-ending films.

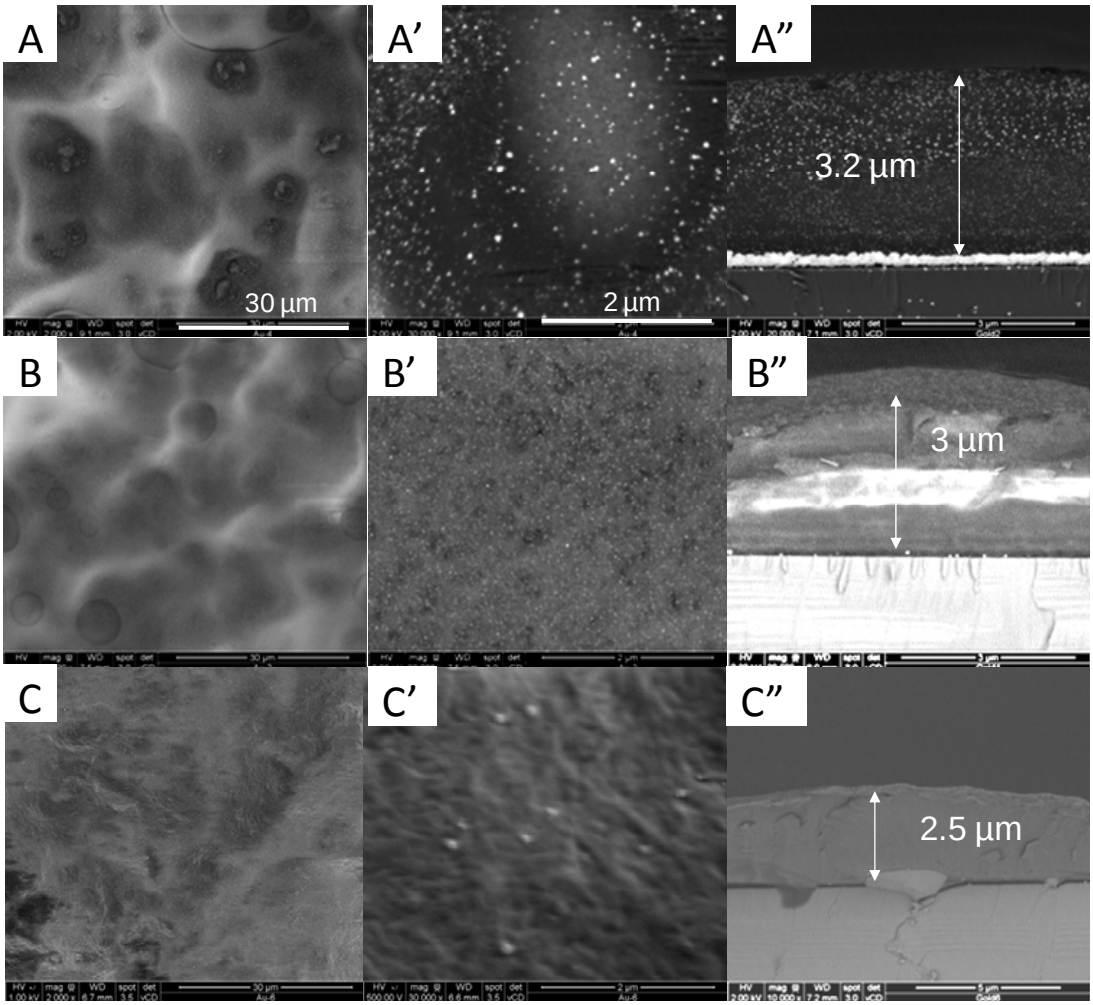

Figure 4.14. SEM images for gold nanoparticles embedded in $(PLL9.5/HA2.9)_8$ films: surface imaging (left and middle columns) and *z*-cross-section (right column). Gold chloride was loaded at different pH of 3 (top row), 6 (middle row), and 9 (bottom row). The scale bars are 30 µm for (A, B, C) and 2 µm for (A', B', C').

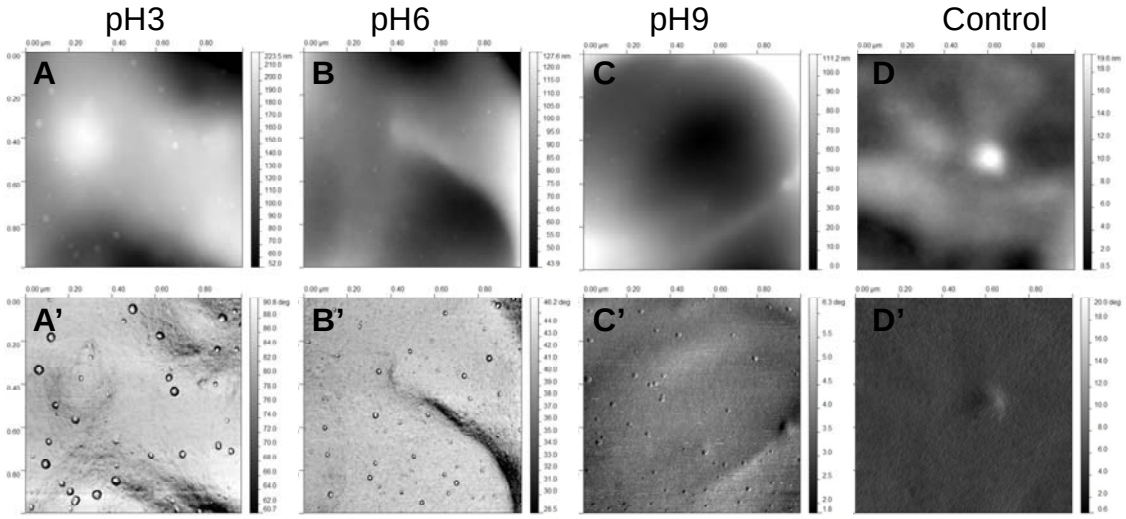

Figure 4.15. AFM images of the surface morphology of $(PLL9.5/HA2.9)_7$-PLL9.5 films imaged after synthesis of the gold NPs. The pH of the gold ion solution was adjusted to pH 3 (A,A'), 6 (B, B') or 9 (C,C'). (A-D) are height images and (A'-D') are phase images. A control UV-irradiated film but without gold salt loaded is also shown (D, D'). Image size is 1 µm x 1 µm.

To further confirm film surface morphology and get a first estimate of the NP size at the film surface, we performed AFM imaging. Height and phase images of the films prepared by loading the gold precursor at the different pH (3, 6 and 9) are shown in **Figure 4.15**. The surface of the films was quite rough with a maximum *Z* distance of ~100 to 200 nm in the area of 1x1 μm^2. Gold NPs were barely visible on height images but could be identified in the phase images. The size of gold NP estimated from these images was of ~18 nm, ~11 nm and ~10 nm for pH 3, pH 6 and pH 9, respectively. This confirms the decrease of NP size when the loading pH of the precursor solution is increased.

We next observed cross-sections of the films by TEM at low and high resolution (HR-TEM) (**Figure 4.16 and Figure 4.17**). TEM images of the film/silicon interface are shown in **Figure 4.16** at different magnifications. First, we noticed that gold NPs were always well dispersed throughout the whole film thickness, regardless of the pH of the gold chloride solution, which indicates that aurochlorate ions could diffuse homogeneously in the film. Here again, we observed that large NPs of 30-60 nm in diameter have nucleated at the silicon/film interface, in the case of pH 3. From these TEM images, we quantified the gold NP size distribution (**Figure 4.16A1-C1**). The median size of gold NPs synthesized from pH 3, 6 and 9 was of 8.6, 2.8 and 1.7 nm, respectively. Thus, increasing the loading pH of gold chloride resulted in a significant decrease of the gold NP size.

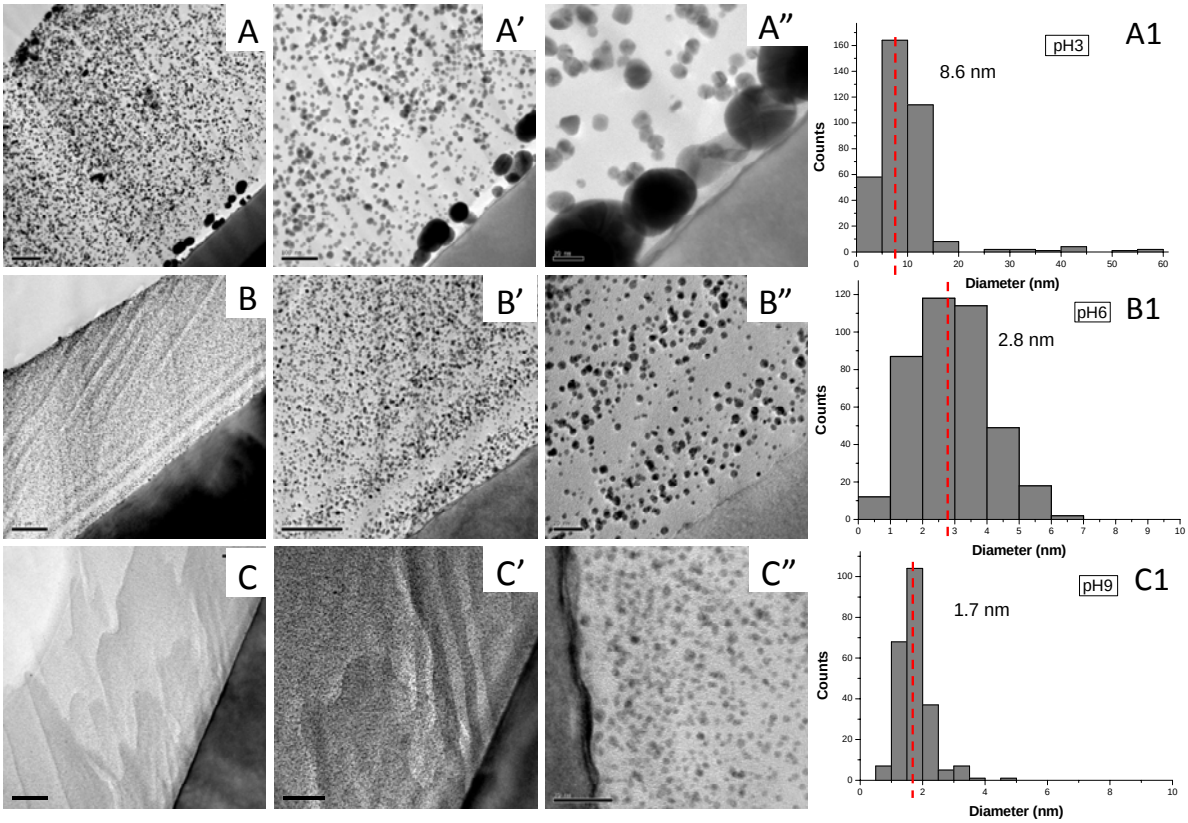

Figure 4.16. Cross-sectional TEM images through $(PLL9.5/HA2.9)_7$-PLL9.5 films showing gold NPs dispersed over the entire film thickness. Gold chloride was loaded at different pH of 3 (A-A"), 6 (B-B"), and 9 (C-C"). Images are shown at different magnifications. The black zone corresponds to the silicon substrate and the white zone to Epoxy resin. The gold NPs were formed homogeneously throughout the whole film thickness, as observed by the presence of very small to large black dots. The corresponding particle size distribution deduced from these TEM images is given in Figure A1, B1 and C1. The red dashed lines indicate the median NP size, which is of 8.6 nm, 2.8 nm and 1.7 nm, respectively for films loaded with gold chloride at pH 3, 6 and 9. Scale bars are 200 nm for (A, B, C) 100 nm for (A', B', C') and 20 nm for (A", B", C").

Of note, the size of particles inside the films, as measured by TEM, was lower than that estimated by AFM for the gold NPs on the film surface. Differences may be due to the formation of larger nanoparticles at the film surface. They may also rise from the measurement method. High resolution TEM imaging of the gold NPs was performed to investigate their nanocrystalline structure (**Figure 4.17**). Parallel lattices of the nanocrystals can be clearly observed for gold NPs synthesized in acid and neutral conditions (**Figure 4.17A' and B'**).

Furthermore, the electron diffraction pattern confirmed the typical rings characteristic of a polycrystalline phase. It could be indexed in the reciprocal space by superposition of the X-ray diffraction of Au powder (**Figure 4.17A", B"**). Conversely, the gold NPs formed at pH 9 were too small to get enough electron diffraction signals (**Figure 4.17C"**). However, the energy dispersive X-ray (EDAX) data confirmed the existence of gold NPs in these films as well (**Figure 4.18**).

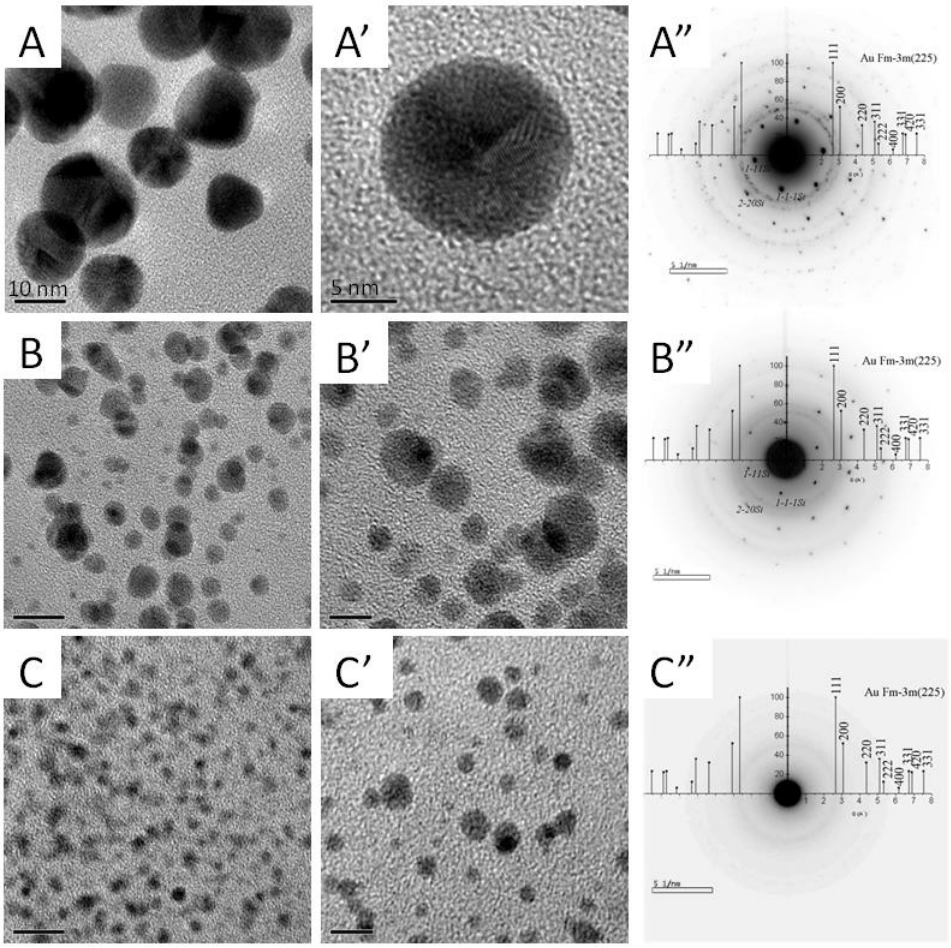

Figure 4.17. High resolution TEM images of gold NPs synthesized *in situ* in $(PLL9.5/HA2.9)_7$-PLL9.5 films. (A, A', B, B', C, C'): the conditions for the pH are the same as for Figure 4.16. The corresponding electron diffraction patterns of the samples are also shown (A", B", C"). Scale bars are 10 nm for (A, B, C) and 5 nm for (A', B', C').

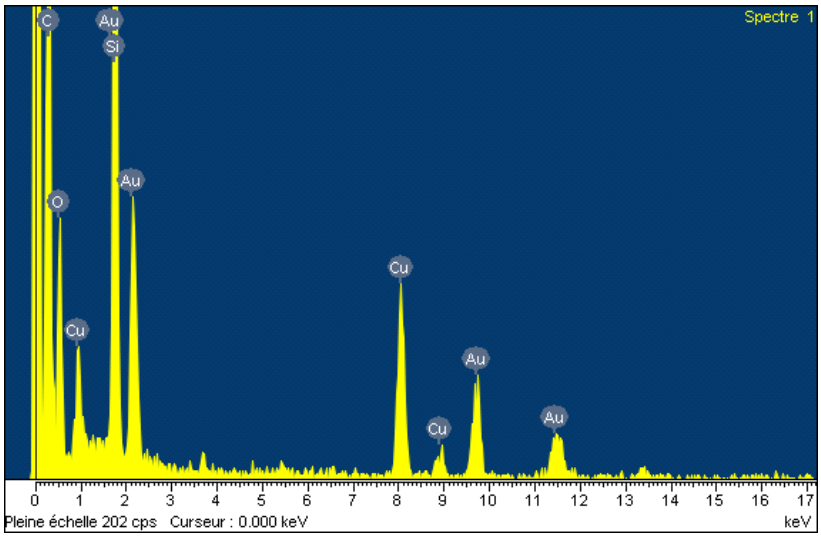

Figure 4.18. EDX spectrum of gold nanoparticles embedded in a $(PLL9.5/HA2.9)_7$-PLL9.5 film, for gold loading at pH 9.

Based on the TEM images, we quantified in the cross sections the gold NP density for the different conditions. A 25-fold increase in NP density was observed when the pH was increased from 3 to 9 (**Table 4.3**).

Table 4.3. Quantification of the gold NP density based on cross-sectional TEM images of the films (shown in Figure 4.16, same PLL-ending films as in Table 4.2). The NP density is given as number of particle/ μm^2 in transverse sections of the films. Mean values are given (uncertainty being of the order of 15%). The fold increase as compared to the values measured at pH 3 is also given.

Gold NP density	**pH 3**	**pH 6**	**pH 9**
PLL-ending films	2 500	26 000	63 000
Fold increase	1	× 10.4	× 25.2

Thus, (PLL9.5/HA2.9) films allow the spatially-confined growth and stabilization of a very large number of gold NPs. The gold NPs embedded in the 2.5 μm thick surface-adsorbed polymeric matrix are well-dispersed and of homogeneous size. The green synthetic chemistry constitutes a promising method to confine gold NPs at a very high density on a surface for applications in biosensing or biodetection.

Possible mechanism of gold NPs photosynthesis in (PLL/HA) films

In order to further understand the molecular mechanism underlying *in situ* synthesis of gold NPs in (PLL9.5/HA2.9) multilayer films, we performed additional experiments in solution using the gold chloride solution at different pH and the individual components of the film. To this end, we acquired the UV-visible spectra of a 1 mM $HAuCl_4$ solution adjusted to different pH and of the same solution in the presence of either HA (3 mg/mL) or PLL (1 mg/mL) (**Figure 4.19A-C**). The corresponding images of the solutions are shown in **Figure 4.20**. The UV-visible spectra were also recorded after UV-irradiation (**Figure 4.19A'-C'**).

As shown in **Figure 4.19A**, the absorbance of the $HAuCl_4$ solution at pH 3 exhibited a peak at ~ 313 nm, which can be attributed to the charge-transfer band from chloride *p* to gold *d* orbitals (Gangopadhayay et al. 1961). The corresponding images showed a slightly yellow color for this solution. This band disappeared when the pH of the solution was increased. The Au-Cl-H_2O system has been studied (Richardson et al. 2006) and it is known that $AuCl_4^-$ is stable over a wide pH range (0-7.5) (Kelsall et al. 1993). However, destabilization of the system at higher pH can lead to a transition to $AuCl_2^-$. Indeed, the Au^+ ions of $AuCl_2^-$ can be more easily reduced in Au^0 than Au^{3+} of $AuCl_4^-$ (Kurihara et al. 1983). Increasing the pH to 6 and 9 probably results in destabilization of $AuCl_4^-$ with a subsequent transition to $AuCl_2^-$, which does not exhibit any specific peak in the UV-visible range.

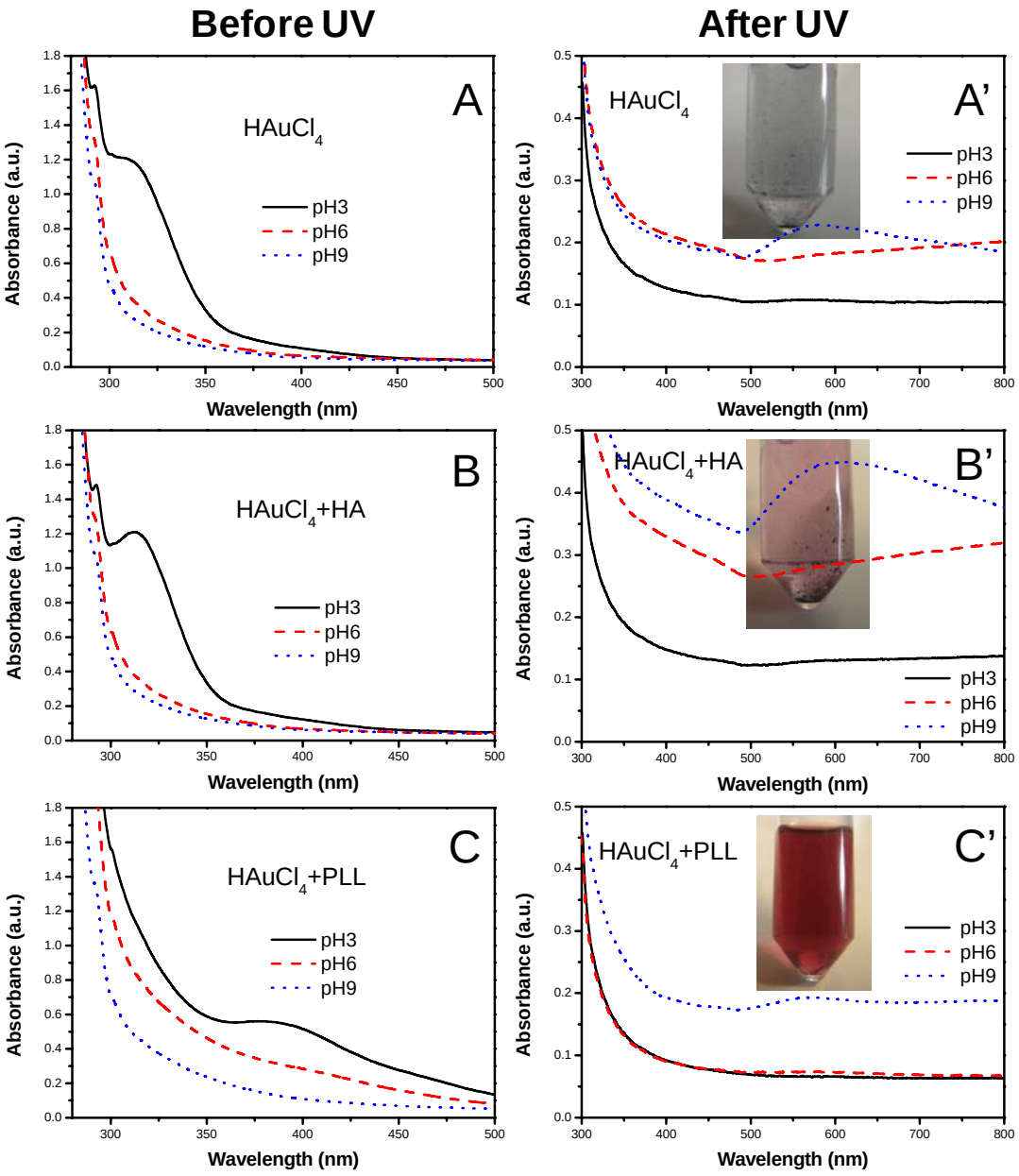

Figure 4.19. UV-visible absorbance spectra of 1 mM $HAuCl_4$ solution (A,A'), 1 mM $HAuCl_4$ and 3 mg/mL hyaluronic acid solution (B,B') and 1 mM $HAuCl_4$ and 1 mg/mL poly(L-lysine) solution (C, C') at different pH before UV irradiation (left column) and after UV irradiation (right column). Inserts are digital images of the same solutions obtained after UV irradiation at pH 9.

When HA was added to the $HAuCl_4$ solution, the UV-visible spectra (**Figure 4.19B**) were very similar to the case where no HA was present (**Figure 4.19A**). In the case where PLL was mixed to the $HAuCl_4$ in solution, the charge-transfer band was shifted to ~385 nm (**Figure 4.19C**) and the complex gave rise to a yellow color (**Figure 4.20**) (Gangopadhayay et al. 1961). The band was also broader and of much lower intensity.

This is compatible with the following ion exchange process between tetrachloride aurate ions and complexed ammonium groups:

$$COO^-NH_3^+ + H^+ + Au^{3+}Cl_4^- \rightarrow COOH + NH_3^+Au^{3+}Cl_4^- \qquad (1)$$

Thus, PLL can first play a role in the stabilization of the $AuCl_4^-$ ions and subsequently in the stabilization of the gold nuclei.

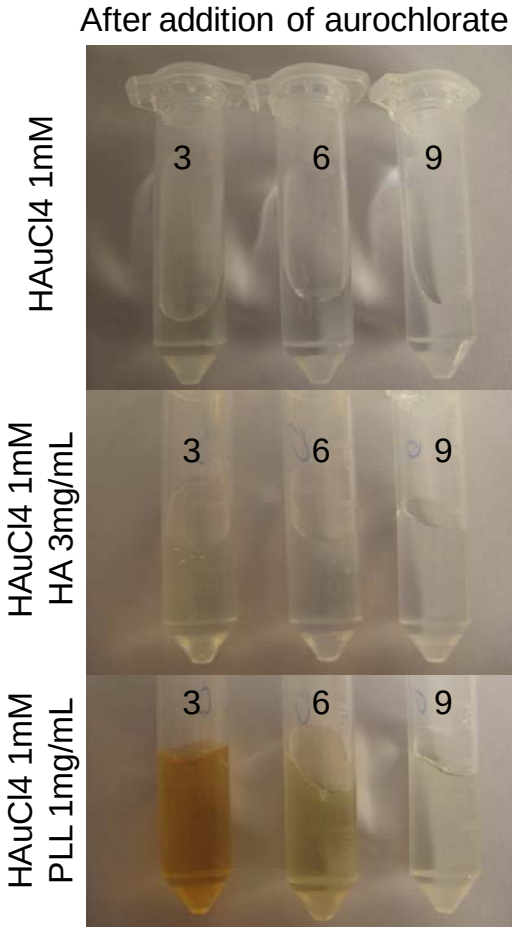

Figure 4.20. Digital images of the $HAuCl_4$ solutions at different pHs and in the absence (upper row) or in the presence of HA at 3 mg/mL (middle row) or PLL at 1 mg/mL (bottom row).

Changes that have occurred upon UV irradiation were also investigated. For the $HAuCl_4$ solution alone, a weak and broad peak ~550 nm was observed only for pH 9 (**Figure 4.19A'**). The image of the solution revealed a blue color, with the formation of large and aggregated clusters (**Figure 4.19A' inset**).

When HA was added to the $HAuCl_4$ solution, the change in the absorbance spectra was even larger, especially at pH 9 (**Figure 4.19B'**). The absorbance peak was broader and shifted to the right (~595 nm). We indeed observed a larger number of precipitated gold clusters in this case (inset of **Figure 4.19B'**).

In the case of PLL addition, a very small increase in UV absorbance at ~550 nm was noted after UV-reduction, especially at pH 9. The mixture at pH 9 exhibited a red color and

contained well-dispersed NP of ~10 nm in size, as was observed by TEM (**Figure 4.21**). Thus, PLL appeared to act as good stabilizer of Au^0 atoms, as was previously observed for poly(ethylene imine) (Richardson et al. 2006).

All together, these results suggest that PLL can first interact with gold ions and then lead to the formation of well-dispersed nanoparticles. Interestingly, they also suggest that HA molecules can be implicated in the photo-reduction process, especially at neutral and basic pH. In fact, several studies have already shown that CH_2-OH groups, which are present on HA backbone, can facilitate gold chloride reduction under photo irradiation (Eustis et al. 2005; Mallick et al. 2005; Mallick et al. 2005).

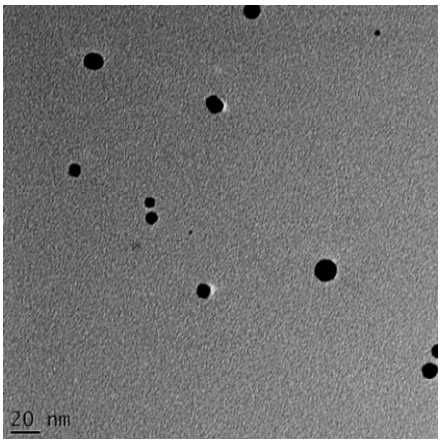

Figure 4.21. TEM image of gold nanoparticles synthesized from 1 mM $HAuCl_4$ and 1 mg/mL poly(L-lysine) solution at pH 9, corresponding to Figure 4.19C' blue short dash line and insert picture.

The direct photolysis of water in the presence of a UV source is:

$$H_2O \rightarrow H^{\bullet} + OH^{\bullet} \qquad (2)$$

According to Mallick *et al.* (Mallick et al. 2005), -CH_2-OH is a scavenger of $H^{\bullet}$ and $OH^{\bullet}$ radicals. It can be excited under UV irradiation to form the following radicals:

$$\text{-}CH_2\text{-}OH \xrightarrow{OH^{\bullet}} \text{-}CH^{\bullet}\text{-}OH + H_2O \qquad (3)$$

$$\text{-}CH_2\text{-}OH \xrightarrow{H^{\bullet}} \text{-}CH^{\bullet}\text{-}OH + H_2 \qquad (4)$$

These radicals are able to reduce gold ions as follows:

$$Au^{n+} + \text{-}CH^{\bullet}\text{-}OH \rightarrow Au^0 + \text{-}CHO + nH^+ \qquad (5)$$

Indeed, it has also been proven that hyaluronic acid can help the formation of silver NP

under UV irradiation by oxidation of CH_2OH groups to CHO (Cui et al. 2008). Furthermore, the COO^- groups of HA is a proton acceptor. The carboxylic group itself might even play a role in the reduction of gold ions, as was recently suggested by Wang et al. (Tan et al. 2009).

To elucidate on the changes in the film internal composition, in particular the appearance or disappearance of specific groups, we further investigated the changes in the FTIR spectra obtained at different steps of the procedure (**Figure 4.22**). We focused on changes that occurred after loading with the gold chloride solution at different pHs (**Figure 4.22A-C**) and after UV-irradiation (**Figure 4.22A'-C'**). In parallel, control experiments were performed in which the films were only soaked in water at different pH, without any gold precursors, before being UV-irradiated.

Upon addition of the aurochlorate solution on a PLL-ending film (final deposition of PLL at pH 9.5), we observed specific differences in the FTIR spectra. The changes exhibited the same trends at all pH conditions, but they were more pronounced at pH 3 (**Figure 4.22A, B, C**).

First, we noticed a strong decrease in the COO^- peaks at 1604 and 1400 cm^{-1} and a concomitant increase in COOH peak at 1735 cm^{-1} (**Figure 4.22A, B** and **Table 4.4**). As the pH of the film is lowered from 9.5 (pH of the PLL-ending layer) to pH 3, COO^- are converted to COOH. This indicated that COO^- became protonated, the change being maximal at pH 3 (-40%). This is due to the lowering of the pH upon immersion of the film at pH3, as the PLL-ending layer was deposited at pH 9.5.

Secondly, we observed a very slight decrease of the peaks at 1047 cm^{-1} and 1078 cm^{-1}, indicating a change in the hydroxyl groups of HA.

Third, we also noticed a significant increase in the amide band of PLL and HA at 1656 cm^{-1}, which was again more pronounced at acidic pH (+18.7%). This may be a consequence of the interaction of PLL with gold ions.

After UV-irradiation, these shifts were further enhanced (**Figure 4.22A'-C'** and **Table 4.4**). Here, the amide I peak at 1656 cm^{-1}, the COO^- peaks as well as the hydroxyl peak all decreased. Again, the changes were more pronounced at pH 3 with a decrease of the order of 11 to 17% (**Table 4.4**). At pH 6 and 9, the changes were of the order of 6 to 9 % at maximum (**Table 4.4**). In parallel, there was a large increase of the COOH peak at 1735 cm^{-1}, which was also higher at pH 3. Of note, HA-ending films behaved very similarly (**Figure 4.23**). For these films, the only structural differences were observed after gold loading at the different pHs (i.e. before UV irradiation), as the final deposited layer was HA at pH 2.9 (instead of pH 9.5 in the

case of PLL-ending films). But importantly, the major bands that changed during UV-irradiation were the same and the amplitude of the changes were similar.

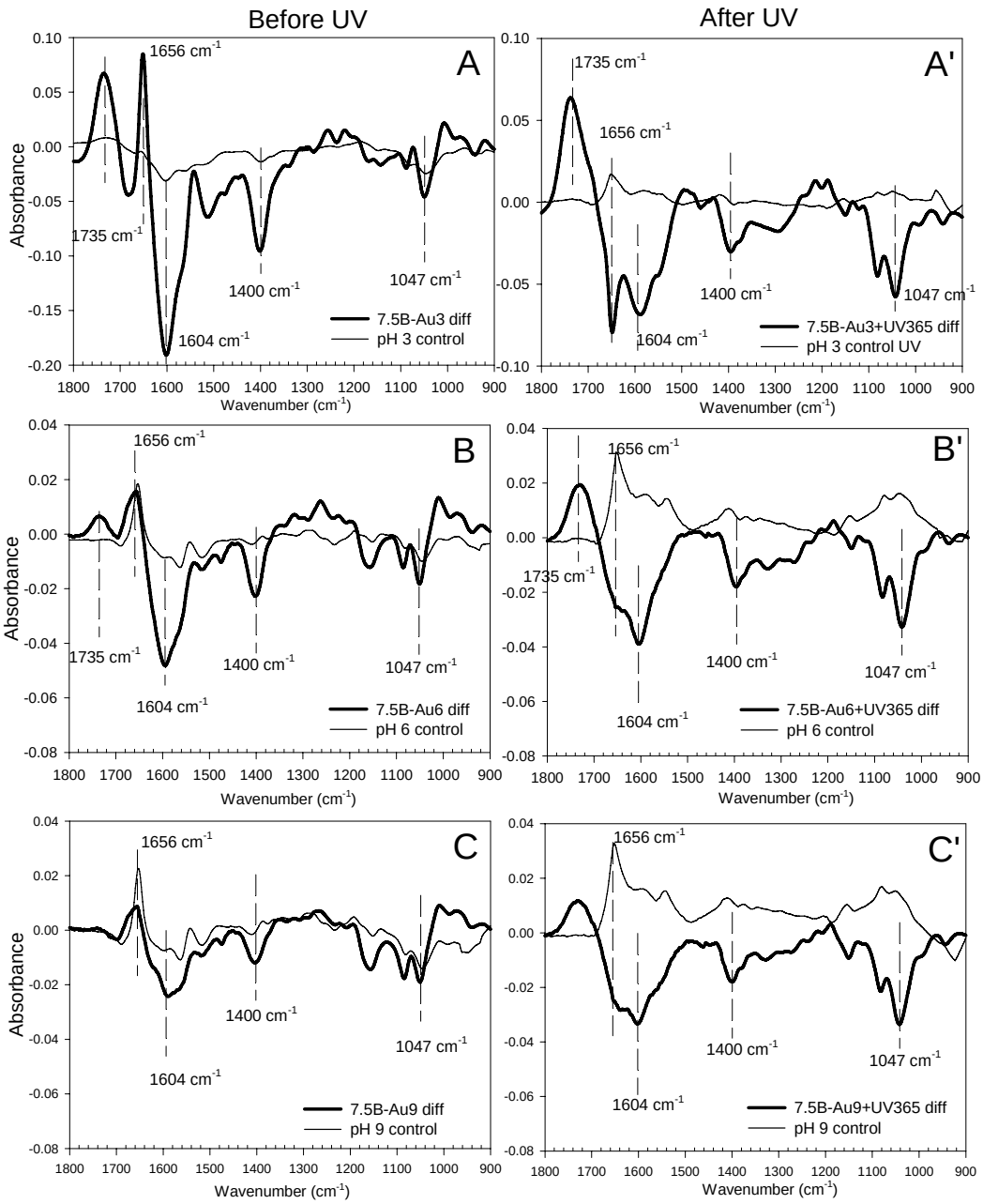

Figure 4.22. FTIR spectra of $(PLL9.5/HA2.9)_7$-PLL9.5 films acquired after gold salt loading and UV irradiation. The pH of the gold ions solution was adjusted to 3 (A, A'), 6 (B, B') or 9 (C, C'). (A, B, C) Differences between FTIR spectra of the film measured after gold chloride loading and before (thick line). The control experiment, i.e. solution at the same pH but without gold ion, is also shown (thin line). (A', B', C') Differences between FTIR spectra of the film measured after and before UV-irradiation (thick line). The control experiment, i.e. solution without gold ion that has been UV-irradiated in similar conditions (thin line) is also shown.

Table 4.4. Changes of the major peaks of the FTIR spectra measured as percentage of the initial value: Amide I (1656 cm^{-1}), COO- (1604 cm^{-1}) and saccharide ring (1047 cm^{-1}) changes after contact with the gold chloride solution (but before irradiation), or after UV irradiation, as compared to the initial value for the $(PLL9.5/HA2.9)_7$-PLL9.5 films.

Peak (cm^{-1})	Before UV (%)			After UV (%)		
	pH 3	pH 6	pH 9	pH 3	pH 6	pH 9
1656 cm^{-1}	+ 18.7	+2.5	+ 1.2	-17.1	-5.7	-5.5
1604 cm^{-1}	-40.5	-9.2	-3.7	-12.7	-8.9	-7.3
1047 cm^{-1}	-9.1	-2.2	-2.2	-10.9	-6.8	-6.6

All together, the FTIR data indicated that the major changes under UV-irradiation occurred: 1) for the COO^-/COOH groups, COO^- being transformed to COOH, 2) for H-bonded C-OH of alcohols and C-O-C in HA, a decrease at 1047 cm^{-1} and 1078 cm^{-1} ; of note, a decrease in hydroxyl (possibly H-bonded) was also observed at 3400 cm^{-1} (data not shown), and 3) for the amide I of PLL and HA, a decrease at 1656 cm^{-1}. The magnitude of the changes was in the order pH 9 < pH 6 < pH 3.

It is already acknowledged that the conformation and structure of an organic template are crucial parameters in the nucleation and/organization of inorganic nanoparticles (Lee et al. 2006; Chen et al. 2008). Also, it is now well accepted that the synthesis of gold NPs involves a two-step process (Mallick et al. 2005). First, there is a nucleation step, in which part of the metal ions are reduced and act as nucleation centers. Second, the nucleation centers catalyze the reduction of the remaining metal ions present in the surrounding. The coalescence of atoms leads to the formation of metal clusters and these are effectively stabilized by ligands, surfactants or polymers. It is also known that Au^+ ions are more easily photoreduced than Au^{3+} ions (Kurihara et al. 1983). Indeed, photo irradiation in the presence of water molecules induces reduction of Au^{3+} into Au^{2+}, which is itself instable and can disproportionate to form Au^+ and Au^{3+} (Eustis et al. 2005). The Au^+ is then photoreduced by absorbing another photon, leading to the net disproportionation equation (Eustis et al. 2005):

$$3\ Au^+Cl_2^- \rightarrow Au^{3+}Cl_4^- + 2\ Au^0 + 2\ Cl^- \qquad (6)$$

Once atoms are formed they can act as catalysts for the reduction of the remaining metal ions present in the solution. After their formation the atoms coalesce, which results in cluster formation, i.e. NP growth (Mallick et al. 2005).

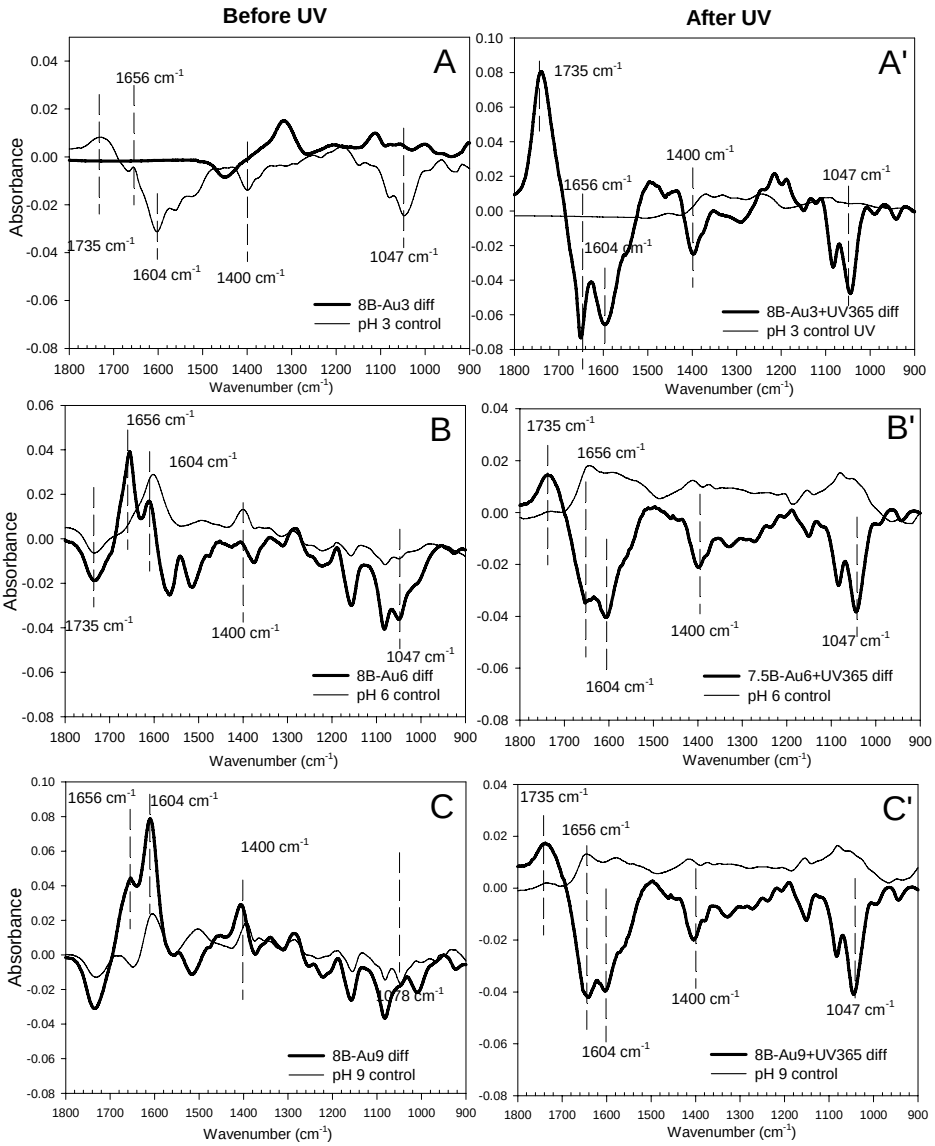

Figure 4.23. FTIR spectrum of $(PLL9.5/HA2.9)_8$ films acquired after gold salt loading and after UV irradiation. The pH of the gold ions solution was adjusted to 3 (A, A'), 6 (B, B') or 9 (C, C'). (A, B, C) Differences between FTIR spectra of the film measured after gold chloride loading and before (thick black line). The control experiment (solution at the same pH but without gold ion) is also shown. (A', B', C') Differences between FTIR spectra of the film measured after UV-irradiation and before (thick black line). The control experiment (solution without gold ion that has been UV-irradiated in similar conditions) is also shown.

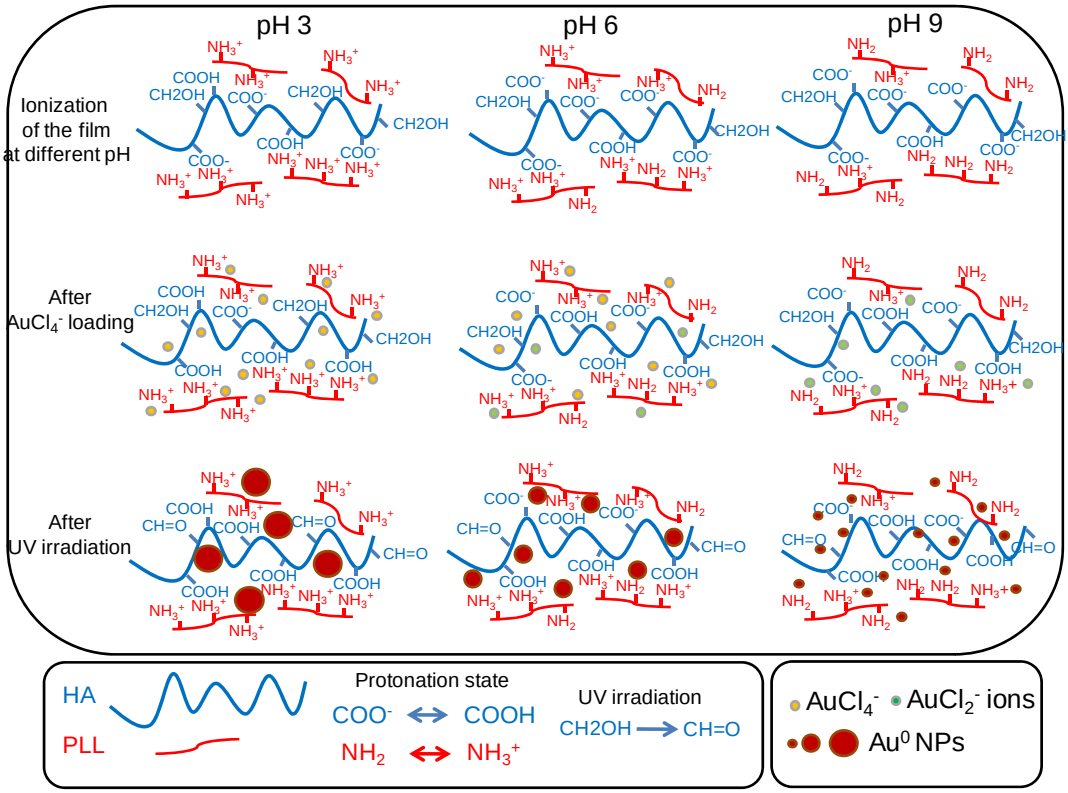

Scheme 4.1. Proposed mechanism for *in situ* formation of gold NP in (PLL9.5/HA2.9) PEM films at different pHs. The protonation degree of HA and PLL both depends on pH; the number of protonated COOH groups is higher at low pH and decreases when the pH is increased; Also, the number of protonated NH_3^+ groups decreases when the pH is increased. After $AuCl_4^-$ loading, the ions interact with NH_3^+ groups that were either free or paired with COO^- groups; thus, a fraction of COO^- groups becomes protonated in COOH; this fraction is higher at low pH of 3. $AuCl_4^-$ ions may also be reduced to $AuCl_2^-$ ions, especially at high pH of 9 and to some extent at pH6. Both ions may associate with free H^+ ions of the films. After UV irradiation, gold NPs are formed in all conditions but the NPs are larger and less numerous at low pH (median size of ~ 8.6 nm). Their size decreases when the pH is increased to reach 3 nm at pH 6; In both conditions, UV-visible spectra showed a clear increase as a function of time and the diffraction pattern of Au was intense. At very high pH of 9, gold NPs have a small median diameter of 1.7 nm, but they have formed at a very high density in the film. However, due to their very small size, the UV-visible spectrum exhibits only a minor increase, the SPR peak is small and there is no diffraction signal. In all case, the CH2OH groups of HA can be reduced to CH=O during UV-irradiation.

Based on UV-visible spectrometry, FTIR data and TEM images of the *in situ* synthesized NPs, we propose the following mechanism for gold NPs formation in the $(PLL9.5/HA2.9)_7$-PLL9.5 films (**Scheme 4.1**). At pH 3 (**Scheme 4.1**), $HAuCl_4$ dissociates into $AuCl_4^-$, which interacts with the NH_3^+ groups of PLL. Indeed, amine groups were mostly protonated in NH_3^+ groups at this pH and carboxyl groups were partially ionized (the pKa of PLL and HA are of ~9 and ~3, respectively), generating more free NH_3^+ groups and allowing maximal interactions with incoming $AuCl_4^-$ ions. Nevertheless, some NH_3^+ groups that were interacting with COO^- groups, probably via loose interactions with diffusible PLL molecules, could be displaced by $AuCl_4^-$ anions. Thus, COO^- groups became more protonated in COOH. The interaction of $AuCl_4^-$ with the ammonium groups of PLL slightly affected the amide I

band at 1656 cm^{-1}. The UV-reduction process leads to further formation of COOH and loss of H-bonds from the C-O-H and C-O-C groups. Different groups of HA are thus important for the stabilization of the as-formed gold NPs. The additional decrease of the amide peak upon UV-irradiation may correspond to structural changes due to the stabilization of the gold NPs by the polyelectrolytes. The gold NPs formed at this pH were numerous and larger in diameter (~8.7 nm) as the condition for nucleation, growth and stabilization seemed optimal.

At pH 6 (**Scheme 4.1**), most of the amine groups were protonated but most of the carboxyl groups were fully ionized, so there were fewer interactions with $AuCl_4^-$ anions. Electrostatic interactions between PLL and HA are more numerous. Thus, the decrease of COO^- peak was lower and the associated changes in the hydroxyl groups and amide I band were also lower. The nucleation process was efficient and NPs grew over the whole film thickness but the growth stopped when the NPs reached only ~2.8 nm in diameter.

At pH 9 (**Scheme 4.1**), about half of the amine groups were protonated and COO^- groups of HA were essentially ionized. At high pH, the $AuCl_2^-$ form can be easily reduced and the number of nuclei is higher (Bhargava et al. 2005). This pH is indeed close to that of sodium borate buffer, which favor the conditions of nucleation of nanoparticles (Pastoriza-Santos et al. 2010). We hypothesize that the nucleation process is faster than for the other pHs. However, the NPs formed *in situ* are rapidly stabilized by the amine groups and their growth is very limited. In this case, a very large number of NPs are effectively formed, but these NPs have a small diameter of ~ 1.7 nm. Indeed, this very small size was associated with the appearance of a small SPR peak (**Figure 4.12C,C'**) and with the absence of a clear diffraction pattern (**Figure 4.17 C"**).

Thus, the large number of ammonium, carboxylic and hydroxyl groups as well as PLL diffusion within the film all contributed to the formation of homogenous NPs that were spatially-confined in the "bulk" of the film.

This simple and efficient method to synthesize *in situ* a large number of well-dispersed and homogenous NPs after gold loading from an aqueous solution appears very promising. The gold NPs spatially-confined in PEM films could advantageously be used to functionalize different types of materials or devices of any shape, as LbL films can be easily deposited on any solid substrates. The PEM-based nanocomposites could be employed as optoelectronic devices or as catalysts for surface reactions. They may also find applications in photo-thermal cancer treatments, as Au NPs efficiently convert the strongly absorbed light into localized heat, which can be exploited for the selective laser photothermal therapy of cancer (Jain et al.

2007).

4.2.4 Conclusions

We prepared a nanocomposite film using (PLL/HA) multilayer films as a template to synthesize *in situ* gold NPs. The process was easily achieved by loading gold ions from an aqueous solution, then irradiating the dry film under UV light. Importantly, gold NPs formed in all conditions regardless of the pH of the gold solution (pH 3, 6 and 9), but their size and density depended on the loading pH. Highly homogeneous and well-dispersed gold NPs of ~2 nm to ~ 9 nm in diameter were successfully prepared and were distributed throughout the whole film thickness (~2.5 μm). This indicated that amino groups were evenly distributed in the film. Furthermore, these groups were able to interact with aurochlorate ions. We also evidenced that, besides the ammonium groups of PLL, the hydroxyl groups and carboxylic groups of HA played a key role in the reaction by allowing the generation of free radicals and of protonated groups. Thus, the efficient nucleation and growth of gold NPs appeared to be dependent on the presence of specific functional groups in the film, but also on the mobility and even distribution of PLL in the films. Other exponentially-growing polypeptide and polysaccharide PEM films that present a charge imbalance between the polyelectrolytes may be further used to synthesize a large variety of gold NPs. The gold NPs/PEM nanocomposites containing a very high amount of gold NPs may find applications as biosensors or as drug delivery reservoir.

Conclusions

Major conclusions and perspectives for the thesis

In this work, two different pH-amplified layer-by-layer assembly films were studied, where the films were constructed by depositing polycation at high pH and polyanion at low pH.

The first one was consisted of poly(ethylene imine) (PEI) and poly(acrylic acid) (PAA). Assembling PEI at high pH with PAA at low pH makes it possible to fabricate a relatively thick film within limited deposit cycles (up to 3.25 μm for films of 7 layer pairs) and provides a facial way to construct micro nano-structured surface morphology, which can be easily turned to superhydrophobic surface via coating with a layer of low surface energy compound. The fast-growing and superhydrophobic (PEI/PAA) film can be peeled away from Teflon substrate in dry state and therefore the asymmetric free-standing film with one surface hierarchically rough and superhydrophobic while the other surface being flat and hydrophilic was obtained. The asymmetric free-standing film showed extraordinary responsiveness to humidity change. Furthermore, when silver nanoparticles were embedded into this asymmetric free-standing film, multifunctional thin membrane with one surface self-cleaning and the other surface being bactericidal was achieved.

The second system was based on poly(L-lysine) (PLL) and hyaluronic acid (HA), where PLL was assembled at high pH and HA was deposited at low pH. The effect of HA molecular weight on film growth as well as film stability was firstly studied with the attempt to get an insight into the mechanism of the pH-amplified assembly. Thereafter, organic/inorganic hybrid multilayer films were constructed via using the pH-amplified (PLL/HA) films as templates to load metal ions and then to reduce them *in situ* into metal nanoparticles. Firstly, silver nanoparticle loaded (PLL/HA) films were constructed and the mechanical properties of the free-standing hybrid films were tested. Secondly, gold nanoparticles with sizes ranging from around 1.7 nm to 8.6 nm were synthesized in (PLL/HA) films by changing the pH of aurochlorate precursor loading solution from pH 9 to pH 3.

Asymmetric (PEI/PAA) free-standing film

Our previous work has demonstrated that deposit PEI at high pH and PAA at low pH can largely enhance the film growth rate and reach a thickness in micrometer level in only 6 deposit cycles on silica substrate. Moreover, the PAA ending film got micro nano hierarchical surface structures, which can be turned to be superhydrophobic after coated with a layer of low surface energy silane. In this thesis, we further developed the pH-amplified (PEI/PAA) system by using Teflon as substrate and releasing them to be free-standing multilayered films. Thanks to the hierarchical-structured nature of the PAA ending film, asymmetric free-standing film with one surface rough and superhydrophobic and the other surface being flat and hydrophilic was obtained.

The film asymmetric properties on surface morphology and wettability were verified by SEM and water contact angle measurement, respectively. The drastic differences on wettability of the two surfaces of free-standing film lead to very different behaviors of the two surfaces when they were in contact with water molecules. The superhydrophobic surface is believed to be water-repellent and can effectively stop water molecules from penetrating in or out of the surface, whereas water molecules can diffuse in and out of the film on the bottom hydrophilic surface freely. In this case, the hydrophilic surface of the free-standing film can expand at higher humidity but contract at lower humidity while the superhydrophobic surface keeps its original dimension whatever the environment humidity is. The mismatch in dimensions of the two surfaces resulted in an obvious bending/unbending movement of the free-standing film when the humidity changes. Furthermore, the asymmetric wettability (superhydrophobic *vs* hydrophilic) also provides the possibility for the free-standing film to find potential applications in wound dressing. A multifunctional free-standing film with one surface self-cleaning and the other surface extensively releasing anti-biotic drug was constructed via incorporating silver nanoparticles into the (PEI/PAA) asymmetric free-standing film. The silver ions releasing test measured by ICP-MS showed that the silver ions released one-directionally from the hydrophilic surface of the free-standing film, and the film bactericidal activity on its hydrophilic bottom surface was confirmed by the Kirby-Bauer assay. On the other hand, the self-cleaning ability on the superhydrophobic top surface as well as the anti-bacteria adhesion properties was verified. The asymmetric properties of the two surfaces of free-standing film may open a new avenue to design and functionalize free-standing films and find more applications of the ultrathin membranes.

pH-amplified (PLL/HA) films

It is also proved that increasing the deposit pH of PLL solution and decreasing the pH of HA solution can accelerate the film growth. In this thesis, we firstly studied the effect of molecular weight and concentration of HA deposit solution on film growth behavior and stability of pH-amplified (PLL/HA) films. QCM and FTIR were used to follow the film growth and found when PLL was layered with HA of higher molecular weight or higher concentration much faster and more steady film growth was observed. Concerning film stability in PBS, it was found that the PLL-ending films were much stable than their HA-ending counterparts, meanwhile, higher molecular weight HA also resulted in much more stable film. FTIR was also applied to investigate PLL secondary structures as well as HA ionization degree. Evidences showed that the PLL chains lost their β-sheet structures when layered with HA and the ionization degree of HA in the films increased when the layer number increased. What's more, PLL chains layered with higher molecular weight HA diffused much faster as measured by fluorescence recovery after photobleaching (FRAF). Finally, it is suggested that higher molecular weight HA provided stronger interaction with PLL molecules and also more inter and intra molecular interactions between HA chains in the solution as well as in the film. These interactions make the films grow much faster and more steadily.

The pH-amplified (PLL/HA) films were then used as template to load silver ions, either by pre-complex or post-loading, and the silver nanoparticles were synthesized *in situ* with the intention to enhancing the mechanical properties of the multilayered film. SEM and TEM images were used to visualize the nanoparticle size and distribution on film surface as well as in the cross-section. It was shown that the nanoparticle size depended on the method for incorporating silver ions, pre-complexed silver ions with PLL chains leaded to bigger size and the post-loading way resulted in smaller size. The nanoparticle distributed over the whole film thickness for post-loaded and PLL-ending pre-complexed films but mostly aggregated at the bottom of HA-ending pre-complexed film. Micro stretch test was carried out to measure the mechanical properties of the silver nanoparticle loaded free-standing multilayers, and found the silver loading amount, the nanoparticle distribution and the nanoparticle size can have effect on the film ultimate stress and elastic modulus. However, the reinforcement of the silver nanoparticles on film mechanical properties was not very satisfying, reached only 2.2× and 2.5× for ultimate stress and elastic modulus, respectively. This may because: the loading amount is not high enough; the nanoparticle distribution in the film is not homogenous; or the interaction between silver nanoparticle and polyelectrolyte is not strong enough.

Finally, gold nanoparticles were synthesized in pH-amplified (PLL/HA) films via *in situ* UV reduction and aurochlorate was used as precursor. Highly homogeneous and well-dispersed gold nanoparticles of ~1.7 nm to ~ 8.6 nm in diameter were successfully synthesized and were distributed throughout the whole film thickness (~3 μm), as evidenced by SEM and TEM images. The nanoparticle size can be tuned just by changing the pH of precursor loading solutions. The effect of pH on aurochlorate ions and the role of HA and PLL molecules in gold nanoparticle UV reduction were also studied. UV-visible spectra and FTIR data showed that increasing solution pH can destabilize aurochlorate ions and facilitate gold nanopartice reduction process, HA molecules (probably the hydroxyl groups) can further accelerate gold reduction rate, and the amino groups on PLL chains can form complex with gold ions and also stabilize reduced gold nanoparticles. The well-dispersed and highly homogeneous distribution of gold nanoparticles originated from the well distributed PLL chains in the whole (PLL/HA) film.

Perspectives

Layer-by-layer assembly has witnessed great development since the first reports by Decher and coworkers. It is proved to be a versatile and effective way for surface modification. Releasing the polyelectrolyte multilayer film from the substrate expands the application of the layer-by-layer technique from surface coating to free-standing membranes. Free-standing films based on layer-by-layer films aroused even more interests especially when dry films in large dimensions can be easily peeled off from hydrophobic substrate without any post-processing step.

One of the great challenges for developing free-standing films based on layer-by-layer is to achieve a very fast film buildup and to provide functionalities to such films.

pH-amplified layer-by-layer assembly, which can provide film dry thicknesses in the micrometer level by depositing about 8 pairs of layers, provides a way for rapid film construction. This technique can be used for most multilayers concerning weak polyelectrolytes. Other methods, like the recently developed co-spray method where the polycation and polyanion were sprayed onto the substrate continuously and simultaneously (Lefort et al. 2010), can make contributions to accelerate the film buildup process. In fact, it is possible to release (PLL/HA) films from an inert substrate, such as Teflon, when the film dry thickness reaches 2-3 μm. The thermal and mechanical properties of the (PLL/HA) multilayer

can be tested.

Poor mechanical properties of the membranes based on natural polymers may limit their future application. Trials to introduce inorganic NPs into natural polymer films showed that the position of the inorganic NPs is important for the enhancement of film mechanical properties (Kharlampieva et al. 2010; Uğur et al. 2011). In my work, the silver NP loaded (PLL/HA) film were only 2 times stiffer than the unloaded ones. This may be due to the inhomogeneous dispersion of the Ag NPs (see chapter 4.1). To achieve well-dispersed NP in the whole film, another method may be used. Silver ions can be complexed with HA or modified HA (to be cross-linkable so as to stabilize the film) in solution via ionic interaction. Then, the same solution can be used to deposit layer after layer using spin coating on a sacrificial layer such as cellulose acetate. Silver NPs can be synthesized either by chemical reduction or by photoreduction after film cross-linking. It can be anticipated that with well-dispersed and a proper loading amount, which can be tuned by Ag^+ concentration, the HA-Ag film can get much better mechanical properties. HA and silver NPs gained lots of interest in wound healing due to the capacity of HA molecules to retain water and to the broad spectrum of antimicrobial activity of Ag NPs. The HA-Ag film may find applications in the repair of tissue defects after surgery.

In contrary to Ag NP, *in situ* synthesized Au NPs in (PLL/HA) films were found to be homogenous and distributed throughout the whole film thickness (see chapter 4.2). By releasing the Au NPs loaded (PLL/HA) films from their substrate, it would be possible to study the effect of NP size (by tuning the loading pH), of the amount of Au NPs (by adjusting the precursor concentration) on film mechanical properties. Control experiments of layering prefabricated Au NP into (PLL/HA) films can also carried out to study the effect of NP position on film mechanical properties. Besides mechanical properties, the effect of NP size, amount, and position on electrical and optical properties could also be explored. Moreover, considering the biocompatibility of both the film and Au NP and the special optical and photothermal properties of Au NP, the Au NPs loaded (PLL/HA) films may find applications in the fields of controlled drug delivery, bioimaging and biosensor.

Composite films made of multiple strata provide a convenient way to combine different functionalities together. Free-standing films made of (PLL/HA) films as underlying layer and (PEI/PAA) as top layer may found applications in wound dressing. The (PEI/PAA) top layer can be superhydrophobic and self-cleaning so as to keep the defect from the environment. And the underlying (PLL/HA) film, due to its hydration nature, may keep the contacted defect in a humid atmosphere and retain the enzyme and other useful molecules expressed by the

defect. This is expected to facilitate wound healing (Korting et al. 2011).

Also, composite free-standing film made of tough natural polymers as underlying layer and hydrated films as top layer may be interesting. The tough underlying layer, such as silk fibroin whose mechanical properties can be further reinforced by introducing inorganic NPs, can provide the film with good mechanical properties for easy manipulation. Meanwhile, the top layer, such as (PLL/HA) or (CHI/HA) which is easy to be biofunctionalized, could be used to tune cell behavior by cross-linking or by incorporating functional species. For instance, grafting REDV peptide on soft film surface can selectively promote endothelial cell adhesion and growth and prevent thrombosis (Monchaux et al. 2007; Plouffe et al. 2007; Lin et al. 2010). In case the film is constructed inside a tube with suitable diameter, man-made blood-vessels may be obtained.

Indeed, the functionalization of supported multilayered films that has now been realized for numerous applications can be employed to the free-standing films. Moreover, the asymmetric properties of the two surfaces of the membrane may bring another way to functionalize the free-standing film.

Bibliographic references

Agarwal, A., Shao, X., Rajian, J. R., Zhang, H., Chamberland, D. L., Kotov, N. A. and Wang, X. (2011). "Dual-mode imaging with radiolabeled gold nanorods." Journal of Biomedical Optics 16(5): 051307.

Agarwal, A., Weis, T. L., Schurr, M. J., Faith, N. G., Czuprynski, C. J., McAnulty, J. F., Murphy, C. J. and Abbott, N. L. (2010). "Surfaces modified with nanometer-thick silver-impregnated polymeric films that kill bacteria but support growth of mammalian cells." Biomaterials 31(4): 680-690.

Anker, J. N., Hall, W. P., Lyandres, O., Shah, N. C., Zhao, J. and Van Duyne, R. P. (2008). "Biosensing with plasmonic nanosensors." Nature Materials 7(6): 442-453.

Argun, A. A., Ashcraft, J. N. and Hammond, P. T. (2008). "Highly conductive, methanol resistant polyelectrolyte multilayers." Advanced Materials 20(8): 1539-1543.

Argun, A. A., Ashcraft, J. N., Herring, M. K., Lee, D. K. Y., Allcock, H. R. and Hammond, P. T. (2010). "Ion Conduction and Water Transport in Polyphosphazene-Based Multilayers." Chemistry of Materials 22(1): 226-232.

Ashcraft, J. N., Argun, A. A. and Hammond, P. T. (2010). "Structure-property studies of highly conductive layer-by-layer assembled membranes for fuel cell PEM applications." Journal of Materials Chemistry 20(30): 6250-6257.

Ayache, J. and Albarede, P. H. (1995). "Application of the ionless tripod polisher to the preparation of YBCO superconducting multilayer and bulk ceramics thin films." Ultramicroscopy 60: 195-206.

Bason, S., Oren, Y. and Freger, V. (2011). "Ion transport in the polyamide layer of RO membranes: Composite membranes and free-standing films." Journal of Membrane Science 367(1-2): 119-126.

Belfiore, L. A. and Indra, E. M. (2000). "Transition metal compatibilization of poly(vinylamine) and poly(ethylene imine)." Journal of Polymer Science Part B-Polymer Physics 38: 552-561.

Bernsmann, F., Richert, L., Senger, B., Lavalle, P., Voegel, J.-C., Schaaf, P. and Ball, V. (2008). "Use of dopamine polymerisation to produce free-standing membranes from (PLL-HA)(n) exponentially growing multilayer films." Soft Matter 4(8): 1621-1624.

Bhargava, S. K., Booth, J. M., Agrawal, S., Coloe, P. and Kar, G. (2005). "Gold nanoparticle formation during bromoaurate reduction by amino acids." Langmuir 21: 5949-5956.

Bhushan, B. and Jung, Y. C. (2011). "Natural and biomimetic artificial surfaces for superhydrophobicity, self-cleaning, low adhesion, and drag reduction." Progress in Materials Science 56(1): 1-108.

Bigelow, W. C., Pickett, D. L. and Zisman, W. A. (1946). "The preparation of a monomolecular layer by adsorption of a surfactant onto a clean metal surface." Journal

of Colloid and Interface Science 1: 513-538.

Blodgett, K. B. and Langmuir, I. (1937). "Built-up films of barium stearate and their optical properties." Physical Review 51: 964-982.

Boateng, J. S., Matthews, K. H., Stevens, H. N. E. and Eccleston, G. M. (2008). "Wound Healing Dressings and Drug Delivery Systems:A Review." Journal of Pharmaceutical Sciences 97: 2892-2923.

Boisselier, E. and Astruc, D. (2009). "Gold nanoparticles in nanomedicine: preparations, imaging, diagnostics, therapies and toxicity." Chemical Society Reviews 38(6): 1759-1782.

Bolto, B., Hoang, M. and Xie, Z. (2011). "A review of membrane selection for the dehydration of aqueous ethanol by pervaporation." Chemical Engineering and Processing 50(3): 227-235.

Boudou, T., Crouzier, T., Auzely-Velty, R., Glinel, K. and Picart, C. (2009). "Internal Composition versus the Mechanical Properties of Polyelectrolyte Multilayer Films: The Influence of Chemical Cross-Linking." Langmuir 25(24): 13809-13819.

Boudou, T., Crouzier, T., Ren, K., Blin, G. and Picart, C. (2010). "Multiple Functionalities of Polyelectrolyte Multilayer Films: New Biomedical Applications." Advanced Materials 22(4): 441-467.

Bravo, J., Zhai, L., Wu, Z., Cohen, R. E. and Rubner, M. F. (2007). "Transparent Superhydrophobic Films Based on Silica Nanoparticles." Langmuir 23: 7293-7298.

Bromberg, L. (1998). "Properties of aqueous solutions and gels of poly(ethylene oxide)-b-poly(propylene oxide)-b-poly(ethylene oxide)-g-poly(acrylic acid)." Journal of Physical Chemistry B 102(52): 10736-10744.

Bucur, C. B., Sui, Z. and Schlenoff, J. B. (2006). "Ideal mixing in polyelectrolyte complexes and multilayers: Entropy driven assembly." Journal of the American Chemical Society 128(42): 13690-13691.

Byon, H. R., Lee, S. W., Chen, S., Hammond, P. T. and Shao-Horn, Y. (2011). "Thin films of carbon nanotubes and chemically reduced graphenes for electrochemical micro-capacitors." Carbon 49(2): 457-467.

Cao, X., Pettitt, M. E., Wode, F., Sancet, M. P. A., Fu, J., Ji, J., Callow, M. E., Callow, J. A., Rosenhahn, A. and Grunze, M. (2010). "Interaction of Zoospores of the Green Alga Ulva with Bioinspired Micro- and Nanostructured Surfaces Prepared by Polyelectrolyte Layer-by-Layer Self-Assembly." Advanced Functional Materials 20(12): 1984-1993.

Caruso, F. and Mohwald, H. (1999). "Protein multilayer formation on colloids through a stepwise self-assembly technique." Journal of the American Chemical Society 121(25): 6039-6046.

Caruso, F., Niikura, K., Furlong, D. N. and Okahata, Y. (1997). "1. Ultrathin multilayer polyelectrolyte films on gold: Construction and thickness determination." Langmuir 13(13): 3422-3426.

Caruso, F., Niikura, K., Furlong, D. N. and Okahata, Y. (1997). "Ultrathin multilayer polyelectrolyte films on gold: Construction and thickness determination .1." Langmuir

13(13): 3422-3426.

Cebeci, F. C., Wu, Z. Z., Zhai, L., Cohen, R. E. and Rubner, M. F. (2006). "Nanoporosity-driven superhydrophilicity: A means to create multifunctional antifogging coatings." Langmuir 22(6): 2856-2862.

Chen, C. L. and Rosi, N. L. (2010). "Peptide-Based Methods for the Preparation of Nanostructured Inorganic Materials." Angewandte Chemie-International Edition 49(11): 1924-1942.

Chen, C. L., Zhang, P. and Rosi, N. L. (2008). "A new peptide-based method for the design and synthesis of nanoparticle superstructures: construction of highly ordered gold nanoparticle double helices." Journal of the American Chemical Society 130: 13555-13557.

Chen, J. Y., Huang, L., Ying, L. M., Luo, G. B., Zhao, X. S. and Cao, W. X. (1999). "Self-assembly ultrathin films based on diazoresins." Langmuir 15: 7208-7212.

Chia, K.-K., Cohen, R. E. and Rubner, M. F. (2008). "Amine-Rich Polyelectrolyte Multilayer Nanoreactors for in Situ Gold Nanoparticle Synthesis." Chemistry of Materials 20(21): 6756-6763.

Chia, K. K., Cohen, R. E. and Rubner, M. F. (2008). "Amine-Rich Polyelectrolyte Multilayer Nanoreactors for in Situ Gold Nanoparticle Synthesis." Chemistry of Materials 20(21): 6756-6763.

Cho, J. H. and Caruso, F. (2005). "Investigation of the interactions between ligand-stabilized gold nanoparticles and polyelectrolyte multilayer films." Chemistry of Materials 17(17): 4547-4553.

Choi, I., Suntivich, R., Pamper, F. A., Synatschke, C. V., Mueller, A. H. E. and Tsukruk, V. V. (2011). "pH-Controlled Exponential and Linear Growing Modes of Layer-by-Layer Assemblies of Star Polyelectrolytes." Journal of the American Chemical Society 133(24): 9592-9606.

Choi, J. and Rubner, M. F. (2005). "Influence of the degree of ionization on weak polyelectrolyte multilayer assembly." Macromolecules 38(1): 116-124.

Connor, E. E., Mwamuka, J., Gole, A., Murphy, C. J. and Wyatt, M. D. (2005). "Gold nanoparticles are taken up by human cells but do not cause acute cytotoxicity." Small 1(3): 325-327.

Correa-Duarte, M. A., Grzelczak, M., Salgueirino-Maceira, V., Giersig, M., Liz-Marzan, L. M., Farle, M., Sierazdki, K. and Diaz, R. (2005). "Alignment of carbon nanotubes under low magnetic fields through attachment of magnetic nanoparticles." Journal of Physical Chemistry B 109(41): 19060-19063.

Crespo-Biel, O., Dordi, B., Reinhoudt, D. N. and Huskens, J. (2005). "Supramolecular layer-by-layer assembly: Alternating adsorptions of guest- and host-functionalized molecules and particles using multivalent supramolecular interactions." Journal of the American Chemical Society 127: 7594-7600.

Crisp, M. T. and Kotov, N. A. (2003). "Preparation of nanoparticle coatings on surfaces of complex geometry." Nano Letters 3(2): 173-177.

Crouzier, T. and Picart, C. (2009). "Ion Pairing and Hydration in Polyelectrolyte Multilayer Films Containing Polysaccharides." Biomacromolecules 10(2): 433-442.

Crouzier, T. and Picart, C. (2009). "Ion pairing and hydration in polyelectrolyte multilayer films containing polysaccharides." Biomacromolecules 10(2): 433-442.

Crouzier, T., Ren, K., Nicolas, C., Roy, C. and Picart, C. (2009). "Layer-By-Layer Films as a Biomimetic Reservoir for rhBMP-2 Delivery: Controlled Differentiation of Myoblasts to Osteoblasts." Small 5(5): 598-608.

Crouzier, T., Szarpak, A., Boudou, T., Auzely-Velty, R. and Picart, C. (2010). "Polysaccharide-Blend Multi layers Containing Hyaluronan and Heparin as a Delivery System for rhBMP-2." Small 6(5): 651-662.

Cui, X., Li, C. M., Bao, H., Zheng, X. and Lu, Z. (2008). "In situ fabrication of silver nanoarrays in hyaluronan/PDDA layer-by-layer assembled structure." Journal of Colloid and Interface Science 327: 459-465.

Cui, X. Q., Li, C. M., Bao, H. F., Zheng, X. T. and Lu, Z. S. (2008). "In situ fabrication of silver nanoarrays in hyaluronan/PDDA layer-by-layer assembled structure." Journal of Colloid and Interface Science 327(2): 459-465.

Cui, X. Q., Li, C. M., Bao, H. F., Zheng, X. T., Zang, J. F., Ooi, C. P. and Guo, J. (2008). "Hyaluronan-assisted photoreduction synthesis of silver nanostructures: From nanoparticle to nanoplate." Journal of physical Chemistry C 112: 10730-10734.

Dai, J. and Bruening, M. L. (2002). "Catalytic Nanoparticles Formed by Reduction of Metal Ions in Multilayered Polyelectrolyte Films." Nano Letters 2: 497-501.

Decher, G. (1997). "Fuzzy nanoassemblies: Toward layered polymeric multicomposites." Science 277(5330): 1232-1237.

Decher, G. and Hong, J. D. (1991). "Buildup of ultrathin multilayer films by a self-assembly process. 2. Consecutive adsorption of anionic and cationic bipolar amphililes and polyelectrolytes on charged surfaces." Berichte Der Bunsen-Gesellschaft-Physical Chemistry Chemical Physics 95(11): 1430-1434.

Decher, G., Lvov, Y. and Schmitt, J. (1994). "Proof of multilayer structural organization in self-assembled polycation polyanion molecular films." Thin Solid Films 244(1-2): 772-777.

Decher, G., Schlenoff, J. B. and Ed. (2003). "Multilayer Thin Films: Sequential Assembly of Nanocomposite Materials." Germany: Wily-VCH, Weinheim.

Delcea, M., Mohwald, H. and Skirtach, A. G. (2011). "Stimuli-responsive LbL capsules and nanoshells for drug delivery." Advanced Drug Delivery Reviews 63(9): 730-747.

DeLongchamp, D. M. and Hammond, P. T. (2004). "Highly ion conductive poly(ethylene oxide)-based solid polymer electrolytes from hydrogen bonding layer-by-layer assembly." Langmuir 20(13): 5403-5411.

DeRocher, J. P., Mao, P., Kim, J. Y., Han, J., Rubner, M. F. and Cohen, R. E. (2011). "Layer-by-Layer Deposition of All-Nanoparticle Multilayers in Confined Geometries." Acs Applied Materials & Interfaces 3: ASAP.

Detry, J. G., Sindic, M. and Deroanne, C. (2010). "Hygiene and Cleanability: A Focus on

Surfaces." Critical Reviews in Food Science and Nutrition 50(7): 583-604.

Dong, W. F., Sukhorukov, G. B. and Mohwald, H. (2003). "Enhanced Raman imaging and optical spectra of gold nanoparticle doped microcapsules." Physical Chemistry Chemical Physics 5(14): 3003-3012.

Dontsova, D., Keller, V., Keller, N., Steffanut, P., Felix, O. and Decher, G. (2011). "Photocatalytically Active Polyelectrolyte/Nanoparticle Films for the Elimination of a Model Odorous Gas." Macromolecular Rapid Communications 32(15): 1145-1149.

Dubas, S. T., Farhat, T. R. and Schlenoff, J. B. (2001). "Multiple membranes from "true" polyelectrolyte multilayers." Journal of the American Chemical Society 123(22): 5368-5369.

Duffel, B. v., Schoonheydt, R. A., Grim, C. P. M. and Schryver, F. C. D. (1999). "Multilayered Clay Films: Atomic Force Microscopy Study and Modeling." Langmuir 15: 7520-7529.

Eckle, M. and Decher, G. (2001). "Tuning the performance of layer-by-layer assembled organic light emitting diodes by controlling the position of isolating clay barrier sheets." Nano Letters 1(1): 45-49.

Elbert, D. L., Herbert, C. B. and Hubbell, J. A. (1999). "Thin polymer layers formed by polyelectrolyte multilayer techniques on biological surfaces." Langmuir 15(16): 5355-5362.

Esumi, K., Suzuki, A., Aihara, N., Usui, K. and Torigoe, K. (1998). "Preparation of gold colloids with UV irradiation using dendrimers as stabilizer." Langmuir 14(12): 3157-3159.

Eustis, S. and El-Sayed, M. A. (2005). "Aspect ratio dependence of the enhanced fluorescence intensity of gold nanorods: Experimental and simulation study." Journal of physical Chemistry B 109: 16350-16356.

Eustis, S. and El-Sayed, M. A. (2006). "Molecular mechanism of the photochemical generation of gold nanoparticles in ethylene glycol: Support for the disproportionation mechanism." journal of Physical Chemistry B 110: 14014-14019.

Eustis, S. and El-Sayed, M. A. (2006). "Why gold nanoparticles are more precious than pretty gold: Noble metal surface plasmon resonance and its enhancement of the radiative and nonradiative properties of nanocrystals of different shapes." Chemical Society Reviews 35: 209-217.

Eustis, S., Hsu, H.-Y. and El-Sayed, M. A. (2005). "Gold Nanoparticle Formation from Photochemical Reduction of Au3+ by Continuous Excitation in Colloidal Solutions. A Proposed Molecular Mechanism." Journal of Physical Chemistry B 109: 4811-4815.

Fendler, J. H. (1996). "Self-assembled nanostructured materials." Chemistry of Materials 8(8): 1616-1624.

Feng, L., Li, S., Li, Y., Li, H., Zhang, L., Zhai, J., Song, Y., Liu, B., Jiang, L. and Zhu, D. (2002). "Super-Hydrophobic Surfaces: From Natural to Artificial." Advanced Materials 14: 1857-1860.

Ferri, J. K., Dong, W. F. and Miller, R. (2005). "Ultrathin free-standing polyelectrolyte nanocomposites: A novel method for preparation and characterization of assembly

dynamics." Journal of Physical Chemistry B 109(31): 14764-14768.

Ferri, J. K., Dong, W. F., Miller, R. and Mohwald, H. (2006). "Elastic moduli of asymmetric ultrathin free-standing polyelectrolyte nanocomposites." Macromolecules 39(4): 1532-1537.

Fery, A., Scholer, B., Cassagneau, T. and Caruso, F. (2001). "Nanoporous thin films formed by salt-induced structural changes in multilayers of poly(acrylic acid) and poly(allylamine)." Langmuir 17(13): 3779-3783.

Forrest, J. A., Dalnoki-Veress, K. and Dutcher, J. R. (1997). "Interface and chain confinement effects on the glass transition temperature of thin polymer films." Physical Review E 56: 5705-5716.

Fu, J., Ji, J., Shen, L., Kueller, A., Rosenhahn, A., Shen, J. and Grunze, M. (2009). "pH-Amplified Exponential Growth Multilayers: A Facile Method to Develop Hierarchical Micro- and Nanostructured Surfaces." Langmuir 25(2): 672-675.

Fujie, T., Kinoshita, M., Shono, S., Saito, A., Okamura, Y., Saitoh, D. and Takeoka, S. (2010). "Sealing effect of a polysaccharide nanosheet for murine cecal puncture." Surgery 148(1): 48-58.

Fujie, T., Matsutani, N., Kinoshita, M., Okamura, Y., Saito, A. and Takeoka, S. (2009). "Adhesive, Flexible, and Robust Polysaccharide Nanosheets Integrated for Tissue-Defect Repair." Advanced Functional Materials 19(16): 2560-2568.

Fujie, T., Okamura, Y. and Takeoka, S. (2007). "Ubiquitous transference of a free-standing polysaccharide nanosheet with the development of a nano-adhesive plaster." Advanced Materials 19(21): 3549-3553.

Fujie, T., Okamura, Y. and Takeoka, S. (2009). "Selective surface modification of free-standing polysaccharide nanosheet with micro/nano-particles identified by structural color changes." Colloids and Surfaces a-Physicochemical and Engineering Aspects 334(1-3): 28-33.

Galyean, A. A., Day, R. W., Malinowski, J., Kittredge, K. W. and Leopold, M. C. (2009). "Polyelectrolyte-linked film assemblies of nanoparticles and nanoshells: Growth, stability, and optical properties." Journal of Colloid and Interface Science 331(2): 532-542.

Gangopadhayay, A. K. and Chakravorty, C. (1961). "Charge Transfer Spectra of some Gold(III) Complexes." Journal of Physical Chemistry 35: 2206-2209.

Gill, R., Mazhar, M., Felix, O. and Decher, G. (2010). "Covalent Layer-by-Layer Assembly and Solvent Memory of Multilayer Films from Homobifunctional Poly(dimethylsiloxane)." Angewandte Chemie-International Edition 49(35): 6116-6119.

Goulet, P. J. G., David S. dos Santos, J., Alvarez-Puebla, R. A., Osvaldo N. Oliveira, J. and Aroca, R. F. (2005). "Surface-Enhanced Raman Scattering on Dendrimer/Metallic Nanoparticle Layer-by-Layer Film Substrates." Langmuir 21: 5576-5581.

Grossin, L., Cortial, D., Saulnier, B., Felix, O., Chassepot, A., Decher, G., Netter, P., Schaaf, P., Gillet, P., Mainard, D., Voegel, J.-C. and Benkirane-Jessel, N. (2009). "Step-by-Step Build-Up of Biologically Active Cell-Containing Stratified Films Aimed at Tissue

Engineering." Advanced Materials 21(6): 650-655.

Gui, Z., Qian, J., Du, B., Yin, M. and An, Q. (2009). "Fabrication of free-standing polyelectrolyte multilayer films: A method using polysulfobetaine-containing films as sacrificial layers." Journal of Colloid and Interface Science 340(1): 35-41.

Gunawidjaja, R., Jiang, C., Peleshanko, S., Ornatska, M., Singamaneni, S. and Vladimir V. Tsukruk (2006). "Flexible and Robust 2D Arrays of Silver Nanowires Encapsulated within Freestanding Layer-by-Layer Films." Advanced Functional Materials 16: 2024-2034.

Hübsch, E., Fleith, G., Fatisson, J., Labbé, P., Voegel, J. C., Schaaf, P. and Ball, V. (2005). "Multivalent ion/polyelectrolyte exchange processes in exponentially growing multilayers." Langmuir 21: 3664-3669.

Haes, A. J., Zou, S. L., Schatz, G. C. and Van Duyne, R. P. (2004). "Nanoscale optical biosensor: Short range distance dependence of the localized surface plasmon resonance of noble metal nanoparticles." Journal of Physical Chemistry B 108: 6961-6968.

Hajicharalambous, C. S., Lichter, J., Hix, W. T., Swierczewska, M., Rubner, M. F. and Rajagopalan, P. (2009). "Nano- and sub-micron porous polyelectrolyte multilayer assemblies: Biomimetic surfaces for human corneal epithelial cells." Biomaterials 30(23-24): 4029-4036.

Hammond, P. T. (2011). "Engineering Materials Layer-by-Layer: Challenges and Opportunities in Multilayer Assembly." Aiche Journal 57(11): 2928-2940.

Hao, E. C. and Lian, T. Q. (2000). "Buildup of polymer/Au nanoparticle multilayer thin films based on hydrogen bonding." Chemistry of Materials 12(11): 3392-3396.

Haxaire, K., Marechal, Y., Milas, M. and Rinaudo, M. (2003). "Hydration of polysaccharide hyaluronan observed by IR spectrometry. I. Preliminary experiments and band assignments." Biopolymer 72: 10-20.

Hillberg, A. L., Holmes, C. A. and Tabrizian, M. (2009). "Effect of genipin cross-linking on the cellular adhesion properties of layer-by-layer assembled polyelectrolyte films." Biomaterials 30: 4463-4470.

Hiller, J. A., Mendelsohn, J. D. and Rubner, M. F. (2002). "Reversibly erasable nanoporous anti-reflection coatings from polyelectrolyte multilayers." Nature Materials 1: 59-63.

Hoshi, T., Sagae, N., Daikuhara, K., Takahara, K. and Anzai, J.-i. (2007). "Multilayer membranes via layer-by-layer deposition of glucose oxidase and Au nanoparticles on a Pt electrode for glucose sensing." Materials Science and Engineering C 27: 890-894.

Hu, M., Chen, J. Y., Li, Z. Y., Au, L., Hartland, G. V., Li, X. D., Marquez, M. and Xia, Y. N. (2006). "Gold nanostructures: engineering their plasmonic properties for biomedical applications." Chemical Society Reviews 35(11): 1084-1094.

Hu, Z., Zhang, X. and Li, Y. (1995). "Synthesis and Application of Modulated Polymer Gels." Science 269: 525-527.

Hua, F., Cui, T. H. and Lvov, Y. M. (2004). "Ultrathin cantilevers based on polymer-ceramic nanocomposite assembled through layer-by-layer adsorption." Nano Letters 4(5): 823-825.

Huang, X. H., Jain, P. K., El-Sayed, I. H. and El-Sayed, M. A. (2007). "Gold nanoparticles: interesting optical properties and recent applications in cancer diagnostic and therapy." Nanomedicine 2(5): 681-693.

Huang, Y. and Paul, D. R. (2004). "Experimental methods for tracking physical aging of thin glassy polymer films by gas permeation." Journal of Membrane Science 244(1-2): 167-178.

Iler, R. K. (1966). "Multilayers of colloidal particles." Journal of Colloid and Interface Science 21: 569-594.

Iost, R. M., Madurro, J. M., Brito-Madurro, A. G., Nantes, I. L., Caseli, L. and Crespilho, F. N. (2011). "Strategies of Nano-Manipulation for Application in Electrochemical Biosensors." International Journal of Electrochemical Science 6(7): 2965-2997.

Itano, K., Choi, J. Y. and Rubner, M. F. (2005). "Mechanism of the pH-induced discontinuous swelling/deswelling transitions of poly(allylamine hydrochloride)-containing polyelectrolyte multilayer films." Macromolecules 38(8): 3450-3460.

Jaber, J. A. and Schlenoff, J. B. (2007). "Counterions and water in polyelectrolyte multilayers: a tale of two polycations." Langmuir 23(2): 896-901.

Jain, P. K., El-Sayed, I. H. and El-Sayed, M. A. (2007). "Au nanoparticles target cancer." Nano Today 2: 18-29.

Jiang, C. Y., Ko, H. Y. and Tsukruk, V. V. (2005). "Strain-sensitive Raman modes of carbon nanotubes in deflecting freely suspended nanomembranes." Advanced Materials 17(17): 2127-2131.

Jiang, C. Y., Markutsya, S., Pikus, Y. and Tsukruk, V. V. (2004). "Freely suspended nanocomposite membranes as highly sensitive sensors." Nature Materials 3(10): 721-728.

Jiang, C. Y., Markutsya, S., Shulha, H. and Tsukruk, V. V. (2005). "Freely suspended gold nanoparticle arrays." Advanced Materials 17(13): 1669-1673.

Jiang, C. Y., Markutsya, S. and Tsukruk, V. V. (2004). "Compliant, robust, and truly nanoscale free-standing multilayer films fabricated using spin-assisted layer-by-layer assembly." Advanced Materials 16(2): 157-161.

Jiang, C. Y. and Tsukruk, V. V. (2006). "Freestanding nanostructures via layer-by-layer assembly." Advanced Materials 18(7): 829-840.

Joly, S., Kane, R., Radzilowski, L., Wang, T., Wu, A., Cohen, R. E., Thomas, E. L. and F, R. M. (2000). "Multilayer Nanoreactors for Metallic and Semiconducting Particles." Langmuir 16(3): 1354 -1359.

Joly, S., Kane, R., Radzilowski, L., Wang, T., Wu, A., Cohen, R. E., Thomas, E. L. and Rubner, M. F. (2000). "Multilayer Nanoreactors for Metallic and Semiconducting Particles." Langmuir 16: 1354 -1359.

Jourdainne, L., Lecuyer, S., Arntz, Y., Picart, C., Schaaf, P., Senger, B., Voegel, J.-C., Lavalle, P. and Charitat, T. (2008). "Dynamics of poly(L-lysine) in hyaluronic acid/poly(L-lysine)multilayer films studied by fluorescence recovery after pattern photobleaching." Langmuir 24(15): 7842-7847.

Kadi, S., Cui, D., Bayma, E., Boudou, T., Nicolas, C., Glinel, K., Picart, C. and Auzély-Velty, R. (2009). "Alkylamino Hydrazide Derivatives of Hyaluronic Acid: Synthesis, Characterization in Semidilute Aqueous Solutions, and Assembly into Thin Multilayer Films." Biomacromolecules 10: 2875-2884.

Kar, T., Dutta, S. and Das, P. K. (2010). "pH-Triggered conversion of soft nanocomposites: in situ synthesized AuNP-hydrogel to AuNP-organogel." Soft Matter 6(19): 4777-4787.

Kelsall, G. H., Welham, N. J. and Diaz, M. A. (1993). "Thermodynamics of CL-H2O,BR-H2O, I-H2O, AU-CL-H2O, AU-BR-H2O and AU-I-H2O systems at 298 K." Journal of Electroanalytical Chemistry 361: 13-24.

Kharlampieva, E., Kozlovskaya, V., Gunawidjaja, R., Shevchenko, V. V., Vaia, R., Naik, R. R., Kaplan, D. L. and Tsukruk, V. V. (2010). "Flexible Silk-Inorganic Nanocomposites: From Transparent to Highly Reflective." Advanced Functional Materials 20: 840-846.

Kharlampieva, E., Kozlovskaya, V., Wallet, B., Shevchenko, V. V., Naik, R. R., Vaia, R., Kaplan, D. L. and Tsukruk, V. V. (2010). "Co-cross-linking Silk Matrices with Silica Nanostructures for Robust Ultrathin Nanocomposites." Acs Nano 4: 7053-7063.

Kharlampieva, E., Slocik, J. M., Tsukruk, T., Naik, R. R. and Tsukruk, V. V. (2008). "Polyaminoacid-induced growth of metal nanoparticles on layer-by-layer templates." Chemistry of Materials 20(18): 5822-5831.

Kharlampieva, E., Zimnitsky, D., Gupta, M., Bergman, K. N., Kaplan, D. L., Naik, R. R. and Tsukruk, V. V. (2009). "Redox-Active Ultrathin Template of Silk Fibroin: Effect of Secondary Structure on Gold Nanoparticle Reduction." Chemistry of Materials 21: 2696-2704.

Kim, B.-S., Park, S. W. and Hammond, P. T. (2008). "Hydrogen-Bonding Layer-by-Layer-Assembled Biodegradable Polymeric Micelles as Drug Delivery Vehicles from Surfaces." Acs Nano 2: 386-392.

Kim, T. H. and Sohn, B. H. (2002). "Photocatalytic thin films containing TiO2 nanoparticles by the layer-by-layer self-assembling method." Applied Surface Science 201(1-4): 109-114.

Klitzing, R. V. (2006). "Internal structure of polyelectrolyte multilayer assemblies." Physical Chemistry Chemical Physics 8: 5012-5033.

Komarala, V. K., Rakovich, Y. P., Bradley, A. L., Byrne, S. J., Corr, S. A. and Gun'ko, Y. K. (2006). "Emission properties of colloidal quantum dots on polyelectrolyte multilayers." Nanotechnology 17(16): 4117-4122.

Korkut, S., Keskinler, B. and Erhan, E. (2008). "An amperometric biosensor based on multiwalled carbon nanotube-poly(pyrrole)-horseradish peroxidase nanobiocomposite film for determination of phenol derivatives." Talanta 76: 1147-1152.

Korting, H., Schöllmann, C. and White, R. (2011). "Management of minor acute cutaneous wounds: importance of wound healing in a moist environment." Journal of the European Academy of Dermatology and Venereology 25: 130-137.

Kotov, N. A., Magonov, S. and Tropsha, E. (1998). "Layer-by-layer self-assembly of alumosilicate-polyelectrolyte composites: Mechanism of deposition, crack resistance,

and perspectives for novel membrane materials." Chemistry of Materials 10(3): 886-895.

Kurihara, K., Kizling, J., Stenius, P. and Fendler, J. H. (1983). "Laser and pulse radiolytically induced colloidal gold formatoin in water and in water-in-oil microemulsions." Journal of the American Chemical Society 105: 2574-2579.

Lakard, B., Magnin, D., Deschaume, O., Vanlancker, G., Glinel, K., Demoustier-Champagne, S., Nysten, B., Jonas, A. M., Bertrand, P. and Yunus, S. (2011). "Urea potentiometric enzymatic biosensor based on charged biopolymers and electrodeposited polyaniline." Biosensors & Bioelectronics 26: 4139-4145.

Larkin, A. L., Davis, R. M. and Rajagopalan, P. (2010). "Biocompatible, Detachable, and Free-Standing Polyelectrolyte Multilayer Films." Biomacromolecules 11(10): 2788-2796.

Lavalle, P., Boulmedais, F., Ball, V., Mutterer, J., Schaaf, P. and Voegel, J. C. (2005). "Free standing membranes made of biocompatible polyelectrolytes using the layer by layer method." Journal of Membrane Science 253(1-2): 49-56.

Lavalle, P., Picart, C., Mutterer, J., Gergely, C., Reiss, H., Voegel, J. C., Senger, B. and Schaaf, P. (2004). "Modeling the buildup of polyelectrolyte multilayer films having exponential growth." Journal of Physical Chemistry B 108(2): 635-648.

Lavalle, P., Vivet, V., Jessel, N., Decher, G., Voegel, J. C., Mesini, P. J. and Schaaf, P. (2004). "Direct evidence for vertical diffusion and exchange processes of polyanions and polycations in polyelectrolyte multilayer films." Macromolecules 37(3): 1159-1162.

Lee, D., Rubner, M. F. and Cohen, R. E. (2006). "All-nanoparticle thin-film coatings." Nano Lett 6(10): 2305-2312.

Lee, H., Choi, S. H. and Park, T. G. (2006). "Direct visualization of hyaluronic acid polymer chain by self-assembled one-dimensional array of gold nanoparticles." Macromolecules 39: 23-25.

Leff, D. V., Brandt, L. and Heath, J. R. (1996). "Synthesis and Characterization of Hydrophobic, Organically-Soluble Gold Nanocrystals Functionalized with Primary Amines." Langmuir 12: 4723-4730.

Lefort, M., Popa, G., Seyrek, E., Szamocki, R., Felix, O., Hemmerle, J., Vidal, L., Voegel, J.-C., Boulmedais, F., Decher, G. and Schaaf, P. (2010). "Spray-On Organic/Inorganic Films: A General Method for the Formation of Functional Nano- to Microscale Coatings." Angewandte Chemie-International Edition 49(52): 10110-10113.

Leguen, E., Chassepot, A., Decher, G., Schaaf, P., Voegel, J.-C. and Jessel, N. (2007). "Bioactive coatings based on polyelectrolyte multilayer architectures functionalized by embedded proteins, peptides or drugs." Biomolecular Engineering 24(1): 33-41.

Lehn, J. M. and Sanders, J. (1995). "Supramolecular chemistry: concepts and perspectives." Germany: Weiheim-VCH: 1-9.

Li, Z., Lee, D., Sheng, X., Cohen, R. E. and Rubner, M. F. (2006). "Two-Level Antibacterial Coating with Both Release-Killing and Contact-Killing Capabilities." Langmuir 22: 9820-9823.

Liao, H. W., Nehl, C. L. and Hafner, J. H. (2006). "Biomedical applications of plasmon

resonant metal nanoparticles." Nanomedicine 1: 201-208.

Lin, Q., Ding, X., Qiu, F., Song, X., Fu, G. and Ji, J. (2010). "In situ endothelialization of intravascular stents coated with an anti-CD34 antibody functionalized heparin-collagen multilayer." Biomaterials 31(14): 4017-4025.

Link, S. and El-Sayed, M. A. (2000). "Shape and size dependence of radiative, non-radiative and photothermal properties of gold nanocrystals." International Reviews in Physical Chemistry 19: 409-453.

Liu, K. and Jiang, L. (2011). "Bio-inspired design of multiscale structures for function integration." Nano Today 6(2): 155-175.

Loh, K. J., Kim, J., Lynch, J. P., Kam, N. W. S. and Kotov, N. A. (2007). "Multifunctional layer-by-layer carbon nanotube-polyelectrolyte thin films for strain and corrosion sensing " Smart Materials and Structures 16: 429-458.

Lutkenhaus, J. L. and Hammond, P. T. (2007). "Electrochemically enabled polyelectrolyte multilayer devices: from fuel cells to sensors." Soft Matter 3(7): 804-816.

Lutkenhaus, J. L., Hrabak, K. D., McEnnis, K. and Hammond, P. T. (2005). "Elastomeric flexible free-standing hydrogen-bonded nanoscale assemblies." Journal of the American Chemical Society 127(49): 17228-17234.

Lutkenhaus, J. L., McEnnis, K. and Hammond, P. T. (2007). "Tuning the glass transition of and ion transport within hydrogen-bonded layer-by-layer assemblies." Macromolecules 40(23): 8367-8373.

Lutkenhaus, J. L., McEnnis, K. and Hammond, P. T. (2008). "Nano- and microporous layer-by-layer assemblies containing linear poly(ethylenimine) and poly(acrylic acid)." Macromolecules 41(16): 6047-6054.

Lvov, Y., Decher, G. and Mohwald, H. (1993). "Assembly, structural characterization, and thermal-behavior of layer-by-layer deposited ultrathin films of poly(vinyl sulfate) and poly(allylamine)." Langmuir 9(2): 481-486.

Lvov, Y., Decher, G. and Sukhorukov, G. (1993). "Assembly of Thin-Films by Means of Successive Deposition of Alternate Layers of DNA and Poly(Allylamine)." Macromolecules 26: 5396-5399.

Ma, Y. and Sun, J. (2009). "Humido- and Thermo-Responsive Free-Standing Films Mimicking the Petals of the Morning Glory Flower." Chemistry of Materials 21: 898-902.

Ma, Y., Sun, J. and Shen, J. (2007). "Ion-triggered exfoliation of layer-by-layer assembled poly(acrylic acid)/poly(allylamine hydrochloride) films from substrates: A facile way to prepare free-standing multilayer films." Chemistry of Materials 19(21): 5058-5062.

Malikova, N., Pastoriza-Santos, I., Schierhorn, M., Kotov, N. A. and Liz-Marzan, L. M. (2002). "Layer-by-layer assembled mixed spherical and planar gold nanoparticles: Control of interparticle interactions." Langmuir 18(9): 3694-3697.

Mallick, K., Witcomb, M. J. and Scurrell, M. S. (2005). "Polymer-stabilized colloidal gold: a convenient method for the synthesis of nanoparticles by a UV-irradiation approach." Applied Physics A: Materials Science & Processing 80: 395-398.

Mallick, K., Witcomb, M. J. and Scurrell, M. S. (2005). "Polymer-stabilized colloidal gold: a convenient method for the synthesis of nanoparticles by a UV-irradiation approach." Applied Physics a-Materials Science & Processing 80(2): 395-398.

Mallick, K., Witcomb, M. J. and Scurrell, M. S. (2005). "Redox catalytic property of gold nanoclusters: evidence of an electron-relay effect." Applied Physics A: Materials Science & Processing 80: 797-801.

Mamedov, A., Ostrander, J., Aliev, F. and Kotov, N. A. (2000). "Stratified assemblies of magnetite nanoparticles and montmorillonite prepared by the layer-by-layer assembly." Langmuir 16(8): 3941-3949.

Mamedov, A. A. and Kotov, N. A. (2000). "Free-standing layer-by-layer assembled films of magnetite nanoparticles." Langmuir 16(13): 5530-5533.

Mamedov, A. A., Kotov, N. A., Prato, M., Guldi, D. M., Wicksted, J. P. and Hirsch, A. (2002). "Molecular design of strong single-wall carbon nanotube/polyelectrolyte multilayer composites." Nature Materials 1(3): 190-194.

Manevitch, O. L. and Rutledge, G. C. (2004). "Elastic Properties of a Single Lamella of Montmorillonite by Molecular Dynamics Simulation." The Journal of Physical Chemistry B 108: 1428-1435.

Markutsya, S., Jiang, C. Y., Pikus, Y. and Tsukruk, V. V. (2005). "Freely suspended layer-by-layer nanomembranes: Testing micromechanical properties." Advanced Functional Materials 15(5): 771-780.

Mattsson, J., Forrest, J. A. and Borjesson, L. (2000). "Quantifying glass transition behavior in ultrathin free-standing polymer films." Physical Review E 62(4): 5187-5200.

McAloney, R. A., Sinyor, M., Dudnik, V. and Goh, M. C. (2001). "Atomic force microscopy studies of salt effects on polyelectrolyte multilayer film morphology." Langmuir 17(21): 6655-6663.

Mei, Y., Sharma, G., Lu, Y., Ballauff, M., Drechsler, M., Irrgang, T. and Kempe, R. (2005). "High catalytic activity of platinum nanoparticles immobilized on spherical polyelectrolyte brushes." Langmuir 21(26): 12229-12234.

Mendelsohn, J. D., Barrett, C. J., Chan, V. V., Pal, A. J., Mayes, A. M. and Rubner, M. F. (2000). "Fabrication of microporous thin films from polyelectrolyte multilayers." Langmuir 16(11): 5017-5023.

Mendelsohn, J. D., Yang, S. Y., Hiller, J., Hochbaum, A. I. and Rubner, M. F. (2003). "Rational design of cytophilic and cytophobic polyelectrolyte multilayer thin films." Biomacromolecules 4(1): 96-106.

Mjahed, H., Porcel, C., Senger, B., Chassepot, A., Netter, P., Gillet, P., Decher, G., Voegel, J.-C., Schaaf, P., Benkirane-Jessel, N. and Boulmedais, F. (2008). "Micro-stratified architectures based on successive stacking of alginate gel layers and poly(L-lysine)-hyaluronic acid multilayer films aimed at tissue engineering." Soft Matter 4(7): 1422-1429.

Monchaux, E. and Vermette, P. (2007). "Bioactive microarrays immobilized on low-fouling surfaces to study specific endothelial cell adhesion." Biomacromolecules 8: 3668-3673.

Muller, W., Ringsdorf, H., Rump, E., Wildburg, G., Zhang, X., Angermaier, L., Knoll, W., Liley, M. and Spinke, J. (1993). "Attempts to Mimic Docking Processes of the Immune-System-Recognition-Induced Formation of Protein Multilayers." Science 262: 1706-1708.

Murphy, C. J., Gole, A. M., Hunyadi, S. E., Stone, J. W., Sisco, P. N., Alkilany, A., Kinard, B. E. and Hankins, P. (2008). "Chemical sensing and imaging with metallic nanorods." Chemical Communications(5): 544-557.

Nam, K. T., Kim, D. W., Yoo, P. J., Chiang, C. Y., Meethong, N., Hammond, P. T., Chiang, Y. M. and Belcher, A. M. (2006). "Virus-enabled synthesis and assembly of nanowires for lithium ion battery electrodes." Science 312(5775): 885-888.

Nazaran, P., Bosio, V., Jaeger, W., Anghel, D. F. and Klitzing, R. v. (2007). "Lateral Mobility of Polyelectrolyte Chains in Multilayers." The Journal of Physical Chemistry B 111: 8572-8581.

Nepal, D., Balasubramanian, S., Simonian, A. L. and Davis, V. A. (2008). "Strong Antimicrobial Coatings: Single-Walled Carbon Nanotubes Armored with Biopolymers." Nano Letters 8: 1896-1901.

Newman, J. D. S. and Blanchard, G. J. (2006). "Formation of gold nanoparticles using amine reducing agents." Langmuir 22(13): 5882-5887.

Neyertz, S. and Brown, D. (2008). "Molecular dynamics simulations of oxygen transport through a fully atomistic polyimide membrane." Macromolecules 41(7): 2711-2721.

Ngankam, A. P. and Van Tassel, P. R. (2005). "In situ layer-by-layer film formation kinetics under an applied voltage measured by optical waveguide lightmode spectroscopy." Langmuir 21(13): 5865-5871.

Nolte, A. J., Rubner, M. F. and Cohen, R. E. (2004). "Creating Effective Refractive Index Gradients within Polyelectrolyte Multilayer Films: Molecularly Assembled Rugate Filters." Langmuir 20: 3304-3310.

Nolte, A. J., Rubner, M. F. and Cohen, R. E. (2005). "Determining the young's modulus of polyelectrolyte multilayer films via stress-induced mechanical buckling instabilities." Macromolecules 38(13): 5367-5370.

Nolte, A. J., Takane, N., Hindman, E., Gaynor, W., Rubner, M. F. and Cohen, R. E. (2007). "Thin film thickness gradients and spatial patterning via salt etching of polyelectrolyte multilayers." Macromolecules 40(15): 5479-5486.

Okamura, Y., Kabata, K., Kinoshita, M., Saitoh, D. and Takeoka, S. (2009). "Free-Standing Biodegradable Poly(lactic acid) Nanosheet for Sealing Operations in Surgery." Advanced Materials 21(43): 4388-4392.

Olek, M., Kempa, K. and Giersig, M. (2006). "Multiwall carbon nanotubes-based composites - mechanical characterization using the nanoindentation technique." International Journal of Materials Research 97(9): 1235-1238.

Olek, M., Ostrander, J., Jurga, S., Mohwald, H., Kotov, N., Kempa, K. and Giersig, M. (2004). "Layer-by-layer assembled composites from multiwall carbon nanotubes with different morphologies." Nano Letters 4(10): 1889-1895.

Ono, S. S. and Decher, G. (2006). "Preparation of ultrathin self-standing polyelectrolyte multilayer membranes at physiological conditions using pH-responsive film segments as sacrificial layers." Nano Letters 6(4): 592-598.

Orozco, V. H., Kozlovskaya, V., Kharlampieva, E., b, B. L. L. and Tsukruk, V. V. (2010). "Biodegradable self-reporting nanocomposite films of poly(lactic acid) nanoparticles engineered by layer-by-layer assembly." Polymer 51: 4127-4139.

Paeng, K. and Ediger, M. D. (2011). "Molecular Motion in Free-Standing Thin Films of Poly(methyl methacrylate), Poly(4-tert-butylstyrene), Poly(α-methylstyrene), and Poly(2-vinylpyridine)." Macromolecules 44: 7034-7042.

Park, S. Y., Barrett, C. J., Rubner, M. F. and Mayes, A. M. (2001). "Anomalous adsorption of polyelectrolyte layers." Macromolecules 34(10): 3384-3388.

Park, S. Y., Rubner, M. F. and Mayes, A. M. (2002). "Free energy model for layer-by-layer processing of polyelectrolyte multilayer films." Langmuir 18(24): 9600-9604.

Parks, G. (1965). "The isoelectric points of solid oxides, solid hydroxides, and aqueous hydroxo complex systems." Chemical Reviews 65: 177-198.

Pastoriza-Santos, I., Alvarez-Puebla, R. A. and Liz-Marzan, L. M. (2010). "Synthetic Routes and Plasmonic Properties of Noble Metal Nanoplates." European Journal of Inorganic Chemistry(27): 4288-4297.

Petrov, A. I., Antipov, A. A. and Sukhorukov, G. B. (2003). "Base-acid equilibria in polyelectrolyte systems: From weak polvelectrolytes to interpolyelectrolyte complexes and multilayered polyelectrolyte shells." Macromolecules 36(26): 10079-10086.

Philippova, O. E., Hourdet, D., Audebert, R. and Khokhlov, A. R. (1997). "pH-responsive gels of hydrophobically modified poly(acrylic acid)." Macromolecules 30(26): 8278-8285.

Picart, C., Lavalle, P., Hubert, P., Cuisinier, F. J. G., Decher, G., Schaaf, P. and Voegel, J.-C. (2001). "Buildup mechanism for poly(L-lysine)/hyaluronic acid films onto a solid surface." Langmuir 17(23): 7414-7424.

Picart, C., Lavalle, P., Hubert, P., Cuisinier, F. J. G., Decher, G., Schaaf, P. and Voegel, J. C. (2001). "Buildup mechanism for poly(L-lysine)/hyaluronic acid films onto a solid surface." Langmuir 17(23): 7414-7424.

Picart, C., Mutterer, J., Arntz, Y., Voegel, J. C., Schaaf, P. and Senger, B. (2005). "Application of fluorescence recovery after photobleaching to diffusion of a polyelectrolyte in a multilayer film." Microscopy Research and Technique 66(1): 43-57.

Picart, C., Mutterer, J., Richert, L., Luo, Y., Prestwich, G. D., Schaaf, P., Voegel, J.-C. and Lavalle, P. (2002). "Molecular basis for the explanation of the exponential growth of polyelectrolyte multilayers." Proceedings of the National Academy of Sciences of the United States of America 99(20): 12531-12535.

Picart, C., Mutterer, J., Richert, L., Luo, Y., Prestwich, G. D., Schaaf, P., Voegel, J. C. and Lavalle, P. (2002). "Molecular basis for the explanation of the exponential growth of polyelectrolyte multilayers." Proceedings of the National Academy of Sciences of the United States of America 99(20): 12531-12535.

Pichon, B. P., Louet, P., Felix, O., Drillon, M., Begin-Colin, S. and Decher, G. (2011).

"Magnetotunable Hybrid Films of Stratified Iron Oxide Nanoparticles Assembled by the Layer-by-Layer Technique." Chemistry of Materials 23(16): 3668-3675.

Plouffe, B. D., Njoka, D. N., Harris, J., Liao, J., Horick, N. K., Radisic, M. and Murthy, S. K. (2007). "Peptide-mediated selective adhesion of smooth muscle and endothelial cells in microfluidic shear flow." Langmuir 23: 5050-5055.

Podsiadlo, P., Arruda, E. M., Kheng, E., Waas, A. M., Lee, J., Critchley, K., Qin, M., Chuang, E., Kaushik, A. K., Kim, H.-S., Qi, Y., Noh, S.-T. and Kotov, N. A. (2009). "LBL Assembled Laminates With Hierarchical Organization from Nano- to Microscale: High-Toughness Nanomaterials and Deformation Imaging." Acs Nano 3(6): 1564-1572.

Podsiadlo, P., Kaushik, A. K., Arruda, E. M., Waas, A. M., Shim, B. S., Xu, J., Nandivada, H., Pumplin, B. G., Lahann, J., Ramamoorthy, A. and Kotov, N. A. (2007). "Ultrastrong and Stiff Layered Polymer Nanocomposites." Science 318: 80-83

Podsiadlo, P., Liu, Z., Paterson, D., Messersmith, P. B. and Kotov, N. A. (2007). "Fusion of seashell nacre and marine bioadhesive analogs: High-strength nanocompoisite by layer-by-layer assembly of clay and L-3,4-dihydroxyphenylaianine polymer." Advanced Materials 19(7): 949-955.

Podsiadlo, P., Michel, M., Lee, J., Verploegen, E., Kam, N. W. S., Ball, V., Lee, J., Qi, Y., Hart, A. J., Hammond, P. T. and Kotov, N. A. (2008). "Exponential growth of LBL films with incorporated inorganic sheets." Nano Letters 8(6): 1762-1770.

Podsiadlo, P., Paternel, S., Rouillard, J. M., Zhang, Z. F., Lee, J., Lee, J. W., Gulari, L. and Kotov, N. A. (2005). "Layer-by-layer assembly of nacre-like nanostructured composites with antimicrobial properties." Langmuir 21(25): 11915-11921.

Podsiadlo, P., Qin, M., Cuddihy, M., Zhu, J., Critchley, K., Kheng, E., Kaushik, A. K., Qi, Y., Kim, H.-S., Noh, S.-T., Arruda, E. M., Waas, A. M. and Kotov, N. A. (2009). "Highly Ductile Multilayered Films by Layer-by-Layer Assembly of Oppositely Charged Polyurethanes for Biomedical Applications." Langmuir 25(24): 14093-14099.

Podsiadlo, P., Shim, B. S. and Kotov, N. A. (2009). "Polymer/clay and polymer/carbon nanotube hybrid organic-inorganic multilayered composites made by sequential layering of nanometer scale films." Coordination Chemistry Reviews 253(23-24): 2835-2851.

Podsiadlo, P., Tang, Z., Shim, B. S. and Kotov, N. A. (2007). "Counterintuitive effect of molecular strength and role of molecular rigidity on mechanical properties of layer-by-layer assembled nanocomposites." Nano Letters 7(5): 1224-1231.

Porcel, C., Lavalle, P., Decher, G., Senger, B., Voegel, J. C. and Schaaf, P. (2007). "Influence of the polyelectrolyte molecular weight on exponentially growing multilayer films in the linear regime." Langmuir 23(4): 1898-1904.

Recksiedler, C. L., Deore, B. A. and Freund, M. S. (2006). "A novel layer-by-layer approach for the fabrication of conducting polymer/RNA multilayer films for controlled release." Langmuir 22: 2811-2815.

Ren, K. F., Wang, Y. X., Ji, J., Lin, Q. K. and Shen, J. C. (2005). "Construction and deconstruction of PLL/DNA multilayered films for DNA delivery: Effect of ionic strength." Colloids and Surfaces B-Biointerfaces 46(2): 63-69.

Richardson, M. J., Johnston, J. H. and Borrmann, T. (2006). "Monomeric and polymeric amines as dual reductants/stabilisers for the synthesis of gold nanocrystals: A mechanistic study." European Journal of Inorganic Chemistry: 2618-2623.

Richardson, M. J., Johnston, J. H. and Borrmann, T. (2006). "Monomeric and polymeric amines as dual reductants/stabilisers for the synthesis of gold nanocrystals: A mechanistic study." European Journal of Inorganic Chemistry(13): 2618-2623.

Richert, L., Arntz, Y., Schaaf, P., Voegel, J. C. and Picart, C. (2004). "pH dependent growth of poly(L-lysine)/poly(L-glutamic) acid multilayer films and their cell adhesion properties." Surface Science 570(1-2): 13-29.

Richert, L., Engler, A. J., Discher, D. E. and Picart, C. (2004). "Elasticity of Native and Cross-Linked Polyelectrolyte Multilayer Films." Biomacromolecules 5: 1908-1916.

Richert, L., Engler, A. J., Discher, D. E. and Picart, C. (2004). "Elasticity of native and cross-linked polyelectrolyte multilayers." Biomacromolecules 5(5): 1908-1916.

Richert, L., Lavalle, P., Payan, E., Shu, X. Z., Prestwich, G. D., Stoltz, J. F., Schaaf, P., Voegel, J. C. and Picart, C. (2004). "Layer by layer buildup of polysaccharide films: Physical chemistry and cellular adhesion aspects." Langmuir 20(2): 448-458.

Rogalski, A. (2003). "Infrared detectors: status and trends." Progress in Quantum Electronics 27: 59-210.

Ruths, J., Essler, F., Decher, G. and Riegler, H. (2000). "Polyelectrolytes I: Polyanion/polycation multilayers at the air/monolayer/water interface as elements for quantitative polymer adsorption studies and preparation of hetero-superlattices on solid surfaces." Langmuir 16(23): 8871-8878.

Salomaki, M., Vinokurov, I. A. and Kankare, J. (2005). "Effect of temperature on the buildup of polyelectrolyte multilayers." Langmuir 21(24): 11232-11240.

Sardar, R., Bjorge, N. S. and Shumaker-Parry, J. S. (2008). "pH-controlled assemblies of polymeric amine-stabilized gold nanoparticles." Macromolecules 41(12): 4347-4352.

Schneider, G. F., Subr, V., Ulbrich, K. and Decher, G. (2009). "Multifunctional Cytotoxic Stealth Nanoparticles. A Model Approach with Potential for Cancer Therapy." Nano Letters 9(2): 636-642.

Schrof, W., Rozouvan, S., Van Keuren, E., Horn, D., Schmitt, J. and Decher, G. (1998). "Nonlinear optical properties of polyelectrolyte thin films containing gold nanoparticles investigated by wavelength dispersive femtosecond degenerate four wave mixing (DFWM)." Advanced Materials 10(4): 338-341.

Sepulveda, B., Angelome, P. C., Lechuga, L. M. and Liz-Marzan, L. M. (2009). "LSPR-based nanobiosensors." Nano Today 4(3): 244-251.

Shen, J. C., Sun, J. Q. and Zhang, X. (2000). "Polymeric nanostructured composite films." Pure and Applied Chemistry 72(1-2): 147-155.

Shen, L., Chaudouet, P., Ji, J. and Picart, C. (2011). "pH-Amplified Multilayer Films Based on Hyaluronan: Influence of HA Molecular Weight and Concentration on Film Growth and Stability." Biomacromolecules 12: 1322-13231.

Shen, L., Chaudouet, P., Ji, J. and Picart, C. (2011). "pH-Amplified Multilayer Films Based on

Hyaluronan: Influence of HA Molecular Weight and Concentration on Film Growth and Stability." Biomacromolecules 12(4): 1322-1331.

Shi, X. Y., Sanedrin, R. J. and Zhou, F. M. (2002). "Structural characterization of multilayered DNA and polylysine composite films: Influence of ionic strength of DNA solutions on the extent of DNA incorporation." Journal of Physical Chemistry B 106: 1173-1180.

Shim, B. S., Tang, Z., Morabito, M. P., Agarwal, A., Hong, H. and Kotov, N. A. (2007). "Integration of conductivity transparency, and mechanical strength into highly homogeneous layer-by-layer composites of single-walled carbon nanotubes for optoelectronics." Chemistry of Materials 19(23): 5467-5474.

Shim, B. S., Zhu, J., Jan, E., Critchley, K., Ho, S., Podsiadlo, P., Sun, K. and Kotov, N. A. (2009). "Multiparameter Structural Optimization of Single-Walled Carbon Nanotube Composites: Toward Record Strength, Stiffness, and Toughness." Acs Nano 3(7): 1711-1722.

Shim, B. S., Zhu, J., Jan, E., Critchley, K. and Kotov, N. A. (2010). "Transparent Conductors from Layer-by-Layer Assembled SWNT Films: Importance of Mechanical Properties and a New Figure of Merit." Acs Nano 4(7): 3725-3734.

Shimomura, H., Gemici, Z., Cohen, R. E. and Rubner, M. F. (2010). "Layer-by-Layer-Assembled High-Performance Broadband Antireflection Coatings." Acs Applied Materials & Interfaces 2: 813-820.

Shiratori, S. S. and Rubner, M. F. (2000). "pH-dependent thickness behavior of sequentially adsorbed layers of weak polyelectrolytes." Macromolecules 33(11): 4213-4219.

Sohn, B. H. and Seo, B. H. (2001). "Fabrication of the Multilayered Nanostructure of Alternating Polymers and Gold Nanoparticles with Thin Films of Self-Assembling Diblock Copolymers." Chemistry of Materials 13: 1752-1757.

Soltwedel, O., Ivanova, O., Hohne, M., Gopinadhan, M. and Helm, C. A. (2010). "Aggregation and Rearrangement within a Silver Nanoparticle Layer during Polyelectrolyte Multilayer Formation." Langmuir 26: 15219-15228.

Stockton, W. B. and Rubner, M. F. (1997). "Molecular-level processing of conjugated polymers .4. Layer-by-layer manipulation of polyaniline via hydrogen-bonding interactions." Macromolecules 30: 2717-2725.

Struth, B., Eckle, M., Decher, G., Oeser, R., Simon, P., Schubert, D. W. and Schmitt, J. (2001). "Hindered ion diffusion in polyelectrolyte/montmorillonite multilayers: Toward compartmentalized films." European Physical Journal E 6(5): 351-358.

Sukhishvili, S. A. and Granick, S. (2002). "Layered, erasable polymer multilayers formed by hydrogen-bonded sequential self-assembly." Macromolecules 35: 301-310.

Sun, B., Flessner, R. M., Saurer, E. M., Jewell, C. M., Fredin, N. J. and Lynn, D. M. (2011). "Characterization of pH-induced changes in the morphology of polyelectrolyte multilayers assembled from poly(allylamine) and low molecular weight poly(acrylic acid)." Journal of Colloid and Interface Science 355(2): 431-441.

Sun, B., Jewell, C. M., Fredin, N. J. and Lynn, D. M. (2007). "Assembly of multilayered films using well-defined, end-labeled poly(acrylic acid): Influence of molecular weight on

exponential growth in a synthetic weak polyelectrolyte system." Langmuir 23(16): 8452-8459.

Sun, J., Wang, X. and Ji, J. (2009). "Layer-by-Layer Assembly: the New Approach for Advanced Drug Release System." Progress in Chemistry 21(12): 2682-2688.

Sun, T., Wang, G., Feng, L., Liu, B., Ma, Y., Jiang, L. and Zhu, D. (2004). "Reversible switching between superhydrophilicity and superhydrophobicity." Angewandte Chemie International Edition 43: 357-360.

Tan, Y. N., Lee, J. Y. and Wang, D. I. C. (2009). "Morphosynthesis of Gold Nanoplates in Polypeptide Multilayer Films." journal of physical Chemistry C 113: 10887-10895.

Tan, Y. N., Lee, J. Y. and Wang, D. I. C. (2009). "Morphosynthesis of Gold Nanoplates in Polypeptide Multilayer Films." Journal of Physical Chemistry C 113(25): 10887-10895.

Tan, Y. N., Lee, J. Y. and Wang, D. I. C. (2010). "Uncovering the Design Rules for Peptide Synthesis of Metal Nanoparticles." Journal of the American Chemical Society 132(16): 5677-5686.

Tang, Z., Wang, Y., Podsiadlo, P. and Kotov, N. A. (2006). "Biomedical Applications of Layer-by-Layer Assembly: From Biomimetics to Tissue Engineering." Advanced Materials 18: 3203-3224.

Tang, Z. Y., Kotov, N. A., Magonov, S. and Ozturk, B. (2003). "Nanostructured artificial nacre." Nature Materials 2(6): 413-418.

Terzi, F., Zanardi, C., Zanfrognini, B., Pigani, L., Seeber, R., Lukkari, J., aritalo, T. A. and Kankare, J. (2009). "Preparation and Characterization of a Redox Multilayer Film Containing Au Nanoparticles." Journal of Physical Chemistry B 113: 4868-4874.

Tian, S., Liu, J., Zhu, T. and Knoll, W. (2004). "Polyaniline/Gold Nanoparticle Multilayer Films: Assembly, Properties, and Biological Applications." Chemistry of Materials 16: 4103-4108.

Toroz, D. and Corni, S. (2011). "Peptide Synthesis of Gold Nanoparticles: The Early Steps of Gold Reduction Investigated by Density Functional Theory." Nano Letters 11(3): 1313-1318.

Torres, J. A., Nealey, P. F. and de Pablo, J. J. (2000). "Molecular simulation of ultrathin polymeric films near the glass transition." Physical Review Letters 85(15): 3221-3224.

Uğur, Ş. S., Sarıışık, M. and Aktaş, A. H. (2011). "Nano-Al2O3 multilayer film deposition on cotton fabrics by layer-by-layer deposition method." Materials Research Bulletin 46: 1202-1206.

Van Ackern, F., Krasemann, L. and Tieke, B. (1998). "Ultrathin membranes for gas separation and pervaporation prepared upon electrostatic self-assembly of polyelectrolytes." Thin Solid Films 327: 762-766.

Van den Beucken, J. J. J. P., Walboomers, X. F., Boerman, O. C., Vos, M. R. J., Sommerdijk, N. A. J. M., Hayakawa, T., Fukushima, T., Okahata, Y., Nolte, R. J. M. and Jansen, J. A. (2006). "Functionalization of multilayered DNA-coatings with bone morphogenetic protein 2." Journal of Controlled Release 113: 63-72.

Van den Beucken, J. J. J. P., Walboomers, X. F., Nillesen, S. T. M., Vos, M. R. J., Sommerdijk,

N. A. J. M., Van Kuppevelt, T. H., Nolte, R. J. M. and Jansen, J. A. (2007). "In vitro and in vivo effects of deoxyribonucleic acid-based coatings funtionalized with vascular endothelial growth factor." Tissue engineering 13: 711-720.

Vendamme, R., Onoue, S. Y., Nakao, A. and Kunitake, T. (2006). "Robust free-standing nanomembranes of organic/inorganic interpenetrating networks." Nature Materials 5(6): 494-501.

Vodouhe, C., Le Guen, E., Garza, J. M., Francius, G., Dejugnat, C., Ogier, J., Schaaf, P., Voegel, J. C. and Lavalle, P. (2006). "Control of drug accessibility on functional polyelectrolyte multilayer films." Biomaterials 27(22): 4149-4156.

Volodkin, D., Skirtach, A. and Moehwald, H. (2011). LbL Films as Reservoirs for Bioactive Molecules. Bioactive Surfaces. H. G. L. J. F. Borner. 240: 135-161.

Volodkin, D. V., Delcea, M., Moehwald, H. and Skirtach, A. G. (2009). "Remote Near-IR Light Activation of a Hyaluronic Acid/Poly(L-lysine) Multilayered Film and Film-Entrapped Microcapsules." Acs Applied Materials & Interfaces 1(8): 1705-1710.

Volodkin, D. V., Madaboosi, N., Blacklock, J., Skirtach, A. G. and Moehwald, H. (2009). "Surface-Supported Multilayers Decorated with Bio-active Material Aimed at Light-Triggered Drug Delivery." Langmuir 25(24): 14037-14043.

Von Klitzing, R. and Tieke, B. (2004). "Polyelectrolyte membranes." Polyelectrolytes with Defined Molecular Architecture I 165: 177-210.

Vuillaume, P. Y., Jonas, A. M. and Laschewsky, A. (2002). "Ordered Polyelectrolyte "Multilayers". 5. Photo-Cross-Linking of Hybrid Films Containing an Unsaturated and Hydrophobized Poly(diallylammonium) Salt and Exfoliated Clay." Macromolecules 35: 5004-5012.

Waite, J. H. and Tanzer, M. L. (1981). "Polyphenolic Substance of Mytilus edulis: Novel Adhesive Containing L-Dopa and Hydroxyproline." Science 212: 1038-1040

Wang, T. C., Cohen, R. E. and Rubner, M. F. (2002). "Metallodielectric photonic structures based on polyelectrolyte multilayers." Advanced Materials 14(21): 1534-1537.

Wang, X. and Ji, J. (2009). "Postdiffusion of Oligo-Peptide within Exponential Growth Multilayer Films for Localized Peptide Delivery." Langmuir 25(19): 11664-11671.

Wang, X., Sun, J. and Ji, J. (2011). "pH modulated layer-by-layer assembly as a new approach to tunable formulating of DNA within multilayer coating." Reactive & Functional Polymers 71(3): 254-260.

Wolkers, W. F., van Kilsdonk, M. G. and Hoekstra, F. A. (1998). "Dehydration-induced conformational changes of poly-L-lysine as influenced by drying rate and carbohydrates." Biochimica et Biophysica Acta-General Subjects 1425: 127-136.

Yang, H. C., Aoki, K., Hong, H. G., Sackett, D. D., Arendt, M. F., Yau, S. L., Bell, C. M. and Mallouk, T. E. (1993). "Growth and Characterization of Metal(Ii) Alkanebisphosphonate Multilayer Thin-Films on Gold Surfaces." Journal of the American Chemical Society 115: 11855-11862.

Yeom, B., Kim, S., Cho, J. H., Hahn, J. and Char, K. (2006). "Effect of interfacial adhesion on the mechanical properties of organic/inorganic hybrid nanolaminates." Journal of

Adhesion 82(5): 447-468.

Yin, M., Qian, J., An, Q., Zhao, Q., Gui, Z. and Li, J. (2010). "Polyelectrolyte layer-by-layer self-assembly at vibration condition and the pervaporation performance of assembly multilayer films in dehydration of isopropanol." Journal of Membrane Science 358(1-2): 43-50.

Yoo, D., Shiratori, S. S. and Rubner, M. F. (1998). "Controlling bilayer composition and surface wettability of sequentially adsorbed multilayers of weak polyelectrolytes." Macromolecules 31: 4309-4318.

Yoo, D., Shiratori, S. S. and Rubner, M. F. (1998). "Controlling bilayer composition and surface wettability of sequentially adsorbed multilayers of weak polyelectrolytes." Macromolecules 31(13): 4309-4318.

Yoo, P. J., Zacharia, N. S., Doh, J., Nam, K. T., Belcher, A. M. and Hammond, P. T. (2008). "Controlling surface mobility in interdiflusing polyelectrolyte multilayers." Acs Nano 2(3): 561-571.

Yu, D.-G., Lin, W.-C. and Yang, M.-C. (2007). "Surface Modification of Poly(L-lactic acid) Membrane via Layer-by-Layer Assembly of Silver Nanoparticle-Embedded Polyelectrolyte Multilayer." Bioconjugated Chemistry 18: 1521-1529.

Yu, M.-F., Louire, O., Dyer, M. J., Moloni, K., Kelly, T. F. and Ruoff, R. S. (2000). "Strength and Breaking Mechanism of Multiwalled Carbon Nanotubes Under Tensile Load." Science 287: 637-640.

Yuan, W., Fu, J., Su, K. and Ji, J. (2010). "Self-assembled chitosan/heparin multilayer film as a novel template for in situ msynthesis of silver nanoparticles." Colloids and Surfaces B-Biointerfaces 76: 549-555.

Yuan, W., Ji, J., Fu, J. and Shen, J. (2008). "A facile method to construct hybrid multilayered films as a strong and multifunctional antibacterial coating." Journal of Biomedical Materials Research Part B-Applied Biomaterials 85B(2): 556-563.

Zacharia, N. S., DeLongchamp, D. M., Modestino, M. and Hammond, P. T. (2007). "Controlling diffusion and exchange in layer-by-layer assemblies." Macromolecules 40(5): 1598-1603.

Zacharia, N. S., Modestino, M. and Hammond, P. T. (2007). "Factors influencing the interdiffusion of weak polycations in multilayers." Macromolecules 40(26): 9523-9528.

Zan, X. and Su, Z. (2009). "Incorporation of nanoparticles into polyelectrolyte multilayers via counterion exchange and in situ reduction." Langmuir 25: 12355-12360.

Zhai, L., Berg, M. C., Cebeci, F. C., Kim, Y., Milwid, J. M., Rubner, M. F. and Cohen, R. E. (2006). "Patterned superhydrophobic surfaces: Toward a synthetic mimic of the Namib Desert beetle." Nano Letters 6(6): 1213-1217.

Zhai, L., Cebeci, F. C., Cohen, R. E. and Rubner, M. F. (2004). "Stable superhydrophobic coatings from polyelectrolyte multilayers." Nano Letters 4(7): 1349-1353.

Zhai, L., Nolte, A. J., Cohen, R. E. and Rubner, M. F. (2004). "pH-gated porosity transitions of polyelectrolyte multilayers in confined geometries and their application as tunable Bragg reflectors." Macromolecules 37(16): 6113-6123.

Zhang, H. and Rühe, J. (2003). "Polyelectrolyte Multilayers on Weak Polyelectrolyte Brushes." Macromolecular Rapid Communications 24: 576-579.

Zhang, X. and Shen, J. C. (1999). "Self-assembled ultrathin films: From layered nanoarchitectures to functional assemblies." Advanced Materials 11(13): 1139-1143.

Zhao, Q., Qian, J., An, Q. and Sun, Z. (2010). "Layer-by-layer self-assembly of polyelectrolyte complexes and their multilayer films for pervaporation dehydration of isopropanol." Journal of Membrane Science 346(2): 335-343.

Zhu, J., Shim, B. S., Di Prima, M. and Kotov, N. A. (2011). "Transparent Conductors from Carbon Nanotubes LBL-Assembled with Polymer Dopant with pi-pi Electron Transfer." Journal of the American Chemical Society 133(19): 7450-7460.

Zou, Y., Xiang, C., Sun, L. and Xu, F. (2008). "Amperometric glucose biosensor prepared with biocompatible material and carbon nanotube by layer-by-layer self-assembly technique." Electrochimica Acta 53: 4089-4095.

Curriculum vitae

Liyan SHEN

Born on 31st Oct. 1982
Married

3 parvis L.NEEL 38016 GRENOBLE, FRANCE
38 Zheda Road, 310027 HANGZHOU, CHINA

Tel: +86 571 87953755; +33 456 52 93 42
Cell phone: +86 13588869389
E-mail: liyanshen@zju.edu.cn

Academic background

2009.01-2012.03 **Co-trained doctorate between Zhejiang University and Grenoble Institute of Technology** on materials science under the supervision of professor Jian JI and professor Catherine Picart. The thesis mainly concerns on functional free-standing film fabrication and hybrid nanocomposite construction based on polyelectrolyte multilayer.

2006.09-2008.12 Research work under the supervision of professor Jian Ji account for the **doctoratal degree at Zhejiang University on polymer materials**. The work concerns about the fabrication of superhydrophobic surface and about the mechanism of pH-amplified layer-by-layer assembly.

2002.10-2006.06 **Bachelor** degree at Zhejiang University in the department of **polymer material science and engineering.**

Skills

Polymer-physics-chemistry-Biophysics

- Physic/biophysic characterization: AFM, SEM, QCM, SPR, Ellipsometry, Microscopy…
- Chemical characterization: NMR, FTIR, XPS…
- Cell/bacteria culture
- Basic polymer manipulation and characterization skills: extrusion, injection, pressure molding… tensile test, viscosity test, TGA, DSC…

Languages

- Chinese: mother tongue
- English: scientific level
- French: beginning level

Computer: Familiar with Word, Excel, PowerPoint

Publications

1. **Liyan Shen**, Jian Ji, Jiacong Shen, Silver mirror reaction as an Approach to Construct Superhydrophobic surfaces with high reflectivity, ***Langmuir***. 2008, 24, 9962.
2. Jinhong Fu, Jian Ji, **Liyan Shen**, Alexander Küller, Axel Rosenhahn, Jiacong Shen, Michael Grunze, pH Amplified Exponential Growth Multilayers: Toward Hierarchal Micro- and Nanostructuring Surface, ***Langmuir***. 2009, 25, 672.
3. **Liyan Shen**, Jinhong Fu, Ke Fu, Catherine Picart, Jian Ji, Humidity Responsive Asymmetric Free-Standing Multilayered Film, ***Langmuir***. 2010, 26, 16634.
4. Wei Sun, **Liyan Shen**, Jiaming Wang, Ke Fu and Jian Ji, Netlike Knitting of Polyelectrolyte Multilayers on Honeycomb-Patterned Substrate, ***Langmuir***. 2010, 26, 14236.
5. **Liyan Shen**, Patrick Chaudouet, Jian Ji, Catherine Picart, pH-amplified multilayer films based on hyaluronan : influence of HA molecular weight and concentration on film growth and stability, ***Biomacromolecules***. 2011, 12, 1322.
6. **Liyan Shen**, Bailiang Wang, Jinlei Wang, Jinhong Fu, Catherine Picart, Jian Ji, Asymmetric Free-Standing Film with Multifunctional Anti-Bacterial and Self-Cleaning Properties, Submitted to ***ACS Applied Materials & Interfaces.***
7. **Liyan Shen**, Laetitia Rapenne, Patrick Chaudouet, Jian Ji, Catherine Picart, *In-situ* synthesis of gold nanoparticles in exponentially-growing layer-by-layer films, to be submitted.

Conferences

1. **Liyan Shen**, Jinhong Fu, Jian Ji, Jiacong Shen, Fabrication of superhydrophobic free-standing films via layer-by-layer assembly, ***9th International Symposium on Polymer for Advanced Technologies***, 2007, Shanghai, China.
2. **Liyan Shen**, Ke Fu, Gongyan Liu, Qiao Jin, Jian Ji, Synthesis and characterization of coumarin modified reversible photo-crosslinkable hyaluronic acid, ***4th International Symposium on Polymer Chemistry***, 2010, Suzhou, China.
3. **Liyan Shen**, Patrick Chaudouet, Jian Ji, Catherine Picart, pH-Amplified Multilayer Films Based on Hyaluronan: Influence of HA molecular weight and concentration on film growth and stability, ***LBL symposium 2011 "20 Years Layer-by-Layer Assembly: New Frontiers for Fundamental Science and for Applications"***, 2011, Strasbourg, France.